# Understanding changes in the DCD kidney degradome associated with warm ischaemia

**Rebecca Vaughan**

Nuffield Department of Surgical Sciences

St Catherine's College, University of Oxford




**Thesis submitted for the degree of**

**'Doctor of Philosophy in Surgical Sciences'**

**Michaelmas term, 2024**

Word count: 49,338

# Supervisors

**Maria E. Kaisar DPhil**

Associate Professor of Transplantation Science

Nuffield Department of Surgical Sciences, University of Oxford

Scientific Programme Lead in Organ Donation and Transplantation, NHS Blood & Transplant

**Philip D. Charles PhD**

Bioinformatician and Statistician in Proteomics and Mass Spectrometry

Big Data Institute, Nuffield Department of Medicine, University of Oxford

**Rutger J. Ploeg MD, PhD, FRCS, FEBS**

Professor of Transplant Biology & Consultant Transplant Surgeon

Nuffield Department of Surgical Sciences, University of Oxford

# Acknowledgements

I would like to extend heartfelt thanks to my supervisors and my colleagues at the University of Oxford and NHS Blood and Transplant. I have been fortunate to benefit from your vast expertise and guidance.

**To Maria**, your energy and enthusiasm for research is contagious, as is your drive to elevate and support fellow scientists. I am grateful for your ongoing encouragement and support, and for the role you've played in shaping me as a scientist and critical thinker.

**To Phil**, your patience, guidance and understanding – and your love for a good R code – has been invaluable in progressing this study and helping me develop as a researcher. I appreciate the kindness and understanding you have shown me, especially during this challenging final year.

**To Rutger**, your unwavering commitment to research and 'bench to the bedside' approach is an inspiration. Thank you for your insight and support, and the timely reminders that the most important endpoints are the donor and recipient.

I would like to extend my gratitude to Professor Benedikt Kessler, Dr Leonie van Leeuwin, Dr Sarah Fawaz and Dr Ioannis Michelakis for their expertise and technical guidance to support my research. I am also grateful to my employer NHSBT for the opportunity and funding to undertake my DPhil. To the generous people who contributed to my GoFundMe campaign and enabled me to achieve this career ambition, I will always be grateful.

I want to acknowledge the donors and their families whose selflessness enables research such as this to be conducted. I would also like to recognise the NHS teams who work tirelessly to facilitate transplantation and prioritise patient care.

**To my husband Chris**, I could not have achieved this without your unwavering love, support, and tireless encouragement. Thank you for being my rock.

**To my sweet Ezra**, the love, enthusiasm and excitement with which you approach each day makes the world a better place. I hope I have shown you that with persistence and hard work you can achieve anything.

**To my Mum, Robyn, and my sister, Kate**, your love and support have got me to this point. Thank you for everything you've done for me; I hope I've made you proud.

Finally, I would like to honour my friend and colleague, **Jonathan Dixey**. When I first joined NHSBT, you offered to teach me the art of culturing cells and always made yourself available to share your knowledge and offer support. Your kindness and generosity knew no bounds, and I will always treasure the laughter, love, and time we spent together. The call of a bird or smell of cake will always make me think of you.

# Declaration

All research described in this thesis is my own work, undertaken by me unless otherwise stated. The hypothesis and aims behind this research were conceptualised with the support of my supervisors.

The degradomics protocol used in Chapter 4 was suggested following my transfer of status by Professor Benedikt Kessler. Dr Leonie Van Leeuwen and Dr Darragh O'Brien provided support in kidney sample preparation for mass spectrometry analysis according to the HUNTER protocol. Samples were analysed using mass spectrometry in the Target Discovery Institute, by Dr Iolanda Vendrell. Raw mass spectrometry data was processed, using MaxQuant software with the guidance of Svenja Hester. I performed mass spectrometry data analysis using R Studio, under the guidance of my supervisor Dr Philip Charles.

The immortalised human podocyte and proximal tubule epithelial cells utilised in this study were gifted to Diagnostics in Organ Transplantation, Research & Development at NHSBT by Professor Gavin Welsh, from the Bristol Renal Group, University of Bristol.

# Table of Contents

Chapter 1 Introduction ..... 1

1.1 Introduction ..... 2

1.2 The kidney structure and its function ..... 2

1.3 Chronic kidney disease and end stage kidney disease ..... 7

1.4 Kidney transplantation is the best treatment for ESKD yet remains limited ..... 9

*1.4.1 Kidney transplantation statistics, UK ..... 10*

*1.4.2 Kidney transplantation outcomes ..... 12*

*1.4.3 Clinical limitations of kidney transplantation ..... 14*

1.5 The history of kidney transplantation ..... 16

1.6 Donor types ..... 19

*1.6.1 Living donation ..... 20*

*1.6.2 Donation after brain death (DBD) ..... 21*

*1.6.3 Donation after circulatory death (DCD) ..... 23*

*1.6.4 Recipients of DCD kidneys have increased incidences of delayed graft function (DGF) and primary non-function (PNF) ..... 27*

1.7 Warm ischaemia and associated kidney injury ..... 29

*1.7.1 Studies addressing the length of warm ischaemia ..... 30*

*1.7.2 Studies describing pathophysiological implications of warm ischaemia ..... 31*

*1.7.3 Cellular hypoxic response to warm ischaemia ..... 34*

*1.7.4 Molecular limitation associated with WI and DCD KTx ..... 35*

1.8 Proteostasis and degradation in the kidney ..... 36

*1.8.1 The role of proteases in proteostasis ..... 37*

1.9 Measurement of subclinical markers of kidney injury ..... 38

Chapter 2 Thesis overview and research aims ..... 41
2.1 Background ..... 42
2.2 Hypothesis and aims ..... 42
2.3 Overview of experimental work presented in this thesis ..... 43

Chapter 3 Materials and methods ..... 47
3.1 Introduction ..... 48
3.2 Ethical approval for research work ..... 48
3.3 Clinical samples ..... 48
*3.3.1 QUality in Organ Donation (QUOD) biobank samples ..... 48*
3.4 Homogenisation of kidney tissue ..... 50
3.5 Conditionally immortalised human kidney cells ..... 51
*3.5.1 Conditional immortalisation of podocytes and proximal tubule epithelial cells (PTECs) ..... 51*
3.6 Bicinchoninic acid (BCA) assay for protein quantification ..... 54
3.7 Gel electrophoresis, protein staining and Western immunoblotting ..... 55
*3.7.1 Preparing samples into Laemmli buffer ..... 55*
*3.7.2 Gel electrophoresis 4-12% Bis-Tris gels ..... 55*
*3.7.3 Gel transfer for Western immunoblotting. ..... 56*
*3.7.4 Western blotting – protein of interest ..... 56*
*3.7.5 Chemiluminescent imaging of Western blot membranes ..... 57*
*3.7.6 β-actin probing – housekeeping gene for normalisation ..... 58*
*3.7.7 Analysis of Western blots ..... 58*
3.8 Quantitative Polymerase Chain Reaction (qPCR) ..... 59

*3.8.1 RNA purification from cultured cells ..... 59*

*3.8.2 Conversion of extracted RNA into cDNA ..... 59*

*3.8.3 Primer preparation and melt curve tests ..... 60*

*3.8.4 Quantitative polymerase chain reaction (qPCR) method ..... 60*

3.9 Analysis of qPCR data ..... 62

3.10 Statistical analysis ..... 62

Chapter 4 Profiling the DCD kidney degradome with prolonged fWIT ..... 63

4.1 Introduction ..... 64

4.2 Hypothesis and Aims ..... 67

4.3 Materials and methods ..... 68

*4.3.1 Profiling fWIT from NHSBT organ registry data for DCD kidney donors between 2012-2022 ..... 68*

*4.3.2 Kidney biopsy selection ..... 68*

*4.3.3 High-efficiency Undecanal-based N-Termini EnRichment (HUNTER) analysis of kidney biopsies ..... 68*

*4.3.4 Mass Spectrometry Analysis ..... 76*

*4.3.5 Data analysis ..... 77*

4.4 Results ..... 79

*4.4.1 Analysis of fWIT to establish clinically relevant experimental groups 79*

*4.4.2 Donor characteristics and recipient outcomes ..... 80*

*4.4.3 Mass spectrometry data pre-processing and normalisation ..... 83*

*4.4.4 There was no difference in raw reporter ion values based on kidney procurement protocol or TMT-kit ..... 85*

*4.4.5 Endogenous peptide abundance increased in kidneys with prolonged fWIT ……85*

*4.4.6 Endogenous peptides were mapped to derivative proteins based on peptide sequences ..... 92*

*4.4.7 Biological pathways associated with changes in the kidney degradome were mapped using Reactome ..... 95*

*4.4.8 Protease activity changes with prolonged fWIT ..... 102*

*4.4.9 Endogenous peptide abundance and protease activity in DCD donor with or without DGF ..... 106*

4.5 Discussion ..... 108

*4.5.1 Principal component analysis showed no differences in tissue composition between biopsies or batch effects during sample processing ..... 109*

*4.5.2 Endogenous peptide abundance increased with fWIT, indicating changes in cytoskeletal protein arrangement and metabolic processes ..... 110*

*4.5.3 Protein level dysregulation in fWIT affected kidneys indicate dysregulation of cytoskeletal proteins ..... 115*

*4.5.4 Biological pathways dysregulated with fWIT associated with metabolic changes and membrane integrity ..... 118*

*4.5.5 Protease activity changes with prolonged fWIT ..... 134*

*4.5.6 The endogenous peptide profile and protease activity of DGF kidneys was different to that of kidneys with prolonged fWIT ..... 137*

*4.5.7 Limitations and suggested expansions to the study ..... 141*

4.6 Conclusions ..... 144

Chapter 5 Optimisation of a hypoxic human kidney cell model ..... 145

5.1 Introduction ..... 146

5.2 Hypothesis and aims ..... 149

5.3 Materials and methods ..... 150

*5.3.1 Culturing and differentiating cells for inducing hypoxia ..... 150*

*5.3.2 Methods to induce hypoxia ..... 150*

*5.3.3 Induction of hypoxia using GasPak-pouches in media +/- glucose .. 152*

*5.3.4 Expression of hypoxia associated genes quantified using qPCR ..... 153*

5.4 Results ..... 154

*5.4.1 Optimising methods to induce hypoxia in podocytes and PTECs ..... 154*

*5.4.2 Hypoxic cell model experimental plan ..... 160*

*5.4.3 Podocytes and PTECs survived in culture under hypoxic and glucose starved conditions ..... 161*

*5.4.4 qPCR analysis of podocytes and PTECs cultured under normoxic and hypoxic conditions ..... 164*

*5.4.5 Comparison of changes in gene expression in podocytes and PTECs cultured under normoxic and hypoxic conditions +/- glucose over culture time 209*

5.5 Discussion ..... 212

*5.5.1 Glucose concentration during cell culturing may influence metabolic processes in podocytes and PTECs ..... 212*

*5.5.2 GasPak-pouches are a reliable method of inducing cell hypoxia ..... 212*

*5.5.3 HIF expression changed over time in Podocytes and PTECs ..... 214*

*5.5.4 PHDs are key oxygen sensors and regulate HIF stability ..... 216*

*5.5.5 HIFs upregulate genes via the hypoxic response element (HRE) ..... 217*

*5.5.6 Conclusions, limitations and future work ..... 221*

Chapter 6 Validation of key HUNTER degradomic findings ..... 224
6.1 Introduction ..... 225
6.2 Hypothesis and aims ..... 226
6.3 Materials and methods ..... 227
*6.3.1 Mapping endogenous peptides to each derivative protein ..... 227*
*6.3.2 Validation of peptidome changes using Western blotting ..... 227*
*6.3.3 Analysis of Western blots ..... 227*
*6.3.4 Evaluation of protease targets ..... 228*
6.4 Results ..... 228
*6.4.1 Validation of peptide and protease changes in DCD kidneys ..... 228*
*6.4.2 FBP1 endogenous peptides validated using Western blotting ..... 228*
*6.4.3 Western blotting to measure NHERF1 ..... 232*
*6.4.4 BHMT endogenous peptides validated using Western blotting ..... 234*
*6.4.5 Abundance of active LGMN is greater than the zymogen form as fWIT increases in DCD kidneys ..... 238*
*6.4.6 Legumain expression was variable in podocytes and PTEC cells, with active LGMN abundance reduced in PTECs cultured without glucose ..... 240*
*6.4.7 Fibronectin expression did not change in podocytes or PTECs cultured under hypoxic conditions ..... 245*
*6.4.8 Active Cathepsin B abundance decreases as fWIT extends ..... 247*
*6.4.9 Cathepsin B abundance is not affected by hypoxia or glucose concentration in podocytes or PTECs ..... 253*
*6.4.10 Granzyme M activity increased in DCD kidneys with prolonged fWIT ..... 257*

*6.4.11 Matrix metalloproteinase-3 activity decreased in DCD kidneys with prolonged fWIT..... 260*

*6.4.12 Tripeptidyl peptidase 1 cleaved itself, shows its autocatalytic activity ……..261*

6.5 Discussion..... 262

*6.5.1 Degradation of fructose-1,6-biphosphate increased with fWIT..... 263*

*6.5.2 Na/H exchange regulatory factor 1 degradation increased with fWIT, but could not be validated using Western blotting..... 265*

*6.5.3 Betaine-homocysteine S-methyltransferase degradation generated several previously described fragments and associates with increased Legumain activity and fWIT ..... 268*

*6.5.4 Legumain activity was significantly increased in ischaemic kidneys, yet its expression was reduced as fWIT increased ..... 270*

*6.5.5 Cathepsin B expression decreased with fWIT..... 274*

*6.5.6 Granzyme M activity increased with fWIT..... 278*

*6.5.7 Matrix metalloproteinase-3 activity reduces with increasing fWIT . 279*

*6.5.8 Tripeptidyl peptidase 1 showed autocatalytic activity which was downregulated as fWIT increased ..... 281*

*6.5.9 Limitations and future work ..... 281*

*6.5.10 Conclusions ..... 284*

Chapter 7 Summary and future work..... 285

7.1 Experimental findings ..... 286

7.2 Study reflections ..... 289

7.3 Future work..... 292

7.4 Study conclusions ..... 294

Chapter 8 Appendix ..... 296

8.1 Buffers ..... 297

*8.1.1 Laemmli buffer ..... 297*

*8.1.2 MOPS buffer ..... 297*

*8.1.3 Transfer buffer ..... 298*

*8.1.4 Tris-buffered saline with tween (TBST) ..... 298*

*8.1.5 Bovine serum albumin (BSA) blocking buffer ..... 298*

*8.1.6 BSA TBST antibody diluent ..... 299*

*8.1.7 5% Milk blocking buffer/Antibody diluent ..... 299*

*8.1.8 6M Guanidine hydrochloride (GuHCl) ..... 299*

*8.1.9 1M HEPES ..... 299*

*8.1.10 1M Sodium hydroxide (NaOH) ..... 299*

*8.1.11 100mM Sodium hydroxide (NaOH) ..... 300*

*8.1.12 5M Sodium hydroxide (NaOH) ..... 300*

*8.1.13 200mM tris-2-carboxyethyl phosphine (TCEP) ..... 300*

*8.1.14 100mM Iodoacetamide (IAA) ..... 300*

*8.1.15 1M Ethanolamine ..... 300*

*8.1.16 Buffer A ..... 300*

8.2 Kidney tissue homogenisation tests ..... 301

*8.2.1 Buffers compared. ..... 301*

*8.2.2 Homogenisation using a bead beater ..... 301*

*8.2.3 Mortar and pestle homogenising ..... 302*

*8.2.4 Sonicator based tissue lysis ..... 302*

*8.2.5 Coomassie gel staining ..... 302*

*8.2.6 Silver gel staining ..... 303*

*8.2.7 Comparison of homogenisation methods using protein staining .... 303*

8.3 HUNTER Study ..... 306

*8.3.1 Comparison between technical replicates across TMT batches ..... 306*

8.4 Podocyte and PTEC Western blot analysis p.values ..... 310

# Table of Figures

Figure 1-A: Diagram of a kidney and nephron ..... 4

Figure 1-B: The glomerular filtration barrier ..... 5

Figure 1-C: Schematic of the nephron outlining the function of the different regions ... 6

Figure 1-D: Number of DCD donors between 2002-2023 ..... 10

Figure 1-E: Adults on the kidney-only waitlist for transplantation as of March 2024 ... 11

Figure 1-F: Adult-only single kidney transplants in the UK between 2014/15 and 2023/24 ..... 12

Figure 1-G: Mean eGFR 1-year posttransplant..... 13

Figure 1-H: Percentage of kidneys retrieved but not transplanted from deceased donors ..... 15

Figure 1-I: History of kidney transplantation ..... 18

Figure 1-J: Schematic of donor types ..... 20

Figure 1-K: International utilisation of DBD and DCD donors (donors per million population) ..... 24

Figure 1-L: DCD donor care pathway..... 26

Figure 1-M: Schematic differentiating warm ischaemia times ..... 30

Figure 1-N: Simplified schematic of cellular changes associated with ischaemia ..... 34

Figure 1-O: Example of Trypsin cleavage and specificity ..... 38

Figure 2-A: Experimental overview ..... 46

Figure 3-A: QUality in Organ Donation (QUOD) sample collection..... 49

Figure 4-A: High-efficiency Undecanal N-Termini EnRichment (HUNTER) protocol and analysis ..... 76

Figure 4-B: Histogram of functional and total warm ischaemia time of DCD kidney donors with available records between 2012-2022 ..... 79

Figure 4-C: Scatter plot of the fWIT of kidney biopsies analysed as part of the HUNTER study ..... 81

Figure 4-D: Comparison of raw reporter ion values for the pooled sample included in each TMT-kit ..... 84

Figure 4-E: Principal component analysis comparison of needle and punch biopsies included in the HUNTER study ..... 87

Figure 4-F: Abundance of endogenous peptides comparing short fWIT to long fWIT .. 89

Figure 4-G: Abundance of endogenous peptides changes with prolonged fWIT ..... 91

Figure 4-H: Change in protein (cumulative) abundance as fWIT increases ..... 93

Figure 4-I: Comparison of FBP1 peptide abundance over fWIT length ..... 95

Figure 4-J: Volcano plot showing changes in the regulation of biological pathways with prolonged fWIT ..... 96

Figure 4-K: Heatmap showing changes in biological pathway associated with prolonged fWIT ..... 102

Figure 4-L: Examples of the protease Legumain target specificity ..... 102

Figure 4-M: Inferred protease activity based on endogenous peptide N-termini cleavage ..... 103

Figure 4-N: Protease cleavages change with prolonged fWIT ..... 104

Figure 4-O: Endogenous peptides associated with immediate function or delayed graft function posttransplant ..... 107

Figure 4-P: Protease activity differences in kidneys with immediate function or delayed graft function ..... 108

Figure 4-Q: Podocytes and the slit diaphragm ..... 121

Figure 4-R: Energy metabolism under aerobic conditions begins typically with glycolysis ..... 125

Figure 4-S: Enzymatic pathways of glycolysis and gluconeogenesis ..... 126

Figure 4-T: The citric acid cycle ..... 127

Figure 4-U: The electron transport chain also referred to as oxidative phosphorylation ..... 128

Figure 4-V: Fatty acid oxidation pathway ..... 131

Figure 4-W: Choline catabolism pathway ..... 133

Figure 5-A Schematic of the glomerulus and proximal tubule highlighting key cell structures ..... 148

Figure 5-B: Photo of cells cultured using the GasPak-pouch system with the gas generating sachet and environmental indicator ..... 152

Figure 5-C: Podocytes cultured in CoCl2 for 24h and 48h ..... 156

Figure 5-D: PTECs cultured in CoCl2 for 24h and 48h ..... 158

Figure 5-E: Podocytes and PTECs cultured in GasPak-pouches for 24h and 48h ..... 159

Figure 5-F: Hypoxic cell model experimental plan ..... 160

Figure 5-G: Podocytes cells cultured under normoxic and hypoxic conditions in media +/- glucose ..... 162

Figure 5-H: PTECs cultured under normoxic and hypoxic conditions in media +/- glucose ..... 163

Figure 5-I: HIF1α mRNA expression in podocytes cultured under normoxic and hypoxic conditions ..... 167

Figure 5-J: HIF1α mRNA expression in PTECs cultured under normoxic and hypoxic conditions ..... 169

Figure 5-K: HIF2α mRNA expression in podocytes cultured under normoxic and hypoxic conditions ..... 171

Figure 5-L: HIF2α mRNA expression in PTECs cultured under normoxic and hypoxic conditions ..... 173

Figure 5-M: PHD2 mRNA expression in podocytes cultured under normoxic and hypoxic conditions ..... 175

Figure 5-N: PHD2 mRNA expression in PTECs cultured under normoxic and hypoxic conditions ..... 177

Figure 5-O: PHD3 mRNA expression in podocytes cultured under normoxic and hypoxic conditions ..... 179

Figure 5-P: PHD3 mRNA expression in PTECs cultured under normoxic and hypoxic conditions ..... 181

Figure 5-Q: BNIP3 mRNA expression in podocytes cultured under normoxic and hypoxic conditions ..... 183

Figure 5-R: BNIP3 mRNA expression in PTECs cultured under normoxic and hypoxic conditions ..... 185

Figure 5-S: Glut1 mRNA expression in podocytes cultured under normoxic and hypoxic conditions ..... 187

Figure 5-T: Glut1 mRNA expression in PTECs cultured under normoxic and hypoxic conditions ..... 189

Figure 5-U: PDK1 mRNA expression in podocytes cultured under normoxic and hypoxic conditions ..... 191

Figure 5-V: PDK1 mRNA expression in PTECs cultured under normoxic and hypoxic conditions ..... 193

Figure 5-W: PFKFB3 mRNA expression in podocytes cultured under normoxic and hypoxic conditions ..... 195

Figure 5-X: PFKFB3 mRNA expression in PTECs cultured under normoxic and hypoxic conditions ..... 197

Figure 5-Y: PGC1α mRNA expression in podocytes cultured under normoxic and hypoxic conditions ..... 199

Figure 5-Z: PGC1α mRNA expression in PTECs cultured under normoxic and hypoxic conditions ..... 201

Figure 5-AA: Caspase-3 mRNA expression in podocytes cultured under normoxic and hypoxic conditions ..... 203

Figure 5-BB: Caspase-3 mRNA expression in PTECs cultured under normoxic and hypoxic conditions ..... 205

Figure 5-CC: Fibronectin mRNA expression in podocytes cultured under normoxic and hypoxic conditions ..... 207

Figure 5-DD: Fibronectin mRNA expression in PTECs cultured under normoxic and hypoxic conditions ..... 209

Figure 5-EE: Summary of mRNA expression for all analytes in cultured podocytes .... 210

Figure 5-FF: Summary of mRNA expression for all analytes in cultured PTECs ..... 211

Figure 5-GG – HIF under normoxic and hypoxic conditions ..... 216

Figure 6-A: Endogenous FBP1 peptides intensity increases with prolonged fWIT ..... 229

Figure 6-B: Western blotting shows increased degradation of FBP1 with increasing fWIT ..... 231

Figure 6-C: Endogenous NHERF1 peptides intensity increases with prolonged fWIT . 233

Figure 6-D: Endogenous BHMT peptides intensity increases with prolonged fWIT .... 235

Figure 6-E: Western blotting shows increased degradation of BHMT with increasing fWIT ..... 237

Figure 6-F: Legumain expression in DCD kidneys with prolonged fWIT ..... 239

Figure 6-G: Legumain cleaved two proteins in DCD kidneys..... 240

Figure 6-H: Legumain abundance in podocyte cells exposed to normoxic and hypoxic conditions in media +/- glucose ..... 242

Figure 6-I: Legumain abundance in PTEC cells cultured under normoxic and hypoxic conditions in media +/- glucose ..... 244

Figure 6-J: Fibronectin measured in podocytes cultured under normoxic and hypoxic conditions in media +/- glucose ..... 246

Figure 6-K: Fibronectin measured in PTECs cultured under normoxic and hypoxic conditions in media +/- glucose ..... 247

Figure 6-L: Cathepsin B abundance in DCD kidneys with prolonged fWIT..... 249

Figure 6-M: STRING analysis of proteins cleaved by Cathepsin B ..... 252

Figure 6-N: Cathepsin B measured in podocytes cultured under normoxic and hypoxic conditions in media +/- glucose ..... 254

Figure 6-O: Cathepsin B measured in PTECs cultured under normoxic and hypoxic conditions in media +/- glucose ..... 256

Figure 6-P: STRING analysis of proteins cleaved by Granzyme M..... 259

Figure 6-Q: STRING analysis of proteins cleaved by Matrix metalloproteinase-3 ..... 261

Figure 8-A: Coomassie and silver staining of kidney tissue homogenised using tissue lysis buffer or RIPA buffer ..... 304

Figure 8-B: Silver staining and β-actin probing of kidney tissue homogenised in RIPA buffer ..... 305

Figure 8-C: Comparison in raw report ion values from technical replicates..... 306

Figure 8-D: Normalisation of peptide data from the HUNTER study ..... 307

Figure 8-E: Normalisation of the protein data from the HUNTER study..... 308

Figure 8-F: Cumulative peptide abundance for proteins ..... 309

# Table of Tables

Table 1-A: Stages of Chronic Kidney Disease ..... 8

Table 1-B: Maastricht classification system ..... 19

Table 3-A: Preparation of additives for the DMEM-12 culture media to culture PTECs 53

Table 3-B – Antibodies use for Western blotting ..... 57

Table 3-C: List of primer sequences used to measure gene expression in normoxic and hypoxic cells ..... 61

Table 4-A: Donor characteristics and recipient outcome data ..... 82

Table 4-B: Pathway changes associated with quantified endogenous peptides ..... 100

Table 4-C: Percentage overlap of significant proteases ..... 105

Table 5-A: Cell culture media for normoxic and hypoxic cell treatments with/out glucose experiments ..... 153

Table 6-A: Endogenous peptides cleaved by Cathepsin B ..... 252

Table 6-B: Endogenous peptides cleaved by Granzyme M ..... 259

Table 6-C: Endogenous peptides cleaved by matrix metalloproteinase-3 ..... 260

Table 6-D: Endogenous peptides cleaved by Tripeptidyl peptidase 1 ..... 261

# Understanding changes in the DCD kidney degradome associated with warm ischaemia

Rebecca Vaughan – Thesis for Degree of Doctor of Philosophy in Transplantation Sciences

## Thesis Aim

To investigate the impact of prolonged functional warm ischaemia on the DCD kidney degradome and describe dysregulation of protease activity and biological pathways

### Clinical Issue

Deceased after circulatory death donors (DCD)

WIT injury

40% UK kidney transplants from DCDs

50% Delayed graft function

### Degradomic Analysis

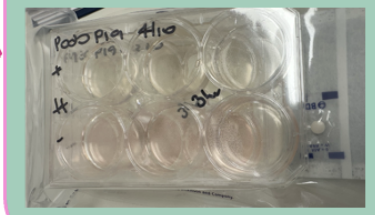
QUOD Quality in Organ Donation

N=42 DCD kidney biopsies

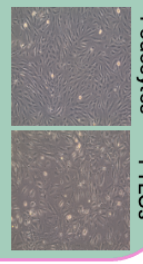
Kidney biopsies prepared according to HUNTER protocol and analysed by Mass Spectrometry

Linear model analysis
- Endogenous peptides
- Protease activity
- Biological pathways

### Hypoxic kidney cell model

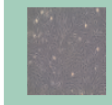


Cultured +/- glucose

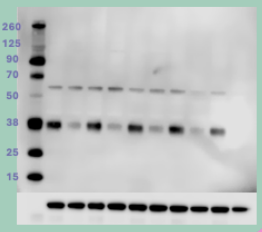



### Validation in kidney biopsies and cells





Validation using Western blotting
- Endogenous peptides
- Proteases




## Conclusions – Prolonged function warm ischaemia associates with dysregulation in glucose metabolism and degradation of matrix proteins in DCD kidneys.

# Abstract

Donation after circulatory death (DCD) has an inherent period of warm ischaemia that strongly associates with inferior kidney posttransplant outcomes. Functional warm ischaemia (fWIT; time donor blood pressure drops below 50mmHg after withdrawal of life support treatment, until cold perfusion) and circulation asystole causes organ hypoperfusion and tissue and cellular energy depletion. This hypoxic period initiates a complex, biological cascade inducing injury, that despite significant clinical implications, remains poorly understood.

Specifically, prolonged fWIT disrupts kidney cell homeostasis and dysregulates endogenous protease activity, which may cause degradation of key proteins integral in kidney physiology. Profiling the degradome of DCD kidney biopsies with variable fWIT using the High-efficiency Undecanal N-Termini EnRichment (HUNTER) protocol and bioinformatic tools was the key objective in this study, to address this hypothesis.

Prolonged fWIT in DCD kidneys is associated with increased degradation of proteins related to proximal tubule injury, metabolism (including FBP1, BHMT and PCBP1) and the cytoskeleton (including NHERF1 and CALD1). The quantified generated protein fragments increased with prolonged fWIT. Notably, legumain (LGMN) activity, a cysteine protease, increased whilst cathepsin B (CATB) activity, a substrate of LGMN, decreased. Pathway analysis suggested that prolonged fWIT induced glucose-driven metabolism dysregulation. This was studied in an *in vitro* hypoxic model of podocytes and proximal tubule epithelial cells (PTECs). Glucose starvation reduced the amount of active LGMN in PTECs but not in podocytes, indicating cell-type specific metabolic disruption associated with glucose availability and hypoxia.

This study describes metabolic and physiological changes in the DCD kidney associated with prolonged fWIT. Newly uncovered changes in active LGMN abundance associated with glucose availability identifies potential considerations for targeted interventions to ameliorate fWIT-induced hypoxic injury in DCD kidneys.

# List of Abbreviations

| | |
|---|---|
| **ACN** | Acetonitrile |
| **AEP** | Asparagine endopeptidase |
| **AKI** | Acute kidney injury |
| **ANOVA** | Analysis of variance |
| **ATP** | Adenosine triphosphate |
| **BCA** | Bicinchoninic acid |
| **BD** | Brain dead/death |
| **BHMT** | Betaine-homocysteine S-methyltransferase |
| **BM** | Basement membrane |
| **BNIP3** | Bcl-2/adenovirus E1B 19-kDa interacting protein |
| **CAC** | Citric acid cycle |
| **CALD1** | Caldesmon |
| **CASP3** | Caspase-3 |
| **CATB** | Cathepsin B |
| **CATD** | Cathepsin D |
| **cDNA** | Complementary DNA |
| **CIT** | Cold ischaemia time |
| **CKD** | Chronic kidney disease |
| **CLIC4** | Chloride intracellular channel protein-4 |
| **CNN3** | Calponin 3 |
| **$CoCl_2$** | Cobalt chloride |
| **CT** | Comparative threshold cycle |

| | |
|---|---|
| **DBD** | Donation after brain death |
| **DCD** | Donation after circulatory death |
| **DCXR** | Dicarbonyl/L-xylulose reductase |
| **DD** | Deceased donor |
| **DGF** | Delayed graft function |
| **DLG2/1** | Disks large homolog 1 and 2 |
| **DMSO** | Dimethyl sulfoxide |
| **ECD** | Extended criteria donor |
| **ECM** | Extracellular matrix |
| **eGFR** | Estimated glomerular filtration rate |
| **EMT** | Epithelial mesenchymal transition |
| **ERM** | Ezrin-radixin-moesin |
| **ESKD** | End Stage Kidney Disease |
| **ETC** | Electron transport chain |
| **FAD** | Flavin adenine dinucleotide |
| **FAO** | Fatty acid oxidation |
| **FCS** | Foetal calf serum |
| **FADH** | Flavin adenine dinucleotide |
| **FBP1** | Fructose-1-6-biophosphatase |
| **FDR** | False discovery rate |
| **FIH** | Factor inhibiting HIF |
| **fWIT** | Functional warm ischaemia time |
| **GBM** | Glomerular basement membrane |
| **GFB** | Glomerular filtration barrier |

| | |
|---|---|
| **Glut 1** | Glucose transporter 1 |
| **GRAM** | Granzyme M |
| **GuHCl** | Guanidine hydrochloride |
| **HIF** | Hypoxia-inducible factor |
| **HIF1α** | Hypoxia-inducible factor 1-alpha |
| **HIF2α** | Hypoxia-inducible factor 2-alpha |
| **HLA** | Human leukocyte antigen |
| **HNRNPC** | Heterogeneous nuclear ribonucleoproteins C1/C2 |
| **HRE** | Hypoxic response elements |
| **HRP** | Horseradish peroxidase |
| **HUNTER** | High-efficiency Undecanal N-Termini EnRichment |
| **IAA** | Iodoacetamide |
| **IF** | Immediate function |
| **IRI** | Ischaemic reperfusion injury |
| **KRT18** | Keratin-18 |
| **KTx** | Kidney transplant/ation |
| **LAD1** | Ladinin 1 |
| **LD** | Living donor |
| **LGMN** | Legumain |
| **MCC2** | 3-methylcrotonoyl-CoA carboxylase |
| **MMPs** | Matrix metalloproteinases |
| **MMP3** | Matrix metalloproteinase 3 |
| **MS** | Mass spectrometry |
| **NAD** | Nicotinamide adenine dinucleotide |

| | |
|---|---|
| **NADH** | Nicotinamide adenine dinucleotide + hydrogen |
| **$NaBH_3CN$** | Sodium cyanoborohydride |
| **NaOH** | Sodium hydroxide |
| **NFκB** | Nuclear factor kappa beta |
| **NHERF1** | Na+/H+ exchanger regulatory factor |
| **NHS** | National Health Service |
| **NHSBT** | National Health Service Blood and Transplant |
| **PBS** | Phosphate-buffered saline |
| **PCA** | Principal component analysis |
| **PCBP1** | Poly(rC)-binding protein |
| **PCR** | Polymerase chain reaction |
| **PDK1** | Pyruvate dehydrogenase kinase 1 |
| **PFKFB3** | 6-phosphofructo-2-kinase/fructose-2,6-biphosphatase 3 |
| **PGC1α** | Peroxisome proliferator-activated receptor gamma coactivator 1-alpha |
| **PHD** | Prolyl hydroxylase domain enzymes |
| **PHD2** | Prolyl hydroxylase domain enzymes-2 |
| **PHD3** | Prolyl hydroxylase domain enzymes-3 |
| **PNF** | Primary non-function |
| **PPP** | Pentose phosphate pathway |
| **PROTOMAP** | PROtein Topography Migration Analysis Platform |
| **PTEC** | Proximal tubule epithelial cells |
| **qPCR** | Quantitative polymerase chain reaction |
| **QUOD** | Quality in organ donation (biobank) |
| **ROS** | Reactive oxygen species |

| | |
|---|---|
| **SCD** | Standard criteria donor |
| **SCr** | Serum creatinine |
| **SD** | Slit diaphragm |
| **SPATS2L** | Spermatogenesis associated serine rich 2 like protein |
| **sWIT** | Standard warm ischaemia time |
| **TAILS** | Terminal Amine Isotopic Labelling of Substrates |
| **TBST** | Tris buffered saline with Tween |
| **TCEP** | tris-2-carboxyethyl phosphine |
| **TEA** | Triethylamine |
| **TFA** | Trifluoracetic acid |
| **TGFβ** | Transforming growth factor-beta |
| **TMT** | Tandem mass tag |
| **TNFα** | Tumour necrosis factor- alpha |
| **TPP1** | Tripeptidyl peptidase 1 |
| **tWIT** | Total warm ischaemia time |
| **UBA1** | Ubiquitin-like modifier activating enzyme-1 |
| **UK** | United Kingdom |
| **UHPLC** | Ultra-high pressure liquid chromatography |
| **USO1** | General vesicular transport factor P115 |
| **WI** | Warm Ischaemia |
| **WIT** | Warm Ischaemia Time |
| **+/-** | With/without glucose |
| **WLST** | Withdrawal of life support treatment |

# Chapter 1 Introduction

## 1.1 Introduction

Kidney transplantation (KTx) is the best treatment for end stage kidney disease (ESKD), the incurable final stage of chronic kidney disease (CKD). KTx improves a patient's quality of life, and estimated survival whilst minimising long-term healthcare costs associated with dialysis therapies[1–6]. Globally CKD affects 13% of the population, with diagnosis rapidly increasing; by 2040, CKD is predicted to be the fifth highest cause of life years lost[7]. In the United Kingdom (UK) 7.2 million people have been diagnosed with CKD, 30,000 of whom rely on dialysis therapies, costing the National Health Service (NHS) £34,000 a year per patient[7]. KTx as the main treatment for ESKD is limited by a shortage of organs available for transplant, a decline in living kidney donation and suboptimal organ quality. Deceased donors (DD) are the primary source of kidneys for transplant and are retrieved from individuals who have been declared dead according to brain or circulatory death criteria. Donation after brain death (DBD) is currently the preferred donation pathways as kidneys from these donors are perceived to have better long-term outcomes posttransplant. Increasing the number of donor kidneys for transplant and improving posttransplant outcomes remains a research priority in this field. Recipients of kidneys from donation after circulatory death (DCD) donors, are more likely to experience posttransplant complications associated with warm ischaemia (WI) inherent to the DCD donation pathway. The pathophysiological implications of WI on the kidney are poorly understood and is the focus of the work presented in this thesis.

## 1.2 The kidney structure and its function

The kidney's primary function is to filter the blood and generate urine *via* its excretory and endocrine functions[8]. Specifically, the kidney regulates water, electrolytes, ions,

glucose and urea concentrations, and removes nitrogenous waste products, toxins, drugs and metabolites from the blood[9]. The kidney also produces the hormones calcitriol (active form of Vitamin D), angiotensin and erythopoietin[10]. The functional unit of the kidney is called the nephron. Each adult kidney has between 1- and 1.2-million nephrons[9]. The nephron consists of the renal corpuscle, glomerulus and Bowman's capsule, and a tubular structure comprised of the proximal convoluted tubule, loop of Henle, distal convoluted tubule and the collecting duct[9]. The glomerulus and convoluted tubules of the nephron are positioned in the kidney cortex, whilst the collecting ducts and loop of Henle are in the medulla (Figure 1-A).

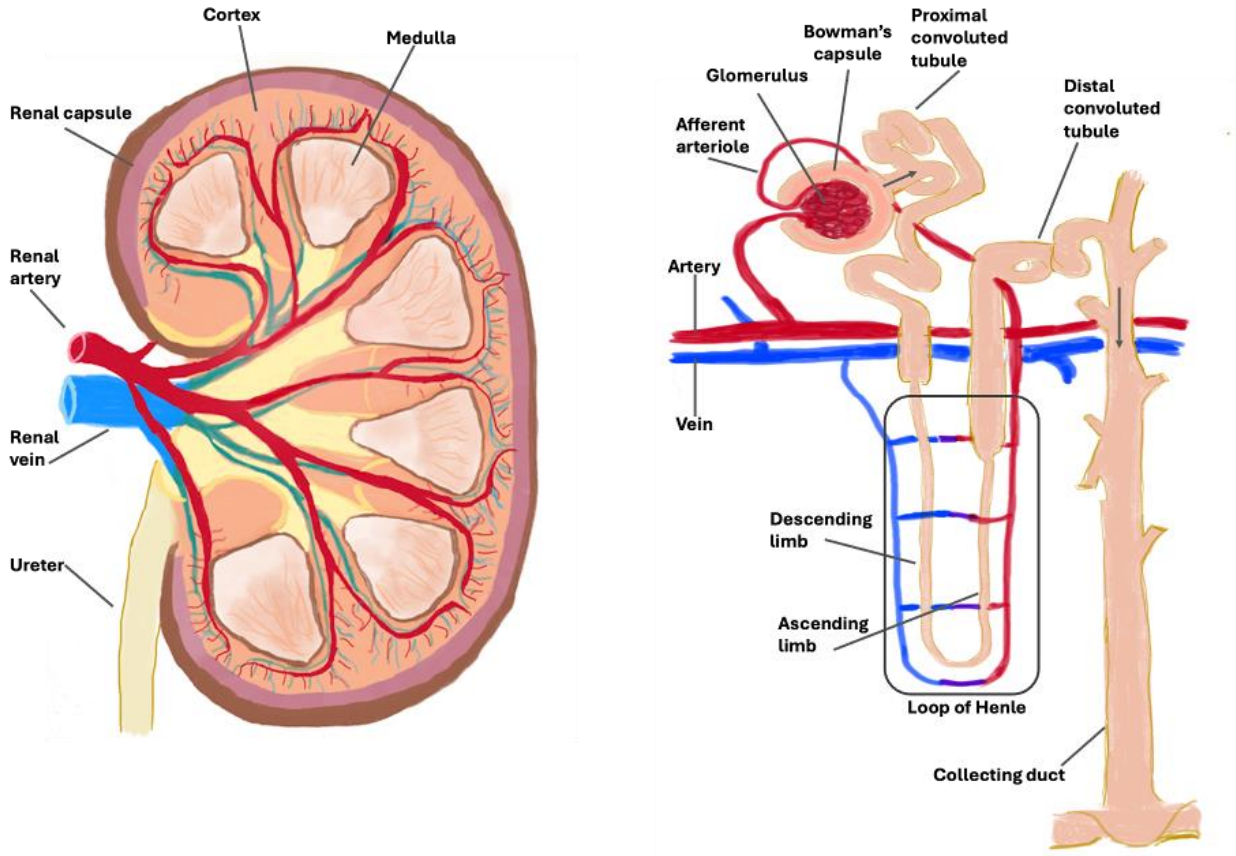



**Figure 1-A: Diagram of a kidney and nephron**

Drawing of a kidney and nephron with key anatomical features labelled for reference. Biopsies used in this study are collected from the kidney cortex.

Each region of the nephron is anatomically and metabolically unique, making the kidney susceptible to pathological insults including hypoxia[11]. Kidney cells are structurally different based on their function. The glomerular filtration barrier (GFB) (Figure 1-B) consists of a capillary endothelium, glomerular basement membrane (GBM) and podocyte layer[9]. The glomerular capillaries are lined with fenestrated endothelial cells that lack diaphragms, allowing for high fluid flux driven by hydrostatic pressure[12]. The GBM is a sheet-like extracellular matrix (ECM) composed of collagen (IV), laminin (LM-521), nidogen and agrin[13] and other key proteins, and is positioned between capillary

endothelial cells and podocytes. The structural composition of the GBM is maintained *via* crosstalk between podocytes and endothelial cells[14]. The unique morphology of podocytes establishes a slit diaphragm between opposing foot processes (that extend from the podocyte cell body) preventing the filtration of plasma proteins, only permitting passage of macromolecules according to size, charge and configuration[9] (Figure 1-B). As podocytes are terminally differentiated, dysregulation to their structure will cause proteinuria[15], affecting kidney function[16]. In the proximal tubules, reabsorption and secretion of the ultrafiltrate occurs. The nephron in Figure 1-C is labelled to highlight the reabsorption and secretory abilities of each segment, which regulates urine concentration.

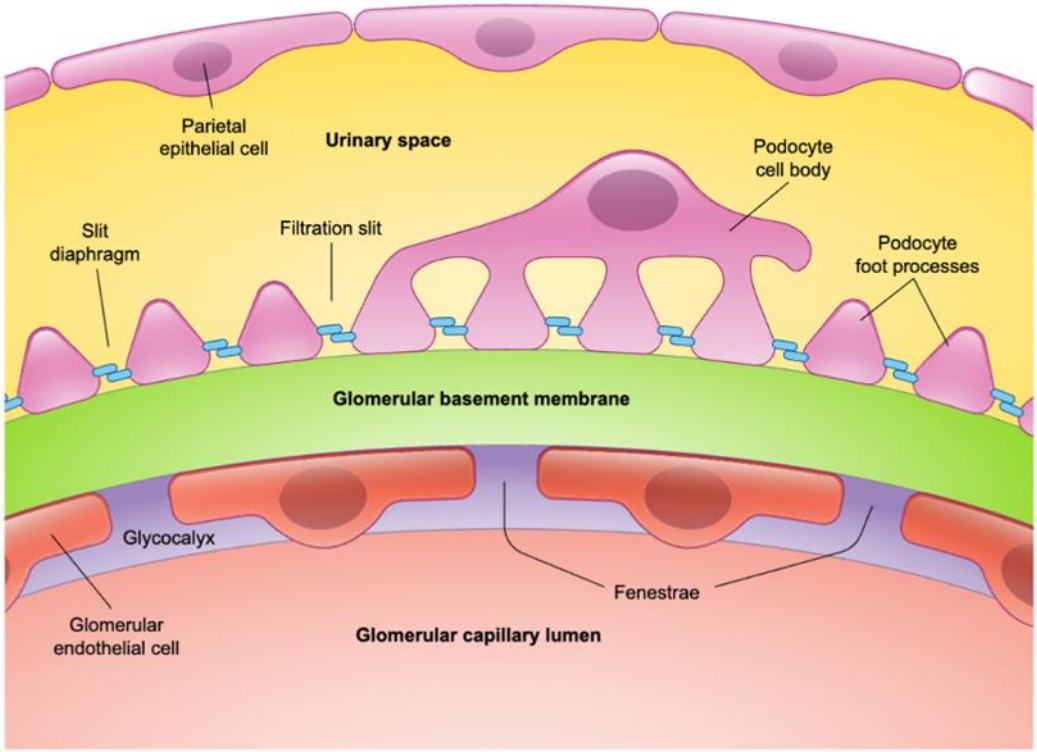



**Figure 1-B: The glomerular filtration barrier**

Schematic showing key structures making up the glomerular filtration barrier. Source: Finch et al (2023)[12].

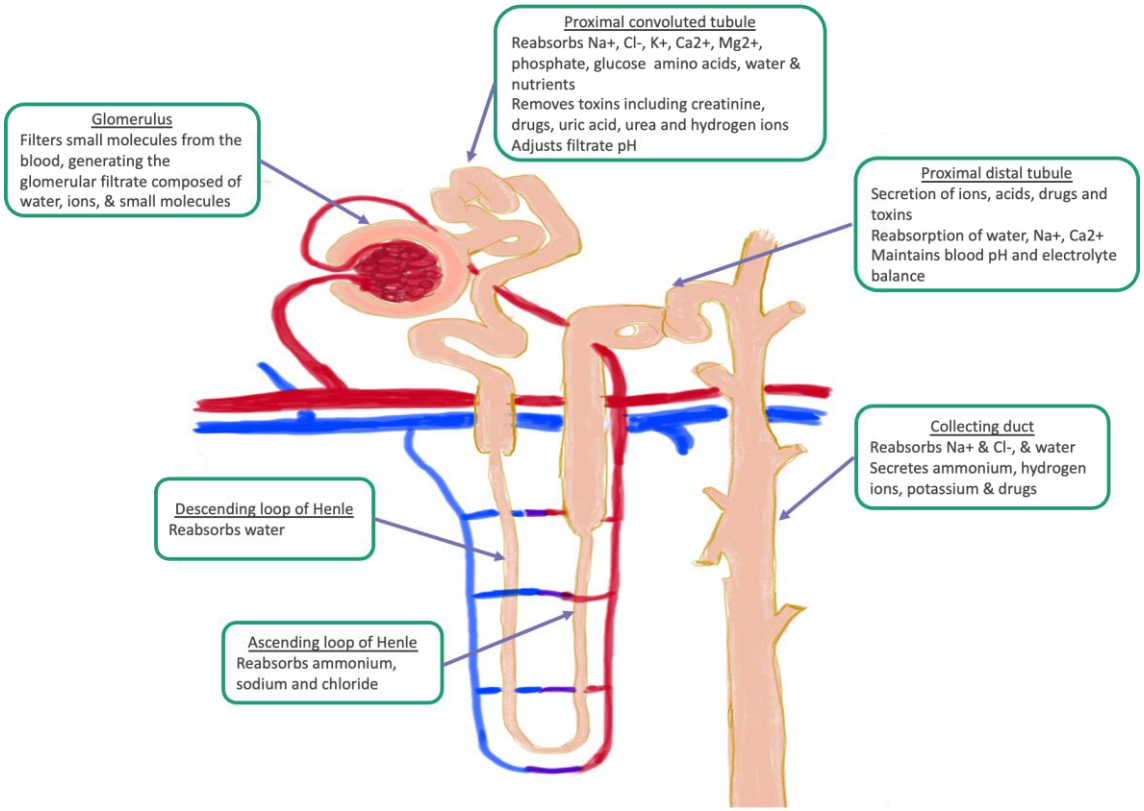



**Figure 1-C: Schematic of the nephron outlining the function of the different regions**

The nephron is the functional unit of the kidney. The reabsorption and secretion functionality of each region is outlined above.

The kidney has a high metabolic demand, necessary to facilitate adenosine triphosphate (ATP)-driven processes essential to maintaining specific functions, including active molecule transport[17]. Although heterogenous, cells in the cortex are typically mitochondria-rich and abundant in oxidative enzymes, facilitating aerobic metabolism. Cells in the medulla rely predominantly on anaerobic glycolysis for ATP production[17]. Glucose is produced in the proximal tubules *via* gluconeogenesis, supporting the vast metabolic needs of the kidney and regulating blood glucose concentration[18]. Metabolic disruption in the kidney caused by ischaemia or acute kidney injury (AKI) will have varying implications. Metabolic demand in the kidney can be satiated for a limited time

by a switch from fatty acid oxidation (FAO) and gluconeogenesis to glycolysis. Metabolic dysregulation is commonly associated with kidney disease, including the transition from AKI to CKD[19].

## 1.3 Chronic kidney disease and end stage kidney disease

Chronic kidney disease is a long-term condition characterised by the gradual decline of renal function in a patient, quantified by reduced (estimated) glomerular filtration rate (eGFR) and an increase in urine albumin:creatinine ratio[20,21]. CKD is a leading cause of mortality[20], affecting 16% of the population[22]. Affecting all socio-economic classes and ethnicities[22], CKD prevalence increases with age and is estimated to cost the NHS in the UK £1.4 billion per year[21]. Although often asymptomatic, early CKD is associated with increased mortality and cardiovascular risk. Advanced CKD (stages ≥3 of the 5-part classification schema; see Table 1-A) is indicative of progression to ESKD and requirement for renal replacement therapies[21], for which KTx is the optimal treatment. Dialysis therapies are more commonly used to treat CKD; however, dialysis has a significant impact on the patient's physical and mental wellbeing, diminishing their quality of life.

| Stage of CKD | eGFR measure (ml/min/1.73m$^2$) | Disease progression |
|---|---|---|
| Stage 1 | >90 | ◊ Indications of kidney damage<br>◊ Kidney works as normal |
| Stage 2 | 60-89 | ◊ Mild kidney damage<br>◊ Kidney still working well |
| Stage 3a | 45-59 | ◊ Mild-moderate kidney damage<br>◊ Kidney function reduced |
| Stage 3b | 30-44 | ◊ Moderate – severe kidney damage<br>◊ Kidney function markedly reduced |
| Stage 4 | 15-29 | ◊ Severe kidney damage<br>◊ Kidney close to not working at all |
| Stage 5 | <15 | ◊ Most severe kidney damage<br>◊ Kidney function minimal or complete kidney failure |

**Table 1-A: Stages of Chronic Kidney Disease**

Stages of CKD are classified by patient eGFR and evidence of disease progression.

## 1.4 Kidney transplantation is the best treatment for ESKD yet remains limited

Kidneys for transplant are retrieved from living donors (LD) and DD with both donor types having excellent 1-year posttransplant survival rates[23]. Yet widespread application of KTx is limited by the longstanding shortage of transplantable donor kidneys. DBD donors are the preferred source of DD kidneys for transplant. However, LD transplants are typically more successful as these donors are healthy, intensely screened and better matched to the recipient[24]. Each year, there are fewer LD transplants as this donation pathway depends upon an individual altruistically donating a kidney. Improvements in donor and recipient care protocols and organ preservation have supported the development of transplant programmes and improved posttransplant outcomes, yet the demand for donor kidneys continues to surpass availability. To counteract this, utilisation of DCDs has increased in the UK (Figure 1-D) as well as other countries during the last two decades, expanding the donor pool by 40%[3].

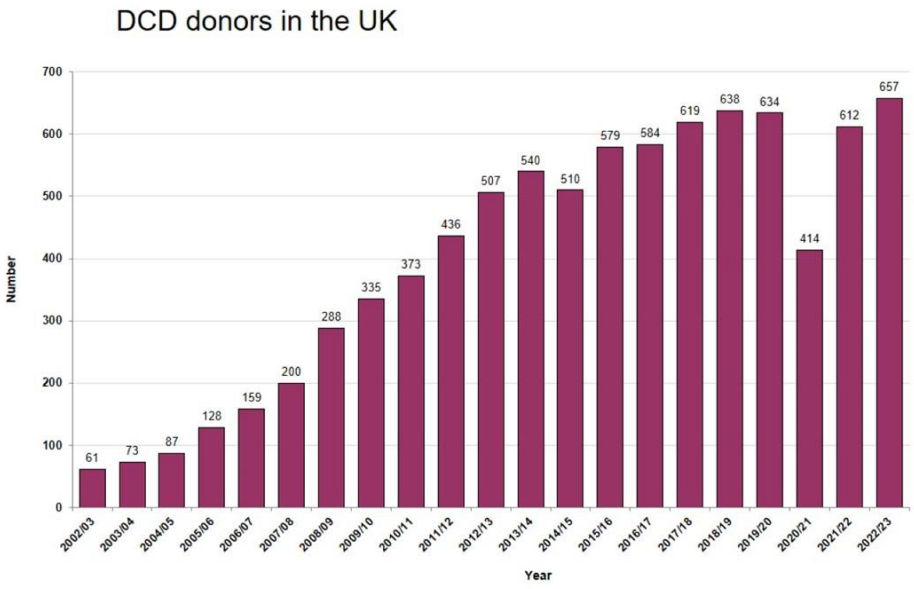



**Figure 1-D: Number of DCD donors between 2002-2023**

Histogram showing utilisation of DCD kidneys between 2002 and 2023. During this time, the utilisation of DCD kidneys has increased substantially in the UK. Between 2020-2021, kidney transplant rates decreased with the COVID-19 pandemic (source: ODT Clinical, NHS Blood and Transplant – Donation after circulatory arrest https://www.odt.nhs.uk/deceased-donation/best-practice-guidance/donation-after-circulatory-death/#:~:text=Number of DCD donors in,organ donors in this year.).

### 1.4.1 Kidney transplantation statistics, UK

As of March 2024, 8,996 patients were awaiting a KTx across the UK, with 5,779 patients active on the waiting list (Figure 1-E). Most ESKD patients wait an average of 536 days for a KTx[23]. Each year approximately 12% of patients on the waiting list are removed due to deteriorating health[25], and 20% of KTx recipients return to the waiting list requiring re-transplantation following kidney graft failure[26]. Between 2023/24, 3,094 adult kidneys were transplanted, with over two-thirds sourced from DD (Figure 1-F).

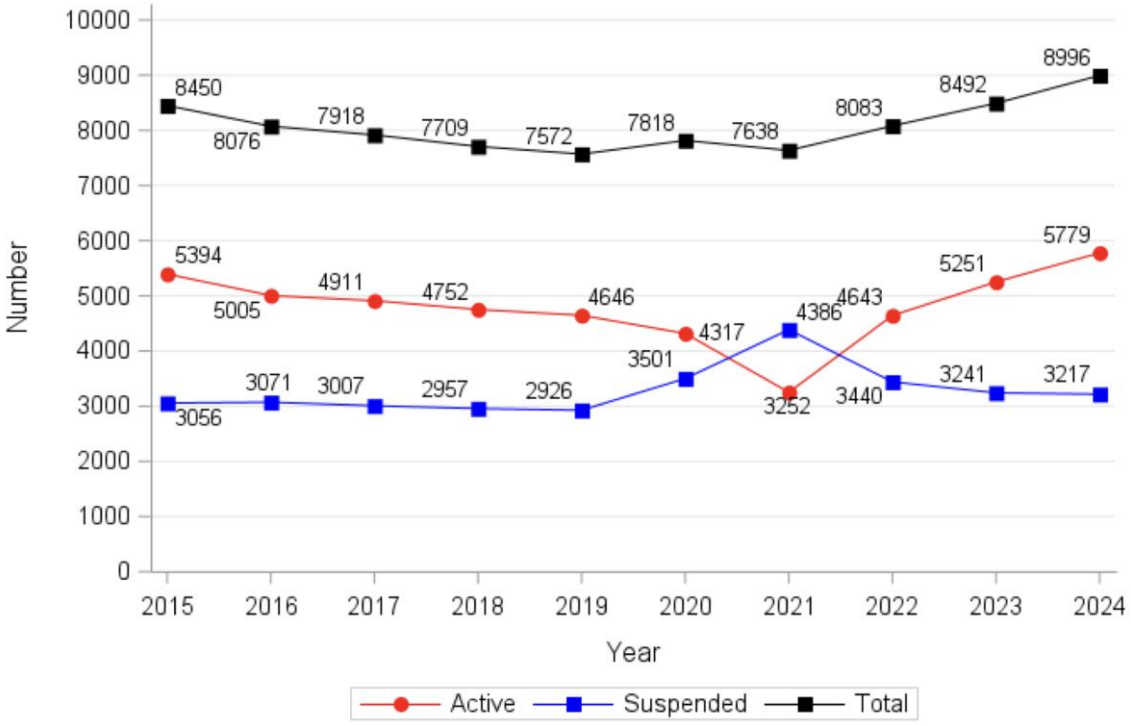



**Figure 1-E: Adults on the kidney-only waitlist for transplantation as of March 2024**

According to the NHS Blood & Transplant Annual Activity Report, at the end of March 2024, 5,779 patients were active on the kidney transplant waiting list (source: NHSBT Annual Kidney Report 2023/24 https://www.odt.nhs.uk/statistics-and-reports/organ-specific-reports/).

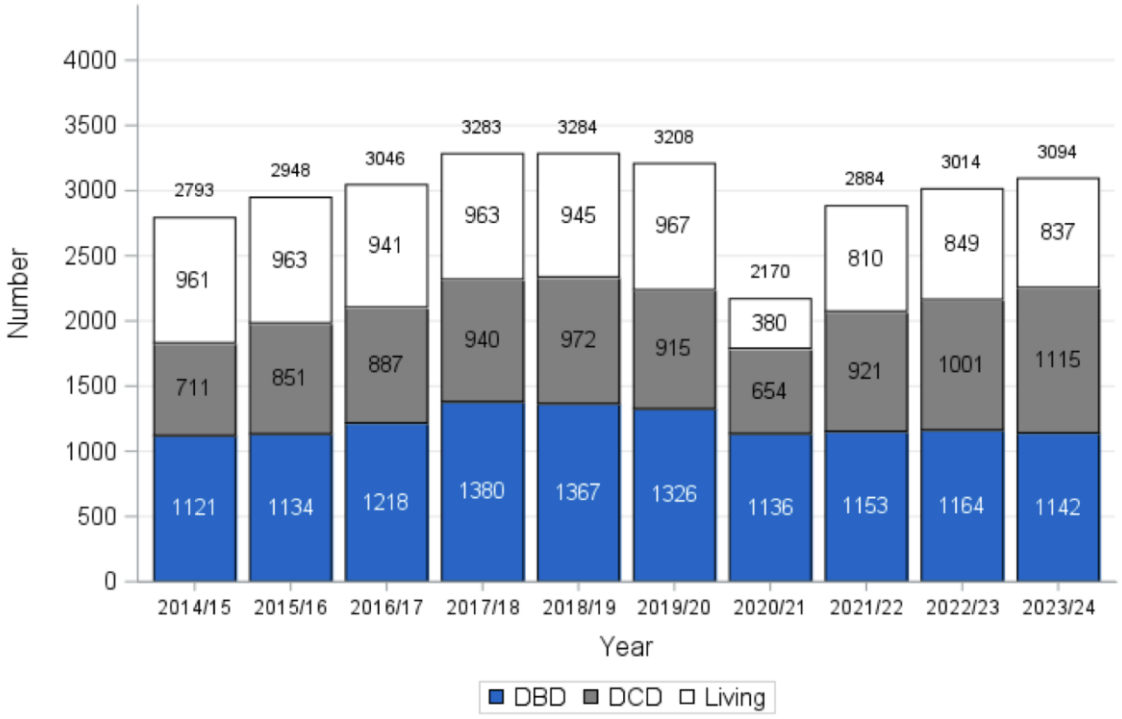



**Figure 1-F: Adult-only single kidney transplants in the UK between 2014/15 and 2023/24**

During 2023/24, 3,094 adult kidneys were transplanted. The number of living donor transplants has slowly decreased during the last 5 years whilst deceased donor numbers have increased. In 2023/24 DCDs contributed 49% of transplanted deceased donor kidneys. Post the COVID-19 pandemic (2020/21), transplant numbers are trending back towards pre-pandemic rates (source: NHSBT Annual Kidney Report 2023/24 https://www.odt.nhs.uk/statistics-and-reports/organ-specific-reports/).

### 1.4.2 Kidney transplantation outcomes

Recipients of LD kidneys have superior short- and long-term outcomes. One-year posttransplant, LD graft survival is 98%; these kidneys have an average eGFR of 56.6ml/min/1.73m$^2$. After five-years LD graft survival remains high at 93%. In DD graft survival at one-year is 95%, dropping to 85% 5-years posttransplant. The average eGFR at 1-year posttransplant for a DBD kidney is 51.8ml/min/1.73m$^2$ compared to 46.9ml/min/1.73m$^2$ for DCD recipients (Figure 1-G)[27]. The impact of donor factors on

kidney graft survival and function is well explored in the literature. Kidneys from LDs function better than DD kidneys as they are retrieved from healthy individuals. Kidneys from DDs are exposed to a cascade of injury relating to cerebral insult, donor management and organ retrieval, which is followed by prolonged periods of cold organ preservation.

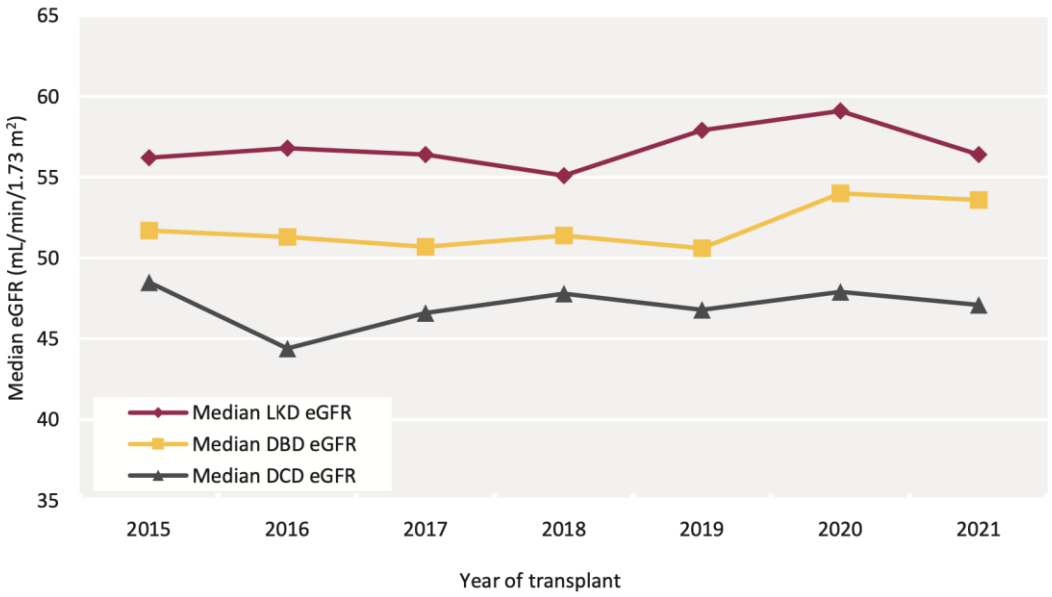



**Figure 1-G: Mean eGFR 1-year posttransplant**

Kidney function posttransplant is measured using eGFR. The average eGFR for each donor type between 2015 and 2021 is shown in this graph (Source: 26th Renal registry report https://ukkidney.org/audit-research/annual-report).

Posttransplant a kidney may function immediately or require additional dialysis treatments to 'kick-start' its function due to donation-related injury. Kidneys that require dialysis support are referred to as having a delayed graft function (DGF), which may detrimentally impact kidney function and longevity. In some instances, transplanted kidneys fail to function immediately posttransplant, and never regain any

function, these kidneys are referred to as primary non-function (PNF). PNF occurs in approximately 3% of DBD and between 3 and 5% of DCD recipients[28].

### 1.4.3 Clinical limitations of kidney transplantation

As a result of developing research and improved success of transplantation as the best treatment for ESKD, the rate of KTx has continuously increased over the last decade. However, the ageing population, increases in co-morbidities and expanding indications for transplant, means that the waiting list continues to increase, whilst the lack of sufficient donor organs persists[26,29,30]. To address this, clinical programmes including those in the UK, have expanded DD selection to include DCDs and extended criteria donors (ECD). First defined by Port *et al* (2002)[29], an ECD donor is aged ≥60 years or aged 50-59 years and meets at least two of the following three criteria: (a) cause of death is cerebrovascular accident, (b) pre-existing history of systemic hypertension; and (c) terminal serum creatinine >1.5mg/dL[30]. Initially, there was reluctance internationally to utilise DCD and ECDs as they pose a higher risk of organ dysfunction and result in poorer transplant outcomes in the short- and long-term. However, as the need for donor organs has continued to increase, clinicians have been forced to accept and transplant higher risk organs, using their understanding of clinical factors to mitigate recipient risk. In this context, risk management protocols are used to match DCD and ECD kidneys to recipients whose survival risk is improved with KTx compared to remaining on dialysis[31]. Utilising ECD kidneys in patients with ESKD can increase life expectancy and minimise dialysis-associated risks, including cardiovascular disease, osteodystrophy and anaemia, especially in elderly recipients or those with diabetes[32].

### 1.4.3.1 Kidney graft allocation and discard

In the UK, DD organs are allocated to waiting recipients according to the organ offer scheme. First established in 2006, the organ offer scheme is regularly reviewed and aims to maximise graft and recipient survival whilst minimising organ discard[4,33,34]. Each year 40% of initial kidney offers are declined and 10 to 12% of DD kidneys are discarded (Figure 1-H), in line with the 8% discard rate reported by Eurotransplant, an organisation of eight countries collaborating in donation and transplantation in Europe[35]. The most common reasons for kidney discard include donor history, organ quality and poor organ perfusion[36,37].

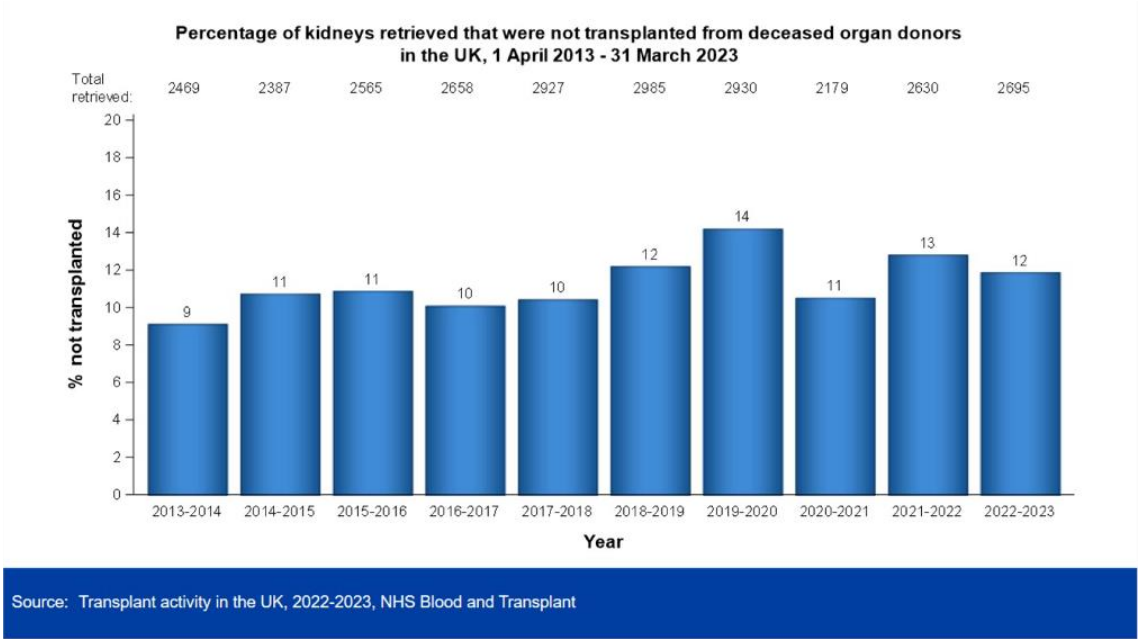



**Figure 1-H: Percentage of kidneys retrieved but not transplanted from deceased donors**

Kidney discard rates between 2013/14 and 2022/23 range between 9 and 14%, with an average discard rate of 11.3% (Source: Organ and tissue donation and transplantation: activity report 2022/2023).

## 1.5 The history of kidney transplantation

Advancements in transplantation research has been guided by pioneers in surgery, immunology and medical technology, establishing modern transplant programmes. Figure 1-I provides a timeline of key milestones throughout the history of KTx. Current research focuses on maximising organ utilisation, minimising organ injury and ensuring graft and recipient survival.

The first successful KTx was performed by Joseph Murray and his team in 1954[38–40], who transplanted a kidney from one brother to his identical twin, overcoming persistent immune rejection issues because of identical twin homology. The recipient twin, who was previously ill with glomerulosclerosis and kidney failure survived eight years posttransplant before succumbing to cardiovascular disease[40–44]. The donor twin lived an additional 56 years following donation. The first successful DD KTx was performed by Murray in 1962; Murray was awarded the Nobel Prize for his contribution to transplantation in 1990[45]

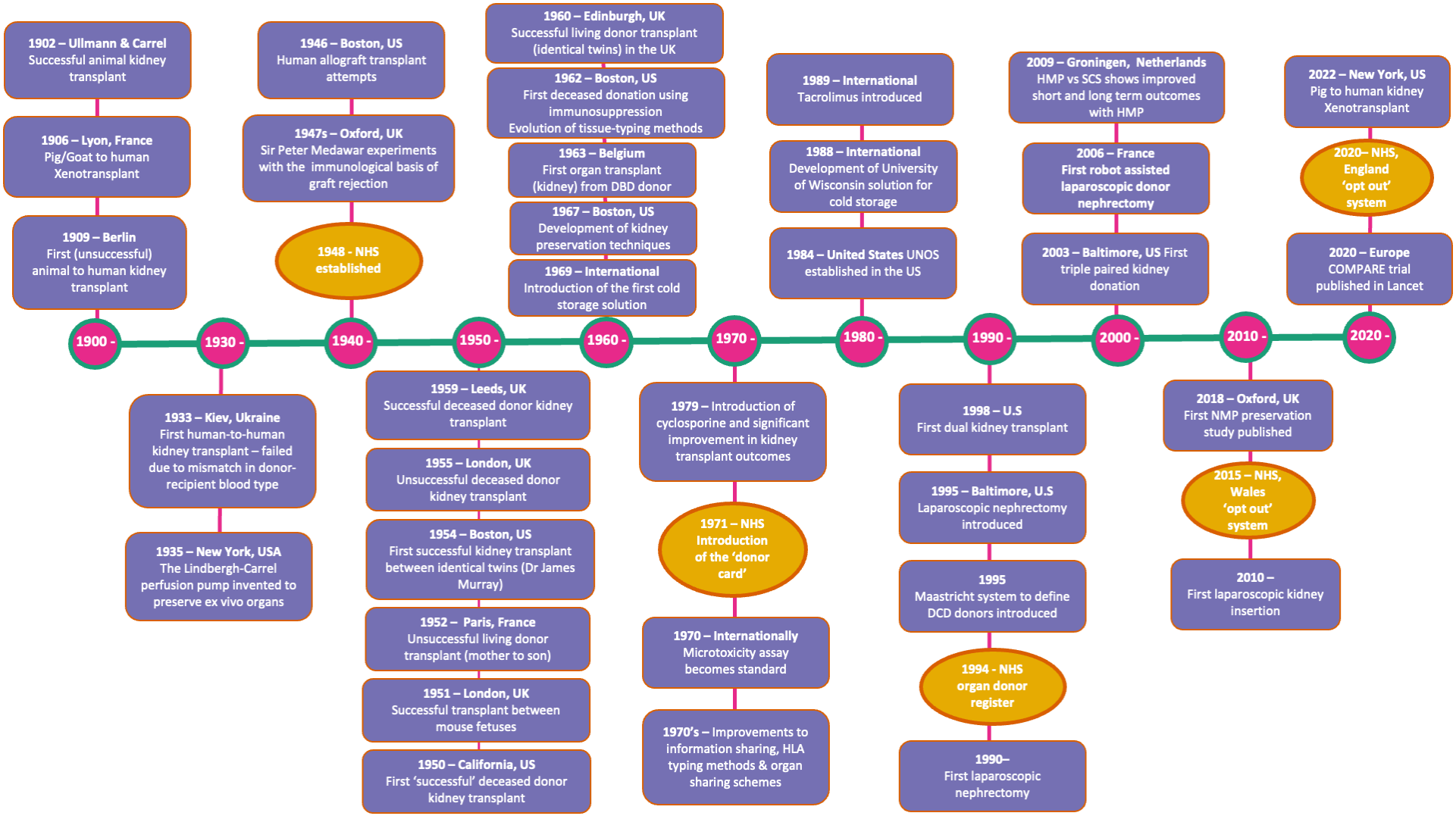

1902 – Ullmann & Carrel
Successful animal kidney transplant
1906 – Lyon, France
Pig/Goat to human Xenotransplant
1909 – Berlin
First (unsuccessful) animal to human kidney transplant
1900 -
1933 – Kiev, Ukraine
First human-to-human kidney transplant – failed due to mismatch in donor-recipient blood type
1935 – New York, USA
The Lindbergh-Carrel perfusion pump invented to preserve ex vivo organs
1930 -
1946 – Boston, US
Human allograft transplant attempts
1947s – Oxford, UK
Sir Peter Medawar experiments with the immunological basis of graft rejection
1948 - NHS established
1940 -
1959 – Leeds, UK
Successful deceased donor kidney transplant
1955 – London, UK
Unsuccessful deceased donor kidney transplant
1954 – Boston, US
First successful kidney transplant between identical twins (Dr James Murray)
1952 – Paris, France
Unsuccessful living donor transplant (mother to son)
1951 – London, UK
Successful transplant between mouse fetuses
1950 – California, US
First 'successful' deceased donor kidney transplant
1950 -
1960 – Edinburgh, UK
Successful living donor transplant (identical twins) in the UK
1962 – Boston, US
First deceased donation using immunosuppression
Evolution of tissue-typing methods
1963 – Belgium
First organ transplant (kidney) from DBD donor
1967 – Boston, US
Development of kidney preservation techniques
1969 – International
Introduction of the first cold storage solution
1960 -
1979 – Introduction of cyclosporine and significant improvement in kidney transplant outcomes
1971 – NHS Introduction of the 'donor card'
1970 – Internationally
Microtoxicity assay becomes standard
1970's – Improvements to information sharing, HLA typing methods & organ sharing schemes
1970 -
1989 – International
Tacrolimus introduced
1988 – International
Development of University of Wisconsin solution for cold storage
1984 – United States UNOS established in the US
1980 -
1998 – U.S
First dual kidney transplant
1995 – Baltimore, U.S
Laparoscopic nephrectomy introduced
1995
Maastricht system to define DCD donors introduced
1994 - NHS organ donor register
1990–
First laparoscopic nephrectomy
1990 -
2009 – Groningen, Netherlands
HMP vs SCS shows improved short and long term outcomes with HMP
2006 – France
First robot assisted laparoscopic donor nephrectomy
2003 – Baltimore, US First triple paired kidney donation
2000 -
2018 – Oxford, UK
First NMP preservation study published
2015 – NHS, Wales 'opt out' system
2010 –
First laparoscopic kidney insertion
2010 -
2022 – New York, US
Pig to human kidney Xenotransplant
2020– NHS, England 'opt out' system
2020 – Europe
COMPARE trial published in Lancet
2020 -

**Figure 1-I: History of kidney transplantation**

Innovation and establishment of kidney transplantation as a potential treatment for kidney disease dates back to 1902. More recently, several previously tested methods including xenotransplantation and organ perfusion have been re-established as potential methods to expand kidney transplantation.

*Acronyms not defined elsewhere: UNOS – United network for organ sharing, HMP – Hypothermic machine perfusion, SCS – Static cold storage, NMP – Normothermic machine perfusion.*

Prior to 1963, all DD organ transplants were from non-heart beating donors (today referred to as DCDs). In 1959, Guy Alexandre introduced the concept of the *coma dépassé,* a state after cerebral injury associated with the deepest coma. Continuation of blood circulation with oxygenation and organ perfusion of *coma dépassé* patients was possible by technical advancement in machinery to support circulation subsequently and resulted in the first successful 'heart-beating donor' (DBD) transplant in 1963. The criteria for neurological death was subsequently defined by the Harvard Committee in 1968[44]. Today, DBDs remain the preferred source of DD organs for transplant[4,23,46,47].

By the end of the 20$^{th}$ century KTx was an established treatment option for ESKD. The embargo on utilising non-heart beating donors (DCD) continued until the 1990s when exponential demand for donor kidneys led to the resurgence of DCD transplant programmes. In 1995, the Maastricht classification system was published by Kootstra *et al,* distinguishing four categories of DCD based on donor status: dead on arrival; death without successful resuscitation; awaiting cardiac arrest; and cardiac arrest with brain death (BD)[48]. The Maastricht classification system was later updated to incorporate the location of where 'death' occurred and to classify DCDs as either controlled or uncontrolled (Table 1-B). However, clinicians remain reluctant to utilise DCD organs[6].

| Category | Type | Classification | Typical location |
|---|---|---|---|
| I | Uncontrolled | Dead on arrival | Emergency department |
| II | Uncontrolled | Unsuccessful resuscitation | Emergency department |
| III | Controlled | Cardiac arrest following planned withdrawal of life support treatments | Intensive care unit |
| IV | Controlled | Cardiac arrest in brain dead patient | Intensive care unit |

**Table 1-B: Maastricht classification system**

The Maastricht classification system used internationally to classify DCDs based on the location and condition of death.

## 1.6 Donor types

As efforts continue to expand the donor pool, there has been significant increases in the utilisation of DCD and ECD kidneys[30] and a push to utilise less conventional donors such as uncontrolled DCDs. Figure 1-J shows a schematic outlining the different types of kidney donors.

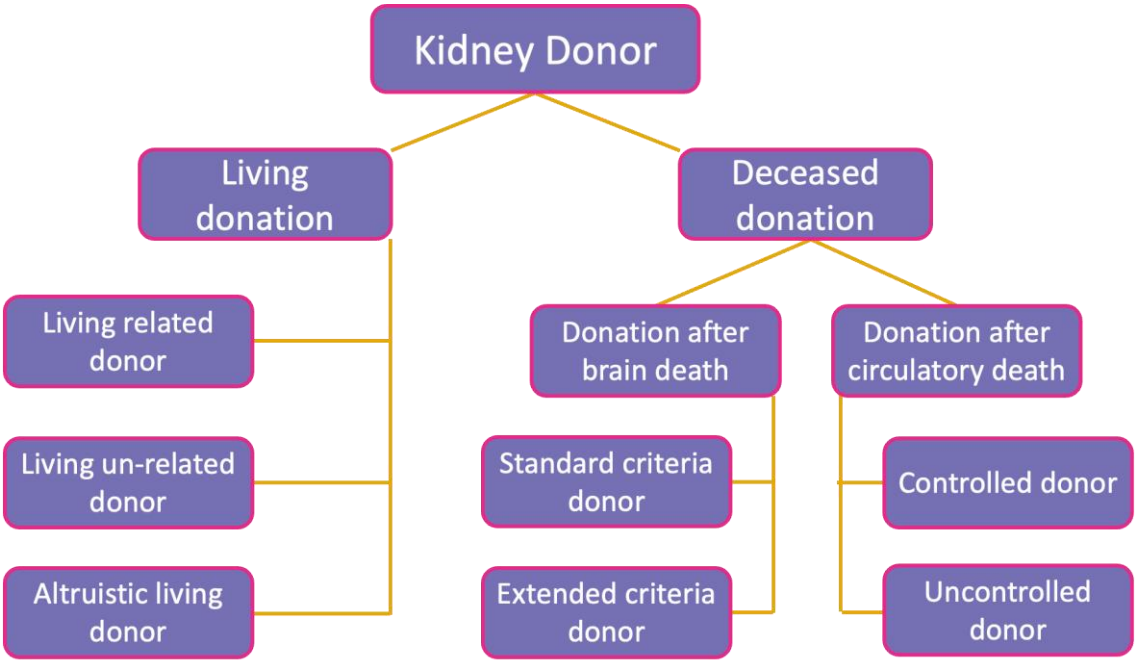



**Figure 1-J: Schematic of donor types**

Schematic of donor types highlighting differences in living and deceased donors. Living donors can be divided into three categories. Deceased donors divide into two groups determined by the donation pathway. In the UK, both standard criteria donors and extended criteria donors (DBD) are utilised whilst only controlled DCDs are transplanted.

### 1.6.1 Living donation

Kidneys from LDs account for one-third of KTx each year in the UK and are donated altruistically or as a directed donation. Kidneys from LD are typically transplanted within 3 to 6 months of consent[47,49,50] often before the recipient commences dialysis, minimising associated health and financial risk[23,50]. KTx from LD have superior outcomes compared to DD[6,23], as they are intensely screened to ensure physical health and donor/recipient compatibility and matchability[23,49]. There is no demonstrable benefit in relative-to-relative LD transplant[23], with human leukocyte antigen (HLA) mismatched LD still outperforming HLA-matched DDs[51]. Recent studies in the UK, USA and Australia

have found that LD and recipients tend to be younger, with the donors more likely to be female, from a white background and of good socioeconomic standing.

### 1.6.2 Donation after brain death (DBD)

Yearly, DBDs account for more than half of DD KTxs and are perceived to have superior outcomes compared to DCD kidneys[3]. Death in DBDs is confirmed using neurological criteria, defined as the cessation of all brain function including the brain stem, confirmed by formal clinical assessment[4,52]. Typically, DBDs have experienced an irreversible catastrophic cerebral injury from which they would die without life support treatment[53].

The pathophysiological implications of neurological death are well described in the literature, and current donor management protocols aim to minimise associated complications and injury. Catastrophic brain death (BD) disrupts physiological homeostasis, inducing autonomic, metabolic and endocrine disturbances affecting multiple systems[54–57]. Mechanical ventilation maintains blood flow and oxygenation of the body. However, as cerebral ischaemia increases, intracranial pressure initiates the systemic storm (catecholamine and autonomic) causing tachycardia, hypertension and systemic vasoconstriction, initiating metabolic changes and apoptosis[58–64]. Donors may also have pulmonary oedema and hormone imbalances leading to conditions including diabetes insipidus[61,65]. Diabetes insipidus occurs in 49-60% of DBD donors caused by a deficiency in antidiuretic hormone and can cause polyuria, hypernatraemia, increased serum osmolarity and low urine osmolarity[66]. The effect of diabetes insipidus on posttransplant kidney function is poorly characterised, but may associate with increased incidences of graft failure[67]. BD associates with systemic pro-inflammatory changes

including increased levels of circulating cytokines, and increased activation of inflammatory markers in the kidneys at the time of donation. Cytokine release following reperfusion may attract the recipient's own leukocytes to the kidney graft increasing the risk of acute rejection[4,59,68]. This can have detrimental effects on both the recipient's immune response and overall graft function[24].

Strategies to ensure adequate organ function must include continuous organ evaluation prior to organ retrieval, during *ex-situ* organ preservation and reconditioning, and before transplant. Organ recovery surgery is performed according to anaesthetic protocols to maintain optimal organ and tissue perfusion and organ quality. More recently there have been calls to delay withdrawal of life support from DCD donors. It is estimated that 28% of cerebral injury in DCDs will progress to BD within 36 hours[69,70], meaning these organs could be retrieved according to DBD criteria, potentially improving graft prognosis. Furthermore, the donation pathway following BD may provide a better experience for the donor family when consenting to organ donation[69]. Once consent is given, the confirmation of BD can alleviate the donor families concerns regarding likelihood of recovery and survival[70]. It also reduces the need for futile treatment[70] and shortens the time donor families spend at the hospital[71], helping them begin the grieving process sooner.

Early graft function is an important determinant of posttransplant function and longevity[72]. Kidney injury associated with ischaemic reperfusion injury (IRI), is an unavoidable insult in DD, and can manifest as slow improvement in kidney function or may act to injure the kidney limiting its function and survival. The mechanisms of injury

associated with IRI remain underexplored, but are associated with tubular injury[73], cell death and systemic inflammation[74]. Inflammatory injury following reperfusion promotes adaptative immunity and graft rejection by predisposing the graft to progressive interstitial fibrosis, tubular atrophy and ultimately graft dysfunction. This risk is particularly relevant in the context of DBDs as these donors experience pro-inflammatory conditions induced by BD, which may cause kidney dysfunction prior to organ retrieval[59,73,75–77], which is exacerbated following reperfusion.

#### 1.6.2.1 Extended criteria donors

To compensate for continuous organ shortages, donor acceptance and allocation criteria is continually being adapted. The variables used to define a donor as ECD, increases graft failure risk by 70% compared to standard criteria donors (SCD)[30]. Therefore, ECDs are typically assigned to a restricted group of recipients: those with an increased age or those experiencing significant difficulties with dialysis therapies, providing a survival advantage over remaining on the waiting list[23,36,37]. ECD kidneys are discarded at a greater rate than that of SCD DBDs, despite considerable evidence of their value in improving transplant rates[78].

### 1.6.3 Donation after circulatory death (DCD)

During the 1990s the exponential demand for donor kidneys for transplantation led to the gradual re-uptake of DCDs in some Western countries including the UK[3,43,79]. Today DCDs are used in several international transplant programmes, including in the USA, Europe, Australia and Japan, and more recently Argentina, Iran, Turkey and Taiwan[54] (Figure 1-K), making DCD the fastest growing form of organ donation. The continued

growth of DCD programs can largely be attributed to overcoming various legal, ethical and facilitation challenges[80]. This progress is particularly evident in the UK and across Europe. In 2020, the UK was reported to have the highest DCD activity in Europe, followed by Spain, Russia, The Netherlands, Belgium and France[79]. Notably, both Spain and France utilise both controlled and uncontrolled DCDs, further expanding the donor pool and increasing the availability of organs for transplantation.

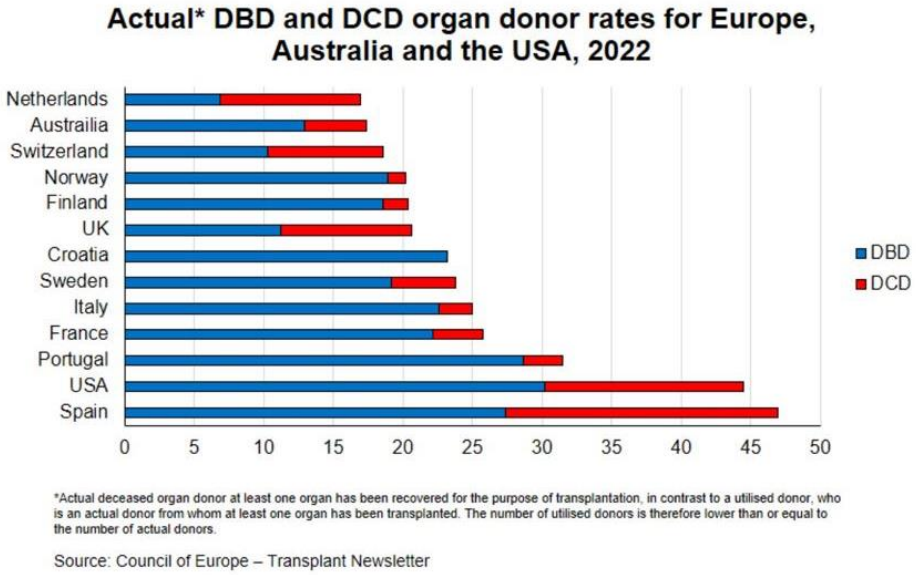



**Figure 1-K: International utilisation of DBD and DCD donors (donors per million population)**

DBDs remain the preferred source of donor kidneys for transplantation, however international programmes are increasingly utilising DCDs to bridge the gap between organ demand and availability. Utilisation of DD in this graph

Death in DCD donation is confirmed using cardio-respiratory criteria, specifically the permanent absence of respiration and circulation without autoresuscitation, confirmed by a no-touch period[10,50]. Patients referred for DCD donation typically have cerebral injuries deemed incompatible with life; however, these potential donors do not meet

the criteria for neurological death and therefore the decision is made to withdraw life support treatment (WLST) irrespective as to whether organ donation is an option or not. The Maastricht system categorises DCDs as either controlled or uncontrolled as described in Table 1-B. In the UK, DCD donors from categories III and IV are used, however following the success of other programmes there has been a push to expand the acceptance criteria to include category I and II donors[81].

During the last two decades, DCD utilisation has increased transplant rates by 85% (Figure 1-D)[3,23]and is now an important donation pathway in the UK[3]. However, DCD still accounts for fewer transplants as many donors do not proceed to donation; often due to prolonged time to asystole following WLST or the donor being deemed medically unsuitable due to donor history, prolonged ischaemia or decline by the retrieval centre[3,33].

#### 1.6.3.1 DCD donation pathway

The clinical pathway for DCD donation in the UK is outlined in Figure 1-L. Irrespective of donation, when a patient's medical treatment is deemed futile, the treating physician will inform and discuss WLST with the patient's family. Common causes of death, for DCDs include catastrophic brain injury such as intracranial haemorrhage, hypoxic brain damage, trauma including head injury or respiratory disease. Conditions such as cardiac arrest are reasonably rare in the UK and would be more typical of uncontrolled DCDs – cardiac arrest introduces additional and variable WI in the donor. Once consent is given to WLST, the family will be asked to consent for organ donation. Donor life support is then withdrawn by extubating the patient; this occurs in either the intensive care unit

or the operating theatre, and results in respiratory and circulatory arrest. Following WLST, the donor's blood pressure drops, reducing blood flow and oxygenation of the organs. Serial haemodynamic, oxygen saturation and urine output measurements are recorded every three to five minutes until circulation has ceased and the donor is declared dead[82]. A five minute 'no touch' period is observed to ensure auto resuscitation does not occur; internationally the 'no touch' period can extend up to 30 minutes[79]. Death is then declared by the responsible physician and the organ retrieval process can commence[82]. Significant to the DCD pathway is the unavoidable period of WI that associates with organ injury and poorer posttransplant outcomes[79].

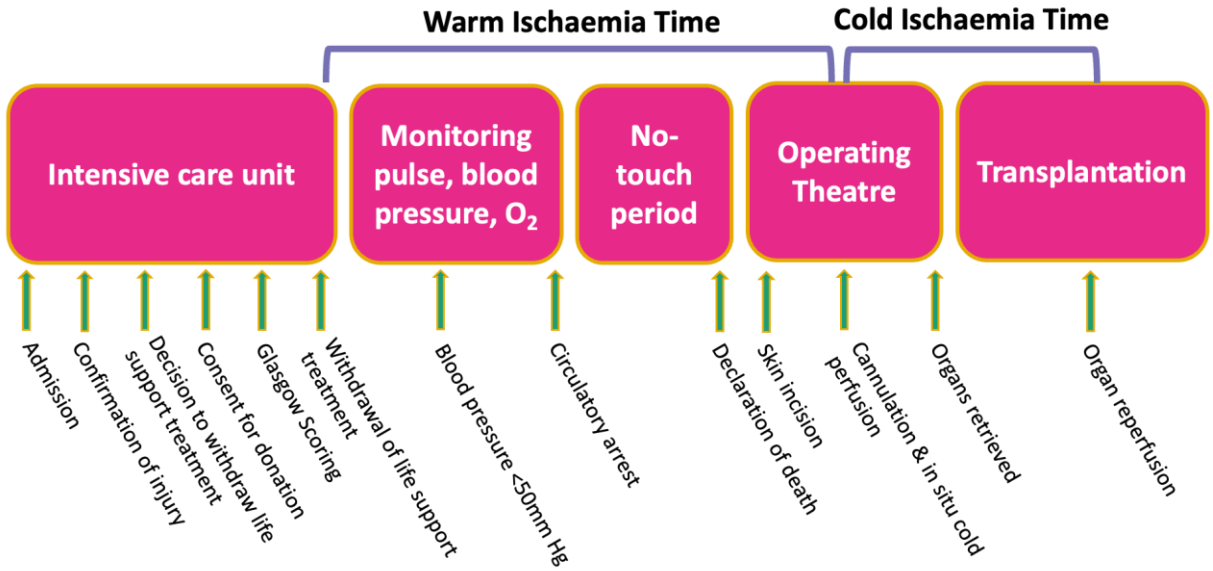



**Figure 1-L: DCD donor care pathway**

This schematic describes the typical donation pathway for a controlled DCD where the medical decision has been made to withdrawal life support. DCD donors can only be declared dead following cardiopulmonary criteria.

### 1.6.4 Recipients of DCD kidneys have increased incidences of delayed graft function (DGF) and primary non-function (PNF)

Kidneys from DCDs are twice as likely to develop DGF compared to DBD, and result in more incidences of PNF. Approximately 40% of DCD kidneys will have DGF posttransplant, and a 40% increased chance of graft loss compared to DBDs[83]. DCD kidneys also have more acute rejection episodes and inferior long-term posttransplant outcomes[84]. DGF is typically defined as a manifestation of AKI in the transplanted graft, requiring at least one dialysis treatment within the initial seven days posttransplant[24,83–85]. Organ injury that causes DGF in DBD and DCD kidneys has different clinicopathologies, demonstrating its heterogeneity between donor types[86]. DGF can only be diagnosed once other pathologies, such as hyperacute rejection, vascular and urinary tract complications, and hyperkalaemia are eliminated as the need for dialysis[84]. In some recipients DGF may result in a prolonged hospital stay for the recipient, including frequent imaging and biopsies of the transplanted kidney with an increased risk of acute graft rejection. DGF may have serious implications for the recipient's physical and mental well-being and graft survival[1,87,88]. Early graft dysfunction also increases the financial burden of care[24], meaning that the likelihood of DGF remains a relative contraindication for many clinicians to utilise DCD organs[89].

#### 1.6.4.1 Consequence of DGF posttransplant

Warm ischaemia characteristic of DCD donation is commonly associated with increased incidences of DGF in DCD recipients[90,91], yet the underlying biological cause and effect of DGF remains under investigated. In 2021, Phillips *et al* reported that DGF alone was not indicative of a suboptimal posttransplant outcome, but rather an extended DGF

duration[83]. Focused on a DCD cohort, Phillips *et al*, reported that DGF incidence correlates with increased donor age, BMI, donor male sex and higher terminal creatinine, resulting in a lower median eGFR at 1-, 3- and 5-years posttransplant compared to grafts with immediate function (IF). Furthermore, recipients who experience DGF for >14-days have a poorer prognosis: limited graft and patient survival[83]. These results indicate that prolonged DGF associates with the severity of ischaemic injury and the potential resilience of the kidney to recover. The findings were later supported by a sophisticated metadata analysis reported by Dumbill *et al* in 2022[86]. In this report, the authors evaluated the UK transplant registry, comparing donors where both donated kidneys had discordant outcomes. The authors reported that HLA matching was predictive of DGF duration, supporting previous findings that innate inflammation and complement activation contributes to the development of DGF[86,92].

Although more susceptible to DGF, DCD recipients tend to recover from the causal AKI and have comparable 1-year functional outcomes to kidneys from DBDs[46,83,93,94]. DBDs with DGF tend to have poor recovery and graft function. It is hypothesised that DCD kidneys have improved tolerance to ischaemic injury[83]; suggesting that WI pre-conditions the kidney, promoting better DGF recovery when supported by dialysis. However, the clinicopathology of DGF in DBDs and DCDs remains elusive.

In a recent gene analysis study of 271 post-retrieval DCD kidney biopsies, upregulation of fibrosis and mitotic spindle associated genes were described in kidneys with DGF. The study also considered donor age but found no overlap between gene modules associated with age and those associated with DGF. Gene changes associated with age,

however, did associate with suboptimal 12-month outcomes. Genes upregulated in kidneys with IF associate with oxidative phosphorylation and immune pathways[95]. Proteomic analysis of DCD kidneys with either short (<7days) or long (14-22 days) DGF posttransplant demonstrated that short DGF associates with dysregulation in protein ubiquitination, autophagy and phagosome maturation, and the upregulation of – eIF2, mTOR and NGAL – proteins associated with kidney injury. In contrast long DGF associated with decreased eIF2 signalling, acute phase response and Nrf2-mediated oxidative stress response[96]. Metabolic dysregulation was also associated with prolonged DGF, including dysregulation of glycolysis, the citric acid cycle (CAC) cycle, and increased catabolism[96]. Kidneys with short DGF had decreased markers of aerobic metabolism and mitochondrial ATP synthase[96].

## 1.7 Warm ischaemia and associated kidney injury

Warm ischaemia is inherent to the DCD donation pathway and is often prolonged (Figure 1-M). Initiated by WLST, WI continues until the organ is cold perfused *in situ* (total warm ischaemia time (WIT) – tWIT). Organ cold perfusion initiates cold ischaemia time (CIT), which is common to both DBD and DCDs. WI confounds CIT-associated injury, worsening IRI, and associates with early graft dysfunction[4,83,87] and increased acute rejection episodes[97]. tWIT is subcategorised into shorter time periods defined by clinical progression of the donor towards death. Agonal WIT refers to the time between WLST until circulatory arrest and is proceeded by standard WIT (sWIT), the time after circulatory arrest until the organ is cold perfused. Functional WIT (fWIT) falls in the middle of agonal WIT and sWIT and marks the time that the donor's blood pressure drops below 50mmHg until the organs are cold perfused *in situ*[3] (Figure 1-M). According

to the British Transplantation Society, fWIT is the most critical period of organ injury during tWIT, as the donor is haemodynamically unstable, blood flow reduces until cessation, and the organs become ischaemic[98,99]. To date most research into WI is from the perspective of IRI, typically using animal models or based on transplant registry metadata analysis, trying to quantify when WIT becomes irreversibly injurious to the kidney.

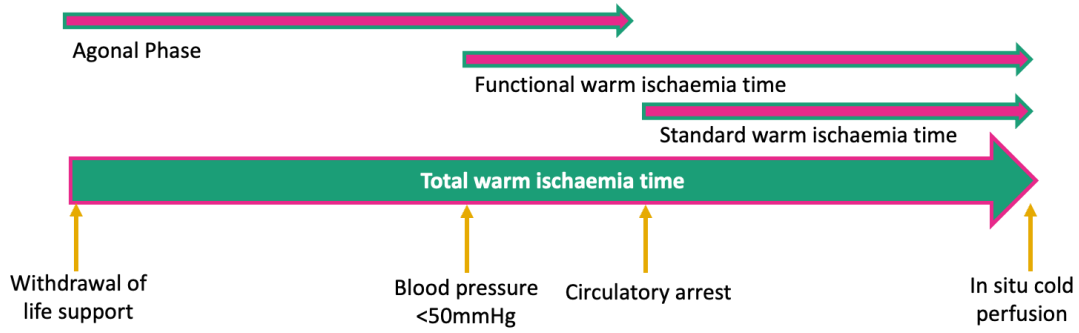



**Figure 1-M: Schematic differentiating warm ischaemia times**

Warm ischaemia refers to the time between withdrawal of life support treatment in the DCD donor until the organ is cold perfused *in situ*.

### 1.7.1 Studies addressing the length of warm ischaemia

The consensus from the transplant community is that prolonged WI drives ischaemic and subsequent reperfusion injury, limiting immediate and long-term graft function posttransplant[87,100–103]. Transplant registry data is commonly used to draw parallels between the length of WI and transplant outcomes, often to describe a 'safe' period of WI in DCDs. Previous studies describing the effects of WI in the kidney do not typically refer to the same WI period and use varying measures of outcomes, making it difficult to implement clinical changes. Analysis of the Eurotransplant registry in 2017, for example, recommended that sWIT should be kept to <17 minutes to preserve kidney

function and ensure comparability to DBDs[91]. In comparison the British Transplantation Society recommend that kidneys with a sWIT >30 minutes can be utilised if organ reconditioning options are available. They also suggest that tWIT is capped at three hours[104]. Coffey *et al* reported subpar outcomes in liver transplant recipients with longer fWIT. In this study, Coffey concluded that fWIT alone did not cause poorer outcomes, but donor factors including age and CIT amplify organ injury[105], highlighting that organ injury in DD is multifactorial.

### 1.7.2 Studies describing pathophysiological implications of warm ischaemia

Studies to investigate the effects of WI on kidney function are limited. Recently, liver cold flush solution was analysed for WI injury markers. In this study lactate dehydrogenase, alanine transaminase and alkaline phosphatase concentrations were all elevated with prolonged WI, but did not correlate to the length of CIT[106]. In the kidney, serum creatinine (SCr) is measured as an indicator of injury, with reduced creatinine clearance commonly associated with ischaemia and the onset of oliguria (reduced urine output)[103]. However, when studying real-time kidney injury associated with WI or cold ischaemia, creatinine is not a reliable marker, as changes in clearance are not immediately measurable[107]. Tubular injury, evidenced by disruption of the brush border, luminal debris and epithelial are also commonly described in animal IRI models[103]. In a recent study, an IRI-mouse model was used to describe changes in kidney injury with progressive WI, between 16 and 30 minutes with samples collected every two minutes. The animals were sacrificed 24 hours later. Post-reperfusion SCr was increased after 24 hours in kidneys with 28- and 30-minutes WI. Histological changes including signs of necrosis, tubular blockage and inflammatory cell infiltration increased in mice with >18

minutes WI. Gene analysis highlighted perturbation in metabolic and immune pathways in these mice as injury progressed from mild to severe after 26 minutes WI[108]. A pilot study by van Leeuwen profiled protein degradation in post-retrieval DCD kidney biopsies with sWIT of <10 minutes, 11-20 minutes and >30 minutes. In this study, kidneys with a longer sWIT had increased degradation in metabolic and cytoskeletal proteins[109].

During fWIT, the donor's blood pressure drops, the organs become hypoperfused, hypoxic and nutrient-starved, invoking a switch from aerobic to anaerobic metabolism[98,99]. The switch to anaerobic glycolysis to generate ATP can moderate ATP levels for a brief period before the cells fall into an energy collapse[98], inducing significant cell death and subsequent decline in renal function[110]. The kidney is highly sensitive to metabolic dysregulation, as energy metabolism is cell and region-specific. Different cells within the nephron preferentially utilise metabolic pathways that are tailored to support their unique functions, allowing for the efficient regulation of kidney function[110]. Anaerobic glycolysis also causes lactate accumulation, cellular acidosis, dysregulating $Na^+/K^+$ ATPase pump and ion exchangers, increasing intracellular sodium, calcium and hydrogen ions concentrations causing cellular oedema and disruption to the cell membrane and organelles[99,111]. The glycolysis pathway soon becomes exhausted, as glycogen and ATP stores are depleted, preventing the ongoing phosphorylation of fructose-6-phosphate[112]. Metabolic dysregulation causes accumulation of toxic metabolites including, protons, creatinine, lactate, nicotinamide adenine dinucleotide (NAD) + hydrogen (NADH), glycolysis products and inorganic phosphate, contributing to cell death[112]. The accumulation of intracellular calcium activates enzymes and proteases such as calpains, which dysregulate proteostasis and induces damage to cellular

compartments including the cytoskeleton, endoplasmic reticulum and mitochondrial proteins, accelerating cell death[112]. Calcium also activates the transition of mitochondrial permeability facilitating the passage of larger molecules though the membrane. Mitochondrial permeability is inhibited as cellular pH decreases but is reactivated upon reperfusion. Ultimately, the mitochondria are progressively compromised as fWIT is prolonged, associating with the malfunction of the CAC and the electron transport chain (ETC). This further depletes redox-active enzymes and electron carrier pools, inducing the arrest of adenine diphosphate phosphorylation to ATP and the accumulation of NADH, flavin mononucleotide, ubiquinol and succinate[99,112]. Electron leak from the ETC promotes reactive oxygen species (ROS) generation, cardiolipin peroxidation, and the loss of cytochrome-C[111], priming the kidney for ROS-driven reperfusion injury (Figure 1-N). The immune response associated with ischaemia is marked by complement activation and neutrophil infilitration[112]. Ischaemia also causes cell swelling, degradation of cytoskeletal proteins, ATP depletion and the subsequent disorder of ATP dependent processes, metabolic dysregulation, fibrosis and cell death[111].

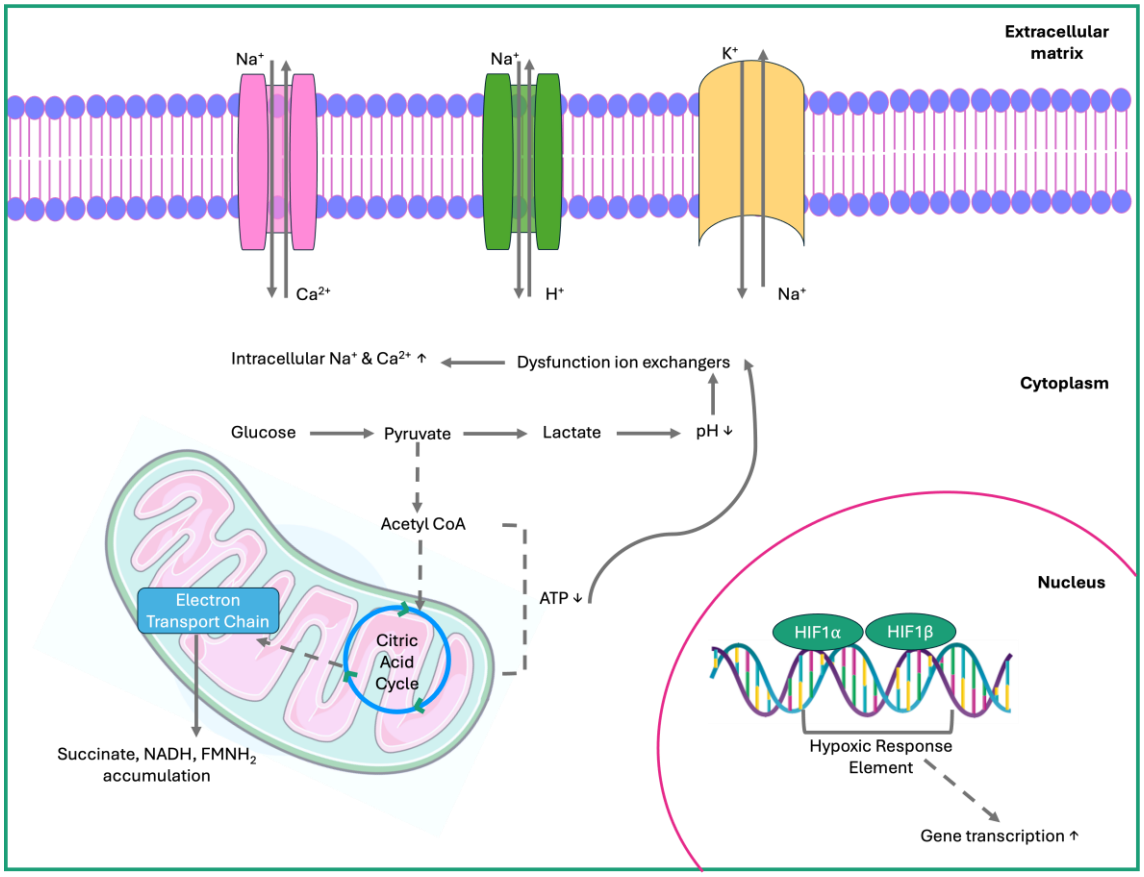



**Figure 1-N: Simplified schematic of cellular changes associated with ischaemia**

Ischaemia in the cell associates with the onset of hypoxia, ion transport dysregulation, mitochondrial dysfunction and the accumulation of toxic metabolic products driving cell injury and death.

### 1.7.3 Cellular hypoxic response to warm ischaemia

Hypoxia associated with WI stabilises hypoxia-inducible factor (HIF) transcription factors[113,114] mediating metabolic adaptations, angiogenesis, cell growth, cell survival, immune adaptation and apoptosis as a protective response to reduced oxygen concentrations[115]. HIF is regarded as the master regulator of the cellular response to hypoxia, with the ability to regulate the expression of hundreds of genes[113,116]. Under normoxic conditions hypoxia-inducible factor 1-alpha (HIF1α) protein is undetectable

due to a very short half-life and hydroxylation leading to degradation *via* the proteasome[117–119]. Hypoxia results in the stabilisation of the HIF1α subunit by inhibiting hydroxylation, with protein abundance increasing to detectable levels; as a result detectable HIF1α abundance is only linked to mRNA expression under hypoxic conditions[120]. As hypoxia persists, HIF1α RNA expression decreases[121], leading to a gradual reduction in the abundance and activity of the HIF1α subunit. This instability in HIF1α mRNA levels, mediates the shift from the HIF1α-dependent cellular response to a more adaptive HIF2α-driven response, typically within a few hours[122]. In addition, HIFs contribute to fibrosis through the differentiation of endothelial cells into myofibroblasts and the promotion of endothelial-mesenchymal transition (EMT). This process increases ECM generation and activates the receptor for advanced glycation end products and triggers mitogen-activated protein kinases and nuclear factor kappa B (NFκB) signalling which accelerates injury[123]. Additionally, HIF activation mediates innate immunity provoking the release of cytokines including interleukins and tumour necrosis factor-alpha (TNFα)[124].

### 1.7.4 Molecular limitation associated with WI and DCD KTx

Ongoing concern regarding the impact of WI remains a major contraindication to the full uptake of DCD organs and requires further research, specifically investigating molecular triggers associated with kidney tolerance and injury associated with WI. Understanding molecular changes that occur with ischaemia would provide novel insight into biological pathways associated with resilience, cellular protection under ischaemic conditions and progressive injurious changes, to describe targets for intervention. Additionally, an understanding of progressive changes in the kidney as WI is prolonged would provide

insight into tolerable ischaemia length, helping define clinical limitations for DCD donation.

## 1.8 Proteostasis and degradation in the kidney

Under physiological conditions proteostasis is maintained by precise regulation of protein synthesis and degradation. Regulated proteolysis maintains the podocyte cytoskeleton and the GFB[125], whilst the tubules actively absorb and degrade proteins including albumin and low molecular weight proteins preventing albuminuria, proteinuria and amyloidosis[126]. Proteolysis is an irreversible posttranslational modification altering protein abundance, and regulating several biological processes including DNA replication, protein turnover, cell cycle progression, cell proliferation, immune responses, inflammation, tissue remodelling, senescence and cell death[127–129]. Protein degradation is essential for protein turnover and to avoid accumulation of misfolded and faulty protein species[130] and is regulated by cell and tissue specific pathological processes[131]. Proteolysis also generates peptides vital to physiological processes including cell growth, cell stress response and immune signalling, or peptides that have a biological function. For example, neuropeptides act as neurotransmitters or neuromodulators, and the peptide hormone insulin is proteolytically cleaved from proinsulin to control blood sugar[132]. Endostatin is another example of an endogenous peptide that, independent to its 'parent' protein collagen XVIII, has essential functions including inhibition of angiogenesis and TNF$\alpha$[133,134].

Ageing can disrupt proteostasis, accelerating organ injury and the progression of age-related diseases[130] including Alzheimer's disease, cardiovascular disease and CKD[128,129].

The kidney is susceptible to metabolic, mechanistic and immune changes[15] that dysregulates proteostasis and induce pathologies. Kidney fibrosis is associated with the excessive accumulation of ECM proteins, reduced proteolysis and dysregulation of matrix metalloproteinases[135], whilst enlargement of the kidney in diabetic kidney disease, although multifactorial, can be caused by reduced proteolysis[136].

### 1.8.1 The role of proteases in proteostasis

Proteolysis is driven by proteases, enzymes that cleave peptide bonds breaking proteins into smaller polypeptides[128]. Proteases are released in an inactive form[128] and become active though autocatalytic activity, post translational modification or by another protease, for example cathepsin D (CATD) activates cathepsin B (CATB)[137], CATB is subsequently inhibited by the protein cystatin-C[138]. Proteases are typically inactivated by protein/peptide interaction[128,138], which are typically specific to the protease class, for example metalloproteinases are inhibited by protein C inhibitor or TIMPs 1-4[138]. There are 6 classes of proteases, grouped according to their mechanisms of action: aspartic, metalloproteases, cysteine, serine and threonine. Glutamic proteases are the sixth class but have not been described in mammals[128]. Proteases do not target specific proteins for cleavage, instead habitually cleave proteins at sequence motif recognition sites, for example the protease trypsin (often used in proteomics) cleaves after lysine or arginine residues not followed by a proline (Figure 1-O). Proteases are currently used to treat a range of conditions including cancers such as breast cancer (ARV-471), multiple myeloma (CC-220) and pancreatic cancer (MS-6105), as well as blood clots (thrombolysis), Alzheimer's disease (QC-01-C175), HIV (Nef-PROTAC), and COVID-19 (MPD2)[139,140]. Several protease therpaies are also being tested in clinical trials for the

treatment of kidney diseases; C5 inhibitor Eculizumab is already used as a complement inhibitor in the treatment of kidney diseases[141,142]. Despite these advancements, the development of protease-based therapies is hindered by several challenges including limited tissue specificity, difficulty in controlling targeted activity, innate biological mechanisms that clear proteases and restrict their therapeutic effectiveness, and significant side effects observed following treatment[140].

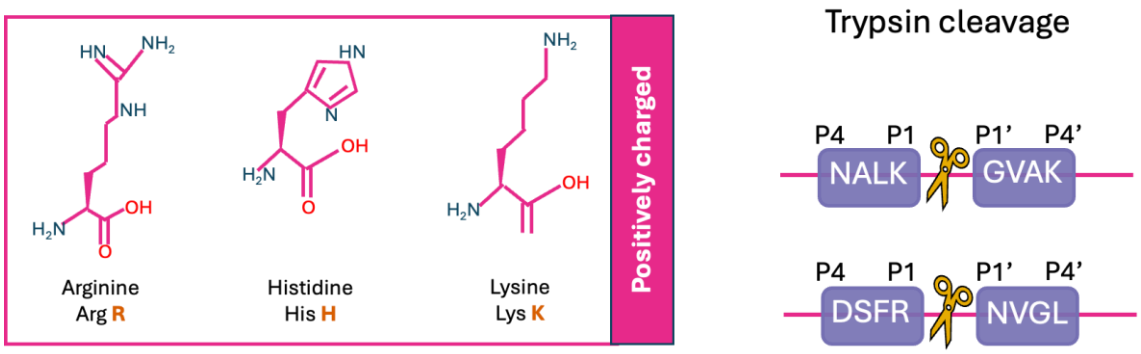



**Figure 1-O: Example of Trypsin cleavage and specificity**

Trypsin is a proteolytic enzyme that has a specificity for cleaving proteins after either a lysine (K) or arginine (R) amino acid that is not followed by proline (P) in the P1' position, resulting in a positive charge on the C-terminus.

## 1.9 Measurement of subclinical markers of kidney injury

Omics methodologies are commonly used to measure and quantify changes in the genome, transcriptome, proteome and metabolome. Utilisation of these methods has rapidly expanded in recent years and has a pertinent role in biomarker and therapeutic discoveries. Proteomics utilises mass spectrometry (MS) technology to study the protein abundance in a biological sample[143,144]. Proteomics has successfully described protein changes in disease states, for instance increased amyloid plaques in amyloidosis and changes in pyruvate kinase expression in diabetes[125]. Another example is the discovery

of a 17-protein signature of CKD[125]. Providing a wider scope than genomics and transcriptomics, proteomics can be used to measure structural and post translational changes in proteins that have a direct effect on the physiology of the tissue. However, proteostasis is a dynamic process which under disease conditions is rapidly dysregulated, altering biological pathways. Static snapshots like those captured using proteomics do not allow for accurate interpretation of changes in proteostasis.

Peptidomics is the use of MS to profile endogenous peptides[145], representative of the irreversible posttranslational modifications of the derivative protein. Degradomics takes this analysis a step further to assess changes in protease activity, providing insight into pathological changes affecting proteostasis, triggered by a catalyst[131]. Due to their functional importance, endogenous peptides are valuable clinical biomarkers whilst proteases are promising drug targets for intevention[146].

Commonly applied to bodily fluid samples such as blood and urine, peptidomics uses methods to reliably enrich for endogenous peptides. Methods to analyse tissue using peptidomics have only recently been optimised and provide novel insight into cellular proteolytic changes associated with physiological and pathophysiological conditions[147]. In the kidney, characterisation of the podocyte protease 'web' has highlighted the importance of proteases and proteolysis in maintaining podocyte function and structure and regulating glomerular physiology[15,148]. Proteolytic dysregulation is associated with development and progression of several kidney pathologies most commonly described in the podocytes, as well as pathological processes associated with the development of cancer, neurodegeneration and cardiovascular disease[127].

Peptidomics has been used to evaluate changes in DD organs. Substantial degradation of kidney cytoskeletal proteins in DBD kidneys is associated with suboptimal outcomes posttransplant, but not in DCD kidneys or LDs[16]. Peptide changes also associate with metabolic pathways in DCD kidneys with varying lengths of sWIT[109].

# Chapter 2 Thesis overview and research aims

## 2.1 Background

As outlined in Chapter 1 DCD remains an underutilised source of donor organs for transplant. In the UK, DCD utilisation has expanded over the last 20 years, and during 2023/24 DCDs contributed 49% of DD transplanted kidneys[149]. Ongoing concern regarding kidney function in the short- and long-term continues to hinder the widespread use of DCDs; DCD kidneys are discarded at a rate ~three times greater than DBD kidneys (~17% vs 6%, respectively)[97]. DGF affects ~40% of DCD recipients and associates with WIT, early graft loss and narrowed kidney function[83]. The long-term implications of DGF following DCD KTx are variable, although according to the UK Renal Report, DBD and DCD function at 1-year posttransplant are comparable (eGFR 51.5ml/min/1.73mm$^2$ and 47.1 ml/min/1.73mm$^2$, respectively)[27]. These figures however do not capture graft losses before one year and therefore do not fully demonstrate the influence WI has on the development of DGF and AKI. A molecular and biological understanding of the implications of WI on the kidney is essential to improving transplant outcomes and minimise organ discard.

## 2.2 Hypothesis and aims

Warm ischaemia remains a primary limitation to the utilisation of DCD kidneys in transplantation. Research to describe the injury associated with WI in relation to transplantation has previously been reported in the context of metadata analysis or IRI, typically in animal models. The mechanisms of kidney-associated injury induced by WI are largely unexplored and would benefit from a granular and mechanistic-focused study approach.

In this thesis I aim to investigate the impact of prolonged fWIT on the kidney peptidome, identifying relevant dysregulated biological mechanisms and delineating some of the key pathways that may be implicated in enhancing proteolytic activity in DCD kidneys. The subsequent study will specifically:

1. Investigate the effects of fWIT on the DCD kidney degradome, by profiling endogenous peptides, proteases and biological pathways.
2. Develop a hypoxic *in vitro* model of immortalised human podocyte and proximal tubule epithelial cells (PTEC) that allows a comparison of the effect of normoxic and hypoxic conditions over time.
3. Validate peptide profiles and proteases using complementary molecular techniques and *in vitro* models.

A research overview is presented in Figure 2-A.

## 2.3 Overview of experimental work presented in this thesis

In Chapter 4 the peptidomic analysis of DCD kidney biopsies across the clinical range of fWIT is described. Kidney biopsies collected immediately post-organ retrieval, i.e. unaffected by CIT and/or recipient influences, reflecting kidney condition immediately post-WI, were obtained from the Quality in Organ Donation (QUOD) biobank. The biopsies were homogenised and prepared for MS analysis according to the High-efficiency Undecanal N-Termini EnRichment (HUNTER) method, enriching for endogenous peptides. Output data was analysed to describe peptide, pathway and protease level changes in the kidney associated with prolonged fWIT. Data was also

analysed to describe degradomic changes associated with DGF, revealing distinct changes in protease activity. Analysis of post-retrieval DCD kidneys indicated the potential implications of hypoxia in the kidney. The impact of ischaemia and more specifically hypoxia on different kidney cell types was then investigated. In Chapter 5 the optimisation of a hypoxic cell model using human immortalised podocytes and PTECs is described. Three methods to induce hypoxia were tested, with the GasPak-pouch system determined to be the best method to simulate hypoxia. Podocytes and PTECs were cultured in media with or without (+/-) glucose under normoxic and hypoxic conditions for up to 24 hours.

Cell hypoxia was confirmed using quantitative polymerase chain reaction (qPCR) to measure expression of known hypoxic markers. This optimised model and kidney homogenates were then used to validate key findings in the peptidomic analysis as outlined in Chapter 6. Three proteins which were found to be degraded with a prolonged fWIT were measured in kidney biopsy samples using Western blotting. The abundance of two proteases were quantified in kidney tissue and hypoxic cells cultured +/- glucose. Significant changes in protease activity were also profiled in relation to peptide cleavages.

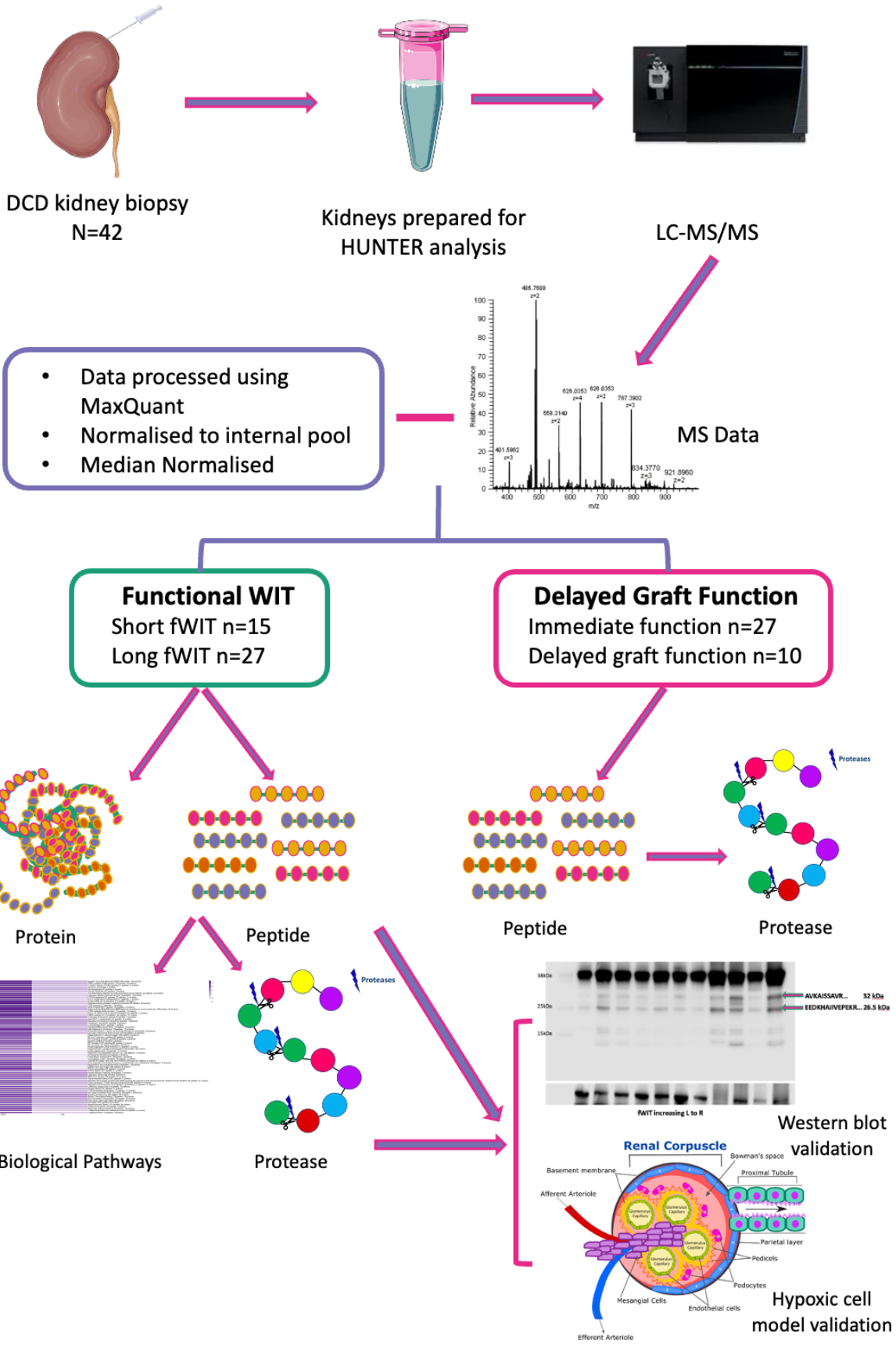

DCD kidney biopsy
N=42
Kidneys prepared for HUNTER analysis
LC-MS/MS
MS Data
Data processed using MaxQuant
Normalised to internal pool
Median Normalised
Functional WIT
Short fWIT n=15
Long fWIT n=27
Delayed Graft Function
Immediate function n=27
Delayed graft function n=10
Protein
Peptide
Peptide
Protease
Proteases
Biological Pathways
Protease
Proteases
AVKAISSAVR... 32 kDa
EEDKHAIIVEPEKR... 26.5 kDa
fWIT increasing L to R
Western blot validation
Renal Corpuscle
Bowman's space
Basement membrane
Proximal Tubule
Afferent Arteriole
Parietal layer
Pedicels
Podocytes
Mesangial Cells
Endothelial cells
Efferent Arteriole
Hypoxic cell model validation

**Figure 2-A: Experimental overview**

Kidney biopsies from DCDs will be analysed by mass spectrometry according to the predefined protocol for High-efficiency Undecanal N-Termini EnRichment peptidomics. Bioinformatics including online tools will be employed to identify peptide and protein changes as well as changes in biological pathways and protease activity associated with increasing fWIT. Data is also to be analysed comparing between kidneys that had an immediate or delayed graft function posttransplant (posttransplant outcomes analysed for the profiled kidney only, when variable reported) top describe degradomic changes.. Changes in peptide and protease abundance measured using Western blotting will be quantified in kidney and a hypoxic cell model, optimised in Chapter 5.

In Chapter 7, the main findings of the work presented in this thesis are summarised. Analysis of the DCD kidney degradome has provided novel insights into potential mechanisms of injury that may associate with prominent clinical outcomes including DGF. Changes in protease activity associated with fWIT and DGF requires additional research to understand the depth of biological implications. Suggestions for future research have been discussed in each chapter and are detailed in Chapter 7**.** Research outcomes from this study have described potential injurious implications of fWIT in DCD kidneys and with further investigations could contribute to the development of future therapeutic interventions.

# Chapter 3 Materials and methods

## 3.1 Introduction

This chapter outlines materials and methods used to undertake the experimental work presented in this thesis. Chapter-specific methods are outlined and cross referenced accordingly. All solutions used in the materials and methods are also cross referenced to Chapter 8.

## 3.2 Ethical approval for research work

Tissue samples used in this research were selected from the QUOD biobank, which retrieves research samples from DD after obtaining written research consent from donor families. All kidney biopsies used in this research were procured from DCDs and obtained from the QUOD biobank, under the ethical approval of the QUOD project 23/NW/0097.

## 3.3 Clinical samples

### 3.3.1 QUality in Organ Donation (QUOD) biobank samples

QUOD is a national bioresource hosted by the University of Oxford, UK, that collects tissue, blood, and urine samples from consented DD. All samples are matched to donor and recipient metadata collected by NHS Blood and Transplant (NHSBT), with donor and recipient data anonymised and linked to samples by a unique identifying number. Metadata specific to samples utilised in each part of this thesis including kidney graft outcomes posttransplant are detailed in the appropriate chapters.

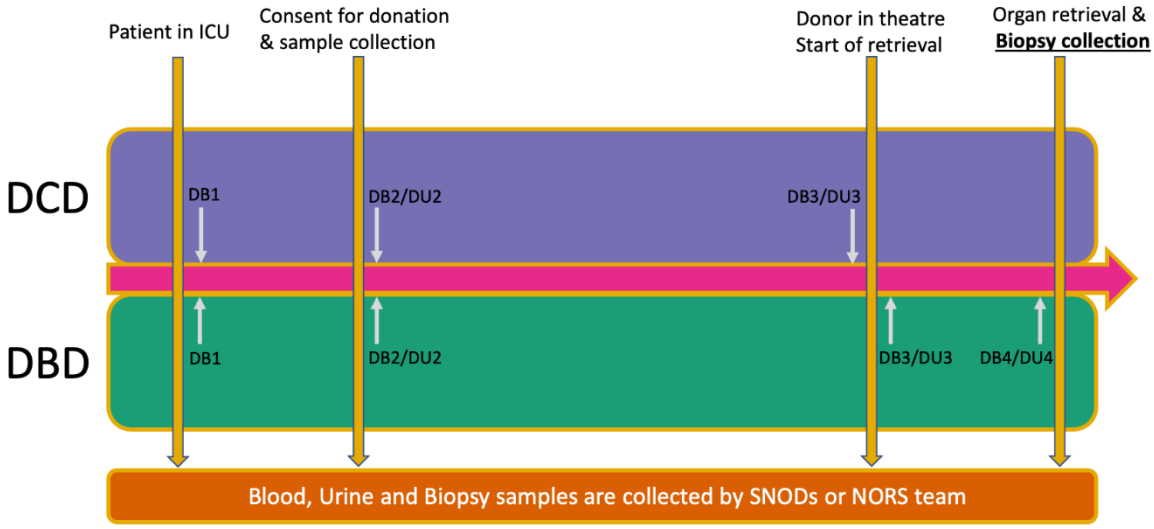



**Figure 3-A: QUality in Organ Donation (QUOD) sample collection**

Longitudinal blood and urine samples are collected from consented deceased donors throughout the donor management process by the SNODs. Organ biopsies are collected by the NORS team during back table preparation of the organs for transport. In this study, kidney biopsies have been utilised.

*DB – Donor Blood, DBD – Donation after Brain Death, DCD – Donation after Circulatory Death, DU- Donor Urine, ICU – Intensive Care Unit, NORS – National Organ Retrieval Service, SNODs – Specialist Nurses in Organ Donation*

Samples collected by QUOD during DD management are outlined in

Figure 3-A. Blood and urine samples are collected from DD at key points during the donation pathway; four longitudinal samples are collected from DBD donors DB/DU1-DB/DU4 and three from DCDs DB/DU1-DB/DU3. Blood and urine samples will not be referred to in this thesis, however it is useful to understand the samples available when considering follow up work. Organ biopsies are collected during back table preparation following retrieval.

#### 3.3.1.1 Deceased donor kidney biopsy collection protocol by QUOD

Kidney biopsies used in this study were collected between 2015 and 2023, *ex situ* from the upper pole of the kidney cortex. Samples were collected using two methods. Up to 2018, biopsies were taken from each donor kidney using a needle biopsy gun (core, 33mm length) and divided into two halves with one half stored in RNA-later and the other fixed in formalin. From 2018, biopsies have been collected according to a revised protocol improving the continuity, quality and quantity of collected tissues. A punch biopsy gun (3mm width and 7mm length) is used to collect samples; the biopsy from the left kidney is stored in formalin and the right-side biopsy stored in RNA-later. All kidney biopsies were stored in RNA-later at -80˚C. For this study, kidney biopsies stored in RNA-later were utilised.

## 3.4 Homogenisation of kidney tissue

To determine the optimal homogenisation technique to maximise protein yield, two commercially available lysis buffers and three homogenisation protocols were compared. Optimisation of these protocols are presented in detail in Chapter 8 (8.2).

Kidney biopsies were weighed and placed in Eppendorf tubes with 100µL of ice-cold RIPA buffer (89901, Thermo Fisher) supplemented with protease inhibitor (P8340, Sigma), phosphatase inhibitor 2 (P5726, Sigma) and phosphatase inhibitor 3 (P0044, Sigma). The biopsies were then homogenised using a sonic dismembrator ultrasonic processor (sonicator) (FN-705, Fisher Scientific) connected to a generator (Fisher Scientific) using a microtip set to 50 amps for 60 seconds. To minimise heat transference,

samples were kept on wet ice during homogenising. Sample protein concentration was later measured using a BCA assay (3.6).

## 3.5 Conditionally immortalised human kidney cells

To investigate the effects of hypoxia on major kidney components, conditionally immortalised human PTEC and podocyte cells were studied. Cells were provided by the Bristol Renal Group, University of Bristol.

### 3.5.1 Conditional immortalisation of podocytes and proximal tubule epithelial cells (PTECs)

The immortalised podocyte cell line was first established and described by Saleem *et al* in 2002[150]. In brief, primary podocyte cells were isolated from a nephrectomy sample *via* a sieving protocol and transfected with a SV40 retroviral construct, immortalising the cells to continually proliferate until culture temperature was increased. Cell growth was subsequently switched off by the increase in culture temperature resulting in the rapid and irreversible loss of cell proliferation capabilities, inducing differentiation[151]. Differentiated immortalised podocytes express key markers definitive of *in vivo* podocytes including nephrin and podocin[151]. Immortalised PTECs were established in 2010 by Wilmer *et al*[152] using a similar SV40 retroviral construct, with cell proliferation arrested at 37˚C. Immortalised PTECs express aminopeptidase N and aquaporin, definitive of PTECs *in vivo*. These cells also form a tight monolayer with limited diffusion and absorption capabilities that mimics *in vivo* PTECs[152].

#### 3.5.1.1 Culturing podocytes and PTECs and cell differentiation

Podocyte and PTECs were cultured in a dedicated cell culture facility, fitted with an air-filtering system. Cell culture work was undertaken in a microflow biological safety cabinet (Holten LaminAir HB2448) under sterile conditions. Cells were cultured in Heraues HeraCell150 incubators (Thermo Scientific) set to either 33˚C or 37˚C and 5% $CO_2$. Laboratory grade ethanol was diluted in MilliQ water to 70% and used to disinfect all implements and during transfer of equipment and cell vessels into the biological safety cabinets. Virkon 2% (220400, Appleton Woods) was used to clean and destroy cellular material prior to discard.

Podocyte cells were cultured in RPMI-1640 (R8758, Sigma) supplemented with 10% foetal calf serum (FCS) (HyClone FetalClone I, GE Lifesciences). The cells were grown in T75cm$^2$ cell culture flasks with vented lids (353136, Corning) to promote cell growth and division. Cell media was replaced every 2-3 days until the cells were 70% confluent. Cells were collected using trypsin (Trypsin EDTA solution, SLCN3107, Sigma-Aldrich/Merck, Dorset, UK) for redistribution into either another flask or 6-well plates (CC7682-7506, CytoOne). Podocytes grown to confluence in 6-well plates were differentiated at 37˚C for 10 days prior to induction of experimental conditions.

Similarly, PTECs were cultured at 33˚C until 70% confluent, with media refreshed every 2-3 days. PTECs were cultured in DMEM-F-12 media (31330-038, Gibco), supplemented with 10% FCS, 36ng/mL Hydrocortisone (1mg, H1035, Sigma), 10ng/mL Epidermal growth factor (0.2mg, 9644, Sigma) and 40pg/mL Triiodo-L-thyronine (1mg, T5516,

Sigma) (details of preparation of media additives are shown in Table 3-A). PTECs were differentiated at 37˚C for 10 days prior to induction of experimental conditions.

| | **Starting concentration** | **Preparation** |
|---|---|---|
| Hydrocortisone | 1mg | Dilute in 1mL ethanol, adjust volume to 20mL with sterile water |
| Epidermal growth factor | 0.2mg | Dilute in 2mL sterile water |
| Triiodo-L-thyronine | 1mg | Dilute in 1mL NaOH, adjust volume to 50mL with sterile water |

**Table 3-A: Preparation of additives for the DMEM-12 culture media to culture PTECs**

Supplements added to DMEM-F-12 for culturing PTECs. Each supplement is purchased as a lyophilised powder and reconstituted as guided in the table.

#### 3.5.1.2 Redistribution of cells in 6-well plates for experimental use

Experiments were performed with cells grown and differentiated in 6-well plates. Cells were collected by removing the culture media and replacing it with warmed trypsin. Cells were manually dislodged from the culture flask and trypsin activity quenched with culture media, then collected and centrifuged for 3 minutes at 10,000rpm. The trypsin was removed and replaced with fresh culture media, and the cells evenly distributed into the wells of each plate. Plated cells were incubated until 70% confluent at 33˚C then moved to 37˚C to differentiate for 10 days.

#### 3.5.1.3 Collection of cells for homogenisation

Cultured and treated cells were collected by removing the culture solution and washing with phosphate-buffered saline (PBS). RIPA supplemented with phosphatase and protease inhibitors (see 3.4) was then used to collect and lyse the cells. Cells were stored at -80˚C until needed.

## 3.6 Bicinchoninic acid (BCA) assay for protein quantification

The bicinchoninic acid (BCA) assay is a colorimetric detection assay used to determine protein concentration of samples. A two-reaction assay, peptide bonds reduce $Cu^{2+}$ ions to $Cu^{1+}$ in proportion to the amount of protein in the solution. Bicinchoninic acid then chelates each $Cu^{1+}$, inducing a colour change (green to purple) that absorbs light at wavelength 562nm and can be measured. The Pierce BCA assay (23225, Thermo Scientific) was used to measure the concentration of protein in the homogenised kidney samples and cells collected in RIPA buffer (89901, Thermo Fisher). BCAs were performed according to the microplate procedure described in the manufacturer's protocol, diluting samples according to sample type. An albumin standard curve was prepared by serially diluting albumin in a dilution buffer, typically matched to the sample buffer. The plate was loaded with samples and reaction buffer and incubated at 37˚C for 30 minutes. BCA plates were read using a BMG LabTech SPECTROstar Nano instrument connected to a PC running SPECTROstar Nano software (version 5.7). BCA data was analysed in MARS software (version 3.42 R6) mapping the standard curve and quantifying the protein concentration of each sample, expressed as µg/mL.

## 3.7 Gel electrophoresis, protein staining and Western immunoblotting

Gel electrophoresis is a method to separate proteins according to size and charge. After electrophoresis, gels can be subsequently stained to investigate the protein profile of the samples or blotted onto a permeable membrane for Western blotting, to visualise and quantitate target proteins.

### 3.7.1 Preparing samples into Laemmli buffer

Following BCA determination of protein concentration, kidney biopsies and cells were prepared into Laemmli buffer (8.1.1) for Western blotting. Based on the sample concentration, samples were prepared to a predetermined concentration (0.5µg/µL or 1µg/µL) and denatured to reduce the intra- and inter-molecular disulphide bonds at 90˚C for 10 minutes using an Eppendorf ThermoMixer (Eppendorf).

### 3.7.2 Gel electrophoresis 4-12% Bis-Tris gels

Pre-cast 4-12% Bis-Tris gels (12 or 15 wells) (NP0322BOX or NP0323BOX, Invitrogen) were prepared by removing the packaging and comb and washing the wells with distilled water and 1x MOPS buffer. The gels were locked into the electrophoresis caddy and the chambers filled with 1x MOPS buffer. Samples were loaded to the maximum volume of 20µL. WesternSure pre-stained chemiluminescent protein ladder (4µL) (926-98000, Li-cor) was loaded into the first well of each gel and additional wells as required. Gels were ran using an Invitrogen PowerEase500 powerpack, set to 200 volts until the running dye reached the gel base.

### 3.7.3 Gel transfer for Western immunoblotting.

Following gel electrophoresis separated proteins were transferred out of the gel to the surface of a permeable membrane using electrophoresis. Prior to transfer, PVDF membranes (LC2005, Invitrogen) were soaked in methanol for 5-10 minutes activating the membrane's positive electron charge. Sponges, filter paper and soaked PVDF membranes were pre-soaked in Transfer buffer. Using a palette knife, the gel cassettes were snapped open, and the gels tidied by removing the well guides and dye front at the base. The transfer sandwich was then assembled. Proteins were transferred at 20 volts for 60 minutes using the Invitrogen PowerEase500 powerpack.

### 3.7.4 Western blotting – protein of interest

Following transfer, membranes were washed in Tris-buffered saline with tween (TBST) solution for five minutes on a gyro-rocker at room temperature. Membranes were blocked in 5% Milk blocking buffer/Antibody diluent for one hour at room temperature. The membranes were washed for five minutes in TBST and incubated overnight at 4˚C in the primary antibody of interest (Table 3-B). Membranes were washed three times in TBST for five minutes per wash and incubated in a target host specific secondary antibody diluted in 5% milk TBST for one hour at room temperature. The secondary antibodies were conjugated to horseradish peroxidase (HRP) for chemiluminescence detection. Finally, membranes were washed another three times for five minutes per wash before imaging.

| Antibody | Host Species | Antibody Type (polycloncal/ monoclonal) | Molecular Weight (kDa) | Epitope | Supplier | Product code |
|---|---|---|---|---|---|---|
| Beta actin | Mouse | Monoclonal | 42 kDa | - | Sigma | A5441 |
| BHMT | Rabbit | Polyclonal | 45 kDa | 1-406 aa | Proteintech | 15965-1-AP |
| Cathepsin B | Goat | Polyclonal | 25-30 kDa | 18-339 aa | R&D Systems | AF953 |
| FBP-1 | Rabbit | Polyclonal | 37 kDa | 1-338 aa | Proteintech | 12842-1-AP |
| Legumain | Goat | Polyclonal | 56 & 37 kDa | 18-433 aa | R&D Systems | AF2199 |
| Anti-mouse IgG HRP conjugated | Horse | Secondary | - | - | Cell Signalling | 7076S |
| Anti-rabbit IgG HRP conjugated | Goat | Secondary | - | - | Cell Signalling | 7074S |
| Anti-Goat IgG HRP conjugated | Rabbit | Secondary | - | - | R&D Systems | HAF017 |

**Table 3-B – Antibodies use for Western blotting**

List of primary and secondary antibodies used for Western blotting. Primary antibodies were selected based on proteins of interest identified as part of the peptidomic analysis for validation in kidney tissue and cultured podocytes and PTECs.

### 3.7.5 Chemiluminescent imaging of Western blot membranes

Western blot membranes were imaged using chemiluminescence, an indirect detection method. In this reaction the secondary-conjugated HRP binds to the substrate catalysing a reaction which generates light.

Western blot membranes were imaged following the application of Super Signal West Dura Extended Duration substrate (34076, Thermo Scientific) for four minutes at room temperature. The membranes were covered with enough substrate (1-2mL) to prevent the membrane drying out during imaging. Membranes were imaged for 10 minutes

using a Li-cor Odyssey FC instrument, connected to a computer running Li-cor Image Studio Software (version 5.2.5).

### 3.7.6 β-actin probing – housekeeping gene for normalisation

Housekeeping genes are used as loading control for Western blotting as they have a fixed stability with minimal changes observed with physiological disturbances. Membranes were probed for β-actin, by washing the membranes in TBST after imaging and re-blocking the membrane in 5% milk TBST for 30-60 minutes at room temperature. The β-actin (Table 3-B) antibody was applied for either one hour at room temperature or overnight at 4˚C, followed by anti-mouse secondary antibody diluted in 5% milk TBST incubated for 60 minutes at room temperature. Membranes were imaged as described in 3.7.5.

### 3.7.7 Analysis of Western blots

Western blots were analysed using Li-cor Empiria studio software (V3.0.0.173), an analysis programme paired with the Li-cor Odyssey FC imaging instrument and software. Membrane images of the protein of interest and the ß-actin loading control were paired. β-actin bands were quantified by measuring the signal of each band; the background signal was automatically subtracted generating a 'normalised signal'.

Quantification of full length and protein fragment bands were done separately so that the ratio of protein fragments to full length protein could be calculated. All bands were normalised to the β-actin loading control by calculating the lane normalisation factor (dividing the β-actin signal by the signal of the lane with the highest β-actin signal). The

target proteins and fragments signal were normalised by dividing their signal by the lane normalisation factor, and these values were compared between samples.

## 3.8 Quantitative Polymerase Chain Reaction (qPCR)

Quantitative polymerase chain reaction (qPCR) is a molecular biology technique using fluorescent reporter dye to measure gene expression in real time. As polymerase chain reaction (PCR) products accumulate there is a proportional increase in fluorescence, used to calculate relative gene expression within a sample. Gene expression measured using qPCR quantified changes in hypoxia related genes in cells cultured under normoxic and hypoxic conditions. β-actin was measured as a loading control for normalisation.

### 3.8.1 RNA purification from cultured cells

RNA was purified from cells, using a Qiagen RNeasy Mini Kit (74104, Qiagen) according to the manufacturer's protocol. In brief, culture media was discarded, and cells washed in fresh PBS and lysed in the provided lysis buffer. Lysed cells were bound to the provided spin column using ethanol, and contaminants washed away using several wash steps and centrifugation. Remaining RNA was eluted in RNase free water and stored at -80˚C until required.

### 3.8.2 Conversion of extracted RNA into cDNA

Cell RNA concentration was quantified using a nanodrop (deNovix DS-11+ spectrophotometer). RNA was converted into complementary DNA (cDNA) using a high-capacity RNA-to-cDNA kit from Applied Biosystems (4387406, Thermo Fisher Scientific), and a PCR thermocycler (Eppendorf). Typically, 1µg of RNA was converted into cDNA,

however when the quantity of collected RNA was low, less RNA was converted, and this was adjusted for when the samples were diluted for qPCR.

### 3.8.3 Primer preparation and melt curve tests

The working concentration of each primer was 10µM. Sample dilution best suited to each primer was determined by comparing the melt curves of serially diluted samples (1:10, 1:100, 1:1,000. 1:10,000). A melting temperature of ~60˚C is indicative of a quality and specific primer and indicates the ideal temperature for hybridisation of primers to the target. For each primer the ideal sample dilution was 1:100 of cDNA. Melt curve analysis confirmed the specificity of each PCR-product. Specifically, the melt curve was reviewed to ensure that the fluorescent detection came from a single amplification product.

### 3.8.4 Quantitative polymerase chain reaction (qPCR) method

A primer master mix was prepared for each primer pair using fast SYBR green master mix (4385612, Applied Biosystems, Thermo Fisher Scientific), RNA free water and the primer pair (forward and reverse primers) (primer list Table 3-C). The reactions were loaded onto a 96 well MicroAmp clear reaction plate (4483354, Life technologies), with samples analysed in triplicate, using an Applied Biosystem QuantStudio 3 instrument (Thermo Fisher Scientific). Plate layouts, PCR run specifics and results were analysed using QuantStudio Design and Analysis software (Version 1.5.1, Thermo Fisher Scientific).

| Protein | | Primer Sequence 5'-3' |
|---|---|---|
| Beta Actin | **F** | ATGTGGCCGAGGACTTTGATT |
| | **R** | AGTGGGGTGGCTTTTAGGATG |
| BNIP3 | **F** | CAGGGCTCCTGG GTAGAACT |
| | **R** | CTACTCCGTCCAGACTCATGC |
| Caspase 3 | **F** | TGTTTGTGTGCTTCTGAGCC |
| | **R** | CACGCCATGTCATCATCAAC |
| Fibronectin | **F** | CAGTGGGAGACCTCGAGAAG |
| | **R** | GTCCCTCGGAACATCAGAAA |
| HIF1a | **F** | CATAAAGTCTGCAACATGGAAGGT |
| | **R** | ATTTGATGGGTGAGGAATGGGTT |
| HIF2a | **F** | GCGCTAGACTCCGAGAACAT |
| | **R** | TGGCCACTTACTACCTGACCCTT |
| Glut1 | **F** | GAACTCTTCAGCCAGGGTCC |
| | **R** | TCACACTTGGGAATCAGCCC |
| NKFB | **F** | CTGGCAGTCCTTCTCAAAGC |
| | **R** | TCCAGGTCTAGAGAGGCTCA |
| PGC1 | **F** | TGAGAGGGCCAAGCAAAG |
| | **R** | ATAAATCACACGGCGCTCTT |
| PDK1 | **F** | ACCAGGACAGCCAATACAAG |
| | **R** | CCTCGGTCACTCATCTTCAC |
| PFKFB3 | **F** | CAGTTGTGGCCTCCAATATC |
| | **R** | GCTTCATAGCAACTGATCC |
| PHD2 | **F** | CAGCATGGACGACCTGATAC |
| | **R** | TACATAACCCGTTCCATTGC |
| PHD3 | **F** | GCTTCCTCCTGTCCCTCAT |
| | **R** | AAGCCACCATTGCCTTAGAC |

**Table 3-C: List of primer sequences used to measure gene expression in normoxic and hypoxic cells**

Primers for qPCR are designed based on the nucleotide sequence of the gene of interest. The primers used in this study were identified in the literature and checked for compatibility using Primer-Blast, an online primer designing tool.

## 3.9 Analysis of qPCR data

Fluorescent data for each sample was analysed with the comparative threshold cycle (CT) method using the 2ΛΛCT (double delta CT) method. Genes of interest were normalised to β-actin. Within each experiment, gene expression was calculated relative to the value in the untreated control.

## 3.10 Statistical analysis

Data preparation and statistical analysis was performed using instrument specific software, Microsoft Excel, and R Studio (Version 2023.03.0+386). Statistical analysis of specific data sets will be described in detail in the methods section of each chapter.

# Chapter 4 Profiling the DCD kidney degradome with prolonged fWIT

## 4.1 Introduction

Globally, under-utilisation of DCD donor kidneys presents a missed opportunity to expand the DD pool to meet the ever-growing need for donor organs. The UK operates a successful DCD transplant programme, with only The Netherlands achieving similar DCD transplant rates per capita/annum[153]. Even so, an excessive number of DCD kidneys are discarded following retrieval due to uncertainty regarding inferior graft outcomes associated with WI[100,154]. DCD KTx results in significantly more incidences of DGF and PNF compared to DBD grafts. DCDs also result in higher incidences of graft loss at 1-year posttransplant[154]. However, functionally, DCD kidneys are comparable to DBDs at 1-year posttransplant[154]. The persistence of poor posttransplant outcomes highlights the importance of evaluating the effect WI has on the DCD kidney.

Warm ischaemia, along with cold ischaemia, are precursors of reperfusion injury. Following WLST, DCD organs become hypoperfused and hypoxic. This induces a switch from physiological aerobic to anaerobic metabolism, inducing cellular dysregulation[155] and a significant increase in cytosolic lactate and ROS production. Protein complexes, part of the ETC, are substantially reduced, leaving electrons to irrevocably leak into the mitochondria; this significantly reduces ATP production and cellular pH[155]. Reduced ATP production dysregulates cellular functions, including ion transport and cytoskeletal rearrangement[19,111], and upregulates cellular catabolism pathways inducing autophagy and cell death[111,155], limiting cellular function. Prolonged WIT associates with morphological changes in the kidney including loss of the brush border[156] characteristic of the apical membrane in tubular cells, tubular dilation, shrinkage of the glomerulus, histone release and cell death[157,158]. These injurious changes are further exacerbated by

lengthy periods of cold ischaemia and accelerated during reperfusion. Ischaemic injury manifests as AKI[159]; mechanisms of AKI are associated with metabolic dysregulation and ATP deprivation, causing metabolic reprogramming, and drives progression to CKD[19,110]. Additionally, ischaemia-associated hypoxia may dysregulate proteostasis; many proteases including metalloproteinases (MMP)[160] are direct targets of HIF1α[161,162]. Proteases are typically autocatalytic and can be triggered by changes in cell conditions, such as changes in pH, oxygen supply, or biological triggers. Changes in one protease's activity also has the potential to cascade and activate multiple proteases[163], compelling disruption to proteostasis.

Two peptidomic approaches have been described in the literature: PROtein Topography Migration Analysis Platform (PROTOMAP) and Terminal Amine Isotopic Labelling of Substrates (TAILS)/High-efficiency Undecanal N-Termini EnRichment (HUNTER). Previously, PROTOMAP methods were used to describe significant dysregulation of the cytoskeleton in DBD kidneys associated with increased transforming growth factor-beta (TGFβ) expression; talin-1 and alpha-actinin-4 were significantly degraded in kidneys that had a low eGFR at 1-year posttransplant[16]. The PROTOMAP method depends upon specialised bioinformatic tools to generate peptographs for each quantified protein. This method is a visualisation tool of degradation products associated with each measured protein yet cannot quantify cleavage sites or predict cleaving proteases. Significantly, this protocol can only compare between two experimental groups, limiting the power of the analysis[127].

In 2019, Weng *et al*[146] described the HUNTER technique, an alternative negative enrichment peptidomic protocol which facilitates the analysis of the degradome using online protease database tools. This technique was developed as a sensitive alternative to previously existing peptidomic methods such as TAILS. This protocol enriches for endogenous peptides by first tagging the N-termini of peptides with a chemical tag, before digesting the proteins in the biological sample with trypsin. Newly generated tryptic peptides are then labelled with an α-amine specific hydrophobic tag (undecanal) and subsequently removed, reducing the sample complexity for MS analysis[164], enabling low abundance endogenous peptides to be reliably measured. Endogenous peptides are sequenced and quantified using MS; the peptide sequence can then be used to qualitatively describe changes in protease activity and biological pathways[127,146]. Crucial to peptidomics and degradomics is quality sample preparation that allows for the enrichment of low abundance peptides and dynamic downstream analysis, maximising peptide detection[127].

Analysis of proteomic – and now peptidomic – data is supported by online resources including UniProt and MEROPS. UniProt is an all-inclusive online protein database that includes protein sequence data and functional information, linked to peer reviewed publications. MEROPS, another online database specific for protease and protease inhibitor data, catalogues hierarchical classification of identified proteases, classifying them and their inhibitors into families and clans[165]. Both databases underpin bioinformatic methodologies to analyse and portray proteomic data and are available for scientific contribution. Additional bioinformatic tools such as the TopFIND

knowledgebase for data processing and bioinformatic programming packages have been coded, drawing on these databases.

This chapter describes the degradomic analysis of DCD kidney biopsies with prolonged fWIT. In this study, the HUNTER method has been used to enrich for endogenous peptide in homogenised kidney samples, collected from DCD donors with either a short (<25 minutes) or long (30-120 minutes) fWIT.

## 4.2 Hypothesis and Aims

It has previously been shown that kidney injury is donor type specific[16]. Ischaemic injury triggered in animal models has shown that hypoxia drives morphological changes in the kidney and metabolic dysregulation, both of which are associated with protease activation including MMPs and cathepsin activity. For this study, it is hypothesised that prolonged fWIT, associated with significant organ hypoperfusion and subsequent ischaemia, may contribute to proteolytic changes in the kidney, inducing kidney injury which limits kidney function posttransplant. Using the HUNTER methodology, changes in the DCD kidney degradome associated with fWIT were profiled. Bioinformatics was used to ascribe changes in endogenous peptide abundance and protease activity as well as biological and metabolic pathways. Variance in peptide abundance and protease activity in kidneys that developed DGF were also quantified.

## 4.3 Materials and methods

### 4.3.1 Profiling fWIT from NHSBT organ registry data for DCD kidney donors between 2012-2022

To establish UK wide trends, functional and total WIT metadata from NHSBT for all DCD donors who donated a kidney for transplant between 2012-2022 was considered. The fWIT and tWIT average and median were calculated. Median fWIT was used to establish the 'divide' between the two experimental cohorts.

### 4.3.2 Kidney biopsy selection

Kidney biopsies from DCDs were selected from the QUOD biobank to establish two distinct cohorts: short fWIT of <25 minutes group (n=15) and a long fWIT group of 30-120 minutes (n=27) (range 7-103 minutes). The selected donors' fWIT represented the fWIT continuum, specific to UK clinical guidelines which cap fWIT length at 120 minutes. The two experimental cohorts were balanced with regards to donor age, sex, and cause of death, to minimise potential effect these variables, have on the kidney degradome. The biopsies used in this study were collected between 2014-2023; collection protocols are described in Chapter 3 (3.3.1.1). Donor characteristics and recipient outcome metadata were provided by NHSBT.

### 4.3.3 High-efficiency Undecanal-based N-Termini EnRichment (HUNTER) analysis of kidney biopsies

High-efficiency Undecanal N-Termini EnRichment (HUNTER) is a sample preparation method, to enrich for endogenous peptides in a biological sample for analysis by MS. The HUNTER protocol is summarised in Figure 4-A. Quantification of HUNTER MS data allows for comparison of endogenous peptide abundance between experimental

cohorts and for protease and biological pathway dysregulation to be ascertained. Here the HUNTER protocol was applied to DCD kidney biopsies; data was compared based on fWIT duration and according to immediate graft function posttransplant (comparing kidneys with immediate and delayed function).

#### 4.3.3.1 Homogenising kidney biopsies for HUNTER

Kidney biopsies selected for the HUNTER study were weighed and placed in Eppendorf tubes with 100µL of RIPA buffer supplemented with protease and phosphatase inhibitors, then homogenised using the sonicator dismembrator (3.4). A BCA (3.6) assay was used to measure the protein concentration of each sample, quantified against the standard curve (20-200µg/mL), expressed as µg/mL.

#### 4.3.3.2 Kidney biopsy preparation for TMT protocol workflow

The total starting protein concentration for each sample for the HUNTER protocol was 90µg, aliquoted into labelled tubes with a generic sample number. Three samples were prepared in duplicate as biological replicates, ran across different TMT-kits.

A sample pool was prepared by adding a volume of each sample to a final concentration of 300µg. The pool was divided into three tubes (90µg each) 1 per TMT-kit and assigned a sample number. The sample pool was prepared as an internal control (technical replicate) and for later normalisation of MS data (across the TMT-kits) to manage for batch effects.

Each sample (labelled 1-48) was topped to a final volume of 200µL with proteomic grade water and treated with 0.5µL of Benzonase (E1014-25KU, Sigma) for 20 minutes on wet ice. Benzonase is an endonuclease that degrades DNA and RNA; in this application Benzonase was used to purify the tissue homogenate by degrading nuclear tissue.

Protein samples were then precipitated using standard methanol/chloroform precipitation protocols, to buffer exchange the sample and remove ruminant detergent from the lysis buffer. In brief, ice-cold methanol (600µL) was added to each sample, followed by 150µL ice-cold chloroform. Samples were vortexed and 450µL of cold ultra-pure water added. Samples were gently mixed by inverting, then centrifuged at top speed for one minute at 4˚C. Using a Pasteur pipette, the aqueous phase was removed from each sample, being careful to maintain the precipitate interface. Ice cold methanol (450µL) was then added to each sample, which was subsequently vortexed and centrifuged at 4˚C at top speed for two minutes. The supernatant was removed, and the protein pellet left to air dry.

#### 4.3.3.3 Reduction and alkylation

Dried protein pellets were rehydrated in 30µL 6M Guanidine hydrochloride (GuHCl) with the volume topped to 80µL with nano pure water, followed by 20µL of 1M HEPES (pH 8.0). Samples were mixed and 200mM tris-2-carboxyethyl phosphine (TCEP) added to a final concentration of 10mM, pH adjusted to 8.0. Samples were incubated at 55˚C on a thermocycler set to 300rpm for 60 minutes. TCEP is a reducing agent used to break disulphide bonds within and between proteins allowing for analysis of proteins/peptides as single subunits. Finally, 100mM Iodoacetamide (IAA) was added to each sample to a

final concentration of 25mM. An alkylating agent, IAA binds covalently to the thiol group of cysteine, preventing disulphide bonds reforming. Samples were incubated at 25˚C for 30 minutes in the dark.

#### 4.3.3.4 TMT labelling

Three 16-plex TMTpro (TMT – tandem mass tag) isobaric label reagent sets (A44521, Thermo Fisher Scientific) were used for this experiment. TMTpro is a commercially available labelling kit that allows for multiplexing. TMT tags are isobaric mass tags that label the N-termini of proteins/peptides in a sample. The isobaric tag can then be used to identify each individual sample according to the unique reporter mass specific tag.

To start, TMT-kits were equilibrated to room temperature. Each TMT tag tube was centrifuged to ensure all powder was at the bottom of the tube prior to reconstitution. The TMT tags were dissolved in a volume of dimethyl sulfoxide (DMSO) equal to that of the total reaction volume, such that labelling was 50% v/v of DMSO (D2650, Sigma). The tags were dissolved in 144µL of DMSO and vortexed repeatedly over 10 minutes.

Kidney sample tubes labelled 1-48 were randomly divided between the three TMT-kits, and TMT tags were then assigned at random to each sample/kit. The paired TMT tag was then added to the assigned sample and the samples incubated at 25˚C for 1 hour in the dark, shaking at 300rpm. The tag binding reaction was stopped by the addition of 25µL of 1M Ethanolamine, followed by incubation at room temperature for 30 minutes.

The samples specific to each TMT-kit were then pooled into a single tube and cleaned up using methanol/chloroform precipitation as described above. Dried protein pellets were resuspended in 100mM Sodium hydroxide (NaOH), then 200µL of water and 1M HEPES (pH 7.2) to a final concentration of 50mM.

#### 4.3.3.5 Trypsin digestion

Trypsin is the most widely used protease in bottom-up proteomics, based on its catalytic activity and specificity in cleavage activity[166–168]. Trypsin is a serine protease that cleaves proteins at the C-termini side of arginine and lysine residues into peptides of relatively similar length (Figure 1-O)[166–168]. Commercially available trypsin enzyme (V5117, Promega) was resuspended in the provided resuspension buffer. Trypsin was then added to each sample at a 1:100 protease/protein ratio, and pH checked to be between 7.5-8. The samples were incubated overnight at 37˚C with gentle shaking.

#### 4.3.3.6 Sample enrichment using undecanal

Following trypsin digestion, ethanol was added to a final concentration of 40% v/v. Undecanal was added at a 50:1 undecanal/peptide ratio. Undecanal is an organic solvent, specifically, an eleven-carbon-aldehyde. Undecanal is used in this protocol as a hydrophobic N-termini tag increasing the hydrophobicity of trypsin generated peptides in the sample, making them a target for subsequent removal using C18 columns. After addition of undecanal, 1M sodium cyanoborohydride ($NaBH_3CN$) was added to a final concentration of 20mM; samples were mixed gently, and the pH adjusted to 7-8. At a higher pH, $NaBH_3CN$ is used to reduce methylation of amines to promote undecanal binding to the N-terminals primary amines. Samples were then incubated on a shaker

for one hour at 37˚C, followed by acidification with 1% trifluoracetic acid (TFA) in 40% ethanol to a pH between 3-4. Sep-pak plus short C18 (WAT020515, Waters) columns were used to remove undecanal tagged tryptic peptides from the samples. Samples were loaded onto C18 columns preconditioned with 5mL methanol, followed by 500µL of 0.1% TFA in 40% ethanol. Samples were then eluted off each column and collected in tubes and dried using speed vacuum centrifugation.

#### 4.3.3.7 Sample fractionation

After drying, each sample was reconstituted in 0.1% TFA. A Pierce High pH Fractionation kit (84868, Thermo Fisher Scientific) was used to reduce sample complexity into an orthogonal dimension prior to MS analysis, according to the manufacturer's protocol. Fractionation tubes were washed with acetonitrile (ACN) and conditioned using 0.1% TFA. 300µL of each sample was loaded onto a labelled column and centrifuged at 3,000g for two minutes. The fractionation column was then placed in a clean Eppendorf tube and 300µL of water added. The samples were centrifuged again (wash step). The flow though was discarded, and the column was again placed in a clean Eppendorf tube. Triethylamine (TEA) buffer was then diluted in 5% ACN and 300µL added to each tube for a TEA wash. The tubes were centrifuged at 300g for two minutes, and columns were then placed in a clean tube ready to fractionate the samples using a ACN gradient (10-50% ACN with 0.1% TEA buffer). Starting with the 10% ACN buffer, 300µL was added to the columns and the samples were centrifuged for two minutes at 3,000g. The first fraction was labelled with the TMT identifier and as Fraction 1. The ACN fractionation process was repeated an additional four times, increasing the ACN concentration by 10% for each run, collecting five fractions in total per sample. The five collected fractions per

sample were dried using speed vacuum centrifugation and stored at -80˚C for MS analysis.

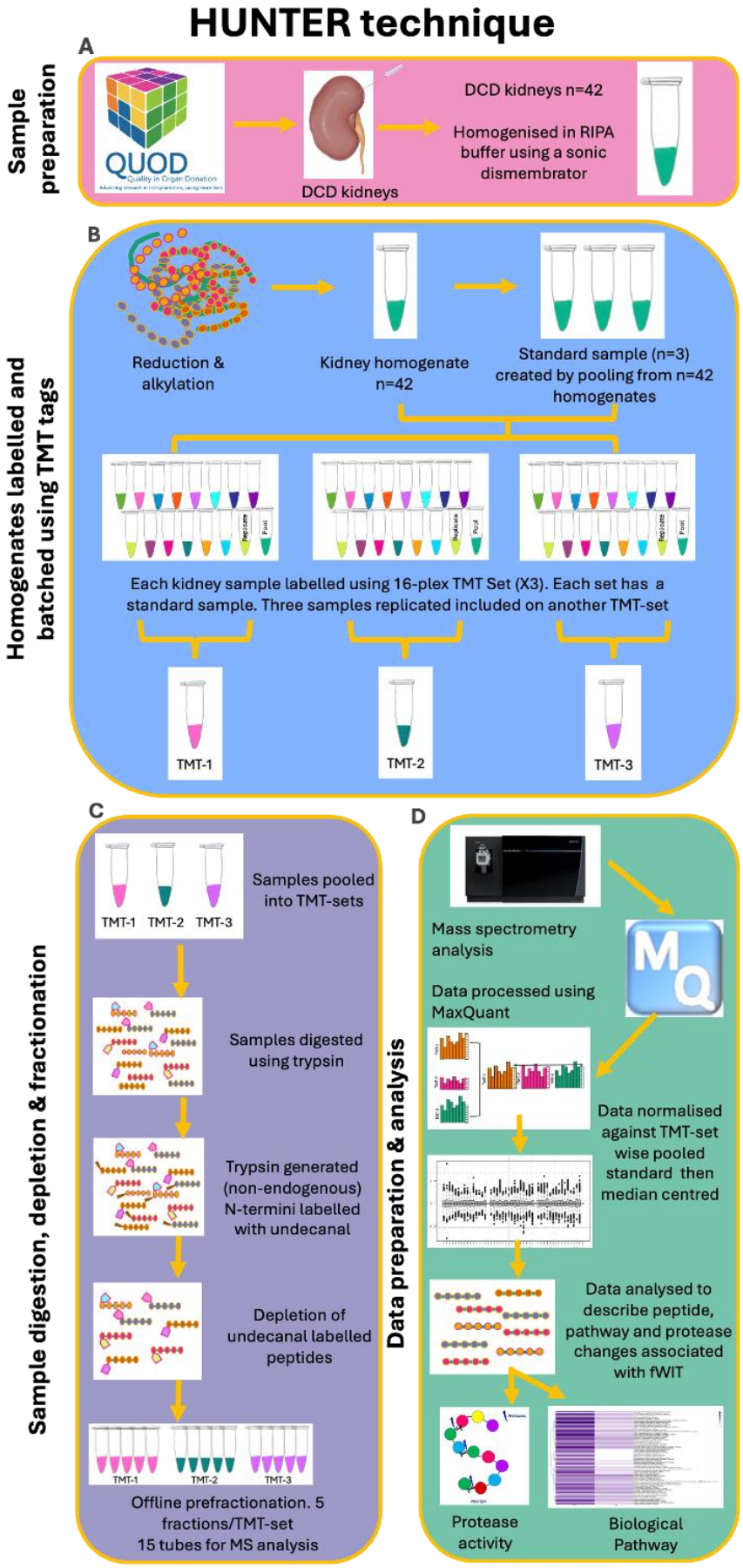

HUNTER technique
A
Sample preparation
QUOD
DCD kidneys
DCD kidneys n=42
Homogenised in RIPA buffer using a sonic dismembrator
B
Homogenates labelled and batched using TMT tags
Reduction & alkylation
Kidney homogenate n=42
Standard sample (n=3) created by pooling from n=42 homogenates
Each kidney sample labelled using 16-plex TMT Set (X3). Each set has a standard sample. Three samples replicated included on another TMT-set
TMT-1
TMT-2
TMT-3
C
Sample digestion, depletion & fractionation
TMT-1 TMT-2 TMT-3
Samples pooled into TMT-sets
Samples digested using trypsin
Trypsin generated (non-endogenous) N-termini labelled with undecanal
Depletion of undecanal labelled peptides
Offline prefractionation. 5 fractions/TMT-set
15 tubes for MS analysis
D
Data preparation & analysis
Mass spectrometry analysis
Data processed using MaxQuant
Data normalised against TMT-set wise pooled standard then median centred
Data analysed to describe peptide, pathway and protease changes associated with fWIT
Protease activity
Biological Pathway

**Figure 4-A: High-efficiency Undecanal N-Termini EnRichment (HUNTER) protocol and analysis**

A schematic outlining the HUNTER sample preparation protocol for analysis using mass spectrometry and data analysis.

### 4.3.4 Mass Spectrometry Analysis

*Sample analysis by mass spectrometry (this section 4.3.4) was performed by the Target Discovery Institute Mass Spectrometry Facility, Oxford, UK.*

Samples were defrosted on ice, resuspended in 10µL of Buffer A (2% ACN, 0.1% TFA in water) and analysed using a NeoVanquish UHPLC in line with an Orbitrap Ascend MS operated in trap and elude mode. The ultra-high pressure liquid chromatography (UHPLC) trap column was a PepMap Neo C18 (5µm, 300µm, 15mm (174500, Thermo Fisher Scientific)) connected to an EasySpray PepMapNeo analytical column (1500 bar max, 72µm x 500mm) (75500, Thermo Fisher Scientific). The gradient total run time for each sample was 80 minutes set to a 0.300µL/min flow rate.

Peptide scans ('MS1') were conducted at 120,000 resolutions with a scan range of 400-1500 mass-to-charge and an AGC target of $4\times10^5$ ions (injection time 251 milliseconds, normalised AGC target 100%). Peptides were selected with an isolation window of 0.7 mass-to-charge and fragmented by Higher-Energy Collisional Dissociation with a collision energy of 38%. Fragment ion scans ('MS2') were conducted at 45,000 resolutions with a scan range of 110-2000 mass-to-charge and an AGC target of $1\times10^5$ ions (injection time 91 milliseconds, normalised AGC target 200%).

### 4.3.5 Data analysis

#### 4.3.5.1 Mass spectrometry raw data search and preparation for analysis

Raw MS data was searched against the UniProt reference proteome database for Homo Sapiens (retrieval date 2018) using MaxQuant Software (version 2.3.1.0). MaxQuant is a quantitative proteomic analysis software programme specialised to support label-based analysis. The following parameters were used during the database search to identify the peptides/proteins: variable modifications were oxidation (methionine) and deamidation (glutamine and asparagine); fixed modifications were carbamidomethylation (cysteine) with a false discovery rate (FDR) of 1%. MaxQuant search parameters enzyme digestion mode was set to N-terminal free semi specific trypsin for TMT-16plex at MS2 level quantification.

#### 4.3.5.2 Analysis of HUNTER data using R Studio

R Studio (R version 2023.03.0+386) was used to analyse donor and recipient data from NHSBT and MS data from MaxQuant based on the HUNTER study analysis. All plots and heatmaps were produced in R Studio.

##### 4.3.5.2.1 Analysis of donor and recipient data

Donor and recipient metadata was provided by NHSBT *via* the QUOD biobank. Donor variables and recipient outcomes were compared between the two experimental groups: short fWIT and long fWIT using a t-test for numeric data and a Fisher's exact test for categorical data. Data are reported as mean and standard deviation and reported p.value where appropriate. A p.value ≤0.05 was considered significant.

#### 4.3.5.2.2 Analysis of HUNTER MS data

Results and NHSBT metadata were analysed in R Studio. Quantitation was performed at the peptide level (peptide.txt) except where specifically noted to be performed at the protein level (protein.txt). MaxQuant infers protein level data by calculating protein ion intensity based on peptide intensity for all peptides uniquely associated with a protein. Contaminants such as human keratin, as well as decoy and sequence reversals, were removed from the data. Quantitation values were log2 transformed, as outlined in Figure 2-A. Samples were normalised to the sample pool specific to each TMT-kit, to account for cross-labelling batch effects. The data was then median normalised.

Protease activity based on the sequenced cleavage sites of each identified endogenous peptides in the HUNTER study was analysed with the online TopFIND tool (https://topfind.clip.msl.ubc.ca), which predicts protease activity based on the observed endogenous peptide cleavage point in the canonical parent protein sequence. TopFIND compares observed cleavage sequence motifs to the MEROPS protease database to determine a responsible protease. The R package 'enrichR' was used to map the proteins identified in the HUNTER study to potentially affected biological pathways in the Reactome database (https://reactome.org).

The MS quantitation data was analysed using a t-test, comparing short and long fWIT or IF and DGF and using a linear model based on the fWIT continuum. Multiple testing correction was performed using the Benjamini Hochberg procedure; raw p.values were plotted in figures while adjusted p.values were used to highlight significant points.

## 4.4 Results

### 4.4.1 Analysis of fWIT to establish clinically relevant experimental groups

Between 2012-2022, 11,851 DCDs donated at least one kidney for transplant. Of these donors, 8,551 did not have a fWIT time documented, whilst 8,169 donors did not have a documented tWIT according to NHSBT records. Of the 3,300 reported fWIT, the mean fWIT length was 26.1 minutes with a median of 18 minutes. The mean length of tWIT was 45.7 minutes with a median of 29 minutes (Figure 4-B).

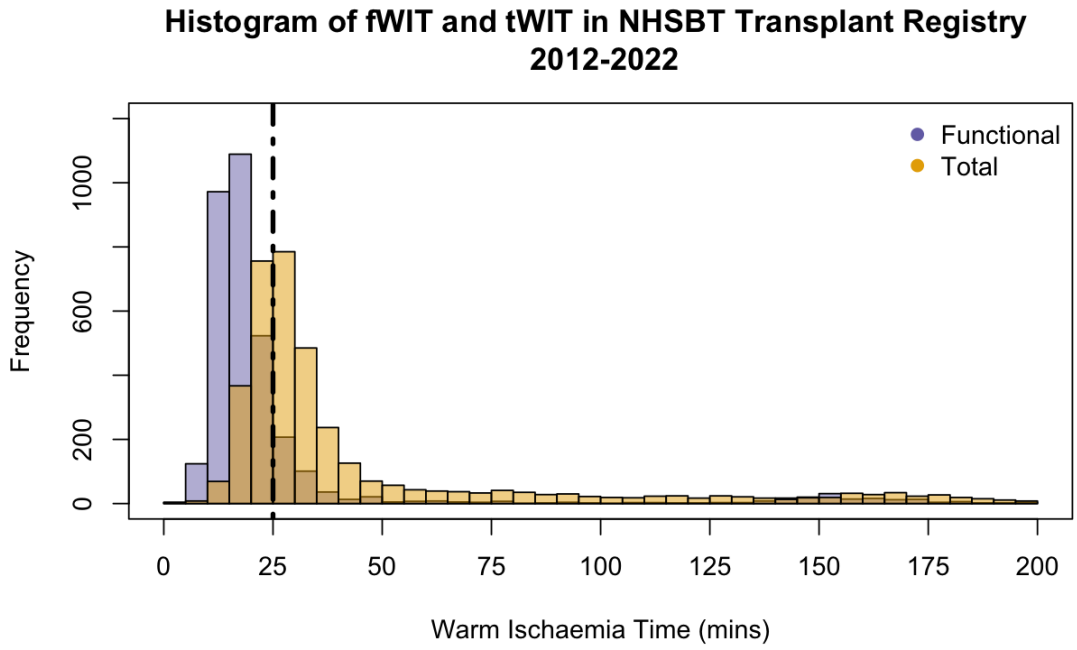



**Figure 4-B: Histogram of functional and total warm ischaemia time of DCD kidney donors with available records between 2012-2022**

Total and functional warm ischaemia times are coloured and overlapped to highlight the relationship between these two time points. The dotted line indicates where the average fWIT for DCD is, and the separation between experimental groups.

The experimental groups were defined for the HUNTER study based on an average UK-wide fWIT of 26 minutes. The short fWIT group was capped to 25 minutes of fWIT, whilst

the long group included donors that had a fWIT of between 30-120 minutes. This selection criteria ensured that the short group, represented the length of fWIT of most DCD donors (80%), whilst the long group reflected the extreme.

### 4.4.2 Donor characteristics and recipient outcomes

Donor kidney biopsies were selected by stratified random sampling across short fWIT (<25 minutes) and long fWIT (30-120 minutes) groups. Donors whose primary cause of death was associated with a physical trauma, such as a car accident or pedestrian accident, were excluded since there were not enough suitable samples for a meaningful study into the influence of trauma on the DCD peptidome, and insufficient detail regarding extent of injury in individual cases of trauma to assess the likely impact on the kidney.

The selected donors represented the continuum of fWIT defined by clinical criteria (Figure 4-C), which limits fWIT to 120 minutes. There was a significant difference ($p=<0.001$) in fWIT between groups and in sWIT ($p=0.01$), but tWIT was unchanged ($p=0.113$). As this study aimed to examine changes in DCD kidneys associated with ischaemia and hypoxia, tWIT was not a key factor in the selection process. Prior to the donor's blood pressure dropping below 50mmHg following WLST, the donor's circulation is sufficient to maintain organ oxygenation and perfusion. The risk of ischaemic injury increases when there is a sustained reduction in blood pressure, below 50mmHg until the organs are cold perfused.

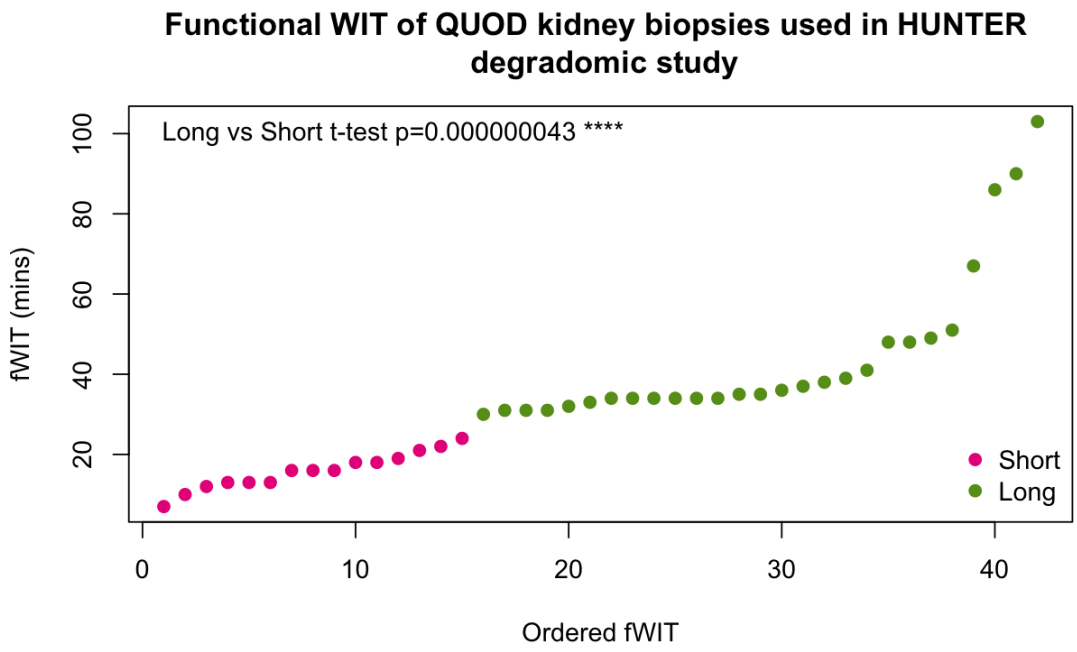



**Figure 4-C: Scatter plot of the fWIT of kidney biopsies analysed as part of the HUNTER study**

Length of fWIT between the experimental groups was significantly different (p=<0.001). Sample fWIT, however, was representative of the clinical fWIT continuum.

There was no significant difference in donor age, sex, height, weight, BMI, ethnicity or cause of death between sampling groups (Table 4-A). There was no difference in terminal SCr in the donors. Donor eGFR was significantly higher (p=0.041) in the long fWIT group. The quantified variance in donor eGFR likely associates with calculated variances that are commonly described in instances when the eGFR value is high; calculation variance associates with differences in donor creatinine levels, age, sex and race[169]. Time between admission to WLST for the two experimental groups had an obvious difference, yet this did not reach significance and is likely associated with an anomaly in the cohort. Recipient outcomes are presented for the donor kidney pair, where both kidneys were transplanted as single transplants (Table 4-A). There was no

difference in early transplant outcomes (p=0.441) or at 1-year posttransplant (eGFR) between the short and long fWIT groups (p=0.772).

| | Short fWIT † | Long fWIT † | p Value |
|---|---|---|---|
| ***Donor characteristics*** | | | |
| n | 15 | 27 | |
| **Donor Age (years)** | 51 ± 16 | 57 ± 13 | 0.261 |
| **Donor Sex (male)** | 11 (73%) | 18 (67%) | 0.739 |
| **Donor Height (cm)** | 174.8 ± 9.8 | 171.9 ± 9.3 | 0.350 |
| **Donor Weight (kg)** | 86.5 ± 19.9 | 77.9 ± 21.7 | 0.203 |
| **Donor BMI** | 28.4 ± 7.1 | 25.3 ± 5.0 | 0.152 |
| **Donor Ethnicity** | | | 0.357 |
| White | 14 (93%) | 27 (100%) | |
| Other | 1 (7%) | | |
| **Donor Serum Creatinine (terminal) µmol/L** ♔ | 67.7 ± 16.0 | 65.1 ± 24.8 | 0.773 |
| **Donor eGFR (mL/min/1.73m2)** | 116.4 ± 33.8 | 147.6 ± 58.5 | 0.041 |
| **Donor Cause of Death** | | | 0.904 |
| Intracranial haemorrhage | 10 | 17 | |
| Hypoxia | 3 | 7 | |
| Other | 2 | 3 | |
| **Admission to withdrawal of life support (hour)** | 102.0 ± 74.4 | 202.1 ± 229.0 | 0.062 |
| **Admission to Cold Perfusion (hour)** | 104.2 ± 75.6 | 197.7 ± 225.8 | 0.071 |
| **Total Warm Ischaemia (min)** ✢ | 43 ± 47 | 66 ± 36 | 0.113 |
| **Functional Warm Ischaemia (min)** † | 15.9 ± 4.6 | 44.3 ± 19.5 | **<0.001** |
| **Standard Warm Ischaemia (min)** ⚓ | 11.9 ± 2.5 | 22.9 ± 20.1 | **0.010** |
| | | | |
| ***Graft outcomes*** | | | |
| n | 29 | 50 | |
| **Cold Ischaemia Time (hour)** | 11.6 ± 3.9 | 13.3 ± 4.5 | 0.201 |
| **Graft Function** | | | 0.431 |
| Immediate Function | 17 (59%) | 30 (60%) | |
| Delayed Graft Function | 11 (38%) | 13 (26%) | |
| Primary Non Function | | 2/50 (4%) | |
| Not Reported | 1 (3%) | 5 (10%) | |
| **Delayed Graft Function Duration (days)** | 6.3 ± 4.6 | 5.5 ± 5.3 | 0.807 |
| **3month eGFR (mL/min/1.73m2)** | 49.8 ± 24.3 | 43.9 ± 23.2 | 0.5 |
| **12month eGFR (mL/min/1.73m2)** | 45.5 ± 25.1 | 43.0 ± 15.6 | 0.772 |

**Table 4-A: Donor characteristics and recipient outcome data**

Donor characteristics and recipient outcomes compared between the short and long fWIT groups. Functional WIT was significantly different (p=<0.001) between the two experimental groups, as was the sWIT (p=0.01). Differences in donor cause of death, donor ethnicity and in graft function outcomes were compared between short and long fWIT using Fisher's exact test; all other comparisons *via* t-test. Donor characteristics such as age, sex, BMI and cause of death previously described as having an impact of transplant outcomes were successfully managed for during selection and were not different between the two groups.

*♲ Last serum creatinine measured in donor before withdrawal of life support*

*✢ Total warm ischaemia refers to the time between withdrawal of the life support until cold perfusion of the organs*

*† Functional warm ischaemia refers to the time between once the donors systolic blood pressure drops below 50mmHg until cold perfusion of the organs*

*♈ Standard warm ischaemia refers to the time between circulatory arrest and cold perfusion of the organs*

### 4.4.3 Mass spectrometry data pre-processing and normalisation

Analysis of DCD kidney biopsies prepared according to the HUNTER protocol by MS identified 2,565 endogenous peptides which mapped to 1,022 unique proteins at a 1% FDR using the UniProt Homo Sapiens database (2018).

Data was first assessed to confirm commonality between internal controls (pool sample and technical replicates) and consistency of sample distribution before and after data normalisation. Raw reporter ion values for each internal control pool were compared (Figure 4-D). The pooled samples reporter ion data was overlayed, showing minimal differences between the three TMT-kits used in the HUNTER study, indicating no overwhelming TMT-kit specific batch effects. The raw intensity values for each sample were normalised (divided by) to that of the pooled sample for each TMT-kit.

As an additional quality control, three samples included in the HUNTER study were duplicated as technical replicates and run in different TMT-sets batches to the original sample (samples L08, L11 and M04 – labelled as L08 R etc). Comparison of the raw reporter ion values from these three samples also showed minimal variance between the replicates across the TMT-kits, providing additional confidence to the reproducibility of the study (Figure 8-C). The quality control duplicates were removed before analysis.

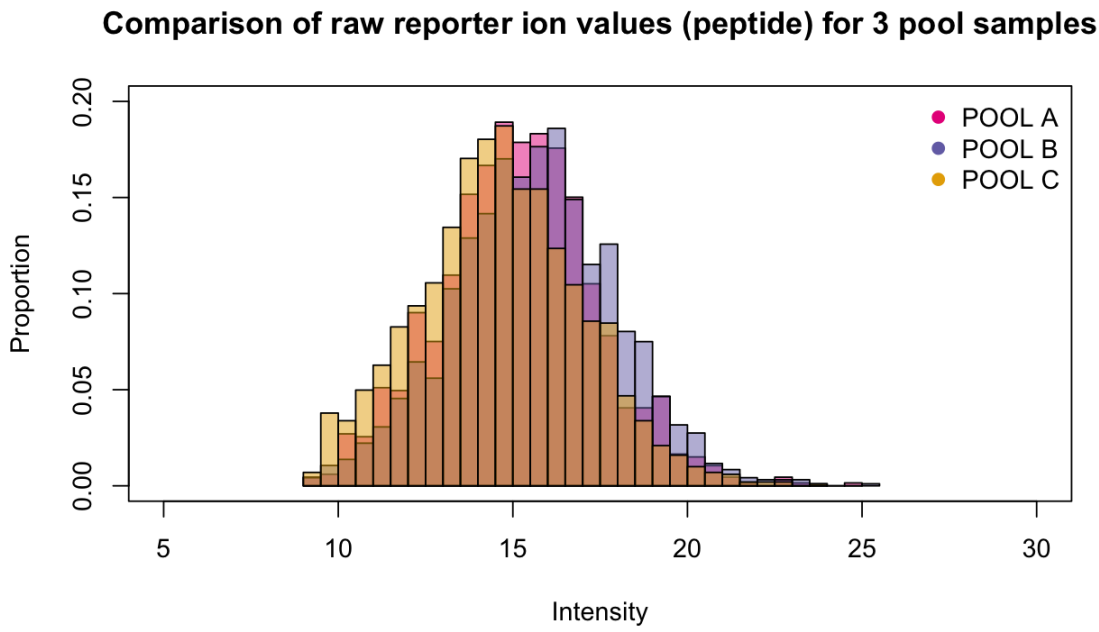



**Figure 4-D: Comparison of raw reporter ion values for the pooled sample included in each TMT-kit**

The pool sample analysed as part of each TMT-kit has minimal variability in the reported ion intensity profile. This analysis provides confidence that there is limited batch effects between the samples ran on the different TMT-kit, and that the samples can be normalised to these pools with confidence.

The pool normalised data was centred to a consistent median across samples by subtracting the mean of each sample from all log-transformed peptide readings from that sample (Figure 8-D). Median centring controls for sample variance associated with sample preparation and processing, ensuring the confidence of acumen drawn from the data. Examination of the pool-normalised, median-centred MS data indicated no evidence of outliers' samples.

### 4.4.4 There was no difference in raw reporter ion values based on kidney procurement protocol or TMT-kit

The collection protocol for kidney biopsies procured by QUOD changed during 2018, switching from a 33mm length needle to a 3mm punch biopsy (see Chapter 3 (3.3.1.1)). This change in tissue collection protocols became necessary to improve the continuity, quality and quantity of tissue collected. Collection of biopsies using the 33mm length gauge needle increased the likelihood that the collected biopsies may include medulla as well as the intended cortex tissue. As the composition of cortex and medulla tissue varies in structure, cell type and function, continuity of sample type is important to ensure a like-for-like comparison between donors. A comparison of peptidome profile for each kidney collected *via* needle or punch biopsy was performed to ensure that the collection protocol did not impact results. Principal component analysis (PCA) (

Figure 4-E) was used to compare the normalised intensity values of each sample. The analysis showed no clustering of the samples according to the collection protocol or according to the TMT-kit. This result shows no pre-analytical variability relating to biopsy procurement protocols or sample processing.

### 4.4.5 Endogenous peptide abundance increased in kidneys with prolonged fWIT

The HUNTER technique measures changes in endogenous peptide abundance, which may be influenced by variations in protease activity or the amount of parent protein. Consequently, any inferences regarding protein abundance from this study should be drawn carefully. In studies that quantify protein phosphorylation, similar challenges related to protein turnover can be addressed by measuring changes in both phosphorylated and total (phosphorylated and unphosphorylated) protein, providing a clearer picture of the ratio of phosphorylated to unphosphorylated protein. In contrast,

this study focused on quantifying endogenous peptides but could not provide direct insight into the cause-and-effect relationship of protein degradation. Analysis of the proteome could reveal changes in protein abundance, but since we only measure a subset of (uniquely assignable) degradation products it provides limited further value for assessment of degradomic changes. Since the likely protease responsible for peptide cleavages can be predicted using online bioinformatic tools, the most robust conclusions in this study can be derived from analysis of biological pathways and protease activity levels that integrate information from multiple protein sources, minimising assumptions about parent protein abundance.

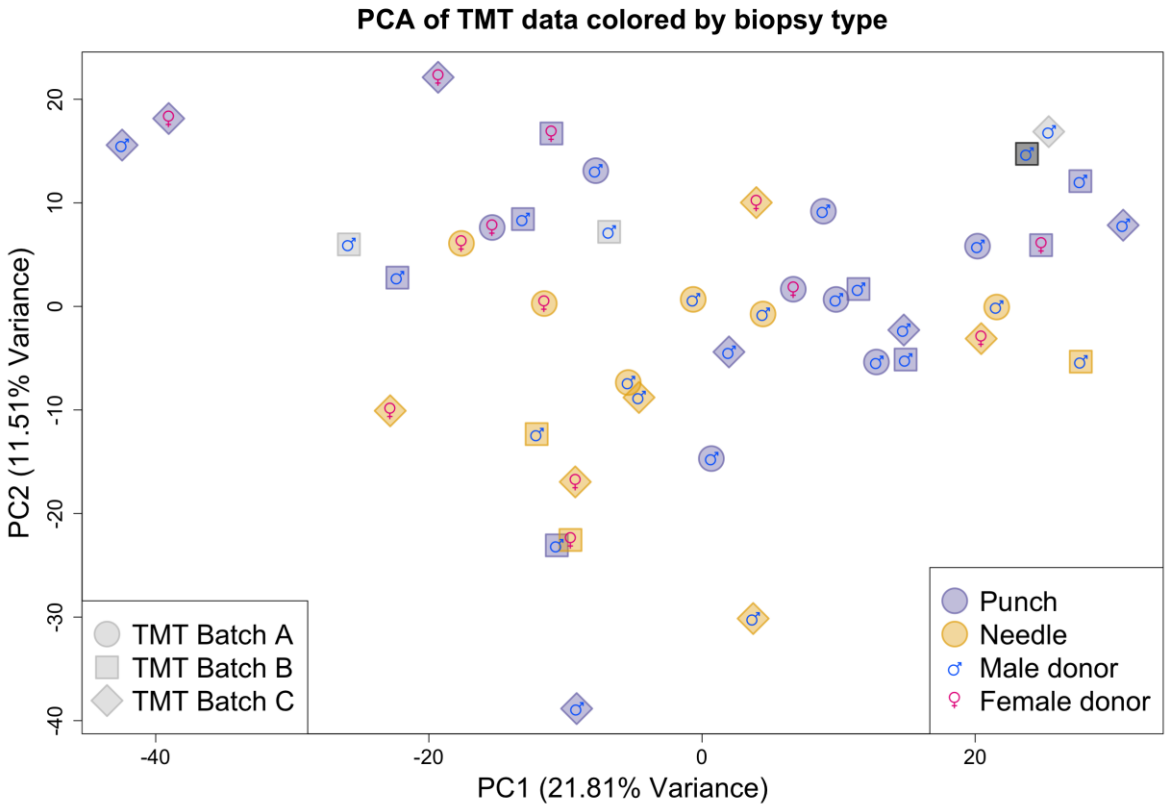



**Figure 4-E: Principal component analysis comparison of needle and punch biopsies included in the HUNTER study**

Principal component analysis (PCA) was used to check for correlations among the kidney biopsies used in the HUNTER study, based on the biopsy collection protocol used by QUOD and TMT-kit assignment during sample preparation. Here samples are colour coded by sample type and donor sex as indicated by the legend. Samples in grey/black did not have a documented biopsy type. The shape of each plotted point differentiates the samples by which TMT-kit the samples were grouped. There is no evidence of sample clustering, showing that donor sex, biopsy type, sample collection date or TMT-kit did not affect the data.

Endogenous peptide abundance in kidneys with a short or long fWIT were compared by t-test. Observation of the distribution of p.values (Figure 4-F (A)) indicated that a large proportion of the peptide tests were underpowered (fold change small relative to variance). To identify differences with an acceptable false discovery rate, the peptide data was filtered to remove peptides with a log2 fold change <0.5 (Figure 4-F (B)). Filtering reduced the number of peptides to n=534. Changes in peptide abundance were

assessed using a volcano plot (Figure 4-F (C)). All peptides are shown, but only those peptides with a significantly different abundance between the groups were highlighted in green or yellow based on the FDR rate (5% or 10%, respectively). Two peptides were significantly increased in the long fWIT group compared to the short fWIT group at 5% FDR: USO1 ($p=0.035$) and AFDN ($p=0.035$).

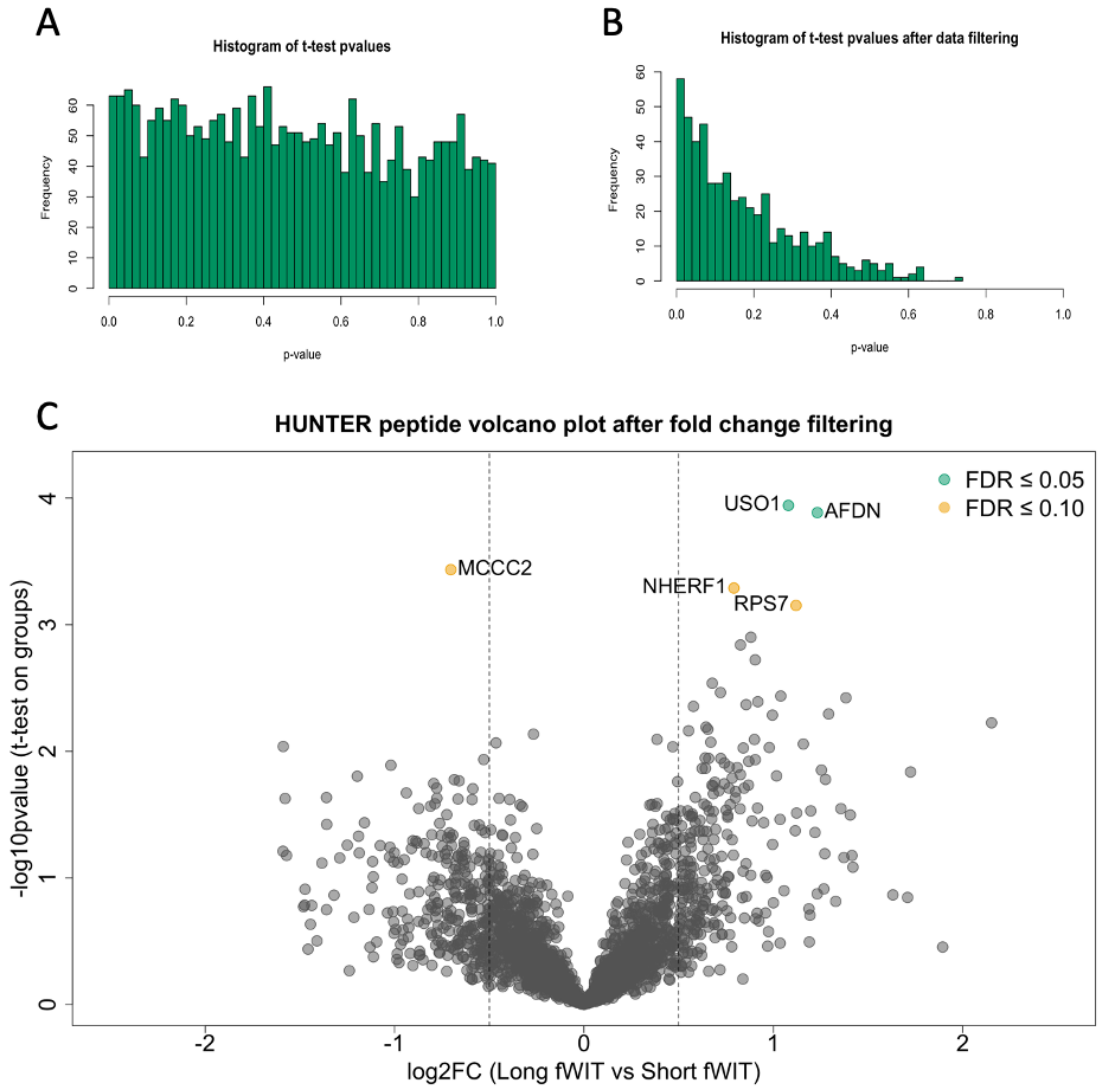



**Figure 4-F: Abundance of endogenous peptides comparing short fWIT to long fWIT**

Endogenous peptide abundance was compared between kidneys with a short fWIT and long fWIT. (A) shows a histogram of t-test p.values before data filtering (n=2565 peptides). (B) shows a histogram of t-test p.values after peptide data was filtered (n=534 peptides). (C) shows a volcano plot of peptide abundance variance between short fWIT (left) and long fWIT (right). The dotted lines indicate the minimum fold change filter; FDR significance is calculated based on those peptides with absolute fold change > 0.5. Two peptides had increased abundance in long FWIT biopsies compared to short fWIT biopsies (green; FDR ≤ 0.05). Only one peptide, MCCC2 had increased abundance in the short fWIT group (10% FDR); the difference in abundance was not significant (p=0.065) following multiple testing correction (0.05 ≤ FDR ≤ 0.1).

For a more sensitive analysis of differences, fWIT was then considered as a continuum, *via* linear regression, to test whether there was a change in peptide abundance as fWIT increased. The x axis (fold change between short and long groups) is retained for comparison purposes, and the same filter of > 0.5 log2 fold change was applied for consistency. Histograms of p.values before and after filtering are presented in Figure 4-G (A and B, respectively). Testing against the continuum of fWIT improved sensitivity highlighting seven peptides that are upregulated as fWIT is prolonged: USO1 (p=0.04), NHERF1 (p=0.04), SPATS2L (p=0.04), HNRNPC (p=0.04), FBP1 (a) (p=0.04), FBP1 (b) (p=0.04), and CALD1 (p=0.05), at a 5% FDR. When the FDR rate is increased to 10% an additional two peptides, PCBP1 (p=0.08) and BHMT (p=0.1), are indicated as increased with fWIT.

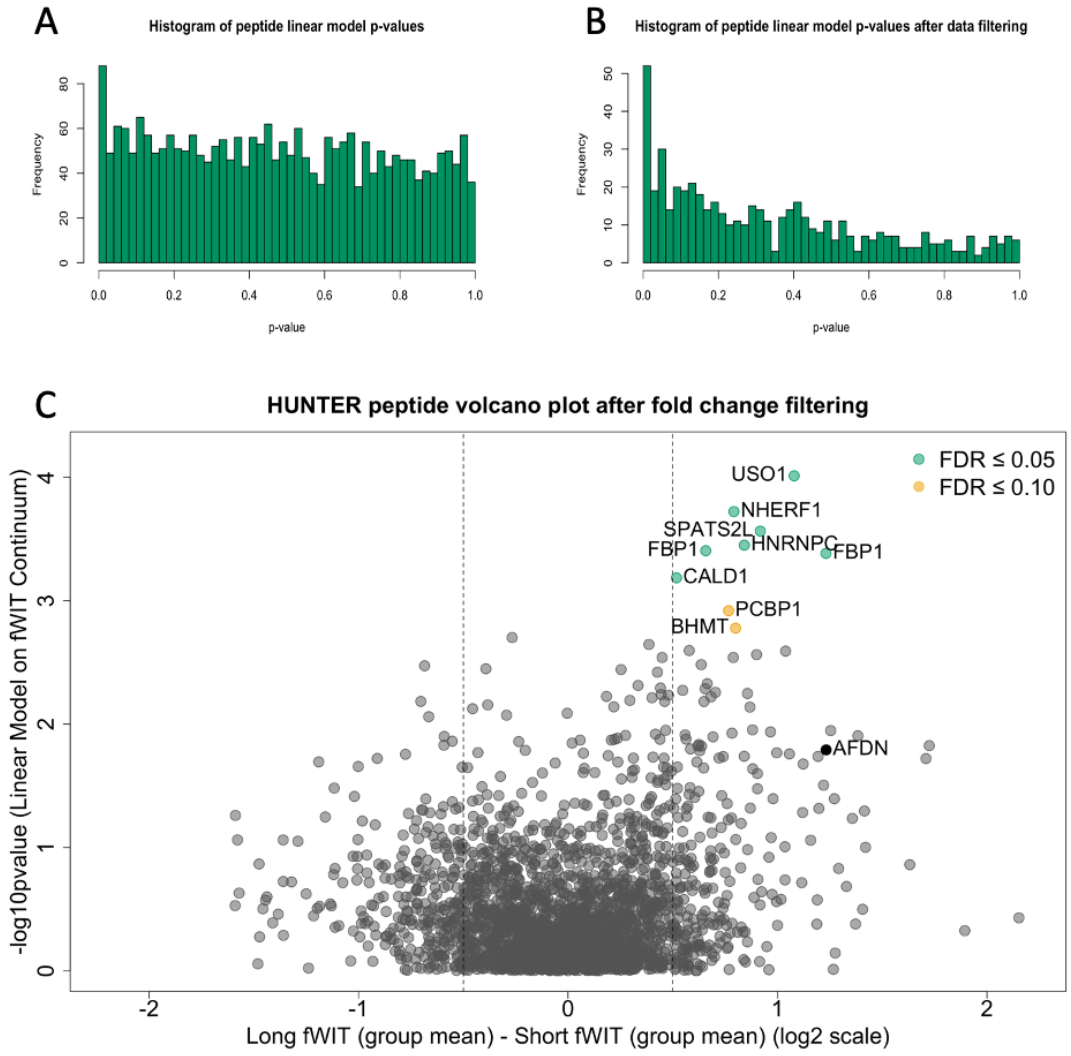



**Figure 4-G: Abundance of endogenous peptides changes with prolonged fWIT**

Using a linear model, changes in endogenous peptide abundance was mapped using a volcano plot after data filtering. (A) shows a histogram of p.values from the linear model before data filtering (n=2565 peptides). (B) shows a histogram of p.values from the linear model after data filtering (n=534 peptides). (C) shows a volcano plot mapping changes in peptide abundance as functional warm ischaemia is prolonged. The abundance of seven endogenous peptides were significantly increased as fWIT was prolonged (FDR 5%).

*N.B AFDN was labelled on this plot to show its position based on linear model analysis.*

### 4.4.6 Endogenous peptides were mapped to derivative proteins based on peptide sequences

Linear modelling was repeated for protein level analysis. During analysis and preparation of the MS raw data, MaxQuant predicts the most likely protein each peptide was derived from based on the peptide sequence. MaxQuant analysis generates a separate list of proteins as standard, which include a protein raw reporter intensity value (sum of all peptide intensities (cumulative abundance) linked to each protein). The protein reporter intensity values were normalised as described for the peptides and is included in the Appendix (Figure 8-E). In standard bottom-up proteomics, data are typically only analysed at the protein level. However, since the HUNTER approach depletes non-endogenous peptides, most proteins will have only one associated peptide detection, undermining the assumptions of the protein inference algorithm and protein-level quantitation calculation. Therefore, this analysis primarily serves as a qualitative comparison to the peptide analysis.

A linear model was used to profile the protein reporter intensity data in relation to the length of fWIT. A total of 1,022 proteins were identified as being the most probable proteins the endogenous peptides were derived from; p.values are presented as histograms in Figure 4-H (A) and (B) before and after fold change filtering (reduced protein number to 165). A volcano plot was then used to map changes in protein abundance with increasing fWIT (Figure 4-H (C)). At a 5% FDR the cumulative abundance of four proteins were increased with fWIT – USO1, PCBP1, SPATS2L and CNN3 – whilst an additional five proteins were upregulated at a 10% FDR. Two proteins were downregulated as fWIT increased (10% FDR): MCCC2 and DCXR. Three proteins – PCBP1,

USO1 and SPATS2L – were significantly increased with fWIT on the peptide and protein level.

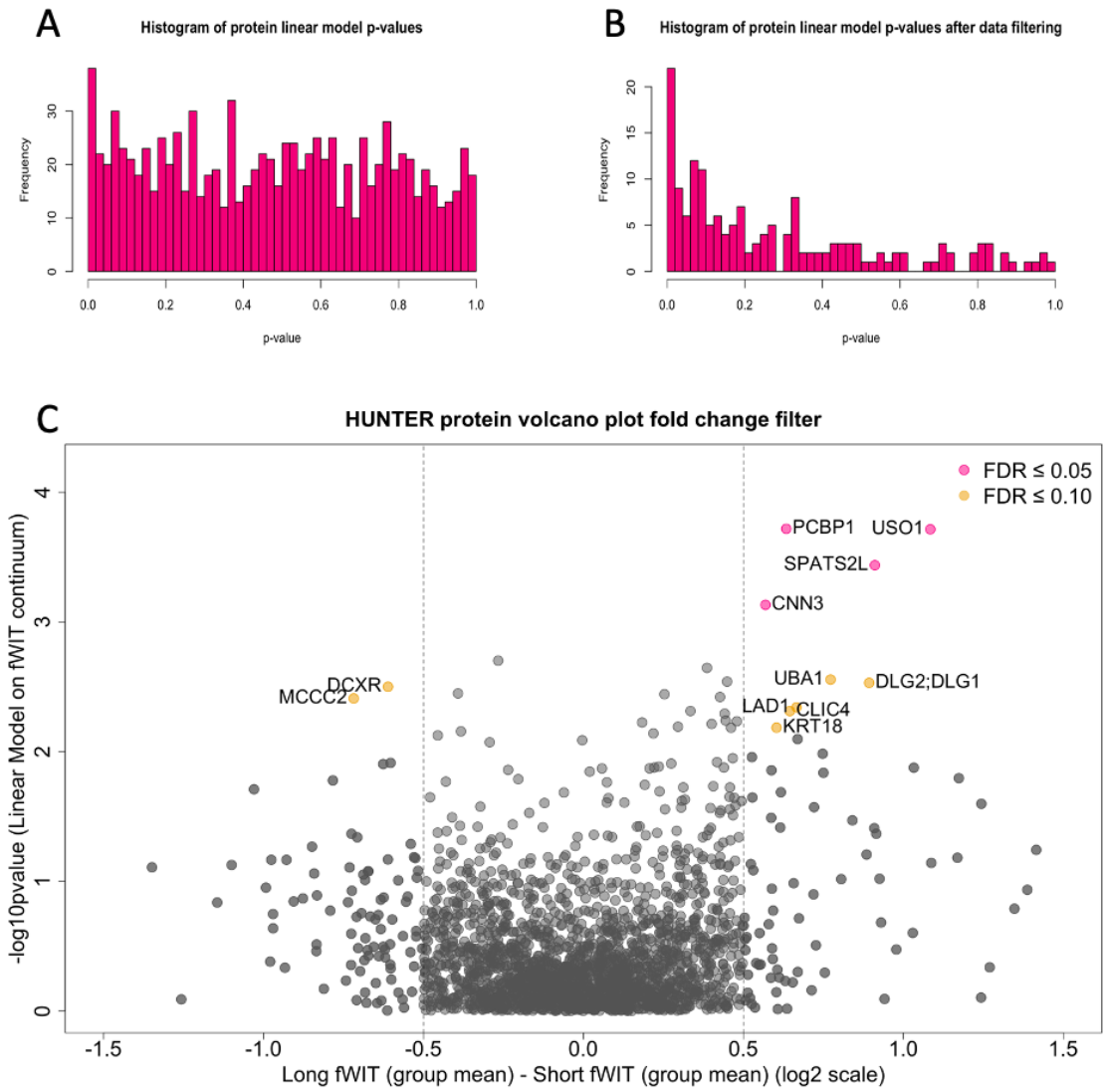



**Figure 4-H: Change in protein (cumulative) abundance as fWIT increases**

Protein raw intensity data was compared between donor samples in relation to the length of fWIT. (A) shows a histogram of p.values from 1,022 identified proteins. (B) shows a histogram of p.values after the data was filtered, comparing 165 proteins. (C) shows a volcano plot of protein raw intensity values as they change as fWIT is increased. Two proteins were downregulated with increasing fWIT at a 10% FDR, whilst nine proteins were increased with fWIT.

Analysis of protein changes with fWIT using HUNTER data is unreliable, evidenced here by the variability in proteins identified as changing with fWIT compared to endogenous peptides. The protein analysis represents changes in protein abundance based on the cumulative abundance of all endogenous peptides specific to each protein. However, the cumulative abundance of peptides for each protein is incomplete as trypsin generated peptides were removed from the samples prior to quantification. An example of this variance in peptide and protein abundance for FBP1 is presented in Figure 4-I. Each FBP1 peptide is represented by a different coloured line; the cumulative abundance of all peptides is represented by the thicker grey line. Abundance of the peptides beginning EEDK and AVKA increased with fWIT, as shown in Figure 4-G. The abundance of the other FBP1 peptides did not change with fWIT, and as a result the cumulative abundance of FBP1 peptides (protein level data) was also unchanged. Therefore, FBP1 protein abundance was not measured as changing with fWIT. Similar peptide abundance maps for CNN3, PCBP1, HNRNPC and CALD1 can be found in the Appendix (Figure 8-F).

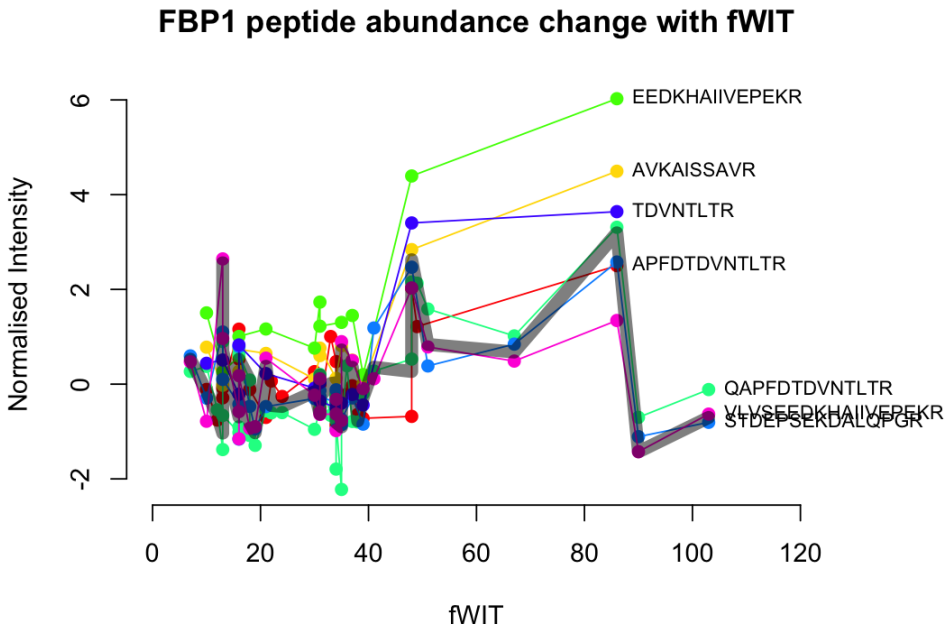



**Figure 4-I: Comparison of FBP1 peptide abundance over fWIT length**

Each coloured line represents a FBP1 endogenous peptide highlighting abundance changes over fWIT length. Two FBP1 peptides abundance (green and yellow lines) significantly increased with fWIT, whilst the abundance of the other peptides remains constant overtime. As the cumulative abundance (grey line) of FBP1 peptides remained constant over the length of fWIT, protein level analysis did not measure changes in the FBP1 cumulative abundance.

### 4.4.7 Biological pathways associated with changes in the kidney degradome were mapped using Reactome

Reactome is an online biological pathway database for the interpretation and analysis of biological pathways associated with a dataset. The peptide intensity data attributed to each parent protein were used to establish the effect of protein degradation on biological pathways. The proteins linked to the endogenous peptides were mapped to 902 biological pathways based on the Reactome search. Pathways were analysed using the linear model approach described above, considering all peptides associated with a pathway (Figure 4-J).

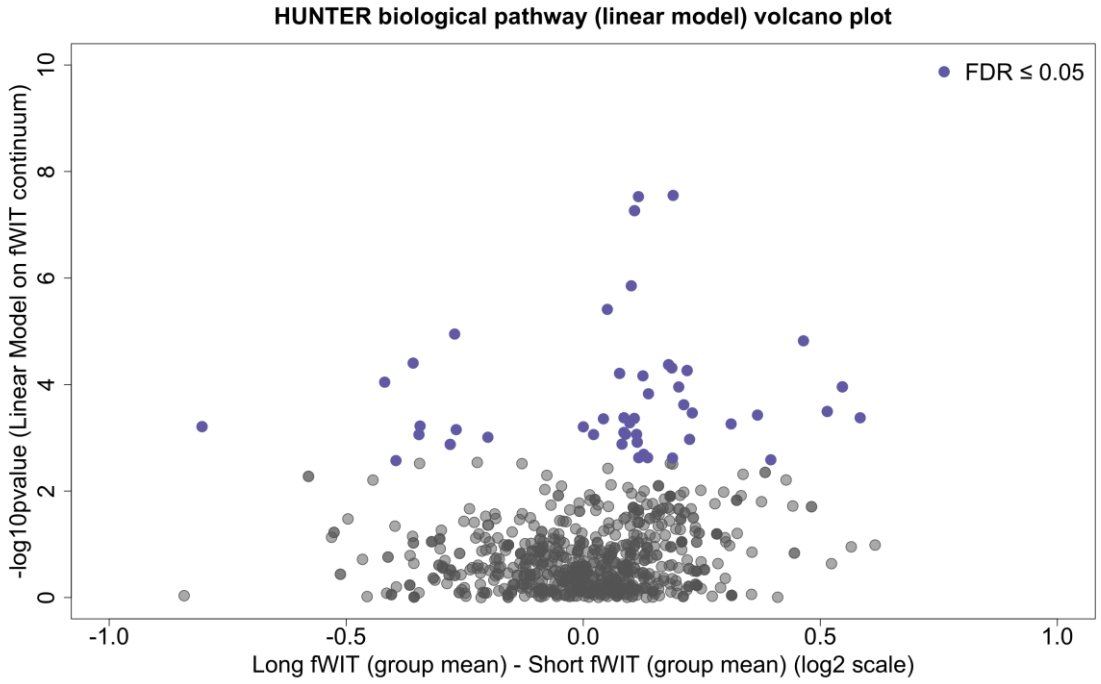



**Figure 4-J: Volcano plot showing changes in the regulation of biological pathways with prolonged fWIT**

The Reactome online database was used to map endogenous peptides quantified in the HUNTER study to biological pathways likely affected by variance in degradation of the native proteins. The volcano plot shows changes in biological pathways with fWIT calculated using a linear model. The pathway names and p.values are presented in Table 4-B.

Table 4-B contains a list of 55 pathways impacted by the increased peptide abundance quantified in the HUNTER study (adjusted p.value <0.05). The linear model calculated the log2 fold change, which is indicative of pathway up-or-down regulation specific to changing endogenous peptide abundance. The adjusted p.value indicates the significance of change in the pathway associated the ascribed degradation and prolonged fWIT. Most pathways in this list associate with metabolism, including glucose and carbohydrate metabolism, or with protein interaction and processing.

| Biological Pathways | Total number of peptides detected across all genes | Number of detected genes | rsquared | log2 Fold Change | Adjusted p.value |
|---|---|---|---|---|---|
| Developmental Biology R-HSA-1266738 | 126 | 70 | 0.01893 | 0.10125 | 0.00030 |
| Metabolism Of RNA R-HSA-8953854 | 105 | 60 | 0.01975 | 0.05080 | 0.00070 |
| Glycolysis R-HSA-70171 | 38 | 6 | 0.02634 | -0.27132 | 0.00175 |
| Nephrin Family Interactions R-HSA-373753 | 14 | 4 | 0.05963 | 0.46447 | 0.00205 |
| Retinoid Metabolism And Transport R-HSA-975634 | 53 | 10 | 0.01714 | 0.18005 | 0.00370 |
| Metabolism Of Fat-Soluble Vitamins R-HSA-6806667 | 53 | 10 | 0.01714 | 0.18005 | 0.00370 |
| Diseases Of Carbohydrate Metabolism R-HSA-5663084 | 31 | 7 | 0.02920 | -0.35892 | 0.00370 |
| Choline Catabolism R-HSA-6798163 | 25 | 3 | 0.03536 | 0.18687 | 0.00370 |
| Visual Phototransduction R-HSA-2187338 | 54 | 11 | 0.01714 | 0.18005 | 0.00370 |
| Sensory Processing Of Sound By Outer Hair Cells Of Cochlea R-HSA-9662361 | 17 | 7 | 0.05219 | 0.21905 | 0.00370 |
| Sensory Processing Of Sound By Inner Hair Cells Of Cochlea R-HSA-9662360 | 17 | 7 | 0.05219 | 0.21905 | 0.00370 |
| Sensory Processing Of Sound R-HSA-9659379 | 17 | 7 | 0.05219 | 0.21905 | 0.00370 |
| Axon Guidance R-HSA-422475 | 95 | 57 | 0.01782 | 0.07660 | 0.00373 |
| Nervous System Development R-HSA-9675108 | 95 | 57 | 0.01782 | 0.07660 | 0.00373 |
| RHO GTPase Cycle R-HSA-9012999 | 74 | 35 | 0.01598 | 0.12580 | 0.00393 |
| Scavenging Of Heme From Plasma R-HSA-2168880 | 23 | 3 | 0.02948 | -0.41891 | 0.00490 |
| Nuclear Events Mediated By NFE2L2 R-HSA-9759194 | 19 | 13 | 0.02893 | 0.20137 | 0.00502 |
| Chylomicron Clearance R-HSA-8964026 | 13 | 1 | 0.03733 | 0.54653 | 0.00502 |

| | | | | | |
|---|---|---|---|---|---|
| Nuclear Signaling By ERBB4 R-HSA-1251985 | 13 | 1 | 0.03733 | 0.54653 | 0.00502 |
| Signaling By ERBB4 R-HSA-1236394 | 13 | 1 | 0.03733 | 0.54653 | 0.00502 |
| Metabolism Of Vitamins And Cofactors R-HSA-196854 | 87 | 28 | 0.01495 | 0.13751 | 0.00647 |
| KEAP1-NFE2L2 Pathway R-HSA-9755511 | 21 | 14 | 0.02683 | 0.21201 | 0.01001 |
| NR1H3 And NR1H2 Regulate Gene Expression Linked To Cholesterol Transport And Efflux R-HSA-9029569 | 14 | 2 | 0.03145 | 0.51467 | 0.01242 |
| NR1H2 And NR1H3-mediated Signaling R-HSA-9024446 | 14 | 2 | 0.03145 | 0.51467 | 0.01242 |
| Antigen Processing: Ubiquitination And Proteasome Degradation R-HSA-983168 | 13 | 10 | 0.03751 | 0.22990 | 0.01278 |
| RHOV GTPase Cycle R-HSA-9013424 | 11 | 4 | 0.04929 | 0.36752 | 0.01356 |
| Signaling By Rho GTPases R-HSA-194315 | 96 | 50 | 0.01596 | 0.08585 | 0.01405 |
| Signaling By ALK Fusions And Activated Point Mutants R-HSA-9725370 | 11 | 8 | 0.06156 | 0.10769 | 0.01405 |
| Golgi Cisternae Pericentriolar Stack Reorganization R-HSA-162658 | 2 | 2 | 0.21262 | 0.58409 | 0.01405 |
| Other Interleukin Signaling R-HSA-449836 | 9 | 2 | 0.06684 | 0.04250 | 0.01405 |
| Syndecan Interactions R-HSA-3000170 | 15 | 3 | 0.04930 | 0.09808 | 0.01619 |
| Cell-Cell Communication R-HSA-1500931 | 27 | 13 | 0.03297 | 0.31180 | 0.01655 |
| Translation R-HSA-72766 | 87 | 56 | 0.01346 | 0.00012 | 0.01690 |
| Negative Regulation Of TCF-dependent Signaling By WNT Ligand Antagonists R-HSA-3772470 | 5 | 1 | 0.06327 | -0.34428 | 0.01690 |
| NGF-stimulated Transcription R-HSA-9031628 | 7 | 1 | 0.08510 | -0.80412 | 0.01690 |

| | | | | | |
|---|---|---|---|---|---|
| Nuclear Events (Kinase and Transcription Factor Activation) R-HSA-198725 | 7 | 1 | 0.08510 | -0.80412 | 0.01690 |
| Platelet Activation, Signaling and Aggregation R-HSA-76002 | 110 | 30 | 0.01095 | -0.26804 | 0.01861 |
| Signaling By Rho GTPases, Miro GTPases And RHOBTB3 R-HSA-9716542 | 97 | 51 | 0.01526 | 0.08568 | 0.02048 |
| Non-integrin membrane-ECM Interactions R-HSA-3000171 | 32 | 8 | 0.02577 | 0.02169 | 0.02056 |
| HS-GAG Biosynthesis R-HSA-2022928 | 18 | 5 | 0.03049 | 0.11251 | 0.02056 |
| Cellular Hexose Transport R-HSA-189200 | 2 | 1 | 0.12860 | -0.34658 | 0.02056 |
| Neuronal System R-HSA-112316 | 17 | 9 | 0.04577 | 0.08916 | 0.02056 |
| Formation Of Xylulose-5-Phosphate R-HSA-5661270 | 9 | 4 | 0.05174 | -0.20120 | 0.02255 |
| Metabolism Of Polyamines R-HSA-351202 | 19 | 10 | 0.02777 | 0.22429 | 0.02419 |
| Neurexins And Neuroligins R-HSA-6794361 | 8 | 3 | 0.06602 | 0.11379 | 0.02623 |
| Protein-protein Interactions At Synapses R-HSA-6794362 | 8 | 3 | 0.06602 | 0.11379 | 0.02623 |
| Platelet Degranulation R-HSA-114608 | 103 | 26 | 0.01098 | -0.28066 | 0.02725 |
| Response To Elevated Platelet Cytosolic Ca2+ R-HSA-76005 | 103 | 26 | 0.01098 | -0.28066 | 0.02725 |
| SUMO E3 Ligases SUMOylate Target Proteins R-HSA-3108232 | 14 | 7 | 0.04351 | 0.08168 | 0.02725 |
| XBP1(S) Activates Chaperone Genes R-HSA-381038 | 20 | 5 | 0.01806 | 0.12732 | 0.04105 |
| Defective EXT1 Causes Exostoses 1, TRPS2 And CHDS R-HSA-3656253 | 17 | 4 | 0.02913 | 0.11699 | 0.04567 |
| Hedgehog Off State R-HSA-5610787 | 15 | 11 | 0.02481 | 0.18820 | 0.04567 |
| Smooth Muscle Contraction R-HSA-445355 | 19 | 5 | 0.03693 | 0.13566 | 0.04567 |

| | | | | | |
|---|---|---|---|---|---|
| Interaction Between L1 And Ankyrins R-HSA-445095 | 10 | 3 | 0.04483 | 0.39559 | 0.04844 |
| Fructose Catabolism R-HSA-70350 | 21 | 3 | 0.02548 | -0.39513 | 0.04932 |

**Table 4-B: Pathway changes associated with quantified endogenous peptides**

The Reactome online database was used to interrogate changes in biological pathways associated with altered endogenous peptide abundance associated with prolonged fWIT. This table contains a list of 55 pathways that are significantly affected by the increase of endogenous peptides associated with fWIT. Pathways included here are not mutually exclusive (genes may contribute to multiple pathways). Significance was calculated using a linear model and multiple testing correction. Amplification of pathways associated with developmental biology, sensory processing etc, are unlikely to be specific to the kidney or injury associated with fWIT, but are likely to indicate commonality between proteins in these pathways and proteins in the kidney – the kidney has approximately 30 different cell types essential to maintaining its structure and function[170].

Changes in biological pathways associated with fWIT were mapped using a heatmap as seen in Figure 4-K. This list of pathways was filtered to include pathways where >20 endogenous peptides were involved in the pathway. It demonstrates that the key pathways dysregulated as fWIT is prolonged are cell-cell communication (cytoskeletal and ECM levels), metabolism specifically affecting glucose, choline and vitamin metabolism, immune response and haemostasis.


Cell-Cell Communication R-HSA-1500931 (27 peptides, 13 genes)
Metabolism Of RNA R-HSA-8953854 (105 peptides, 60 genes)
Developmental Biology R-HSA-1266738 (126 peptides, 70 genes)
Axon Guidance R-HSA-422475 (95 peptides, 57 genes)
Nervous System Development R-HSA-9675108 (95 peptides, 57 genes)
Processing Of Capped Intron-Containing Pre-mRNA R-HSA-72203 (43 peptides, 24 genes)
mRNA Splicing - Major Pathway R-HSA-72163 (42 peptides, 23 genes)
mRNA Splicing R-HSA-72172 (42 peptides, 23 genes)
RHO GTPase Cycle R-HSA-9012999 (74 peptides, 35 genes)
Signaling By Rho GTPases, Miro GTPases And RHOBTB3 R-HSA-9716542 (97 peptides, 51 genes)
Signaling By Rho GTPases R-HSA-194315 (96 peptides, 50 genes)
Choline Catabolism R-HSA-6798163 (25 peptides, 3 genes)
Non-integrin membrane-ECM Interactions R-HSA-3000171 (32 peptides, 8 genes)
Metabolism Of Vitamins And Cofactors R-HSA-196854 (87 peptides, 28 genes)
Sensory Perception R-HSA-9709957 (71 peptides, 18 genes)
Visual Phototransduction R-HSA-2187338 (54 peptides, 11 genes)
Retinoid Metabolism And Transport R-HSA-975634 (53 peptides, 10 genes)
Metabolism Of Fat-Soluble Vitamins R-HSA-6806667 (53 peptides, 10 genes)
Scavenging Of Heme From Plasma R-HSA-2168880 (23 peptides, 3 genes)
Platelet Activation, Signaling And Aggregation R-HSA-76002 (110 peptides, 30 genes)
Platelet Degranulation R-HSA-114608 (103 peptides, 26 genes)
Response To Elevated Platelet Cytosolic Ca2+ R-HSA-76005 (103 peptides, 26 genes)
Glycolysis R-HSA-70171 (38 peptides, 6 genes)
Diseases Of Carbohydrate Metabolism R-HSA-5663084 (31 peptides, 7 genes)
Fructose Catabolism R-HSA-70350 (21 peptides, 3 genes)
Translation R-HSA-72766 (87 peptides, 56 genes)
KEAP1-NFE2L2 Pathway R-HSA-9755511 (21 peptides, 14 genes)
7 10 12 13 16 18 19 21 22 24 30 31 32 33 34 35 36 37 38 39 41 48 49 51 67 86 90 103
1.5
1
0.5
0
-0.5
-1

**Figure 4-K: Heatmap showing changes in biological pathway associated with prolonged fWIT**

This heatmap shows 27 biological pathways with changing activity associated with prolonged fWIT, where >20 endogenous peptides are involved. Changes in heatmap colour intensity represents increased peptide abundance associated with the pathway and fWIT (calculated as a fold change); darker purple suggests upregulation of the pathway. The pathways presented in this heatmap can be grouped into three distinct clusters: glucose metabolism, immune response and metabolic processes.

### 4.4.8 Protease activity changes with prolonged fWIT

Proteases typically target specific amino acid residues (P1 position) or sequences, therefore their activity can be predicted based on the P1 residue at the cleaved site before the new N-termini and the parent protein sequence. For example, the protease Legumain (LGMN), has a specificity for asparagine (ASN - N) or aspartic acid (ASP - D) in the P1 position (Figure 4-L). In this data set, endogenous peptides were matched to their parent protein using the UniProt database – providing the full protein sequence to determine the P1 amino acid at the cleavage point.

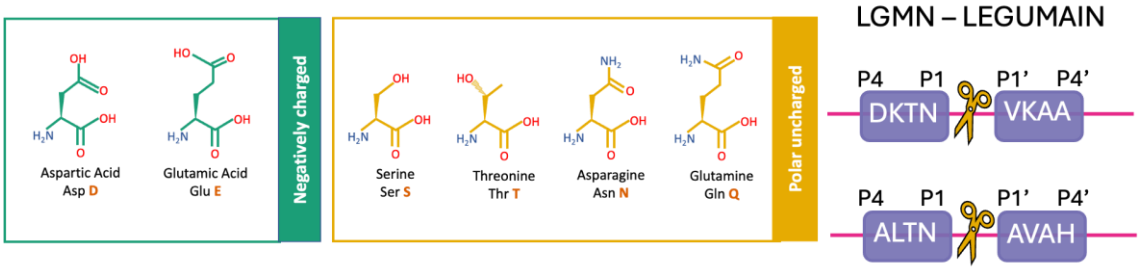



**Figure 4-L: Examples of the protease Legumain target specificity**

Example of endogenous peptides from the HUNTER data set cleaved by Legumin. Cleaving proteases were determined based on the peptide sequence in relation to the parent protein using the online tools TopFIND and MEROPS. Legumain cleaves after an asparagine (ASN – N) or aspartic acid (ASP – D) amino acid in the P1 position.

TopFIND, an online resource, was applied to the HUNTER dataset to determine protease activity based on quantified endogenous peptides. Sixty-three proteases, matching to 14% of the quantified peptides, were mapped to the identified endogenous peptides. The number of endogenous peptides cleaved by each protease is shown in Figure 4-M. Proteases from the granzyme family were some of the most active proteases in these samples. Granzyme M (GRAM) linked to >150 endogenous peptides and Granzyme A (GRAA) and B (GRAB) associated with ~150 and 100 cleavages, respectively. Other proteases such as matrix metalloproteinase 12 (MMP12) or kallikrein-14 (KLK14) have much lower number of cleavage products associated with their activity. This map of protease activity does not reflect changes associated with fWIT duration.

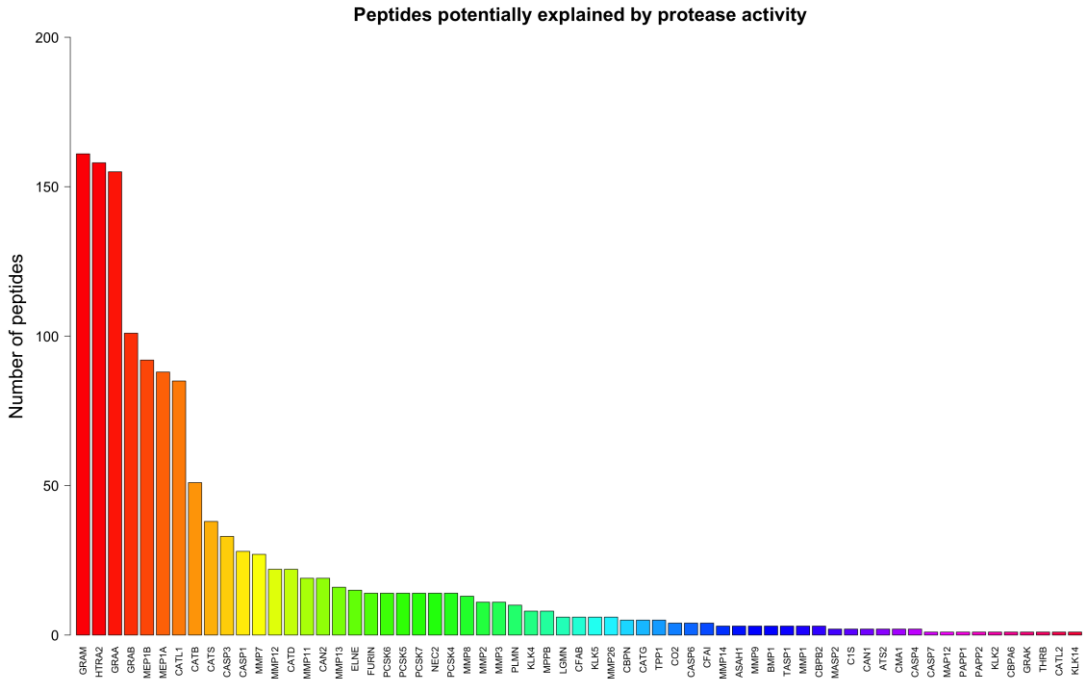



**Figure 4-M: Inferred protease activity based on endogenous peptide N-termini cleavage**

Proteases cleave proteins at specific amino acid sites. This will vary between the protease and is often common within protease families. In this histogram the number of peptides potentially cleaved by each protease is depicted.

Changes in protease activity – quantified according to cleavage motif preferences of each protease – associated with prolonged fWIT were analysed using a linear model and mapped using a volcano plot (Figure 4-N). Five proteases have significant activity changes associated with prolonged fWIT at a 5% FDR and an additional three proteases were detected when the FDR was set to 25%. GRAM (p=<0.001) and legumain (LGMN) (p=<0.001) activity is increased with fWIT. Activity of CATB (p=0.004), matrix metalloprotease 3 (MMP3) (p=0.03) and tripeptidyl peptidase 1 (TPP1) (p= 0.03) activity declines as fWIT increases.

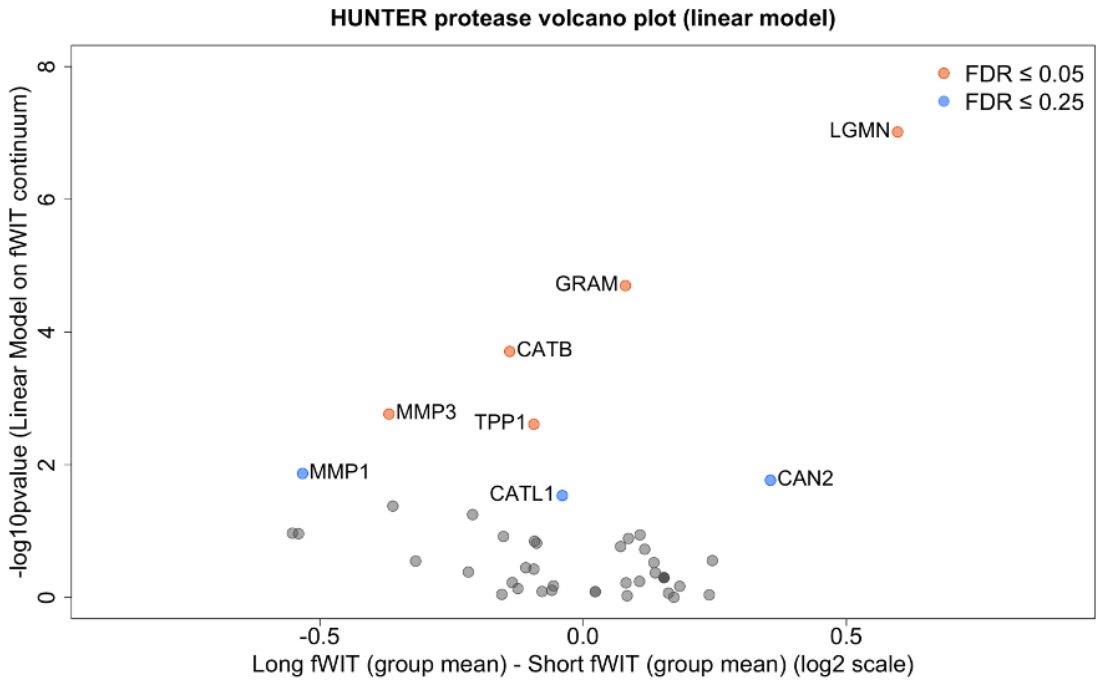



**Figure 4-N: Protease cleavages change with prolonged fWIT**

Protease cleavages were inferred using the TopFIND resource available online. Cleavage products specific to particular proteases changed with fWIT, indicating changes in protease activity. With prolonged fWIT, LGMN and GRAM cleavage products were significantly increased whilst CATB, MMP3 and TPP1 cleavage products were significantly reduced.

As there is likely to be overlap in the identification of 'responsible' proteases due to common specificity for amino acids or sequences, the likelihood of each endogenous peptide being cleaved by an alternative protease was evaluated, based on the five significant proteases at a 5% FDR. In Table 4-C the percentage overlap between proteases is reported. The analysis indicates that the endogenous peptides predicted to be cleaved by LGMN or TPP1 could not have been cleaved by any other of the five significant proteases. The other three proteases cleavage specificity has commonality with other proteases, particularly between CATB and MMP3.

| % | GRAM | CATB | LGMN | MMP3 | TPP1 |
|---|---|---|---|---|---|
| GRAM | 100 | 1.9 | 0 | 0.6 | 0 |
| CATB | 5.9 | 100 | 0 | 7.8 | 0 |
| LGMN | 0 | 0 | 100 | 0 | 0 |
| MMP3 | 9.1 | 36 | 0 | 100 | 0 |
| TPP1 | 0 | 0 | 0 | 0 | 100 |

**Table 4-C: Percentage overlap of significant proteases**

Percentage overlap of active proteases was measured by determining the likelihood that a peptide could have been cleaved by one or more protease. Here, the peptides linked to LGMN and TPP1 could not have been cleaved by any other protease, whilst GRAM-linked peptides have a 1.9% or 0.6% probability of being cleaved by CATB or MMP3, respectively.

### 4.4.9 Endogenous peptide abundance and protease activity in DCD donor with or without DGF

Associations between WI and increased incidences of DGF, determined through meta data analysis are well established in the literature, yet the molecular relationship between DCD donation and increased incidences of DGF is poorly understood. Here, the HUNTER data was reanalysed to identify whether shortlisted peptides and proteases were associated with DGF posttransplant. Twenty-seven of the analysed biopsies had an IF posttransplant, whilst 10 biopsies had DGF. This analysis was performed using t-testing with multiple testing corrections, to provide preliminary data for future studies.

One endogenous peptide, derived from the ketimine reductase mu-crystallin (CRYM) (p=0.01) protein, was significantly upregulated in DGF kidneys at a 5% FDR. AKAP12 (p= 0.08), CNN3 (p=0.1) and HNRNPU (p=0.1) at a 10% FDR were upregulated in kidneys that functioned immediate posttransplant. CDH3 (p=0.06), CD14(p=0.06), PKM (p=0.06) and KNG1 (p=0.1) were upregulated in kidneys that developed DGF posttransplant (10% FDR).

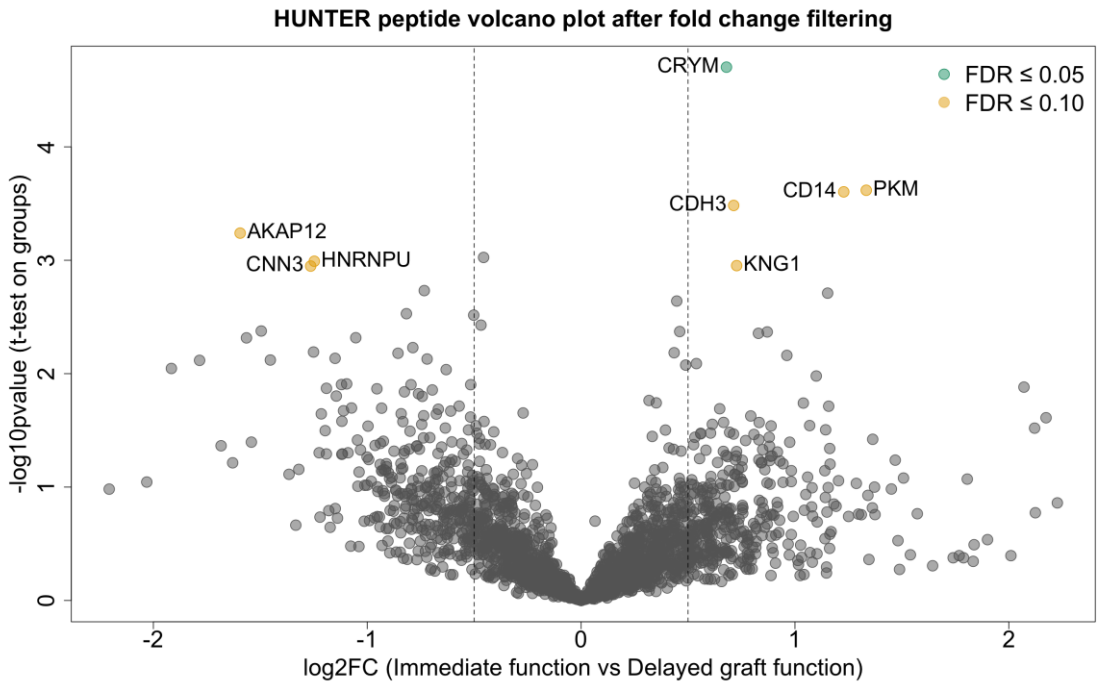



**Figure 4-O: Endogenous peptides associated with immediate function or delayed graft function posttransplant**

Ketimine reductase mu-crystallin (CRYM) (p=0.01) was the only peptide associated with DGF at a 5% FDR.

The endogenous peptides identified were matched to cleaving proteases using TopFIND and the MEROPS database. CATD (p=0.004) activity was significantly increased in kidneys that developed DGF posttransplant. At a 25% FDR, GRAB, MMPB and HTRA2 activity was seen to increase in kidneys that functioned immediately posttransplant, whilst PLMN, MMP7, BMP1, CAN1, CO2, CATG, MMP14, MMP26, CBPN and CBPB2 activity increased in kidneys with DGF (25% FDR).

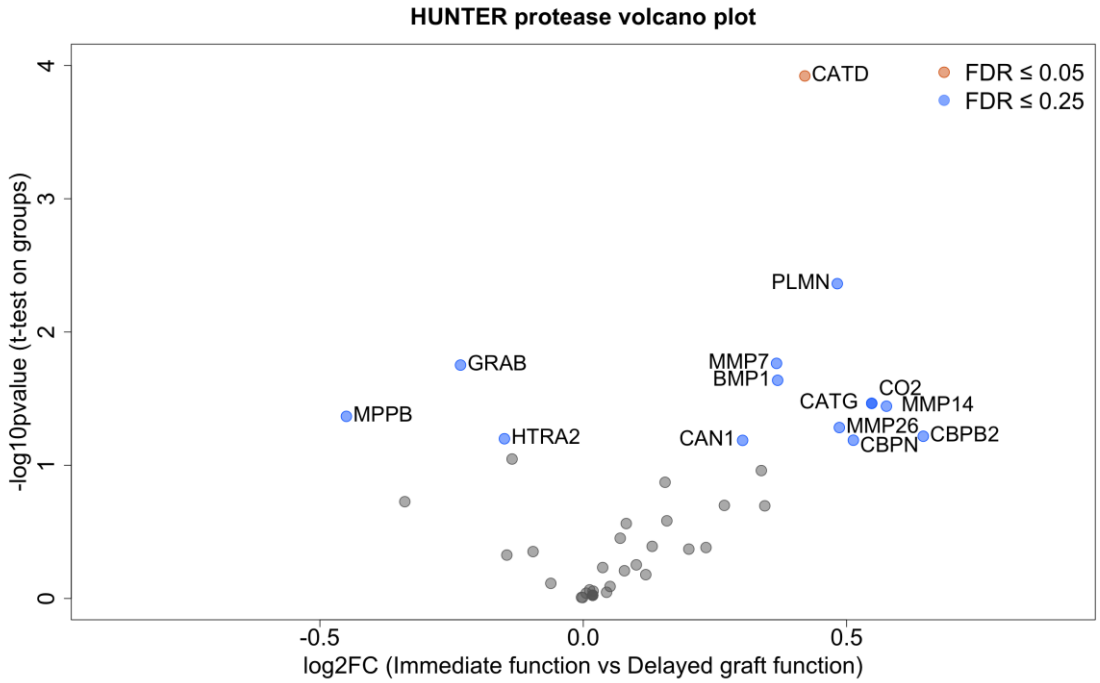



**Figure 4-P: Protease activity differences in kidneys with immediate function or delayed graft function**

Protease activity associated with the cleavage of endogenous peptides was different in kidneys with immediate or delayed graft function posttransplant. Cathepsin D activity was significantly increased in kidneys that developed DGF posttransplant (5% FDR). Adjusting the FDR to 25% highlighted additional protease activity changes associated with both immediate and delayed graft function.

## 4.5 Discussion

This study aimed to use a specialised proteomic method, HUNTER, to quantify changes in the DCD kidney degradome that associates with a prolonged fWIT. Kidney biopsies analysed were procured immediately after organ retrieval by the QUOD biobank, suggesting that the identified degradomic profiles reflect the degradation state associated with WI and are not influenced by additional factors such as CIT or reperfusion. An analysis of NHSBT data was used to establish the fWIT range of the experimental groups, short fWIT (<25 minutes) or long fWIT (30-120 minutes).

### 4.5.1 Principal component analysis showed no differences in tissue composition between biopsies or batch effects during sample processing

The kidney biopsies included in this study were collected between 2014-2023 during back table preparation immediately following retrieval. Biopsies were collected using a needle or a punch biopsy gun. There were limited samples available for this study, restricting its remit; specifically, there were few biopsies with an fWIT >45 minutes. This was further exacerbated by data missingness, as many samples did not have a recorded WIT, which is in line with what was observed during the analysis of the NHSBT registry data. Sample availability was reduced by biobank depletion and research sample consent not always being provided by the donor families. Future studies looking to quantify changes, specific to the donor or donor management pathway could utilise samples collected from discarded kidneys, although immediate and posttransplant outcomes could not be assessed. Donors selected in this study were matched for donor factors including age, sex and cause of death, as these variables have previously been shown to influence transplant outcomes. Matching for these donor factors improves the interpretation confidence of the data, meaning variance was more likely to be associated with fWIT than other factors such as donor age. Donor age is an important factor regarding organ transplant outcomes, however based on the severe shortage of organs for donation, aged donors are now a common part of the transplant landscape. Kidneys from older donors (>65 years) are more susceptible to ischaemic injury and have increased incidences of DGF posttransplant and reduced graft survival, compared to kidneys from younger donors. In a recent proteomic analysis of DD kidneys, our group has shown that donor age independently affects the implications of molecular evidence (Charles, Vaughan *et al*, under review). Managing age-related influences in this study

ensures the robustness of drawn conclusions. There has also been little research studying the impact of donor cause of death on graft outcomes. In this study kidneys donated after a physically traumatic death, such as a road traffic accident, were excluded to minimise variance associated with trauma. The experimental groups were further balanced for cerebrovascular events causing death and hypoxic associated death such as suicide by hanging.

Following MS analysis of the kidneys, a PCA was performed to check that the type of kidney biopsy (needle or punch) did not impact the peptidomic profile of the samples ( Figure 4-E). Despite biopsies being collected according to two different standardised protocols, and the suggestion that needle biopsies may also include medulla tissue, the PCA analysis did not show any clustering of the data based on biopsy type or TMT-kit batching. Additionally, there was no evidence of biopsy variance based on biopsy storage time. These initial checks provided confidence that there were no obvious biases influencing the data and that any observed variances associate with fWIT. Alternative methods to check the constitution of collected biopsies could include haematoxylin and eosin staining of sections to check morphology or measurement of cell specific markers including podocin, nephrin (both podocyte specific proteins) and N-cadherin (proximal tubule marker).

### 4.5.2 Endogenous peptide abundance increased with fWIT, indicating changes in cytoskeletal protein arrangement and metabolic processes

Linear model analysis of endogenous peptide abundance across the fWIT continuum highlighted an increased abundance of seven peptides at a 5% FDR (USO1, NHERF1,

SPATS2L, HNRNPC, FBP1 (two peptides), CALD1) and an additional two peptides at a 10% FDR (PCBP1 and BHMT) (Figure 4-G). The significant increase in endogenous peptide abundance observed is indicative of increased protein degradation in DCD kidneys with a prolonged fWIT.

General vesicular transport factor P115 (USO1) is a vesicle transport factor in the Golgi stack and subsequent binding of vesicles to target membranes. Literature regarding USO1 function in the kidney or in transplantation was not readily available. Similarly, research into spermatogenesis associated serine rich 2 like protein (SPATS2L) was limited. SPATS2L was first described in 2008, in a study of oxidative stress in human myoblasts, and since has remained relatively under investigated. SPATS2L has been identified as a potential cancer biomarker and has a role in chromosome organisation and translational control[171]. Yet its location, function and mode of action remains elusive. In this study SPATS2L degradation may indicate oxidative stress associated with fWIT or enhanced pro-apoptotic signalling[172].

Na+/H+ exchanger regulatory factor (NHERF1) was first described as a scaffold protein found in all epithelial cells, connecting plasma membrane proteins with the actin-binding ezrin-radixin-moesin (ERM) axis. However, NHERF1 is more than a scaffold protein, and has a role in cell interaction, cell structure including organisation of the actin cytoskeleton, trafficking of ions and molecules, inflammatory responses, epithelial cell polarity, and tissue injury[173]. In PTECs, NHERF1 is anchored to the actin cytoskeleton, and defines the brush border, characteristic of the PTEC apical membrane, and regulates sodium ion transporters[174,175]. Loss of the brush border has previously been

characterised as an implication of prolonged WIT in Wistar rats[156], and is characteristic of proximal tubule injury in both AKI and CKD[176]. Dysregulation of NHERF1 influences cell structure, inflammatory response and induces tissue injury[177]. Increased NHERF1 has been reported to cause reversible disruption in the actin cytoskeleton and ubiquitination and degradation of $\alpha$-actinin-IV, another cytoskeletal protein[173]. NHERF1 knockout in mice increases the activity of the pentose phosphate (metabolic) pathway (PPP)[174]. In this study, increased degradation products associated with the NHERF1 protein were associated with increasing fWIT. Degradation of NHERF1 may be indicative of metabolic changes in the kidney, affecting the PPP. NHERF1 degradation is also likely to cause structural dysregulation, affecting the actin cytoskeleton, ERM axis and the PTEC brush border.

Heterogeneous nuclear ribonucleoproteins C1/C2 (HNRNPC) is a member of the heterogenous nuclear ribonucleoprotein family, of RNA binding proteins involved in controlling RNA dynamics within the nucleus[178]. HNRNPC assembles onto new RNA transcripts in the nucleus and can selectively regulate RNA abundance[179]. Research has shown that under stress conditions HNRNPC can translocate to different cellular compartments, where it undergoes post-transcriptional modification, and is associated with several pathologies including multiple cancers, Alzheimer's disease and frontotemporal lobe dementia[179]. Under ischemic conditions and chronic cardiac pathologies, HNRNPC is phosphorylated during ECM remodelling[178] and promotes renal cell carcinoma proliferation and migration *in vitro*[179]. There are no specific references to a role for HNRNPC in KTx or associated with graft outcomes, yet increased degradation

products of HNRNPC in DCD kidneys may associate with RNA processing dysregulation and ECM remodelling in response to the hypoxic insult.

Fructose-1-6-biophosphatase (FBP1) is a rate limiting enzyme in the gluconeogenesis pathway, which synthesises glucose from non-hexose precursors such as lactate. In the kidney, gluconeogenesis is a key metabolic pathway in the proximal tubules regulating glucose homeostasis. However proximal tubule cells cannot metabolise glucose and therefore glucose produced *via* gluconeogenesis is returned to the peritubular capillaries where it is transported to other kidney regions as an energy source for glycolysis[180]. FBP1 in proximal tubule cells is localised to the cytosol, and acts to antagonise glycolytic flux in the proximal tubuless[181]. FBP1 is often cited as a marker for proximal tubule dysfunction[181–184]. In AKI gluconeogenesis is significantly reduced, as is lactate clearance[185], whilst in CKD there is a significant reduction in FBP1 in the kidney[186] as gluconeogenesis is inhibited[187]. FBP1 has also been described as a marker of diabetic nephropathy and can be measured in urine from these patients[181]. FBP1 in the PT decreases as diabetic nephropathy progresses[181]. In the liver, FBP1 loss associates with elevated fibrotic gene expression[188]. In this study, two endogenous peptides mapped to FBP1 had increased abundance as fWIT was prolonged. Degradation of FBP1 likely indicates metabolic dysregulation, specifically dysregulation of glucose metabolism in the kidney, and cellular injury in the proximal tubules. Additionally, as described in AKI and CKD, degradation of FBP1 as seen here likely indicates inhibition of gluconeogenesis in the tubules and may associate with the disruption of glucose metabolism elsewhere in the kidney. Dysregulation of gluconeogenesis likely causes a metabolic switch to glycolysis, limiting ATP dependent processes.

Caldesmon (CALD1) is an actin, myosin and calmodulin binding protein found in smooth muscle and non-muscle cells[189]. Previously, CALD1 has been associated with interstitial phenotypic changes associated with glomerular diseases. Ando *et al* reported that increased CALD1 is associated with IgA nephropathy, associated with increased abundance of the protein observed in mesangial lesions characteristics of the condition[189]. Follow up studies of the role of CALD1 in kidney disease remain limited. Degradation of CALD1 in the DCD biopsies likely indicates cytoskeletal changes, specifically affecting the actin cytoskeleton.

Poly(rC)-binding protein (PCBP1) is a multifunctional protein involved in RNA and iron binding. PCBP1 acts as an iron chaperone, binding iron from the cytosol and delivering it to ferritin *via* direct protein to protein interactions[190–192]. Implicated in liver disease, the deletion of PCBP1 affects mitochondrial morphology, ATP production, and oxygen consumption. PCBP1 also has a role in modulating hypoxia pathways, delivering iron to prolyl hydroxylase domain (PHD) enzymes[191,192], hydroxylating HIF1α and marking it as a target for ubiquitin mediated degradation[191]. When PCBP1 abundance is reduced, iron chaperone activity is subsequently reduced whilst HIF1α is increased[191], making HIF1α available for activation under stress conditions. Degradation of PCBP1 in this study may facilitate HIF1α activation as the kidney becomes hypoperfused and hypoxic during WI. HIF1α is an oxygen-sensitive transcription factor, activated in response to hypoxia and stress conditions to reprogramme metabolic processes and support cellular adaptations under stress conditions[193].

Betaine-homocysteine S-methyltransferase (BHMT) is a zinc metallo-enzyme expressed predominantly in the kidneys and liver[194,195]. In the kidneys, BHMT is restricted to the cortex, specifically the S3 region of the proximal tubules[195]. BHMT acts as part of the homocysteine methylation pathway, catalysing a methyl transfer from betaine to homocysteine forming dimethylglycine and methionine[194,195]. It also acts as an osmoprotectant, and supplements choline metabolism[195]. Hyperhomocysteinemia is linked to inactivity of key enzymes including BHMT in the pathway and has been associated with arteriosclerosis, thrombosis and reduced renal function[196]. Kidneys with increasing fWIT have increased degradation products mapped to BHMT which may reflect metabolic adaptations in the kidney associated with fWIT. BHMT may also serve as a marker of renal function in these kidneys; this will need to be investigated further. All BHMT peptides measured in this study are predicted to have been cleaved by the protease LGMN.

### 4.5.3 Protein level dysregulation in fWIT affected kidneys indicate dysregulation of cytoskeletal proteins

As described, analysis of protein data from the HUNTER study was used to complement the peptide analysis. The abundance of each protein has been cumulatively calculated from the endogenous peptides matched to the protein. Protein data is incomplete as all trypsin-generated peptides were removed from the samples prior to analysis. An 'estimated' protein abundance was calculated by MaxQuant, and therefore any conclusions drawn from protein analysis should be confirmed separately. The abundance of four proteins – PCBP1, USO1, SPATS2L and CNN3 – were measured as increasing with fWIT. All four proteins are associated with the cytoskeleton and/or

degradation of cytosol proteins; PCBP1, USO1 and SPATS2L peptide abundance was also measured as changing with fWIT as described above. Calponin 3 (CNN3) is one of three Calponin proteins that are distinguished from each other by variance in the C-terminal tails. CNN3 is an actin binding protein that is essential during cytoskeletal rearrangement, specifically in stress fibre assembly[197], and is upregulated in tubular cells with fibrotic lesions[198]. The abundance of CNN3 peptides did not significantly change with prolonged fWIT, yet the cumulative abundance of all endogenous peptides increased with fWIT (Figure 8-F). Further validation is required to determine whether CNN3 abundance does change with prolonged fWIT.

Adjusting the FDR to 10% indicated changes three additional proteins not observed at the peptide level. The cumulative abundance of UBA1, DLG2/1, LAD1, CLIC4 and KRT14 increased with fWIT, whilst the abundance of DCXR and MCCC2 decreased. The peptide abundance of these seven proteins did not differ with increased fWIT. Disks large homolog 1 and 2 (DLG2/1) are both scaffolding proteins linking signalling molecules and receptors to signalling proteins[199]. DLG2 interacts specifically with NDMA receptors, potassium channels and cytoskeletal regulators. Both DLG1 and 2 are essential for the developing kidney, but little is known about the role of these proteins in kidney injury or disease. Ladinin 1 (LAD1) is an anchoring filament protein found in the basement membrane (BM) of cells, which has been associated with several cancer types and may be a viable therapeutic target in cancer therapies[200]. LAD1 has been identified in various tissue types including the kidney, specifically the parietal epithelial cells in the glomerulus on the urinary side of the Bowman's capsule[201]. Chloride intracellular channel protein-4 (CLIC4) is enriched in PTECs, and forms chloride channels in the cell

and is a component of the cytoskeleton, binding to α-tubulin, ß-actin and creatine kinase[202]. CLIC4 is activated by local pH changes and cellular stress; CLIC4 deficient mice exhibited impaired renal tubulogenesis[203]. CLIC4 dysregulation also associates with apoptosis[204]. Keratin 18 (KRT18) is a cytoskeletal protein belonging to a larger family of intermediate filaments in epithelial cells[205]. KRT18 is reported to be upregulated under stress conditions, acting as an early response and marker of renal injury of varying causes[206]. Keratin dysregulation is a novel marker of renal epithelial cell injury[205] and has been shown to be upregulated in renal IRI models[205]. Ubiquitin-like modifier activating enzyme-1 (UBA1) was also dysregulated in the kidneys with prolonged fWIT, and acts as the first step for marking cellular proteins for degradation by the ubiquitin proteasome[207]. There is minimal research relating UBA1 to the kidney, yet UBA1 gene mutations are associated with VEXAS syndrome (a rare inflammatory disease), which causes kidney disease in a subset of patients[207]. 3-methylcrotonoyl-CoA carboxylase (MCCC2), is the beta subunit of the 3-methylcrotonoyl-CoA carboxylase enzyme which acts to degrade leucine, generating acetyl-CoA[208]. MCCC is localised at the mitochondrial membrane and is highly expressed in the kidney and liver[208]. Dicarbonyl/L-xylulose reductase (DCXR) is an enzyme that converts L-xylulose to xylitol as part of the carbohydrate metabolism pathway and has a pivotal role in sugar metabolism[209]. DCXR is expressed in the liver and kidneys, specifically in the proximal tubules[209], and is known to be dysregulated with age and metabolic disorders such as diabetes, cancer and nephropathies, yet its function is not fully understood[210]. As with CNN3, further work is required to determine whether the cumulative abundance changes observed in this analysis associate with prolonged fWIT and will not be addressed in this thesis.

Taking the endogenous peptide and protein data together, significant protein degradation of the cytoskeleton, ECM and metabolic proteins were observed in kidneys with prolonged fWIT. Review of literature relating to the identified peptides demonstrates that the dysregulation of proteins reported here likely affects multiple kidney regions and cell types. Dysregulation of proteins associated with metabolism may cause metabolic disruption in the proximal tubules, whilst cytoskeletal changes could impact cells in all regions of the nephron. Given the expected low proportion of glomeruli to tubules in the biopsies analysed in this study, the observed changes are likely specific to tubules. Cell models, such as those described in Chapter 5, or organoids models could be used to further investigate protein changes described here, comparing between glomerular cells such as podocytes and tubule cells. Future studies could quantify region-specific changes associated with fWIT using spatial-'omic methodologies.

### 4.5.4 Biological pathways dysregulated with fWIT associated with metabolic changes and membrane integrity

Measured changes in biological pathways are the sum of changes in the degradome associated with the pathway, thus the degree of variation and direction is difficult to quantify. Based on the endogenous peptides measured in the DCD biopsies, 902 biological pathways were linked to changes in the degradome. Pathways with significant changes (n=55) are listed in Table 4-B and were mapped using a heatmap (27 pathways, >20 contributing endogenous peptides) (Figure 4-K).

Analysis of biological pathways associated with the degradome indicated significant dysregulation in several metabolic pathways, including metabolism of RNA (p=0.0007), glycolysis (p=0.002), retinoid metabolism and transport (p=0.004), metabolism of fat-soluble vitamins (p=0.004), diseases of carbohydrates (p=0.004), and choline catabolism (p=0.004). Pathways associated with cell-cell interactions, signalling and transport, and proteins associated with the BM and ECM were also dysregulated with fWIT. Refining the list of biological pathways based on the number of contributing endogenous peptides (>20) highlighted 27 biological pathways dysregulated with prolonged fWIT. Focus was also drawn to biological pathways associated with cell interaction and response, RNA processing and expression, metabolic pathways, and dysregulation of the cytoskeleton and ECM.

Two pathways in the heat map – cell-cell interactions and KEAP1-NFE2L2 – signal dysregulation in cell interactions and transistasis. The cell-cell interaction pathway includes proteins involved with cell activity, co-ordination and contact with surface receptors that mediate communication between different cells. In the kidney, cell junctions are essential to maintaining the GBM especially the formation, structure, and function of the slit diaphragm (SD). The SD is the intracellular junction between the podocyte foot processes, which function through the synergetic regulation of proteins by the podocytes and are crucial to maintaining cytoskeletal dynamics and signalling in and between the podocytes (Figure 4-Q)[211]. Additionally, under physiological conditions, cell growth, survival, differentiation and permeability is mediated between podocytes and endothelial cells within the GBM[212], moderated by cell communication. Podocytes are susceptible to hypoxia and have been shown to have reduced viability and

expression of SD proteins which likely associates with increased proteinuria in the kidney[211]. Impairment in any part of the GBM will result in proteinuria[212]. Truncation of communication between podocytes and endothelial cells will likely reduce the function of the SD, debilitating the GBM's role in filtration. The KEAP1/NFE2L2 is a regulatory pathway that protects cells against oxidative stress[213], specifically, the activation of NFE2L2 under stress conditions, protects the kidney *via* its antioxidant/electrophile response. In animal IRI models, NFE2L2 reduces tubular injury induced by oxidative stress, but does not completely ameliorate the pathophysiological implications of oxidative and subsequent inflammatory stress[213]. NFE2L2 agonists have been evaluated for their effect in treating several diseases including cancer, neurological disorders, metabolic diseases and kidney disease[214]. Clinical trials evaluating the effects of NFE2L2 agonists in patients with diabetes and CKD have shown promise in improving kidney function and eGFR. However concerns about cardiovascular risks including cardiac failure, have hindered the transition of this treatment into clinical practice[215–218]. In this study, increased degradation products from proteins associated with these pathways were observed in kidneys with prolonged fWIT. Degradation of these proteins is indicative of progressive cellular injury in the GBM, mostly likely affecting podocytes and SD structure and function. Furthermore, degradation of proteins in this pathway may diminishing the kidneys response to oxidative stress and other metabolic processes, potentially limiting kidney function. Proposed deregulation of podocyte and SD interaction is further supported by significant dysregulation of the nephrin family interactions pathway (p=0.002). Nephrin is a transmembrane protein and a major structural component of the SD, acting as a signalling hub, and is crucial in maintaining podocyte cytoskeletal stability[219]. The four proteins degraded from the nephrin family

interaction pathway – ACTN4, WASL, SPTAN1 and SPTBN1 - are all associated with the podocyte cytoskeleton. Degradation of these proteins supports the hypothesis that fWIT induces cytoskeletal degradation in DCD kidneys.

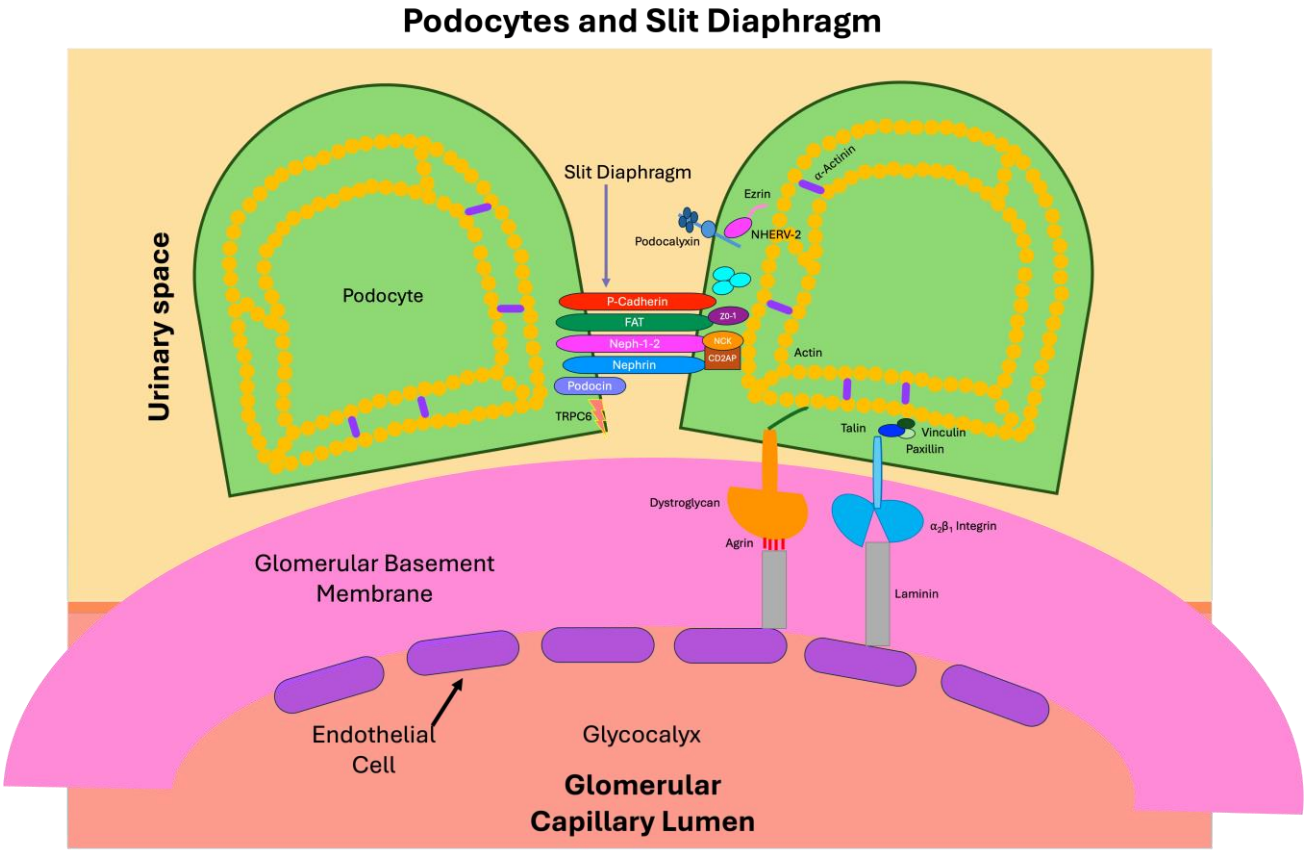



**Figure 4-Q: Podocytes and the slit diaphragm**

The slit diaphragm is the space between podocyte foot processes and are essential for cell-cell communication between podocytes and in regulating podocyte function and maintaining cytoskeletal dynamics.

Pathways dysregulated by fWIT directly associated with cytoskeletal, BM and ECM structure, function and modulation are indicated on the heatmap (Figure 4-K), and include RHO GTPase cycle, signalling by RHO GTPases, micro GTPases and RHOBTB3, signalling by RHO GTPases, and non-integrin membrane ECM interactions. The RHO family of GTPases are a widespread and diverse family of proteins that act as molecular

switches controlling a wide variety of signal transduction pathways, and are considered master regulators of the actin cytoskeleton, regulating cell behaviour and processes associated with cytoskeletal rearrangement[170]. Turbulent regulation of RHO GTPase associated proteins are unlikely to be indicative of injury to a single kidney cell type, as these proteins maintain the structure and dynamics of the actin cytoskeleton common across multiple cell types including podocytes, mesangial cells, and tubular cells. RHO GTPases are also involved in inflammatory cell infiltration[220]. A thorough evaluation of degraded proteins would be required to predict the likely implication of dysregulation to the RHO GTPase pathways which is beyond the scope of this chapter but is an exciting area for further study. Dysregulation of proteins in this family are associated with IRI; in a pig IRI model, increased RAC1 activity induced IRI-injury and also regulated profibrotic cytokines, chemokines and macrophage recruitment[170]. RHO mediated tight junction assembly mechanisms are dysregulated during ATP depletion which induces the rapid breakdown of tight junction permeability barriers[221], linking metabolic dysregulation to cellular disruption. The non-integrin membrane ECM interaction pathway associates with transmembrane proteoglycan and the interaction of integrins with the actin cytoskeleton and, when disrupted, causes unrecoverable injury[222]. An in-depth follow up study is required to comprehensively understand the impact of hypoxia on the RHO GTPase pathways, with a focus on describing cell or nephron-region specific changes. Dysregulation of RHO GTPases has been described in a range of kidney pathologies, including IRI. These changes often manifest as alterations in podocyte function and reduced integrity of the GFB[170], both of which are essential to maintaining kidney function. RHO GTPases are integral in regulating the cytoskeleton, cellular processes such as cell motility, metabolic control and apoptosis, with disruptions to any of these

processes potentially contributing to kidney dysfunction and a loss of kidney filtration capacity in response to ischaemia. As RHO GTPases operate as small molecular switches in the kidney, it is important to consider the cellular consequences of their dysregulation associated with fWIT. To gain a better understanding of this, future research should focus on characterising the function of each protein reported in this study as being degraded with prolonged fWIT, to define the translational effects of RHO GTPase protein degradation. Additionally, future studies should seek to link changes in RHO GTPases with transplant outcomes. Understanding how these molecular shifts correlate with kidney function and recoverability posttransplant could provide novel insight into the mechanisms of cytoskeletal degradation and cell-specific adaptations to ischaemia, whilst contributing to therapeutic strategies to mitigate cellular damage and preserve kidney function posttransplant.

Metabolic pathways were also significantly disrupted in the kidneys with prolonged fWIT. In the heatmap, pathways associated with glycolysis and vitamin metabolism were shown to be disordered with elongated fWIT. Cell metabolism is the process by which cells generate energy (ATP) to fulfil biological functions[110,188,223]. Figure 4-R outlines the typical pathway for aerobic metabolism, starting with a glucose molecule being transported into the cell *via* a GLUT receptor. The glucose molecule is then converted to pyruvate and ATP by 10 successive enzymatic reactions in a pathway known as glycolysis (Figure 4-S). Pyruvate is converted to acetyl-CoA in the mitochondria and is the starting metabolite for the CAC (Figure 4-T). By products of CAC – NADH and Flavin adenine dinucleotide (FADH) – then enter the ETC, which facilitates the transport of protons and electrons from the mitochondrial matrix[110] into the intermembrane space, driving ATP

generation (30-32 molecules on average) by ATP synthase[224] (Figure 4-U). Under anaerobic conditions pyruvate is converted into lactate, which is then converted back into pyruvate by the enzyme lactate dehydrogenase.

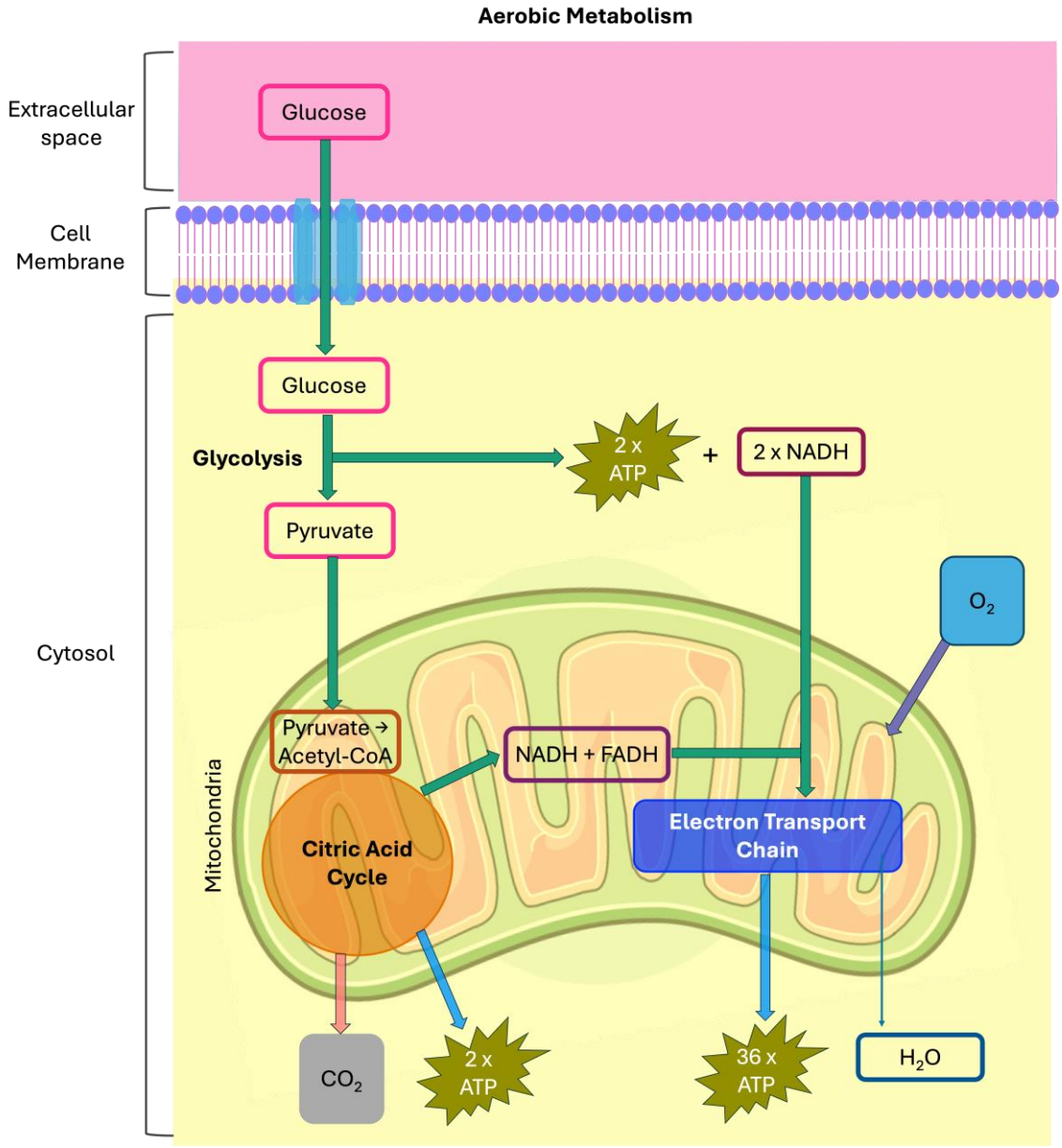



**Figure 4-R: Energy metabolism under aerobic conditions begins typically with glycolysis**

Glycolysis is a successive enzyme driven process converting glucose into pyruvate. Glucose is transported by GLUT membrane receptors into the cell *via* the cell membrane. Under aerobic conditions, pyruvate enters the mitochondria and is converted to acetyl-CoA – the starting metabolite of the citric acid cycle. NADH and FADH generated during the citric acid cycle are then used in the electron transport chain to generate ATP. Each glucose molecule generates two pyruvates.

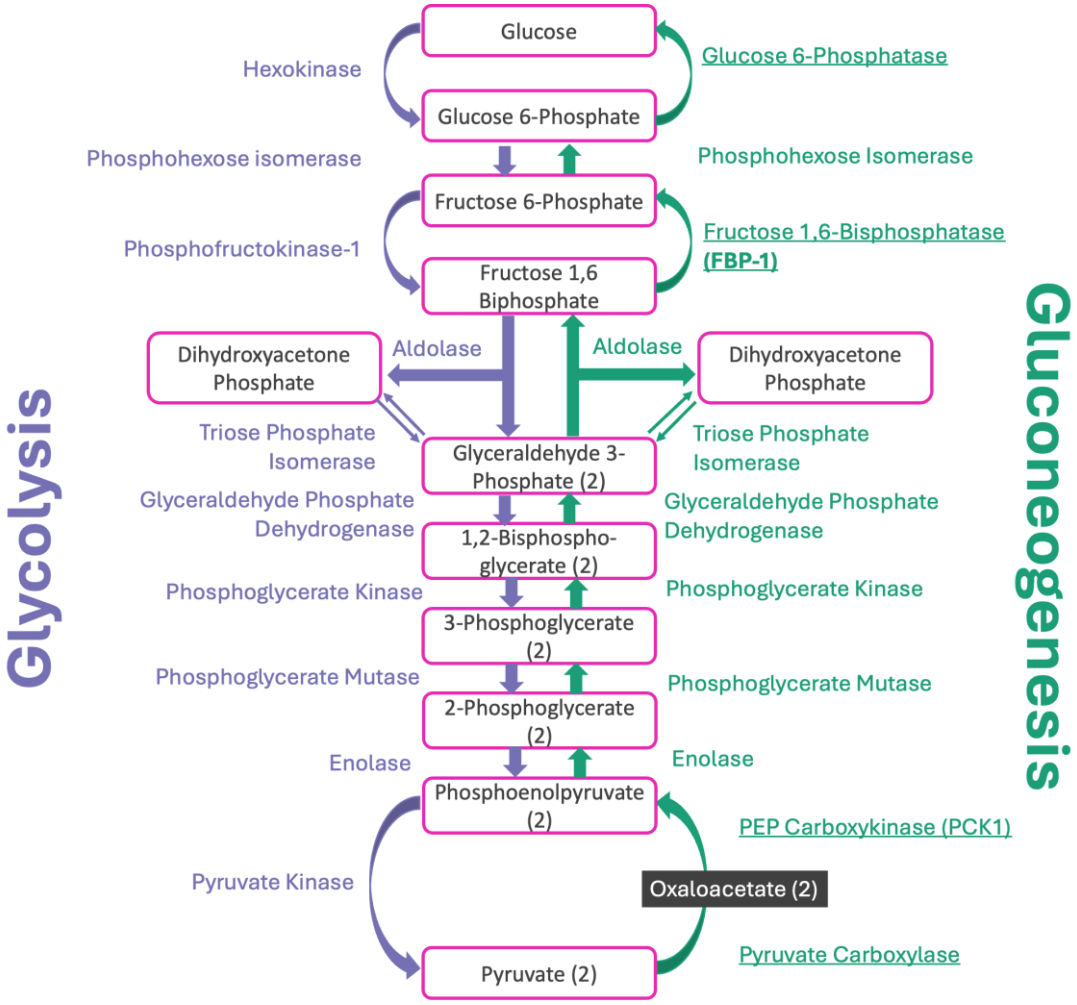



**Figure 4-S: Enzymatic pathways of glycolysis and gluconeogenesis**

Glycolysis is a successive 10 enzyme driven pathway converting glucose molecules into pyruvate. The glycolysis process produces two ATP molecules for each glucose converted[225]. Gluconeogenesis is an 11-step process synthesising glucose from non-hexose precursors such as lactate, glycerol or pyruvate. Gluconeogenesis is essential in maintaining normal glucose levels. Most steps in the gluconeogenesis pathway are the same as that in the glycolysis pathway except four; these four enzymatic reactions are irreversible and are specific to this pathway[187,226].

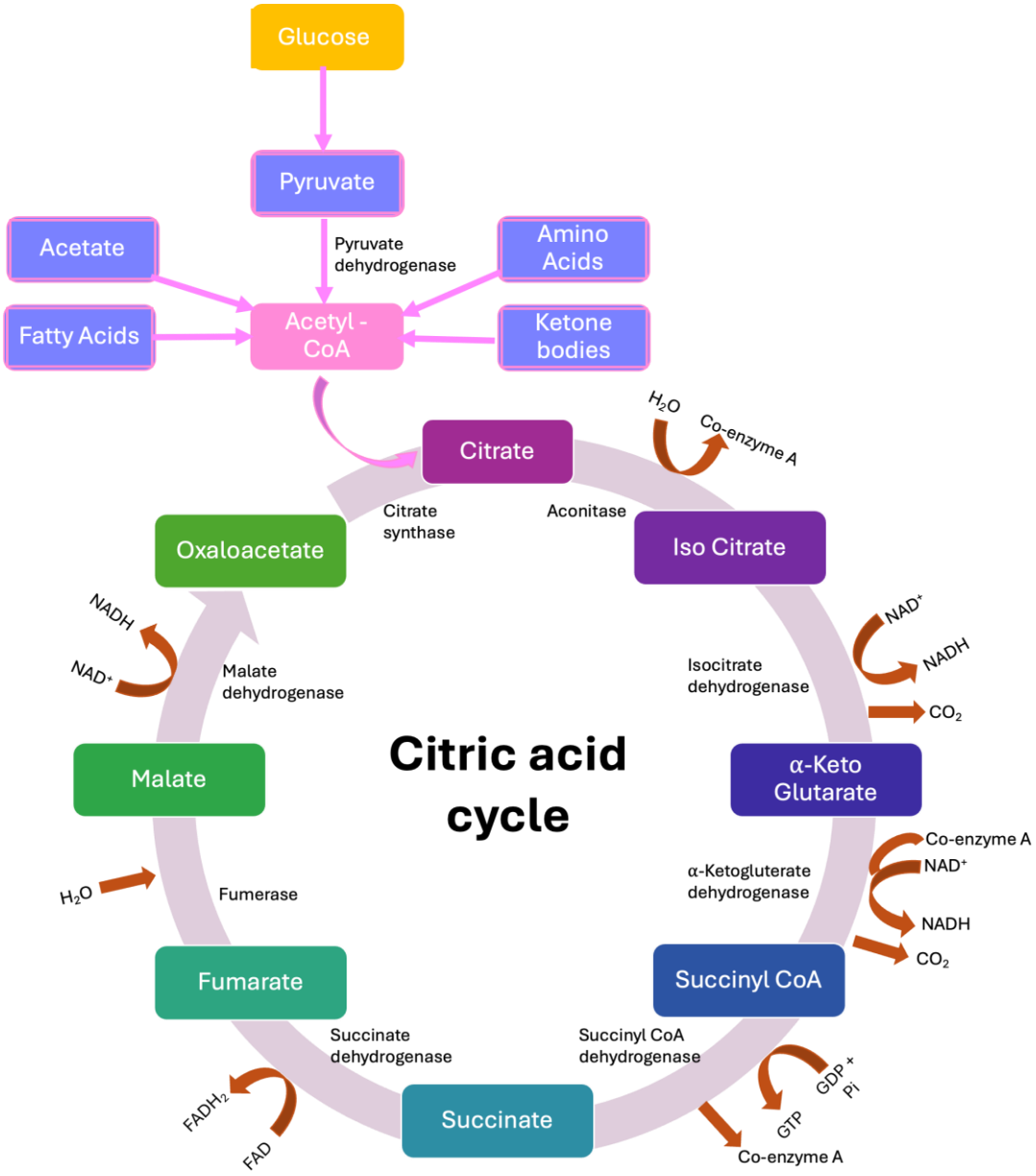



**Figure 4-T: The citric acid cycle**

The citric acid cycle (CAC) is also known as the Kreb's Cycle and tricarboxylic acid cycle. The citric acid cycle is an eight-step enzymatic process converting acetyl-CoA into oxaloacetate. Oxaloacetate is then converted back into glucose *via* downstream processing and the gluconeogenesis pathway. FADH and NADH are bioproducts of the citric acid cycle that are utilised in the electron transport chain[110].

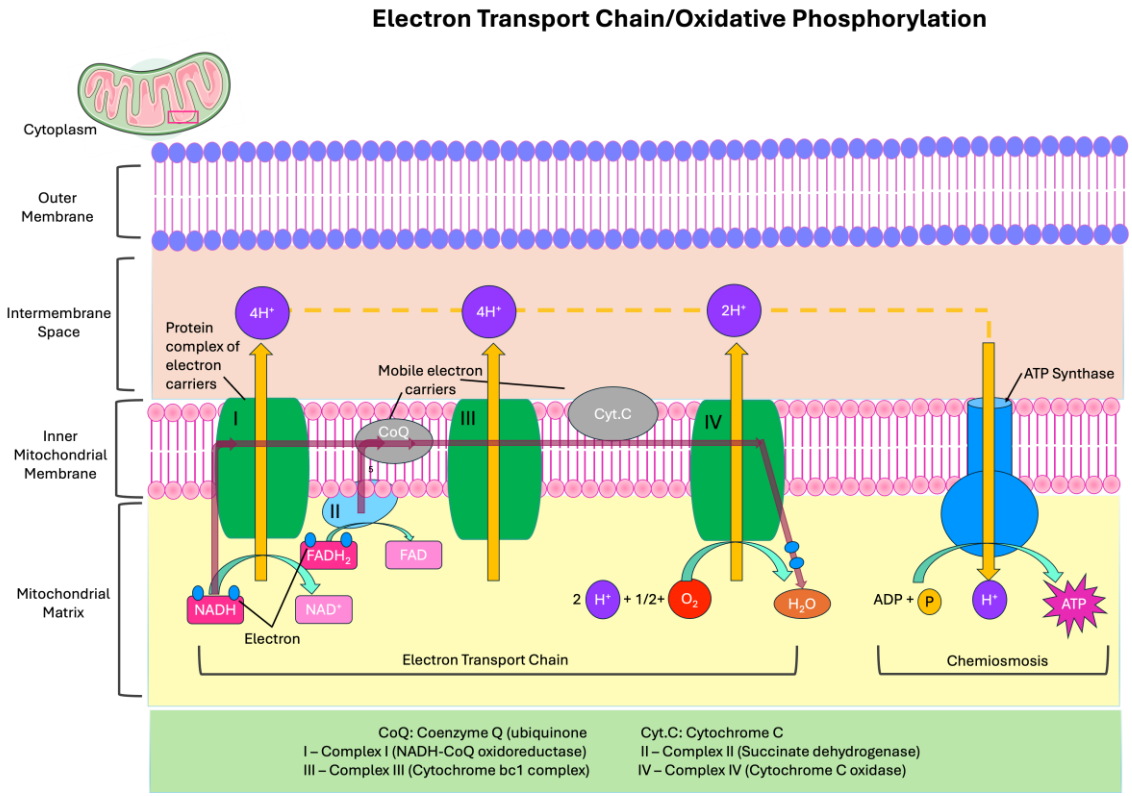



**Figure 4-U: The electron transport chain also referred to as oxidative phosphorylation**

The electron transport chain refers to a series of oxidation-reduction reactions to transfer electrons from NADH and FADH (generated during the citric acid cycle) to oxygen across protein complexes in the inner mitochondrial membrane to synthesise ATP. ATP synthase can generate between 30-32 ATP molecules, and is thus more efficient than glycolysis[224].

The kidney has a high metabolic rate[227], filtering 20% of cardiac output equivalent to 160-180g glucose/day[180,188]. The kidney consumes a large amount of energy to undertake its primary role in filtering the blood, excreting waste products and balancing electrolytes[188]. Blood flow, tissue oxygenation and metabolic requirements vary substantially across the kidney. Partial oxygen pressure in the cortex is four to five times higher than in the medulla; therefore typically nephron regions in the cortex will use oxidative phosphorylation to generate ATP, whilst regions in the medulla depend more

upon glycolysis[227]. In fact different regions of the nephron use and obtain glucose *via* different metabolic pathways[110], typically driven by oxygen availability in that region; the cortex of the kidney is more oxygenated than the medulla[188,227]. Podocytes, for example, have a reduced mitochondrial density compared to other cells types, with metabolomic analysis of podocytes from mice indicating that podocytes generate ATP *via* anaerobic glycolysis[228]. The proximal tubule generates ATP *via* the ETC (Figure 4-U) driven by FAO – see Figure 4-V. These cells have a high metabolic demand to facilitate their role in molecule transport[229], and are abundant in mitochondria[110] facilitating FAO, the CAC and the ETC. Additionally, metabolism under physiological conditions in the proximal tubules is oxygen dependent, making these cells particularly susceptible to hypoxic conditions. Under physiological conditions, proximal tubules have limited capability to utilise glucose to generate ATP[110] but can make a transient switch to glycolysis, as an immediate response to injury[229]. Ongoing metabolic dysfunction in proximal tubules associates with mitochondrial dysfunction, lactic acidosis[230], tubular degeneration, inflammation and fibrosis[188]. In IRI mice models gluconeogenesis is downregulated, as is the RNA expression of the rate limiting enzymes (Figure 4-S) associated with gluconeogenesis[185].

The proximal tubules absorb most of the filtered glucose from the primary kidney filtrate, returning the glucose to the bloodstream or to the distal tubules for glycolysis. The proximal tubules contribute 40% of systemic glucose *via* gluconeogenesis[185] (Figure 4-S), which is also redistributed to the bloodstream or other regions in the nephron. Gluconeogenesis is an anabolic process catalysed by 11 enzymatic reactions converting pyruvate to glucose - sources of pyruvate to drive gluconeogenesis are variable[187]. Most

reactions in the gluconeogenesis pathway are the reverse of those in the glycolysis pathway, bar four steps which are irreversible and specific to the pathway. The four enzymes are pyruvate carboxylase, phosphoenolpyruvate carboxykinase, fructose-1,6-biophosphatase (FBP1) and glucose-6-phosphatase[187]. In kidneys with prolonged fWIT, FBP1 was shown to be significantly degraded, indicating dysregulation in glucose production in the kidney *via* gluconeogenesis. During AKI both FAO and gluconeogenesis are disrupted resulting in renal injury[19]. Degradation of FBP1 has not been investigated in the kidney, yet in the liver FBP1 deficiency is associated with upregulation of fibrotic genes[188]. Loss of other enzymes in the gluconeogenesis pathway associate with fibrosis in the kidney, whilst the build-up of metabolic precursors contributes to mitochondrial dysfunction, decreased ATP production and cellular damage[188]. Dysregulation in glucose metabolism associated with glycolysis and gluconeogenesis is evident in the current study by significant degradation of FBP1 and proteins associated with the glycolysis pathway. This indicates significant disruption in ATP production in the kidneys and may be indicative of AKI-like injury in the DCD kidney. The metabolic dysregulation identified in this study likely impacts different regions of the kidney; further work is required to describe this. A larger in-depth analysis of glucose and metabolic changes in DCD kidneys is also required to describe the impact and long-term effects of glucose metabolism dysregulation in the DCD kidney.

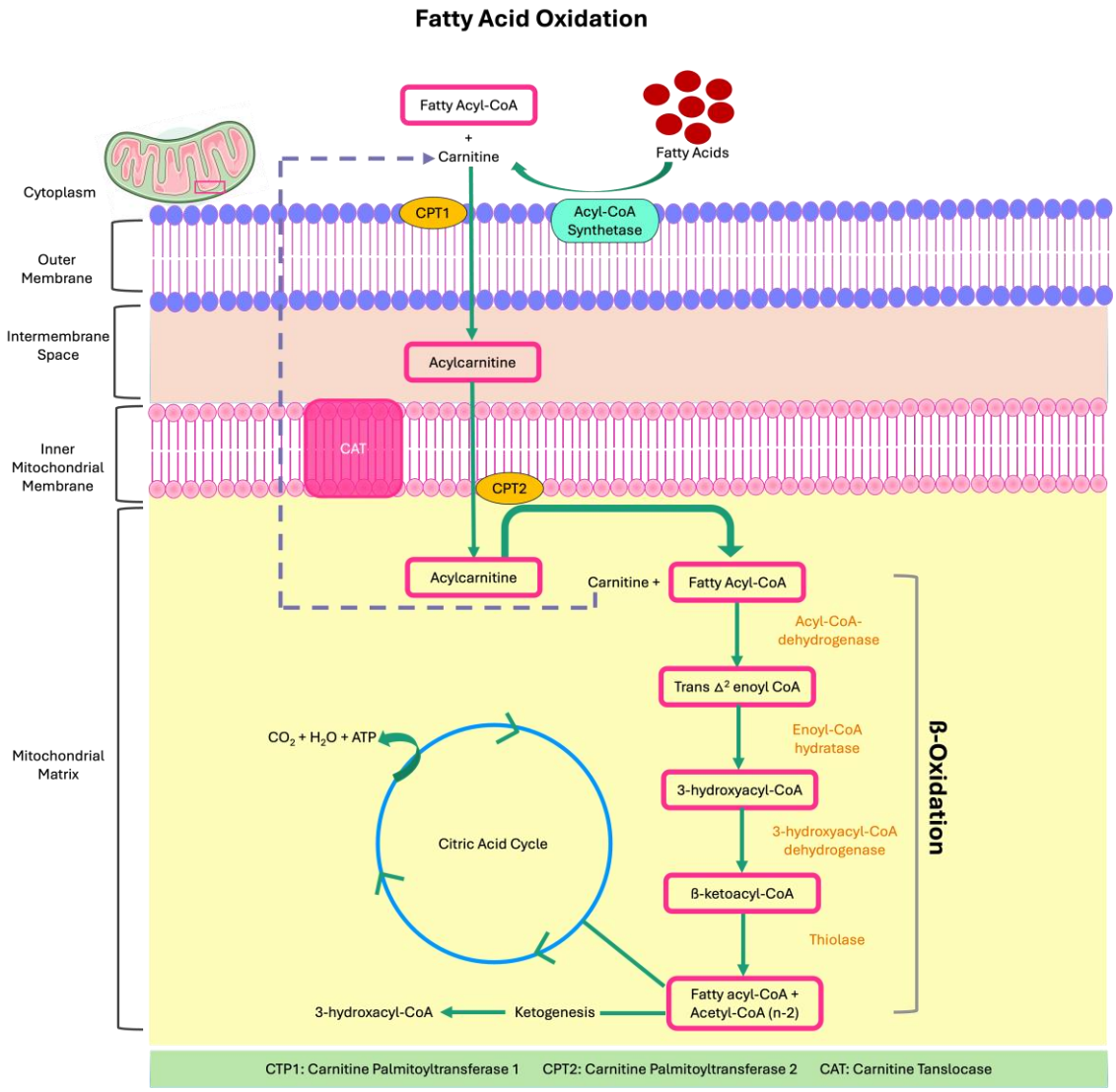



**Figure 4-V: Fatty acid oxidation pathway**

Fatty acid oxidation refers to the process where fatty acids are oxidised to produce acetyl-CoA which is further oxidised *via* the citric acid cycle and electron transport chain to produce ATP.

Oxidation of dietary molecules including vitamins act as co-factors supporting ATP-generation *via* the CAC and ETC. Vitamins such as B2 and B3 are precursors for flavin adenine dinucleotide (FAD) and NAD in the CAC and complexes I and II in the ETC. Biotin is a factor involved in fatty acid and amino acid metabolism, together with CoA and FAD; biotin is also important in heme biosynthesis which is essential in the formation of

cytochromes, for later stages of the ETC[231]. The role of vitamin deficiency in cellular health and disease is an area of growing interest[231]. Choline catabolism is another pathway highlighted in the heatmap as being dysregulated as fWIT increases and is part of a pathway facilitating the conversion of homocysteine to methionine (Figure 4-W). In this pathway dietary choline is transported into the cell where it is irreversible oxidised to form betaine. Betaine maintains glomerular osmolarity and supports reabsorption in the tubule[232], but also acts a methyl donor[232] for homocysteine which is then remethylated to form methionine, a process catalysed by BHMT[233]. Methionine is an essential amino acid, acting as a precursor for succinyl-CoA, cysteine, homocysteine and carnitine. It also has a role in managing oxidative stress, and in lipid metabolism[234]. In this study, BHMT has been shown to be significantly degraded with prolonged fWIT, which may have a limiting effect on the conversion of homocysteine to methionine, causing hyperhomocystemia. Hyperhomocystemia is a side effect of declining renal function and associates with deficiencies in vitamin cofactors B and folic acid. These deficiencies are believe to drive renal injury linked to oxidative stress, inflammation and endoplasmic reticulum stress[233], and ultimately may limit protein transcription.

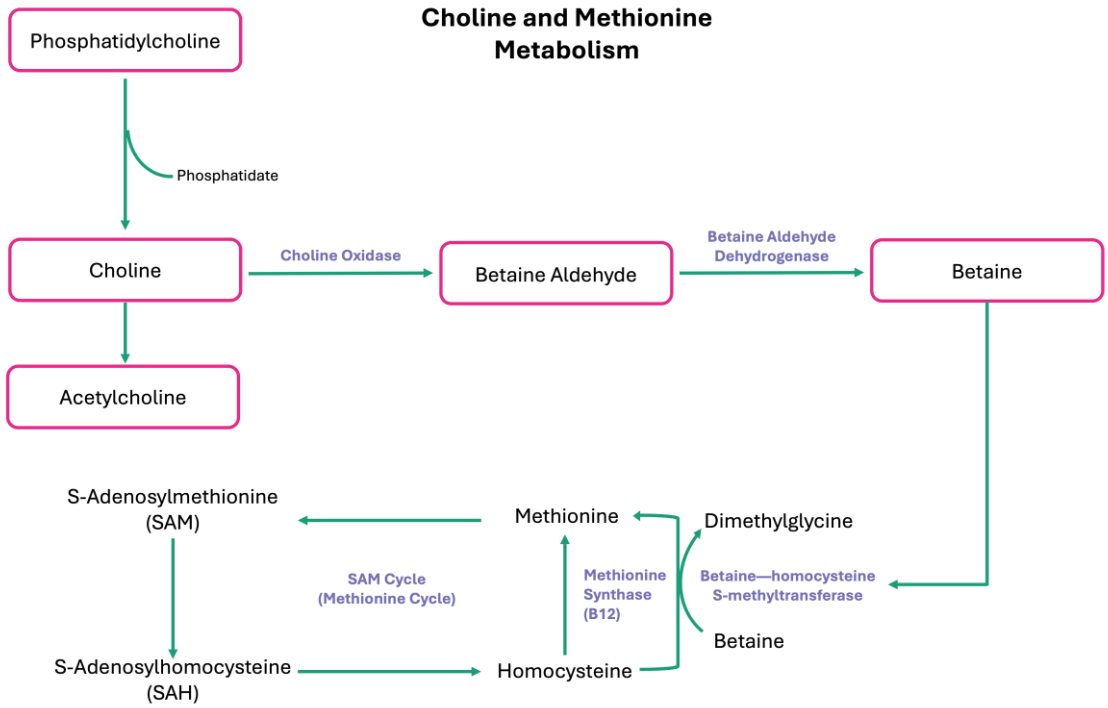



**Figure 4-W: Choline catabolism pathway**

Choline is transported into the cell and oxidised into betaine. Betaine then catalyses the conversion of homocysteine to methionine.

In line with peptide and protein observations, analysis of biological pathways impacted by increasing fWIT strongly indicate that renal injury increases with advance ischaemia. Several endogenous peptides described above are associated with significant dysregulation of biological pathways, including those highlighted in the heatmap. Dysregulation of cytoskeletal and matrix proteins, as well as metabolic processing including glucose metabolism, is likely to affect kidney function posttransplant. To investigate further the effect of the degradomic changes reported here, a wider and more high-powered study is required. The effect of the peptide and pathway changes reported require validation to quantify cell specific changes across the nephron. The results presented here provide initial evidence of injury in the DCD kidney associated

with prolonged fWIT, and further research is required to describe the mechanistic effects of fWIT-associated dysregulation for targeted intervention during deceased donor management.

### 4.5.5 Protease activity changes with prolonged fWIT

The activity of several proteases was shown to differ significantly as fWIT was prolonged. As fWIT increased, there was increased activity of LGMN and GRAM, and reduced activity of CATB, MMP3 and TPP1 (5% FDR) (Figure 4-N). Changes in protease activity with fWIT did not correlate with the number of substrates cleaved by each protease. Figure 4-M shows that GRAM, HTRA2, GRAA, GRAB and MEP1B cleaved the greatest number of peptides. Yet of these proteases, only GRAM activity correlated with prolonged fWIT (Figure 4-N). In Chapter 6, an in-depth analysis of the activity of each significant protease is reported.

Increased protease activity is indicative of increased generation of endogenous peptides associated with prolonged fWIT. Based on this analysis the activity of LGMN and GRAM increased with fWIT. LGMN, also known as asparagine endopeptidase (AEP), is a cysteine protease active in the lysosome[162]. LGMN is abundant in the kidneys and is active under acidic conditions, with a specificity to hydrolyse proteins after an asparagine or aspartic acid amino acid[235]. In this study, increased LGMN activity ($p=<0.001$) was linked to two protein substrates: HBA1 and BHMT. There is little in the literature reporting these proteins as substrates of LGMN, despite LGMN being well characterised. LGMN is important in protein processing and for hydrolysing cathepsin activity; dysregulation of LGMN is associated with multiple disease states, most predominantly cancer[235]. Other

than cathepsins, fibronectin and cystatin-C are commonly known substrates of LGMN[236,237]. LGMN in glioblastoma has been shown to be upregulated by HIF1α, under hypoxic conditions[162]. Experimental data on LGMN in this study cohort suggests that the observed increased activity may associate with fWIT-induced hypoxia.

Granzyme M (GRAM) belongs to the large family of granzyme proteases, expressed by immune cells[238]. GRAM is a serine protease expressed by cytosolic lymphocytes, especially natural killer cells, and mediates non-specific cell death[238,239]. Cleaving after methionine and leucine amino acids GRAM is also known to cleave FADD, ICAD and α-tubulin, disrupting the microtubule network[238]. The specific implications of GRAM dysregulation in the kidney are poorly reported in the literature, highlighting another area of research for future work. GRAM in the DCD kidney cleaved over 150 endogenous peptides, potentially inducing cell death and cytoskeletal disruption.

Cathepsin B (CATB) is a cysteine protease part of the cathepsin family of 19 proteases[240]. CATB also acts as a carboxydipeptidase cleaving amino acids at the C-termini of a peptide. Similar to LGMN, CATB is a lysosomal protease that normally functions at an acidic pH, yet under pathophysiological conditions can leak out of the lysosomes and be active in the cytosol at a higher pH, activating cell death and inflammatory pathways[241]. The specificity of CATB is variable, but CATB is reported by UniProt to have a preference for arginine in the P1 and P2 position. CATB is inhibited by cystatins, serpins and thyropins[240]. In the kidney, CATB is expressed by many cells, including endothelial cells and PTECs, and has been reported to maintain turnover of proteins in the glomerular ECM. Substrates of CATB include perlecan, collagen IV, laminin, fibronectin, TIMP5,

BCL2, BCL-XL, and TFAM. In proximal tubule cells, CATB has been shown to be taken up by megalin receptors mediating endocytosis[240]. Downregulation of CATB, as observed in the current study, reduces glomerular intracellular protein degradation in rat mesangial cells[242] and is associated with increased fibronectin in the glomerulus of diabetic rats[243]. CATB downregulation may also associate with reduced degradation of ECM and BM proteins and may cause fibrotic lesions in the donated kidneys; to confirm this, protocol biopsies would need to be evaluated.

Matrix metalloproteinase-3 (MMP3) is part of the large zinc dependant matrix metalloproteinase family of endopeptidases that can degrade all components of the ECM[244]. MMP3 specifically targets collagens, laminins, aggrecan, fibronectin, fibrinogen, and MCP-1 whilst also activating other MMPs, cleaving between hydrophobic residues[244,245]. In the kidney, MMP3 is found in the tubular regions of the nephron, including the proximal tubule, loop of Henle and distal convoluted tubule, yet not in the glomerulus. MMP3 has been shown to induce EMT in the tubules, which is a known feature of fibrosis[244]. MMP3 serum levels increase as kidney function declines in CKD[246], whilst MMP3 abundance increased in the S3 region of the proximal tubules in mice IRI models [245]. MMP3 can also activate pro-inflammatory mediators including TNFα and osteopontin[247]. In this study, reduced MMP3 activity may associate with reduced protein turn over in the tubular region of the nephron, likely associated with matrix proteins and reduced activity of other MMP substrates.

Tripeptidyl Peptidase 1 (TPP1) is a lysosomal serine protease that has two key functions: N-termini tripeptidyl exopeptidase, cleaving tripeptides at the N-termini at pH 5, and as

a endopeptidase active at pH 3[248,249]. TPP1 cleaves between hydrophobic residues and has been implicated as a potential therapeutic target in Alzheimer's disease[248]. TPP1 has been reported in the distal tubule and, to a lesser extent, the proximal tubule of the kidney, yet not in the glomerulus. There is minimal literature investigating the role of TPP1 in the kidney and in the current study the substrates associated with TPP1 demonstrate auto-catalytic activity.

Taken together, changes in protease activity observed in kidneys as fWIT is prolonged is indicative of significant changes in protein turnover, most probably affecting the BM and ECM of different region of the nephron. Reduced BM and ECM protein turnover, indicated by reduced MMP3 and CATB activity, may associate with fibrotic injury in the kidneys. Increased LGMN activity with prolonged fWIT may be indicative of progressive hypoxia in the kidney, and may be driven by increasing HIF1$\alpha$ or pro-inflammatory mediators[250]. At a lax 25% FDR threshold, an additional three proteases were identified as changing with prolonged fWIT, suggesting that further insight with a larger cohort (higher statistical power) may be possible. As proteases are viable therapeutic targets, future work should look to investigate the implications of changing protease activity in the different regions of the kidney to associate this with changes in protein degradation that may improve or limit kidney function.

### 4.5.6 The endogenous peptide profile and protease activity of DGF kidneys was different to that of kidneys with prolonged fWIT

Delayed graft function occurs in at least 50% of DCD KTxs and can associate with reduced kidney function in the long term[251]. In the current study, due to sample limitations the

biopsies were not selected based on recipient outcomes, resulting in a disproportionate number of kidneys with IF compared to DGF. However, as there were 10 kidneys with DGF, the decision was taken to proceed and evaluate the endogenous peptide profile and protease activity in these kidneys compared to kidneys with an IF posttransplant. PNF kidneys (n=1) were removed from the analysis.

Differences in IF and DGF were calculated using a t-test with multiple testing correction. Significant peptides (Figure 4-O) and proteases (Figure 4-P) identified in this analysis were not common to those identified when the kidneys were profiled according to fWIT length. Ketimine reductase μ-crystallin (CRYM), also known as thyroid binding hormone, is expressed in the brain, muscle, prostate and kidneys, and is linked to several neurological disorders[252]. In this analysis, CRYM was the only significantly degraded protein associated with DGF. CRYM binds thyroid hormones that regulate metabolism – specifically, CRYM reduces ketimine in the lysine degradation pathway[252]. There is little reported about the role of CRYM in the kidney, however in rat kidneys CRYM increases with age and hyperglycaemia, reducing glucose-induced ROS[253].

When the FDR was increased to 10%, the increased degradation of proteins associated with immune response (CDH3 and CD14) and metabolic pathways (PKM) were shown in kidneys with DGF. The abundance of AKAP12, CNN3 and HNRNPU endogenous peptides, however, decreased in kidneys with DGF; CNN3 and HNRNPU are associated with cytoskeletal regulation and RNA binding, respectively. The evaluation of endogenous peptides associated with DGF in this cohort provided very little information to describe potential pathways of injury and therefore warrants a more in-depth evaluation using a

larger cohort. In a recent study by Lo Faro *et al*, the authors reported significant dysregulation of proteins associated with metabolic pathways in kidneys with DGF, which is exacerbated in kidneys with long DGF (more than seven days)[96]. Utilising DCD kidneys from the QUOD biobank, the authors of this study described the downregulation of aerobic respiration and mitochondrial ATP synthesis in DGF kidneys, with proteins associated with the CAC and carboxylic acid metabolism downregulated specifically in kidneys with prolonged DGF. Here, it has been shown that kidneys with prolonged fWIT have significant dysregulation in metabolic processes affecting ATP synthesis. The study by Lo Faro and colleagues is the first to indicate a different proteomic profile of kidneys with IF and DGF posttransplant and key differences between kidneys that have a short and long DGF[96]. The proteomic data presented by Lo Faro *et al* could be further examined and compared with the peptidomic data generated in this study to identify common proteins associated with DGF. Such an analysis would not only validate the findings of both studies but could serve as preliminary data for a larger study.

Cathepsin D (CATD) activity was significantly increased (p=0.006) in DCD kidneys with DGF compared to those with IF posttransplant. CATD is a lysosomal protease belonging to the asparagine family of proteases, known to have a role in ECM proteostasis, glomerular permeability, endothelial functions, inflammation and apoptosis[254]. In the kidney, CATD is expressed in the podocytes, endothelial cells and tubular cells[254]. In the podocytes and tubular cells, CATD has an active role in regulating apoptosis; in endothelial cells, CATD regulates fibrosis and inflammation moderating endothelial dysfunction. Dysregulation of CATD is associated with glomerular disease, AKI and CKD[254]. In IRI mouse models CATD is associated with increased tubular damage including

tubular dilation and apoptosis[255]. Fibrosis in IRI mice can be ameliorated by the addition of CATD inhibitor[256].

As the initial sample selection did not account for associated transplant outcomes, this study did not have the statistical power to identify peptide or protease changes related to transplant outcomes. The samples selected for this study do not reflect the ~50% DGF rate reported following DCD transplant, which is most likely an effect of the small sample number. Additionally, there were insufficient sample replicates at each WI time point, with reported IF or DGF posttransplant to allow for a meaningful analysis. DGF is a complex and multifactorial phenotype that leads to variable outcomes. Although prolonged WI strongly correlates with increased incidence of DGF in DCD kidneys, it is likely that other donor and recipient factors contribute to this outcome, as well as how well a kidney recovers from DGF in the longer term. Future studies should look to analyse DCD kidney biopsies comparing those with IF, DGF and PNF for markers indicative of injury. A comparison between DBD and DCD kidneys with DGF would also be valuable, to identify variances in the DGF phenotype associated with donor type. Based on recent metadata reviews by Philips *et al*[83] and Dumbill *et al*[86] highlighting the important association between DGF duration and long term graft outcomes posttransplant, samples should be selected and grouped according to DGF duration. An in-depth and appropriately powered analysis of DGF in DCD kidneys is required to describe biomarkers and therapeutic targets and could provide valuable insight for future therapeutics.

### 4.5.7 Limitations and suggested expansions to the study

The remit of the study presented in this chapter was limited by several factors. Firstly, missing data during sample selection significantly reduced the number of biopsies that could be selected. Recording of fWIT during donor retrieval was not consistent, which reduced the cohort of donors that could be selected for this study. If more donors had a recorded fWIT, additional factors including immediate and 12-month posttransplant function could have been considered during sample selection to expand the scope of this study. Additionally, several other factors may contribute to organ injury and peri-mortem ischaemia, including the donor's medical history, episodes of cardiac arrest, and haemodynamic instability and inflammation during donor management. These variables cannot be reliably accounted for using standard donor demographic data. As a result, these critical factors are difficult to control in experimental and retrospective studies like the one presented here. Additionally, a more comprehensive oversight of kidney function posttransplant could have enabled correlations between observed protein and pathway changes and transplant outcomes, to provide a better understanding of the implications of prolonged fWIT.

This study was also limited by variability in tissue biopsy size based on different collection protocols. The protein yield obtained from each biopsy varied significantly and in some instances was low. Low protein yield recovered in some biopsies reduced the starting protein concentration for sample preparation and meant that the proteomes of these kidneys could not be concurrently analysed. Profiling the proteome of the same kidneys would have provided additional quantifiable data to support the reported findings, as well as insight into the effects of the measured increase in degradation on

proteostasis in the kidney. However, the current sensitivity of HUNTER is specifically based on the enrichment of endogenous N-termini, which comes at the expense of other peptides generated during digestion. As a result, the current protocol is not compatible with dual proteome/peptidome analysis. Further protocol development alongside advancements in mass spectrometry will likely continue to reduce the required starting material required for both peptidomics and proteomics.

Bioinformatic tools to support the analysis of the mass spectrometry data are readily available online at no cost. However, several of these databases including TopFIND draw on outdated versions of the UniProt (version 2019_07) and MEROPS (version 12.1) databases. As indicated in the results, only a limited number of the endogenous peptides identified in this study were matched to a cleaving protease (14%). To identify the cleaving proteases for the unidentified peptides would require painstaking peptide by peptide analysis. Future studies evaluating the degradome need to take this significant limitation into consideration and may look to update existing resources or establish a new platform.

In this chapter, significant changes in the DCD kidney degradome associated with prolonged fWIT have been described. Specifically, as fWIT increases, metabolic processes in the kidney are dysregulated and are likely to affect posttransplant kidney function. Metabolic dysregulation, specifically glucose metabolism associated with fWIT will likely have a variable impact on different regions and cells of the kidney. Further investigation is necessary to fully understand the effects of metabolic dysregulation in the kidney before clinical interventions can be developed. To explore the impact of

reduced glucose on podocytes and PTECS, a hypoxic immortalised podocyte and PTEC cell model was optimised, as described in Chapter 5. Podocytes and PTECS were cultured under both normoxic and hypoxic conditions for up to 24 hours in media with and without glucose. During this period, changes in cell morphology, protein degradation and protease dysregulation were then measured (Chapter 6). By examining the cell-specific responses to hypoxia and glucose deprivation, cell specific alterations that may mirror kidney injury in DCDs can be further explored. Profiling changes in DCD kidneys and linking them to posttransplant function will offer further insight into the severity of ischaemia- induced injury in DCD kidneys.

Ongoing work will focus on validating protein and protease changes measured in DCD kidneys using alternative techniques, including immunoassays. Changes in protease activity will also be evaluated using protease-based probe assays. In this study, LGMN activity significantly increased with fWIT, however the downstream implications of this increased activity were not measured and should be investigated in the future. CATB activity was also observed as significantly decreasing with fWIT, which is likely to affect proteostasis of matrix proteins which can have significant implications in the glomerulus and tubules. Validation and profiling of protease activity changes associated with fWIT-induced ischaemia is essential, as dysregulated protease activity can have a profound effect on cellular function and biological processes ultimately reducing the function of the transplanted kidney.

## 4.6 Conclusions

Analysis of the DCD kidney degradome has highlighted several significant biological changes affecting glucose metabolism, cellular metabolism, cell interaction and matrix proteins associated with prolonged fWIT. Degradation of multiple cytoskeletal proteins increased with fWIT, as did the gluconeogenesis-specific rate limiting enzyme FBP1. Protease activity was also disturbed by increasing fWIT, which is likely to have downstream implications on kidney function and longevity posttransplant. Marked dysregulation of cytoskeletal and ECM proteins, along with metabolic processes, could associate with increased incidences of adverse posttransplant outcomes in DCD recipients and following validation could serve as therapeutic targets for intervention.

# Chapter 5 Optimisation of a hypoxic human kidney cell model

## 5.1 Introduction

Oxygen is essential to many biological functions, specifically the generation of ATP[257], and is transported around the body *via* the blood. Organ hypoperfusion in the DCD occurs following WLST as the blood pressure of the donor drops until cessation, reducing the oxygen supply to the organs. This induces a period of hypoxia which is later confounded by CIT, prior to reperfusion posttransplant. Under hypoxic conditions tissue damage occurs rapidly, for which the kidney is particularly susceptible due to its high oxygen and metabolic requirement[258]. Prolonged hypoxia is associated with the pathogenesis of AKI.

Production of ATP in the kidney is mostly *via* aerobic respiration and metabolism, yet this is region and cell type specific. Some cells in the medulla are dependent upon anaerobic metabolism due to poorer oxygen supply to this region of the kidney. As described in Chapter 1 (1.2) the nephron is the functional unit of the kidney, with each region of the nephron being anatomically and metabolically unique[11], specific to their function (Figure 1-C). The renal corpuscle is the blood filtering component of the nephron that includes the glomerulus (capillary tuft) and the Bowman's capsule. Blood filters from the glomerulus through the GFM and podocytes into the proximal tubule ( Figure 5-A). Podocytes are terminally differentiated epithelial cells that contribute to the maintenance of the GBM by secreting collagen[259]. Podocytes have a unique cellular structure, composed of a cell body and foot processes, which are maintained by an intricate cytoskeletal network[259]. The podocyte foot processes contract to modulate ultrafiltration in response to mechanical stimuli; podocytes are interconnected by the slit diaphragm which stabilises the glomerular architecture[260]. Several glomerular

pathologies and disorders associate with foot process effacement causing proteinuria and disease progression[219]. Podocyte cells have a high energy requirement to maintain cellular function, with dysregulation in mitochondrial dynamics associated with the development and progression of focal segmental glomerulosclerosis[228,261]. In rats, under hypoxic conditions, there is disruption of the glomerular architecture and increased permeability of the glomerulus, evidenced *via* pas staining[262]. In these animals, there is a substantial decrease in podocyte number and foot process effacement, disrupting the slit diaphragm[262]. Elevated HIF1α in podocytes has previously been associated with a loss of podocyte specific gene expression, including podocin and nephrin[263]. Ischaemic injury also causes significant disruption to the tubules of the nephron[228].

Proximal tubule cells carry out a diverse regulatory and endocrine function, and the active reabsorption of solutes and excretion of waste products[264]. These cells are anchored to a thin BM, supporting cell structure and interaction with the ECM[265]. The proximal tubule cells have a large energetic requirement to maintain their function and rely on oxidative metabolism to facilitate ATP generation[266]. The proximal tubules have limited capacity for glycolysis[267]. Dysregulation of proximal tubule metabolism is associated with onset and progression of AKI and fibrosis[267]. Glucose regulation in the proximal tubules is also of importance to maintaining their function, with glucose reabsorption under physiological conditions controlled by insulin and systemic metabolism[268]. HIF stabilisation in proximal tubule cells during hypoxia has a major role in ischaemia-induced AKI[266]. Importantly, proximal tubule cells have advanced recovery capabilities when ischaemic injury is mild. Under chronic ischaemic conditions, injury will progress to chronic pathologies reducing kidney function in the long-term[266].

Figure 5-A is a schematic of the nephron that highlights key cellular features. Based on previous research and a foundational knowledge of the role each cell type has in maintaining kidney homeostasis, an understanding of the impact hypoxia has on these cells is essential to delineate the effect of ischaemia on the kidney in DCD transplantation.

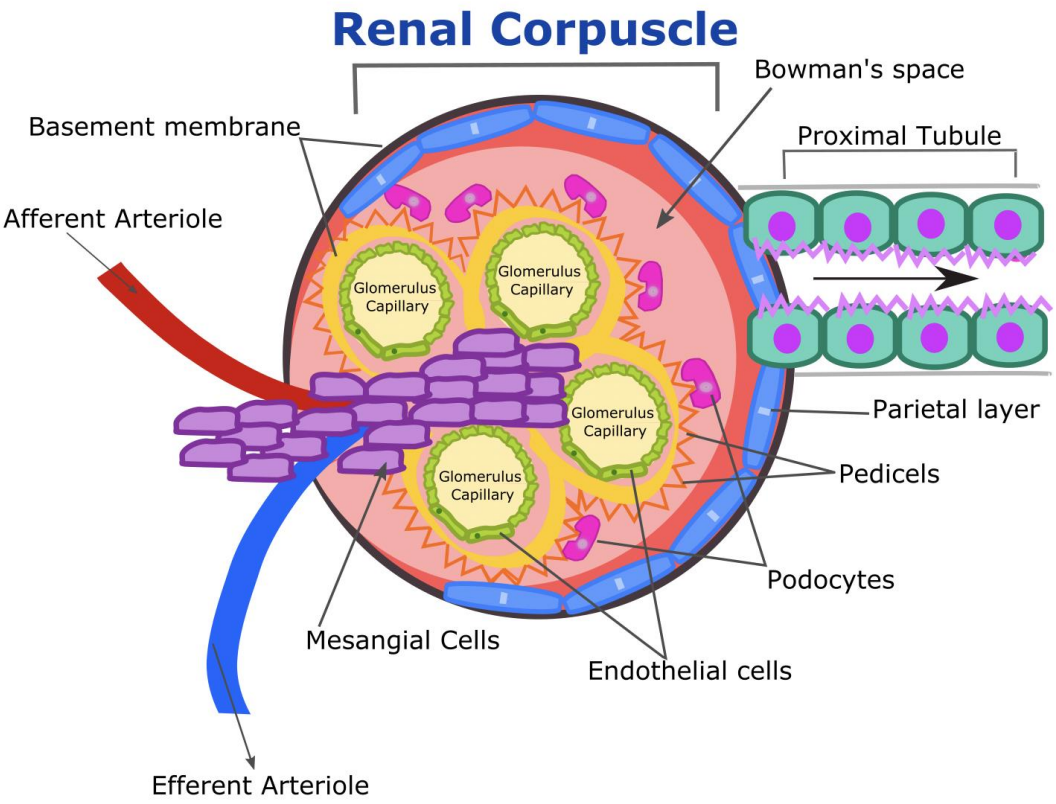



**Figure 5-A Schematic of the glomerulus and proximal tubule highlighting key cell structures**

The glomerulus and proceeding proximal tubule are composed of heterogenous cells working together to maintain the glomerular filtration barrier and nephron function. In this study, podocyte and proximal tubule epithelial cells were cultured under normoxic and hypoxic conditions.

## 5.2 Hypothesis and aims

In this chapter, the development of a hypoxic human kidney cell model is described. Podocytes and PTECs are morphologically, metabolically and functionally unique cells that are essential to maintaining good kidney function. Hypoxia is a consequence of prolonged fWIT and likely has a differential impact on these two cell types. In Chapter 4 extended fWIT was shown to cause morphological and metabolic changes in the kidney, however these changes could not be ascribed to specific cells or nephron regions. To investigate the impact of fWIT and hypoxia on kidney cells, the work presented in this chapter aimed to develop and optimise a hypoxic kidney cell model using immortalised human podocytes and PTECs. Additionally, as glucose metabolism was shown to be dysregulated in DCD kidneys with prolonged fWIT, podocytes and PTECs were cultured under normoxic and hypoxic conditions in media with and without (+/-) glucose. Initially, three methods – nitrogen-fed incubator, cobalt chloride ($CoCl_2$) and GasPak-pouch system – were tested to promote and sustain hypoxia for a defined time-period in the cells.

## 5.3 Materials and methods

### 5.3.1 Culturing and differentiating cells for inducing hypoxia

Podocyte and PTEC cells were grown in T75cm$^2$ culture flasks until they were 70% confluent before being redistributed into 6-well plates as described in Chapter 3 (3.5.1.2). Once confluent the cells were differentiated at 37˚C for 10 days. The number of plates prepared for each experiment was pre-determined based on the experimental design. After the cells were differentiated, the culture media was changed to media without FCS, ready for treatment.

### 5.3.2 Methods to induce hypoxia

Following review of hypoxic cell models reported in the literature, three methods to induce hypoxia were tested.

1. Nitrogen incubator, set to 1% oxygen.
2. Cobalt chloride ($CoCl_2$) treatment.
3. GasPak-pouch system, used as an alternative to hypoxic chambers, as previously described in the literature[269].

Initial method tests compared normoxic to hypoxic conditions in culture media with glucose, for up to 48 hours.

#### 5.3.2.1 Nitrogen incubator

Utilisation of a tri-gas incubator to induce hypoxia is well established in the literature. Nitrogen influx into the incubator displaces and reduces oxygen levels. For this experiment, a tri-gas incubator was set to 37˚C, 1% oxygen and 5% $CO_2$ levels. Cells were incubated up to 48 hours, collected regularly in line with the experimental plan.

#### 5.3.2.2 Cobalt chloride

Cobalt chloride ($CoCl_2$) is a common method to chemically induce a state of elevated HIF' in cells, 'mimicking' hypoxia. When applied to cells $CoCl_2$ artificially stabilises HIF1α stimulating the transcription of hypoxia associated genes[270]. Cobalt substitutes iron in PHDs stabilising HIF under aerobic conditions[257]. Typically, $CoCl_2$ induces hypoxia within two hours, and $CoCl_2$ in excess of 300µM can be cytotoxic leading to cell death[257].

Cobalt chloride was diluted in culture media to a concentration of 1,000µm, then diluted as required. Multiple dilutions of $CoCl_2$ were tested to check cell toxicity. Concentrations compared to an untreated control included 1,000µM, 500µM, 250µM, 100µM, 50µM, 25µM and 10µM. As expected, concentrations over 250µM induced cell death within 24 hours. Final concentrations tested were 250µM, 100µM, 50µM, 25µM and 10µM, in culture media without FCS +/- glucose.

#### 5.3.2.3 Anaerobic GasPak-pouches with oxygen absorbers

The third method to induce hypoxia in the kidney cells used a commercially available single use sealable pouch system: BD GasPak EZ gas generating pouch system (26683, (BD) Fisher Scientific). The GasPak-pouches described in this study were initially developed to culture bacteria under hypoxic conditions. The GasPak-pouch is a sealable bag with a gas-generating sachet, containing inorganic carbonate, activated carbon, ascorbic acid and water that is activated on exposure to air, rapidly reducing the oxygen concentration within the pouch upon sealing. According to the manufacturer specifications, the oxygen concentration within the pouch is reduced to ~1% within two and a half hours, confirmed by the inclusion of the anaerobic indicator on each gas

generating sachet – white indicates the pouch is anaerobic, whilst blue indicates the conditions are aerobic (Figure 5-B). Previous reports using this hypoxic system are limited. For initial survival tests, cells were cultured successfully for up to 48 hours. Induction of hypoxia was then confirmed using qPCR.

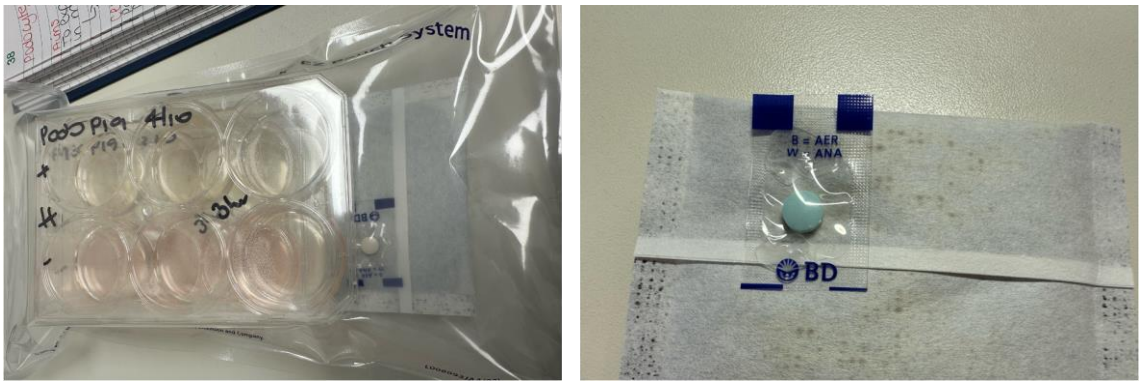



**Figure 5-B: Photo of cells cultured using the GasPak-pouch system with the gas generating sachet and environmental indicator**

Cells were cultured in GasPak-pouches with gas generating sachets to induce hypoxia. Each gas generating pouch has an environmental indicator attached indicating if the pouch system is anaerobic (white) or aerobic (blue).

### 5.3.3 Induction of hypoxia using GasPak-pouches in media +/- glucose

As glucose metabolism was shown to be significantly disrupted by prolonged fWIT, podocytes and PTECs were cultured in media +/- glucose under normoxic and hypoxic conditions for up to 24 hours (h) in serum-starved RPMI or DMEM (medias listed in Table 5-A). DMEM media was supplemented with Hydrocortisone, Epidermal growth factor and Triiodo-L-thyronine, as described in Chapter 3 (3.5.1.1). Cells were collected at regular intervals: 30 minutes (m), 1h, 3h, 6h and 24h for analysis. Cells cultured under normoxic condition with glucose were considered the 'control' for experimental comparisons, as they represented the typical culture conditions for both the podocytes and PTECs.

| Cell Type | Media | Suppliers code and Supplier | Glucose concentration |
|---|---|---|---|
| Podocytes | RPMI-1640 | R8758, Sigma | 1.8-2.2g/L |
| Podocytes | RPMI Medium 1640 | 11879-020, Gibco | 0g/L |
| PTECs | DMEM-F-12 media | 31330-038, Gibco | 3.15g/L |
| PTECs | DMEM 1x | 31885-023, Gibco | 1g/L |

**Table 5-A: Cell culture media for normoxic and hypoxic cell treatments with/out glucose experiments**

Podocytes and PTECs were cultured in media with and without glucose under normoxic and hypoxic conditions to describe the effects of hypoxia and glucose on cells. In this table, the different culture medias used for these experiments are detailed.

### 5.3.4 Expression of hypoxia associated genes quantified using qPCR

Cellular response to hypoxia was quantified using qPCR (3.8). Expression of HIF1α, hypoxia-inducible factor 2-alpha (HIF2α) and prolyl hydroxylase domain enzymes-2 (PHD2) and prolyl hydroxylase domain enzymes-3 (PHD3) were measured as markers of hypoxia. All four genes are regulated by oxygen. Additional genes known to be upregulated by the stabilisation and binding of HIF to hypoxic response elements (HREs) were also measured as markers of the downstream effects of hypoxia.

Cultured podocytes and PTECs were collected and either RNA or protein extracted as described in Chapter 3 (3.8.1 and 3.5.1.3, respectively). Protein extracted from podocytes and PTECs was used in experiments described in Chapter 6.

## 5.4 Results

### 5.4.1 Optimising methods to induce hypoxia in podocytes and PTECs

Three methods were tested to induce hypoxia in immortalised podocytes and PTECs: a nitrogen-fed incubator, $CoCl_2$ treatment and GasPak-pouches. Cell survival was monitored over 48h and hypoxia then confirmed in GasPak-pouch treated cells using qPCR.

The use of a nitrogen incubator had several limitations and was eliminated as initial tests indicated that it was not a viable method to induce hypoxia in cells, namely that the hypoxic environment in the incubator could not be preserved at a constant level while also retaining access for culture maintenance tasks. Oxygen flooded the incubator upon opening the door and took several hours to return to a low oxygen concentration, meaning the cells were not truly 'hypoxic' for the planned incubation time.

Podocytes and PTECs were treated with various concentrations of $CoCl_2$, to determine the optimum concentration to induce hypoxia and check for cell toxicity. Initial tests proved that both cell types could tolerate $CoCl_2$ treatment up to 250µM. Second phase testing confirmed that podocytes (Figure 5-C) and PTECs (Figure 5-D) treated with 250µM $CoCl_2$ would survive in culture for up to 48h.

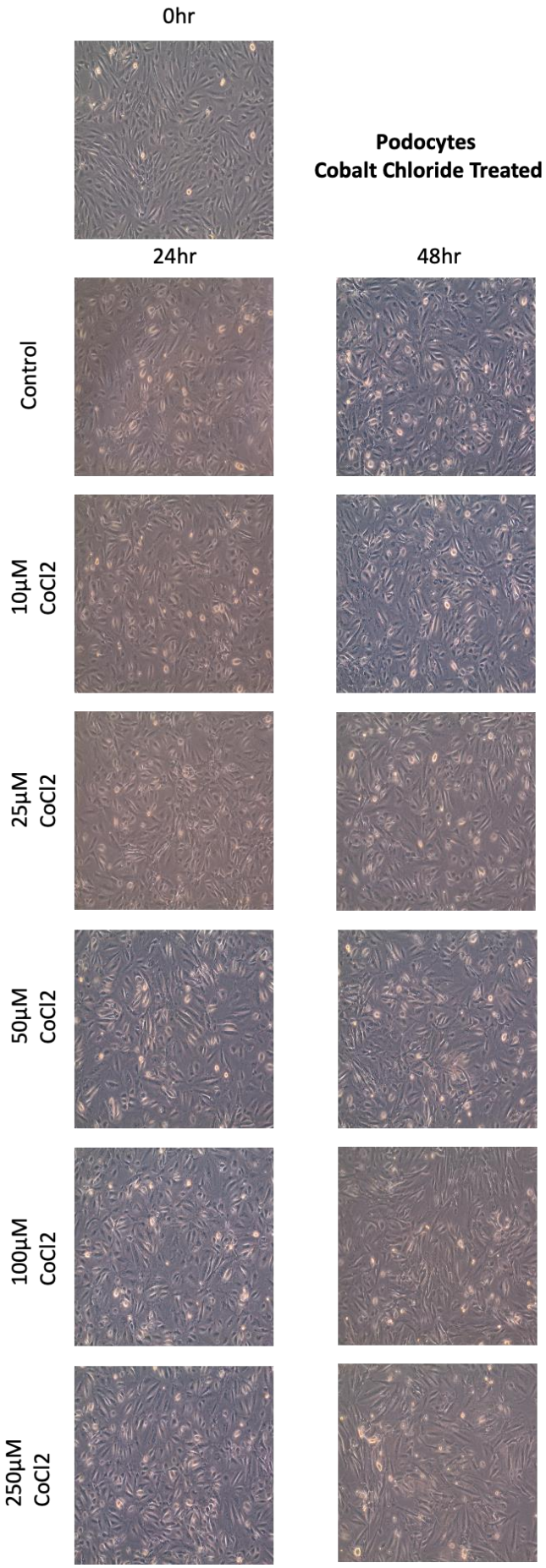

0hr
Podocytes
Cobalt Chloride Treated
24hr
48hr
Control
10µM CoCl2
25µM CoCl2
50µM CoCl2
100µM CoCl2
250µM CoCl2

**Figure 5-C: Podocytes cultured in CoCl2 for 24h and 48h**

Podocytes were cultured in various concentrations of $CoCl_2$ for 24h and 48h to confirm cell tolerance to the treatment and to determine a reliable concentration of $CoCl_2$to induce hypoxia. The podocytes survived for 48h in concentrations up to 250µM.

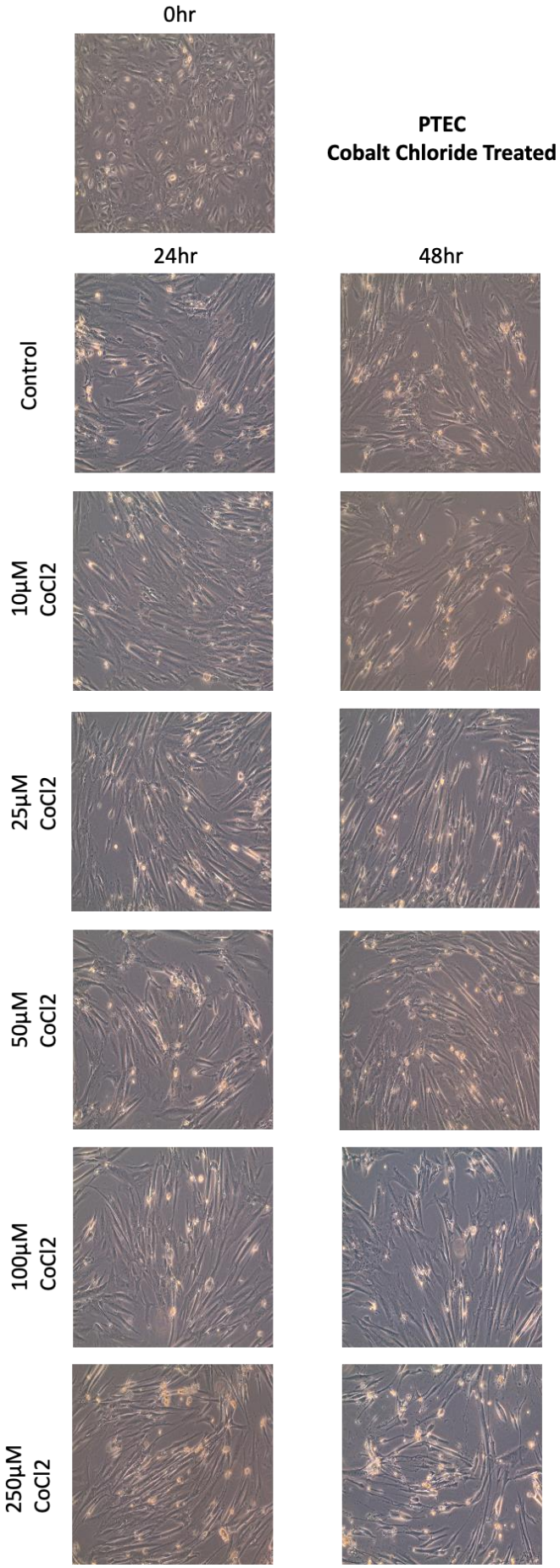

0hr
PTEC
Cobalt Chloride Treated
24hr
48hr
Control
10µM CoCl2
25µM CoCl2
50µM CoCl2
100µM CoCl2
250µM CoCl2

**Figure 5-D: PTECs cultured in CoCl2 for 24h and 48h**

PTECs were cultured in various concentrations of CoCl2 for 24h and 48h to confirm cell tolerance to the treatment and determine a reliable concentration of $CoCl_2$ to induce hypoxia. The PTECs survived for 48h in concentrations up to 250µM.

The use of GasPak-pouches to induce hypoxia in cell culture was recently reported by Moniz *et al*[269]. The GasPak-pouch system did not require any additional specialist equipment and proved to be user friendly, especially as the anaerobic environment could be monitored using the provided indicators. Initial validation tests showed that podocytes and PTEC cells would survive for up to 48h inside the GasPak-pouch in a 37˚C oxygenated incubator (Figure 5-E).

In this study, cell viability and number were not compared across treatment or culture conditions, as it became apparently early on that the nitrogen incubator and $CoCl_2$ models were not viable. Additionally, as the cells cultured in GasPak-pouches were collected for qPCR and Western blot analysis, cells were not available to assess cell viability. Trypan Blue, an azo dye, that penetrates the membranes of dead cells is commonly used to count live cells and calculate viability percentages, and could benefit future studies, as an easy reproducible method to measure changes in cell count and viability associated with different culture conditions.

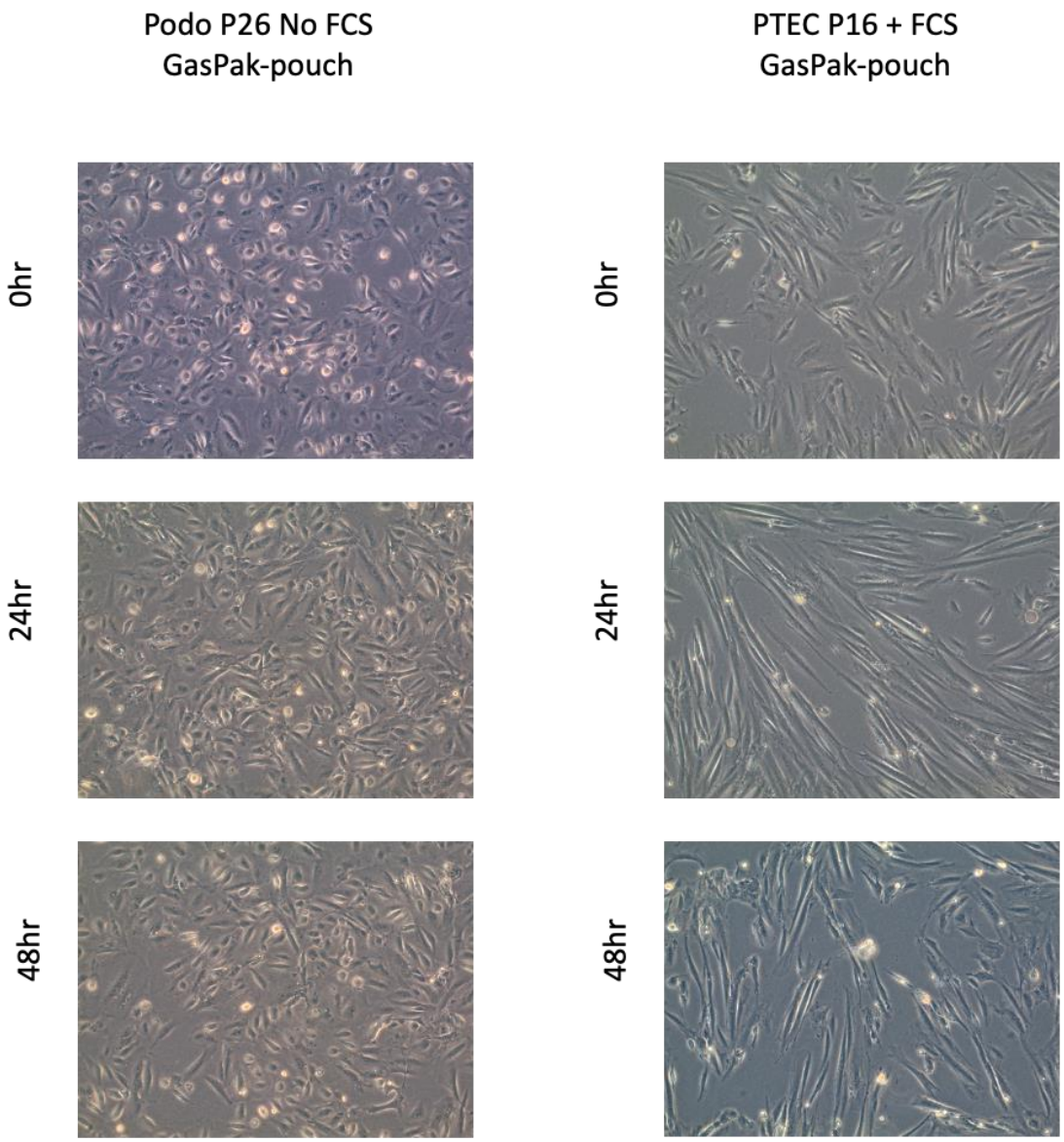



**Figure 5-E: Podocytes and PTECs cultured in GasPak-pouches for 24h and 48h**

Podocytes and PTECs were cultured in a 37˚C normoxic incubator. To induce hypoxia cell plates were put inside a GasPak-pouch with a gas generator that absorbs oxygen. Both cell types survived up to 48h in culture.

### 5.4.2 Hypoxic cell model experimental plan

Figure 5-F outlines the experimental plan for this chapter, starting with the protocol optimisation as described above. As both the podocytes and PTECs survived for up to 48h in the GasPak-pouch, this method was selected for further optimisation as it depleted oxygen *via* the gas-generating inserts rather than chemically induced hypoxia simulation ($CoCl_2$). This approach was reliable, was easy to reproduce, and mimics the *in vivo* environment during fWIT. The next phase of the experiment was to culture the cells under normoxic and hypoxic conditions in media +/- glucose for up to 24h and quantify the expression of hypoxia-associated markers using qPCR.

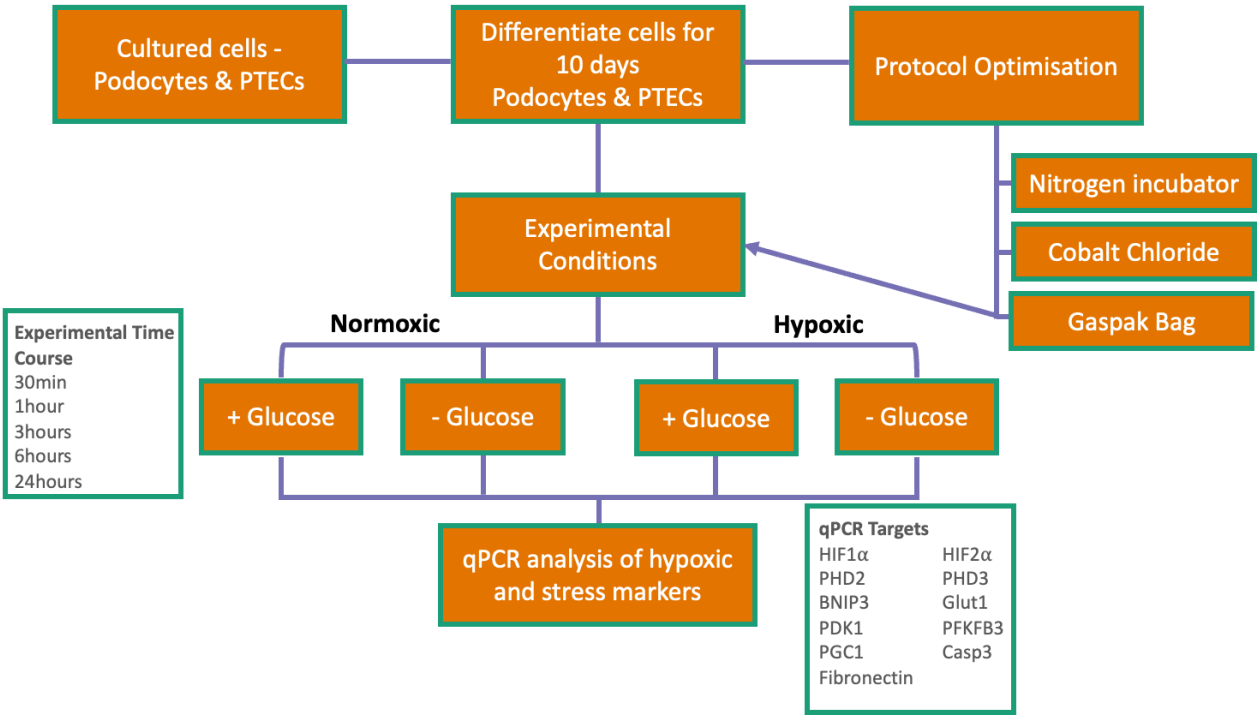



**Figure 5-F: Hypoxic cell model experimental plan**

To establish a hypoxic cell model using immortalised human podocytes and PTECs, three methods to induce hypoxia were tested to confirm cell survival. Cells were then cultured using the GasPak-pouch +/- glucose and the expression of hypoxia-related gene markers were quantified using qPCR. Cells cultured under normoxic conditions with glucose were considered the 'control' experimental group.

### 5.4.3 Podocytes and PTECs survived in culture under hypoxic and glucose starved conditions

Podocytes and PTECs cultured under normoxic and hypoxic conditions (GasPak-pouch) in media +/- glucose survived for up to 24h. Podocytes and PTECs were cultured for 30 minutes (30m), 1 hour (1h), 3 hours (3h), 6 hours (6h) and 24 hours (24h), in four culture conditions:

- Normoxic + glucose (Norm+Gluc)
- Normoxic – glucose (Norm-Gluc)
- Hypoxic + glucose (Hypo+Gluc)
- Hypoxic – glucose (Hypo-Gluc)

Images of cultured cells were collected prior to cell collection.

Podocyte morphology was consistent under both normoxic and hypoxic conditions during the first 3h of culture. At 6h and 24h Hypo-Gluc podocytes showed evolving morphological changes (Figure 5-G). Specifically, podocytes lost their defined structure, and cell-cell connections, which may be indicative of cell death. Figure 5-H shows images of PTECs cultured for up to 24h. Under normoxic and hypoxic conditions +/- glucose, PTECs did not have any obvious morphological changes, however there was evidence of cell loss at 24h in the Hypo-Gluc cells.

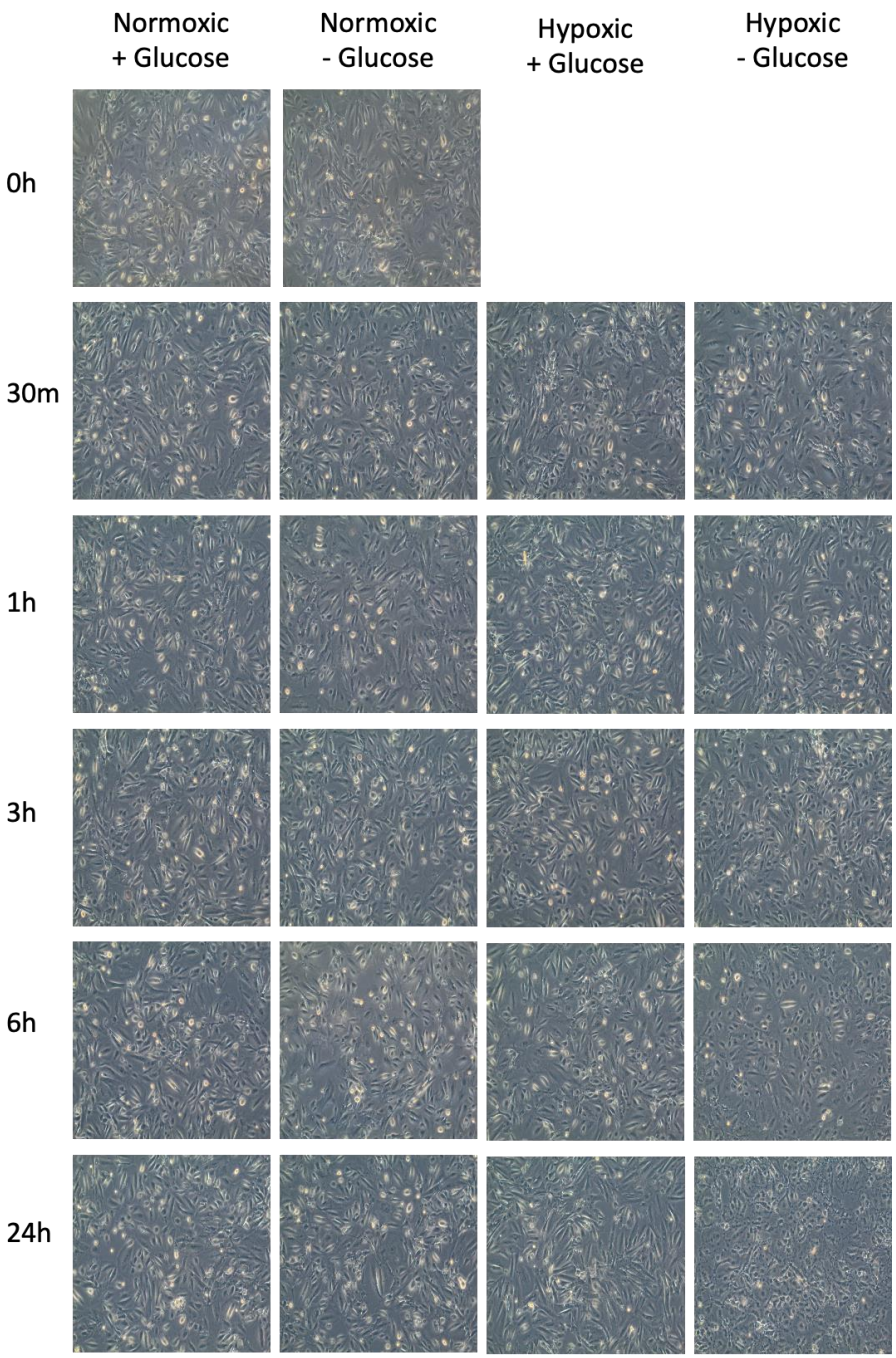



**Figure 5-G: Podocytes cells cultured under normoxic and hypoxic conditions in media +/- glucose**

Podocytes were cultured for up to 24h in media +/-glucose. Cells were imaged at regular intervals as shown in the figure. At 6h and 24h cells cultured under hypoxic minus glucose conditions had reduced cellular granularity and a variable cell structure.

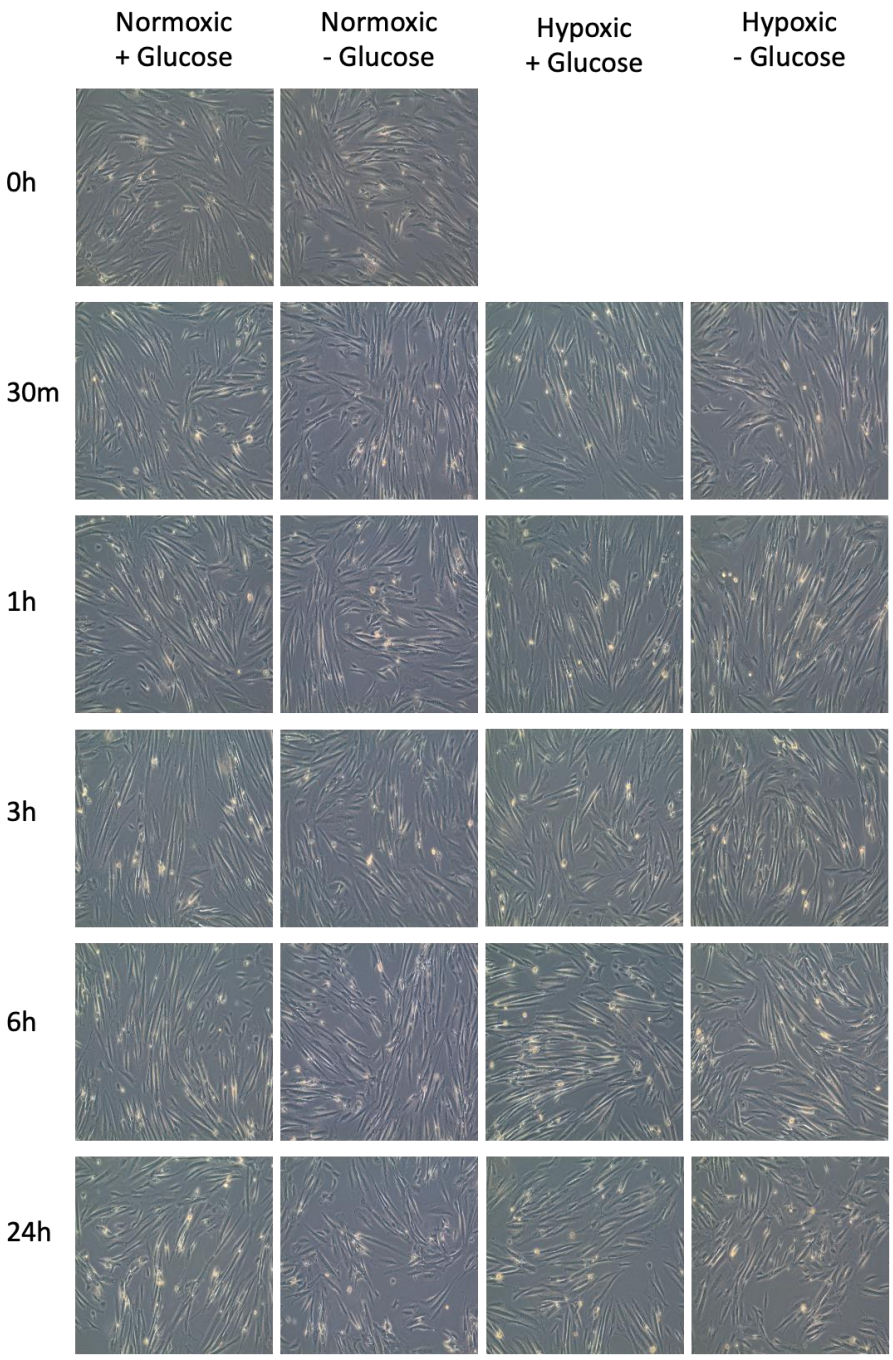



**Figure 5-H: PTECs cultured under normoxic and hypoxic conditions in media +/- glucose**

PTECs were cultured for up to 24h in media +/-glucose. Cells were imaged at regular intervals. There was no evidence of morphological changes in the PTECs under hypoxic conditions or with glucose starvation.

### 5.4.4 qPCR analysis of podocytes and PTECs cultured under normoxic and hypoxic conditions

Quantitative PCR (Chapter 3 (3.8)) was used to quantitate the expression of genes associated with hypoxia in cells cultured under normoxic and hypoxic conditions +/- glucose. Cells were collected at the pre-determined time points, and RNA extracted for qPCR analysis. The expression of each gene was normalised to β-actin. Gene expression for each culture condition was then compared to cells cultured under normoxic condition with glucose (Norm+Gluc) as this treatment represent typical culture conditions. A list of analysed gene primers is shown in Table 3-C.

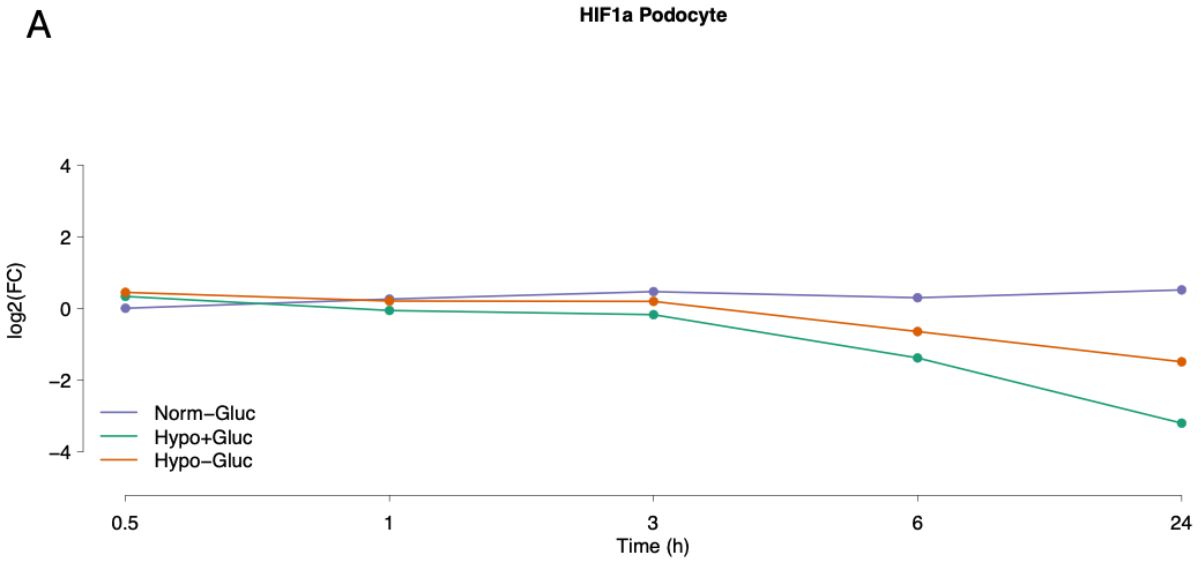
#### 5.4.4.1 HIF1α and HIF2α expression in podocytes and PTECs is indicative of a hypoxic response early during culture

HIF1α and HIF2α are the most common described markers of hypoxia. Yet their expression is also triggered by cellular stress. Under low oxygen conditions, HIF is stabilised and upregulates the expression of genes associated with metabolic reprogramming, extracellular signalling and remodelling, histone modification and modulating transcription factors[271]. Here, HIF1α and HIF2α were measured to quantify whether hypoxia was induced in GasPak-pouch cultured cells.

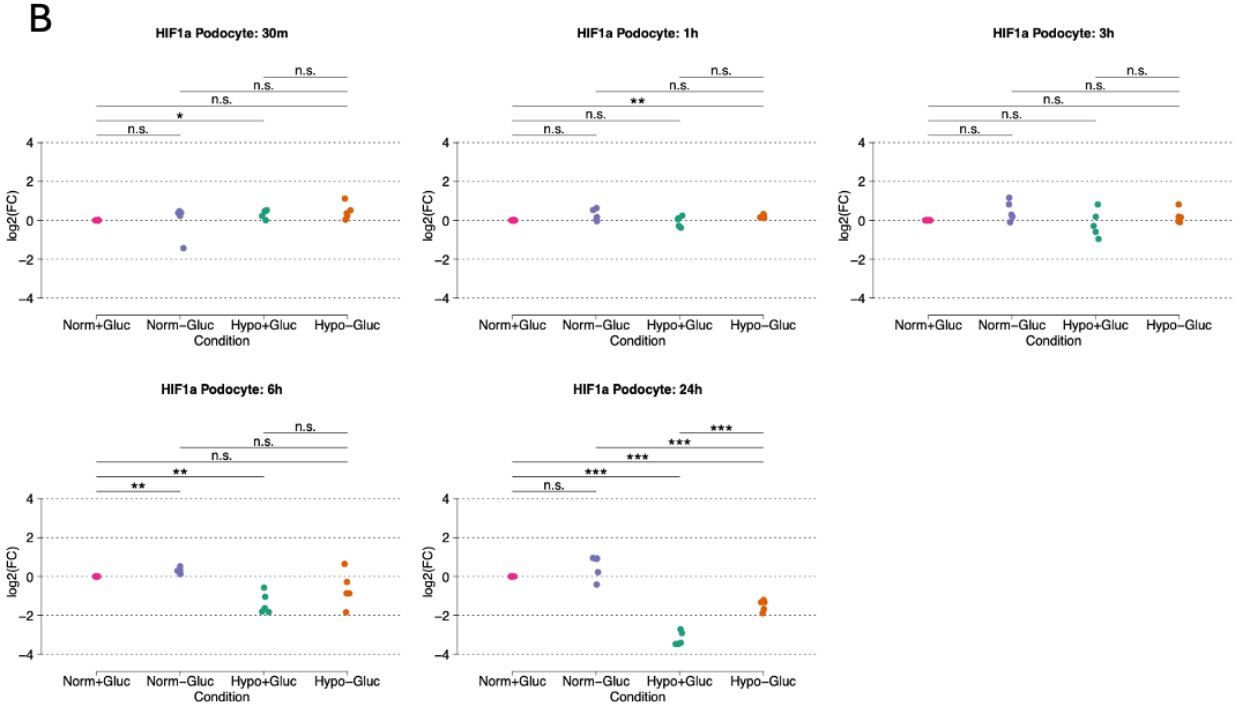
Cultured podocytes had variable expression of HIF1α as culture progressed. After 30m Hypo+Gluc podocytes had more HIF1α expressed compared to the other groups. At 6h and 24h, HIF1α was increased in the Norm-Gluc group demonstrating a probable stress response to the lack of glucose in the culture media; HIF1α was reduced in the hypoxic cells. Additionally, at 6h and 24h there was more HIF1α in Norm-Gluc compared to Hypo-

Gluc cells, and HIF1α expression was lower in the Hypo+Gluc compared to the Hypo-Gluc cells.

A




B




C

**T-test p.values**

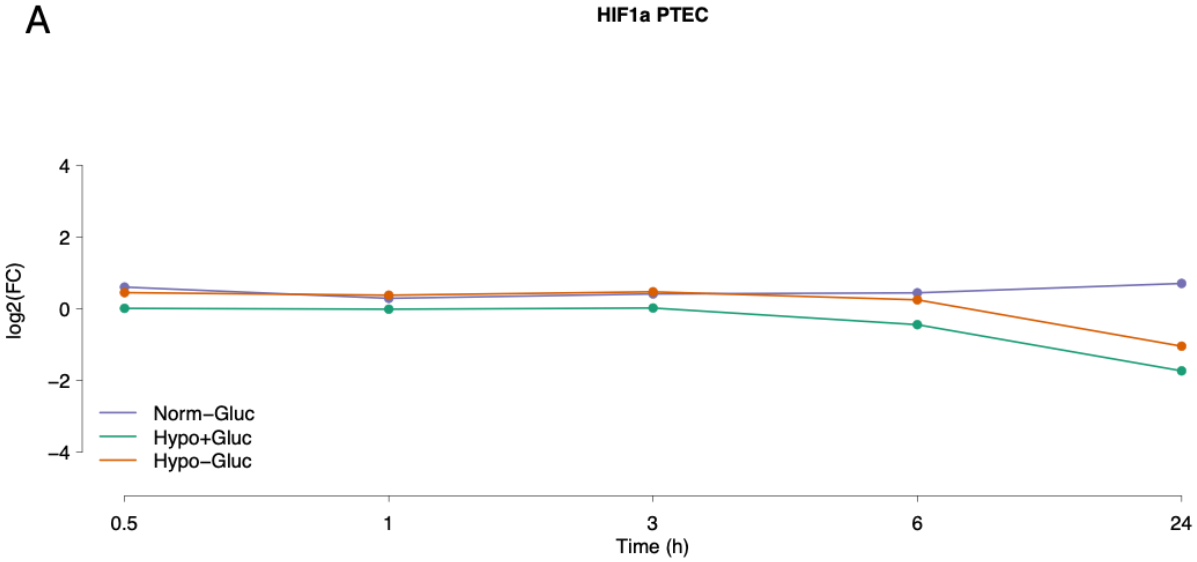
| Time Point | Norm-Gluc | Hypox+Gluc | Hypox-Gluc | Norm-Gluc Vs Hypo-Gluc | Hypo+Gluc Vs Hypo-Gluc |
|---|---|---|---|---|---|
| 30m | 0.98533 | 0.02723 | 0.07156 | 0.31843 | 0.60735 |
| 1h | 0.12285 | 0.66692 | 0.00627 | 0.72074 | 0.09125 |
| 3h | 0.10787 | 0.60843 | 0.29316 | 0.36317 | 0.33066 |
| 6h | 0.00942 | 0.00500 | 0.19034 | 0.08143 | 0.16946 |
| 24h | 0.12792 | 0.00004 | 0.00031 | 0.00067 | 0.00004 |

**Figure 5-I: HIF1α mRNA expression in podocytes cultured under normoxic and hypoxic conditions**

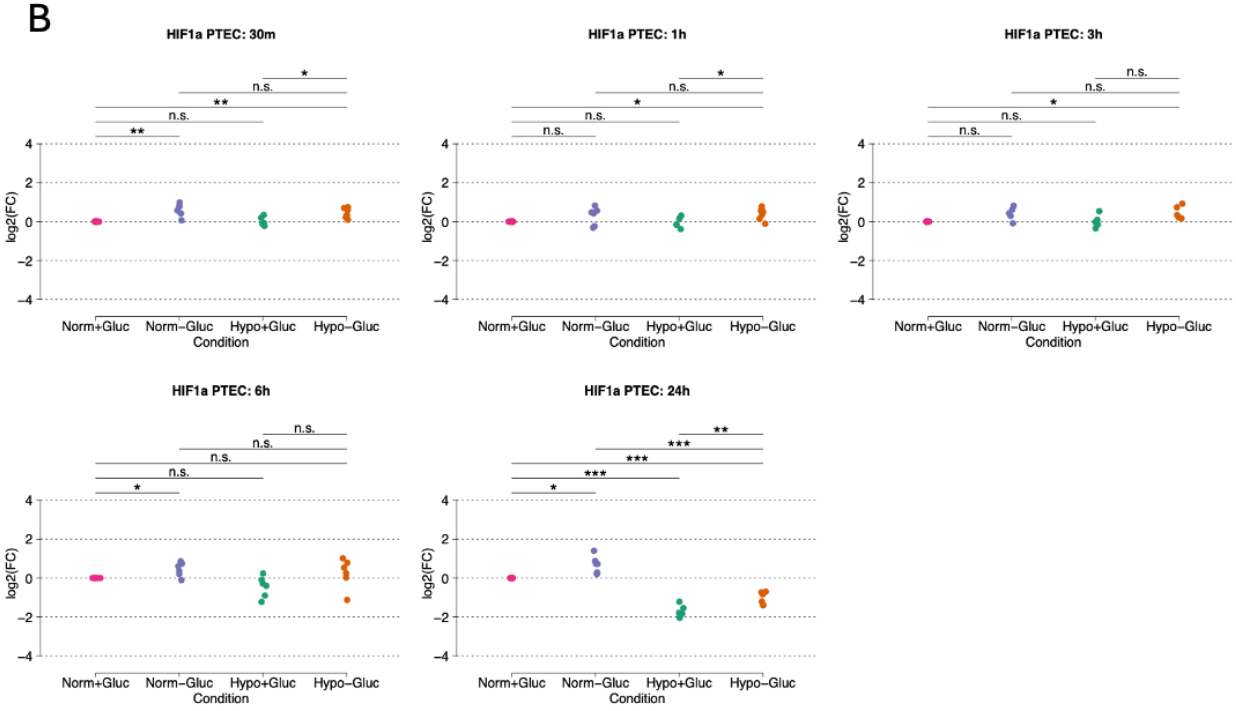
Podocytes were cultured under normoxic and hypoxic conditions for 30m, 1h, 3h, 6h and 24h in media +/- glucose. Cell mRNA was measured for HIF1α expression. (A) depicts expression of HIF1α in podocytes across the time course, highlighting changes in expression at each time point based on treatment. (B) maps change in HIF1α expression with cell treatments across the different time points. (C) shows t-test p.values comparing each condition to Norm+Gluc and between experimental conditions. HIF1α expression increased in Norm-Gluc cells from 6h but decreased in cells exposed to hypoxic conditions +/- glucose.

PTECs cultured without glucose had increased HIF1α expression as early as 30m. At 1h and 3h the HIF1α expression was increased in Hypo-Gluc cells only. At 6h HIF1α expression started trending down and was significantly reduced at 24h. At 24h, HIF1α expression was lower in both the hypoxic groups compared to Norm+Gluc cells whilst expression increased in Norm-Gluc cells.

A




B




C

**T-test p.values**

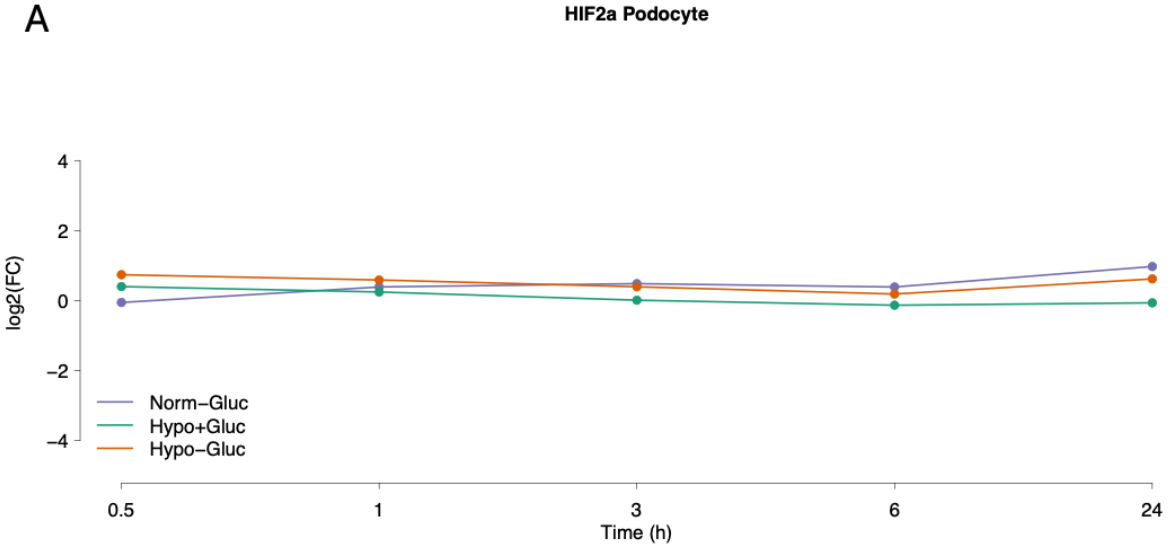
| Time Point | Norm-Gluc | Hypox+Gluc | Hypox-Gluc | Norm-Gluc Vs Hypo-Gluc | Hypo+Gluc Vs Hypo-Gluc |
|---|---|---|---|---|---|
| 30m | 0.00651 | 0.90530 | 0.00894 | 0.39460 | 0.01069 |
| 1h | 0.17997 | 0.91009 | 0.03413 | 0.71427 | 0.04409 |
| 3h | 0.05431 | 0.89689 | 0.03529 | 0.78988 | 0.06514 |
| 6h | 0.03025 | 0.09934 | 0.45988 | 0.58710 | 0.10208 |
| 24h | 0.01046 | 0.00003 | 0.00053 | 0.00002 | 0.00362 |

**Figure 5-J: HIF1α mRNA expression in PTECs cultured under normoxic and hypoxic conditions**

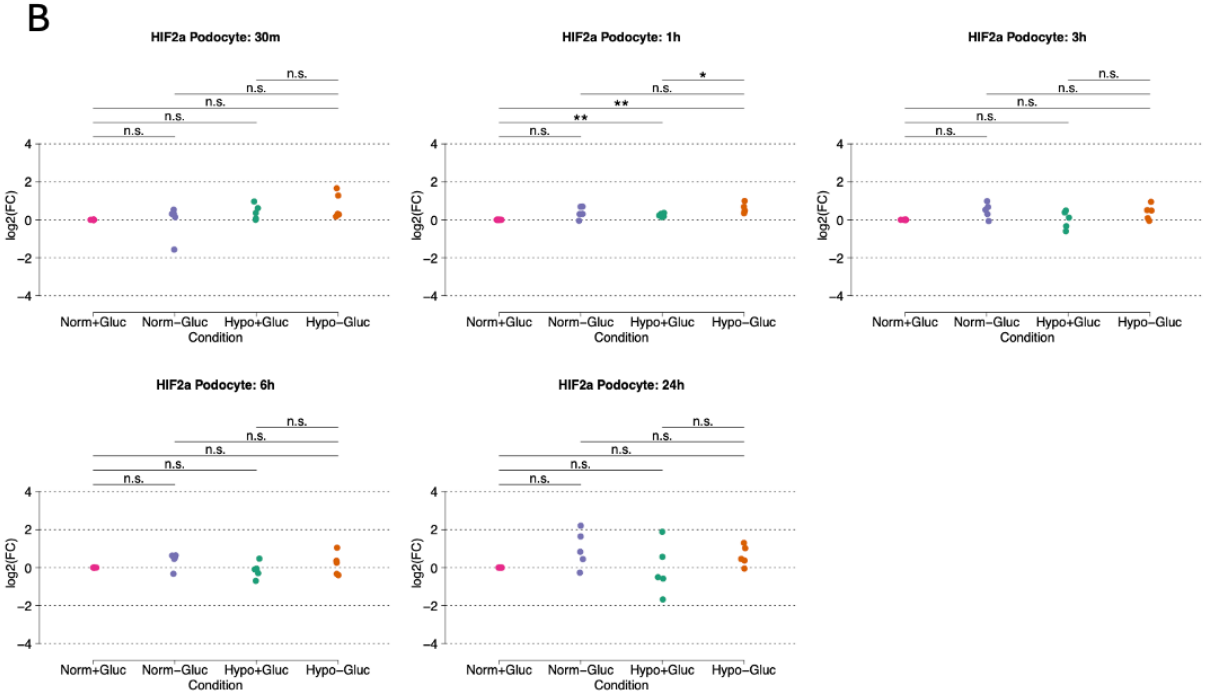
PTECs were cultured under normoxic and hypoxic conditions for 30m, 1h, 3h, 6h and 24h in media +/- glucose. Cell mRNA was measured for HIF1α expression. (A) depicts expression of HIF1α in PTECs across the time course, highlighting changes in expression at each time point based on treatment. (B) maps change in HIF1α expression with cell treatments across the different time points. (C) shows t-test p.values comparing each condition to Norm+Gluc, then between experimental conditions. HIF1α expression increased in Norm-Gluc cells from 30m continuing up to 24h, although expression was not significantly increased at all time points compared to the control group. Initially HIF1α expression was upregulated from 30m in Hypo-Gluc PTECs but expression significantly decreased in these cells and Hypo+Gluc cells at 24h.

Expression of HIF2α increased in hypoxic podocytes within 1h of culture. Hypo-Gluc podocytes had increased HIF2α expression compared to Hypo+Gluc. HIF2α expression did not differ with condition or time points after 3h.

A




B




C

**T-test p.values**

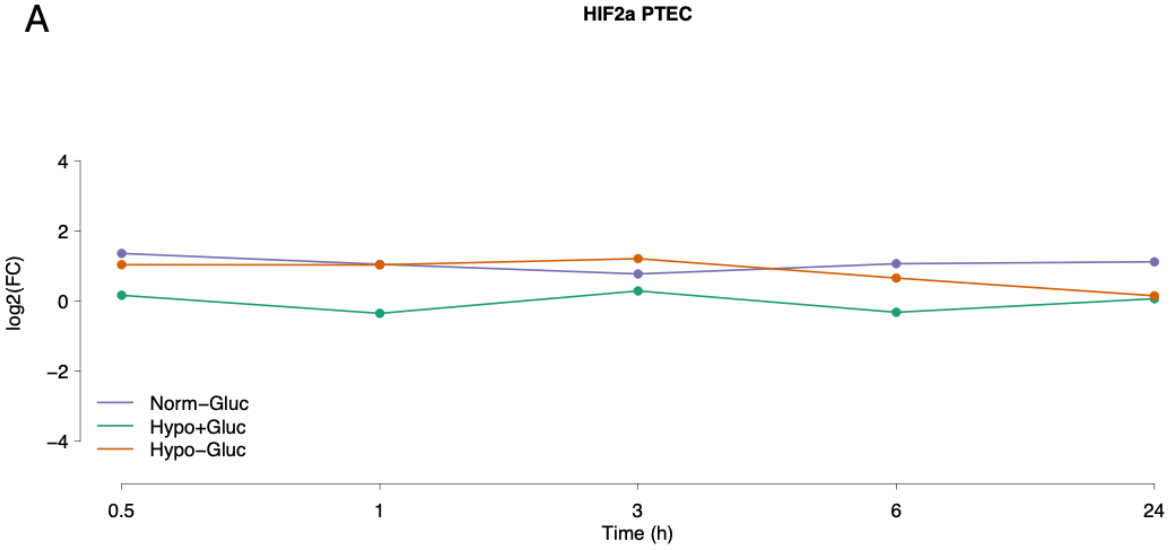
| Time Point | Norm-Gluc | Hypox+Gluc | Hypox-Gluc | Norm-Gluc Vs Hypo-Gluc | Hypo+Gluc Vs Hypo-Gluc |
|---|---|---|---|---|---|
| 30m | 0.89624 | 0.08747 | 0.07232 | 0.14648 | 0.37276 |
| 1h | 0.05004 | 0.00384 | 0.00706 | 0.30806 | 0.03838 |
| 3h | 0.05147 | 0.95853 | 0.08877 | 0.72708 | 0.19931 |
| 6h | 0.09990 | 0.52201 | 0.51636 | 0.54987 | 0.35571 |
| 24h | 0.08924 | 0.92159 | 0.06162 | 0.50376 | 0.33838 |

**Figure 5-K: HIF2α mRNA expression in podocytes cultured under normoxic and hypoxic conditions**

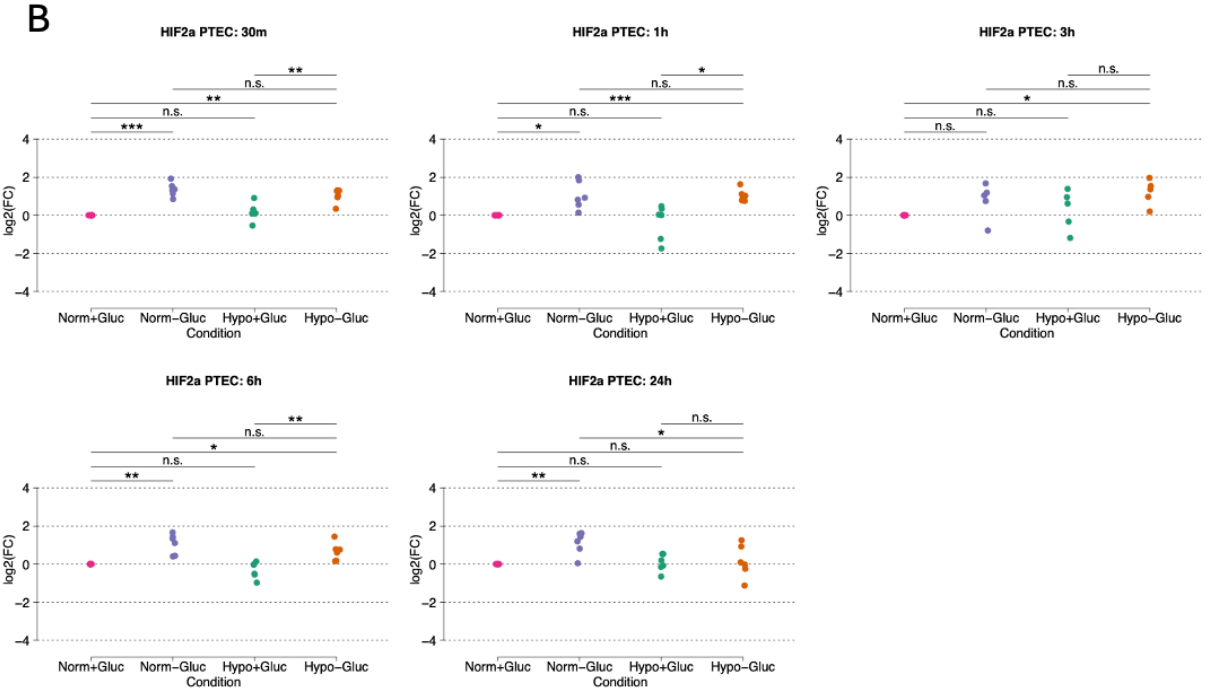
Podocytes were cultured under normoxic and hypoxic conditions for 30m, 1h, 3h, 6h and 24h in media +/- glucose. Cell mRNA was measured for HIF2α expression. (A) depicts expression of HIF2α in podocytes across the time course, highlighting changes in expression at each time point based on treatment. (B) maps change in HIF2α expression with cell treatments across the different time points. (C) shows t-test p.values comparing each condition to normoxic + glucose, then between experimental conditions. HIF2α expression was increased in hypoxic cells at 1h only.

HIF2α expression increased in PTECs cultured without glucose at 30m and at all time points up to and including 6h. Expression of HIF2α trended downwards in the Hypo-Gluc cells at 24h. Expression of HIF2α did not change in the Hypo+Gluc cells, suggesting that HIF2α expression in these cells may be responding to cellular stress associated with hypoglycaemia rather than hypoxia.

A




B




C

**T-test p.values**

| Time Point | Norm-Gluc | Hypox+Gluc | Hypox-Gluc | Norm-Gluc Vs Hypo-Gluc | Hypo+Gluc Vs Hypo-Gluc |
|---|---|---|---|---|---|
| 30m | 0.00025 | 0.42615 | 0.00101 | 0.15905 | 0.00527 |
| 1h | 0.01717 | 0.38837 | 0.00055 | 0.95793 | 0.01216 |
| 3h | 0.14035 | 0.57052 | 0.01534 | 0.42311 | 0.14060 |
| 6h | 0.00441 | 0.12186 | 0.01972 | 0.18952 | 0.00381 |
| 24h | 0.00619 | 0.73982 | 0.68587 | 0.04908 | 0.83719 |

**Figure 5-L: HIF2α mRNA expression in PTECs cultured under normoxic and hypoxic conditions**

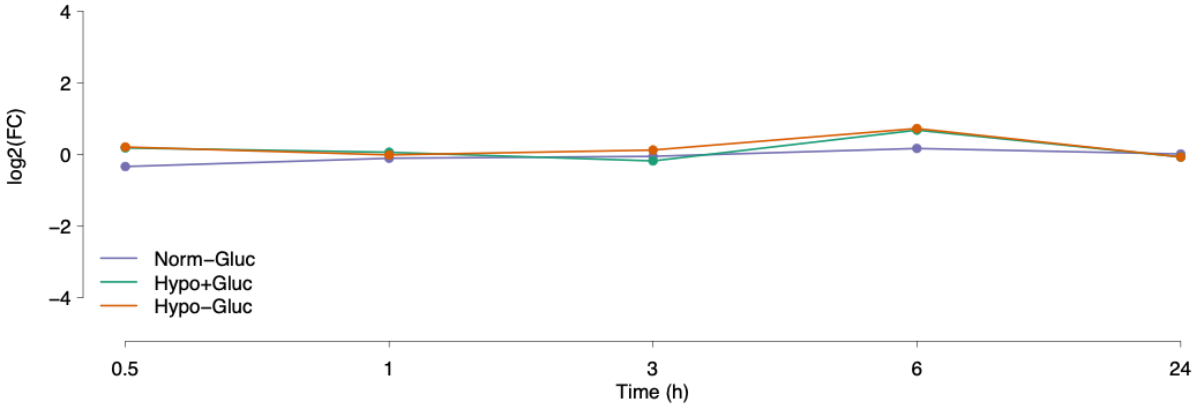
PTECs were cultured under normoxic and hypoxic conditions for 30m, 1h, 3h, 6h and 24h in media +/- glucose. Cell mRNA was measured for HIF2α expression. (A) depicts expression of HIF2α in PTECs across the time course, highlighting changes in expression at each time point based on treatment. (B) maps change in HIF2α expression with cell treatments across the different time points. (C) shows t-test p.values comparing each condition to Norm+Gluc, then between experimental conditions. HIF2α expression increased in cells cultured without glucose from 30m up to including 6h. HIF2α remained increased in Norm-Gluc cells at 24h also. At 6h, expression of HIF2α started to decrease.

#### 5.4.4.2 PHD2 and PHD3 expression indicates hypoxic conditions induced hypoxia in Podocytes and PTECs

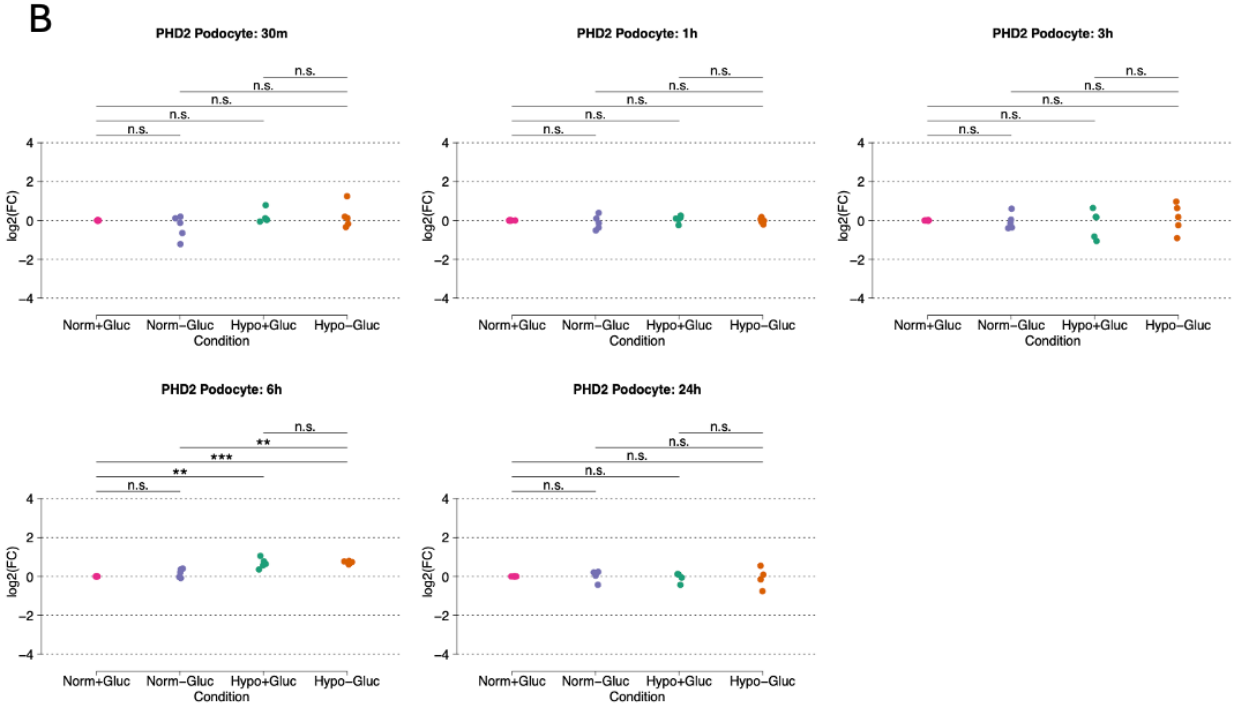
Prolyl hydroxylase domain 2 and 3 (PHD2/3) are oxygen sensing proteins that act as primary regulators of HIFs. Under normoxic conditions, PHDs hydroxylate HIFs marking them for proteasomal degradation. PHD2 is regulated by HIF1α, whilst PHD3 is regulated by both HIF1α and HIF2α[272]. Under hypoxic conditions, PHDs are inactivated. PHD transcription is upregulated in response. In this study, changes in PHD2 and PHD3 expression were measured based on their specificity as oxygen sensors; HIF expression is influenced by various factors not limited to hypoxia.

PHD2 expression in podocytes increased in hypoxic cells at 6h of hypoxia. Expression was not changed in the Norm-Gluc cells at any time point.

A




B




C

**T-test p.values**

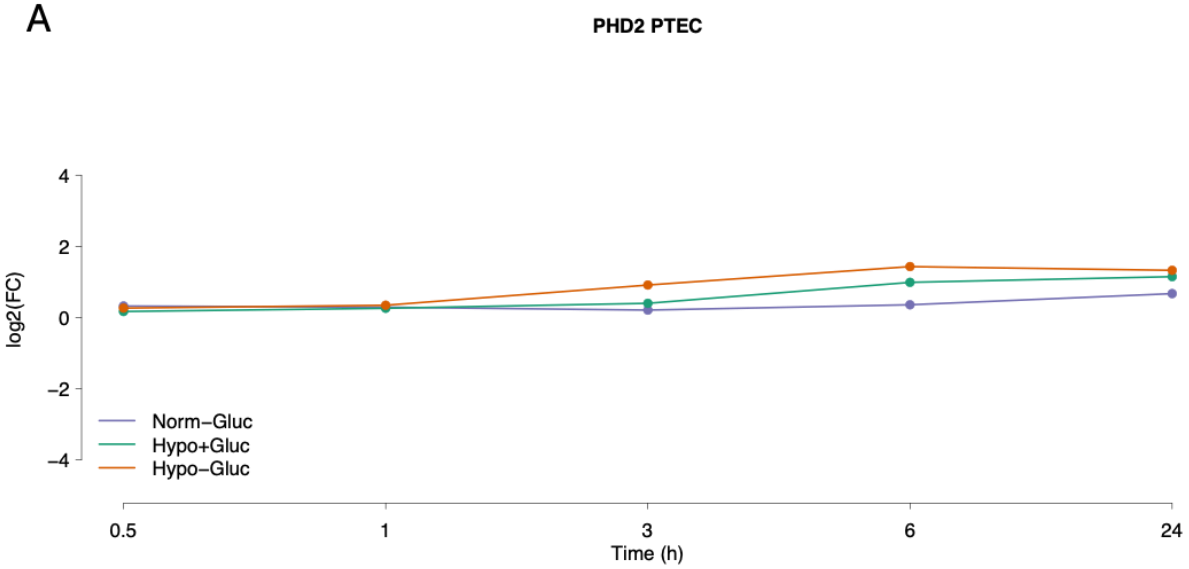
| Time Point | Norm-Gluc | Hypox+Gluc | Hypox-Gluc | Norm-Gluc Vs Hypo-Gluc | Hypo+Gluc Vs Hypo-Gluc |
|---|---|---|---|---|---|
| 30m | 0.27188 | 0.29684 | 0.49366 | 0.19242 | 0.93847 |
| 1h | 0.54932 | 0.49916 | 0.85860 | 0.61379 | 0.50358 |
| 3h | 0.78823 | 0.60901 | 0.72628 | 0.65614 | 0.52987 |
| 6h | 0.16280 | 0.00422 | 0.00002 | 0.00337 | 0.72863 |
| 24h | 0.93998 | 0.62035 | 0.81021 | 0.79965 | 0.99837 |

**Figure 5-M: PHD2 mRNA expression in podocytes cultured under normoxic and hypoxic conditions**

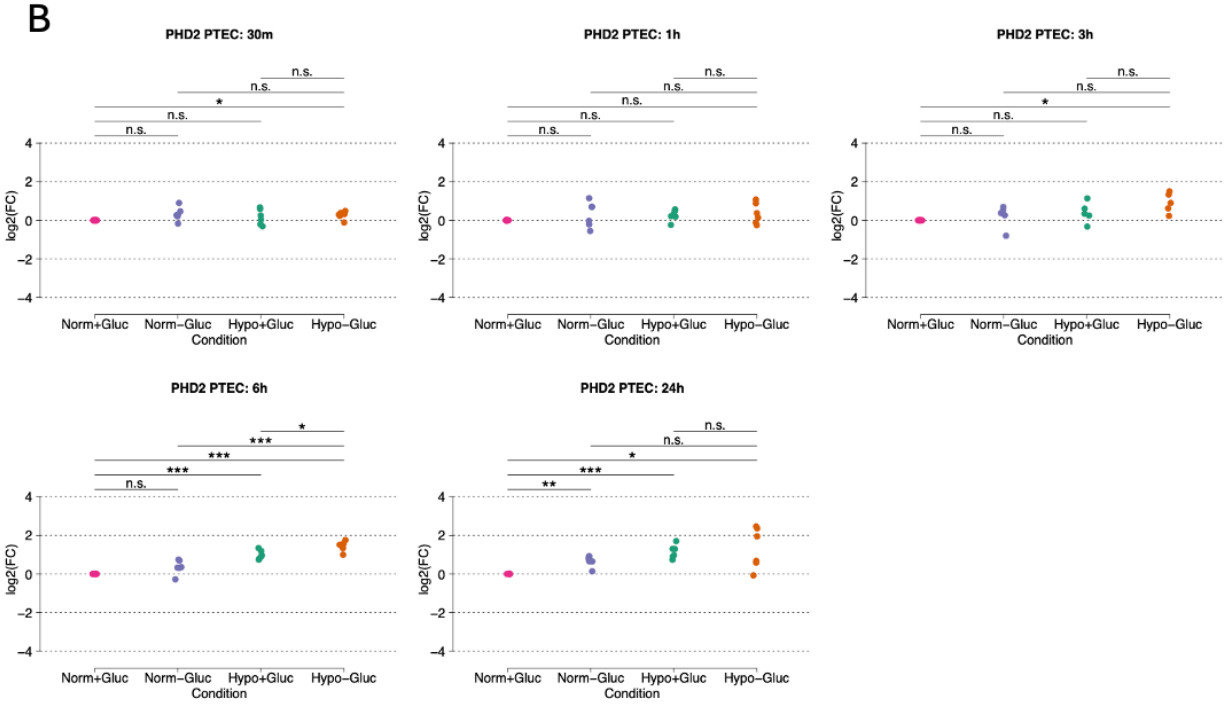
Podocytes were cultured under normoxic and hypoxic conditions for 30m, 1h, 3h, 6h and 24h in media +/- glucose. Cell mRNA was measured for PHD2 expression. (A) depicts expression of PHD2 in podocytes across the time course, highlighting changes in expression at each time point based on treatment. (B) maps change in PHD2 expression with cell treatments across the different time points. (C) shows t-test p.values comparing each condition to Norm+Gluc, then between experimental conditions. PHD2 expression was increased in hypoxic cells at 6h only.

PHD2 expression increased in the Hypo-Gluc PTECs from 30m up to 24h. At 6h and 24h expression of PHD2 was increased in Hypo+Gluc and Hypo-Gluc cells. At 24h there was also an increase in Norm-Gluc PTECs.

A




B




C

**T-test p.values**

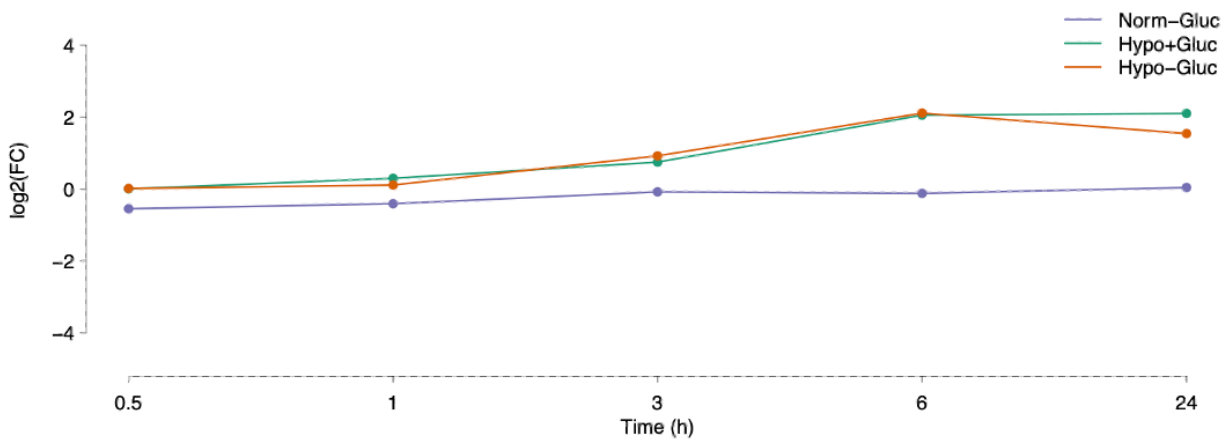
| Time Point | Norm-Gluc | Hypox+Gluc | Hypox-Gluc | Norm-Gluc Vs Hypo-Gluc | Hypo+Gluc Vs Hypo-Gluc |
|---|---|---|---|---|---|
| 30m | 0.07116 | 0.34883 | 0.02490 | 0.73107 | 0.62035 |
| 1h | 0.32502 | 0.07772 | 0.17500 | 0.87574 | 0.74345 |
| 3h | 0.46804 | 0.16767 | 0.01691 | 0.07965 | 0.16027 |
| 6h | 0.06039 | 0.00014 | 0.00004 | 0.00023 | 0.01090 |
| 24h | 0.00218 | 0.00049 | 0.02848 | 0.19928 | 0.71181 |

**Figure 5-N: PHD2 mRNA expression in PTECs cultured under normoxic and hypoxic conditions**

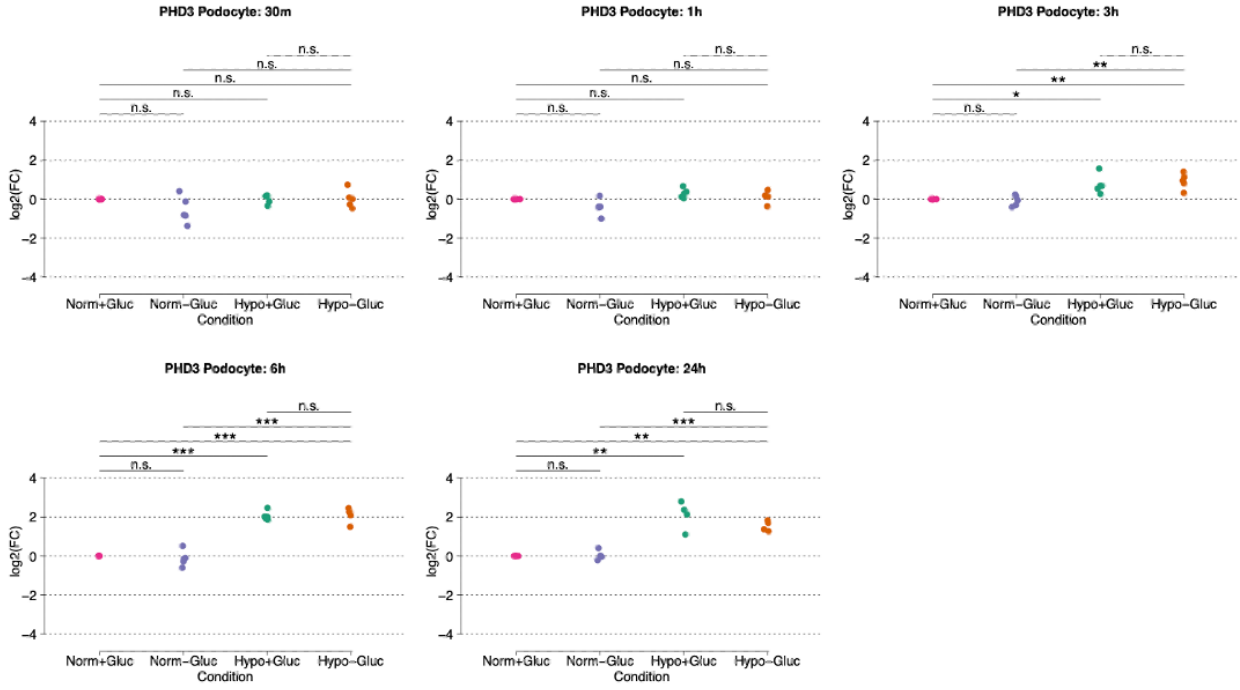
PTECs were cultured under normoxic and hypoxic conditions for 30m, 1h, 3h, 6h and 24h in media +/- glucose. Cell mRNA was measured for PHD2 expression. (A) depicts expression of PHD2 in PTECs across the time course, highlighting changes in expression at each time point based on treatment. (B) maps change in PHD2 expression with cell treatments across the different time points. (C) shows t-test p.values comparing each condition to Norm+Gluc, then between experimental conditions. PHD2 expression increased in Hypo-Gluc cells from 30m until 24h. PHD2 expression increased in Hypo+Gluc cells at 6h and 24h. PHD2 increased in Norm-Gluc cells at 24h.

In podocytes, PHD3 expression increased comparatively in both hypoxic cell groups at 3h, continuing until 24h. There was no increase in PHD3 expression in the Norm-Gluc cells.

A




B




C

**T-test p.values**

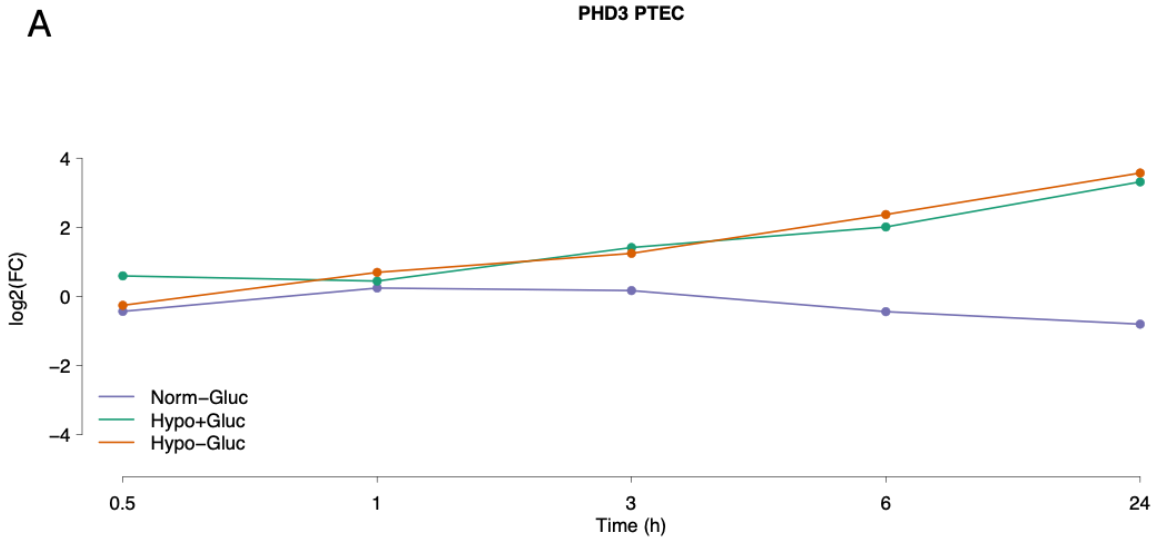
| Time Point | Norm-Gluc | Hypox+Gluc | Hypox-Gluc | Norm-Gluc Vs Hypo-Gluc | Hypo+Gluc Vs Hypo-Gluc |
|---|---|---|---|---|---|
| 30m | 0.15241 | 0.96644 | 0.94731 | 0.17544 | 0.96741 |
| 1h | 0.09162 | 0.05082 | 0.45548 | 0.05569 | 0.30979 |
| 3h | 0.55391 | 0.02674 | 0.00697 | 0.00249 | 0.55816 |
| 6h | 0.54182 | 0.00004 | 0.00021 | 0.00002 | 0.78265 |
| 24h | 0.76999 | 0.00996 | 0.00136 | 0.00020 | 0.22125 |

**Figure 5-O: PHD3 mRNA expression in podocytes cultured under normoxic and hypoxic conditions**

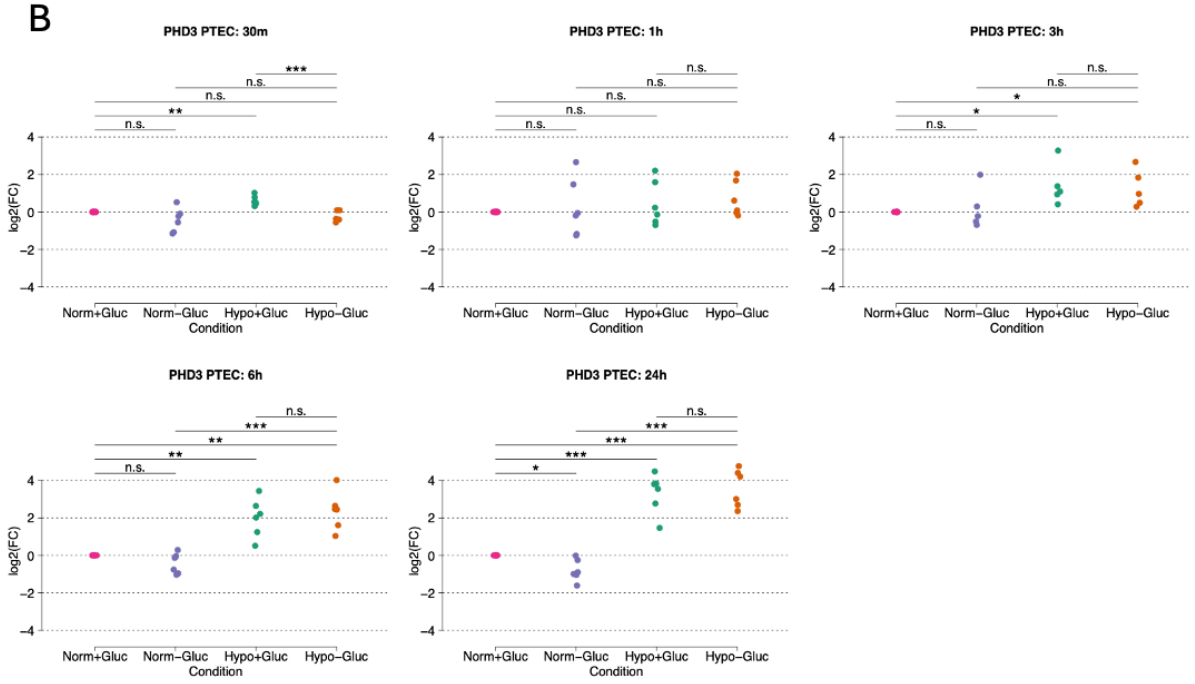
Podocytes were cultured under normoxic and hypoxic conditions for 30m, 1h, 3h, 6h and 24h in media +/- glucose. Cell mRNA was measured for PHD3 expression. (A) depicts expression of PHD3 in podocytes across the time course, highlighting changes in expression at each time point based on treatment. (B) maps change in PHD3 expression with cell treatments across the different time points. (C) shows t-test p.values comparing each condition to Norm+Gluc, then between experimental conditions. PHD3 expression was increased in hypoxic cells from 3h until 24h.

In PTECs PHD3 expression increased in Hypo+Gluc cells with 30m of hypoxia. At the 3h time point PHD3 expression increased in both hypoxic cell groups and continued to increase until 24h. At 24h the expression of PHD3 decreased in the Norm-Gluc cells compared to expression in the Norm+Gluc cells. The expression of PHD3 in Norm-Gluc cells trended downwards at all time points.

A




B




C

**T-test p.values**

| Time Point | Norm-Gluc | Hypox+Gluc | Hypox-Gluc | Norm-Gluc Vs Hypo-Gluc | Hypo+Gluc Vs Hypo-Gluc |
|---|---|---|---|---|---|
| 30m | 0.15619 | 0.00245 | 0.07363 | 0.55420 | 0.00027 |
| 1h | 0.71356 | 0.40015 | 0.13124 | 0.55603 | 0.69322 |
| 3h | 0.74210 | 0.04468 | 0.04863 | 0.14023 | 0.80465 |
| 6h | 0.10696 | 0.00496 | 0.00230 | 0.00040 | 0.55641 |
| 24h | 0.01947 | 0.00061 | 0.00033 | 0.00002 | 0.67668 |

**Figure 5-P: PHD3 mRNA expression in PTECs cultured under normoxic and hypoxic conditions**

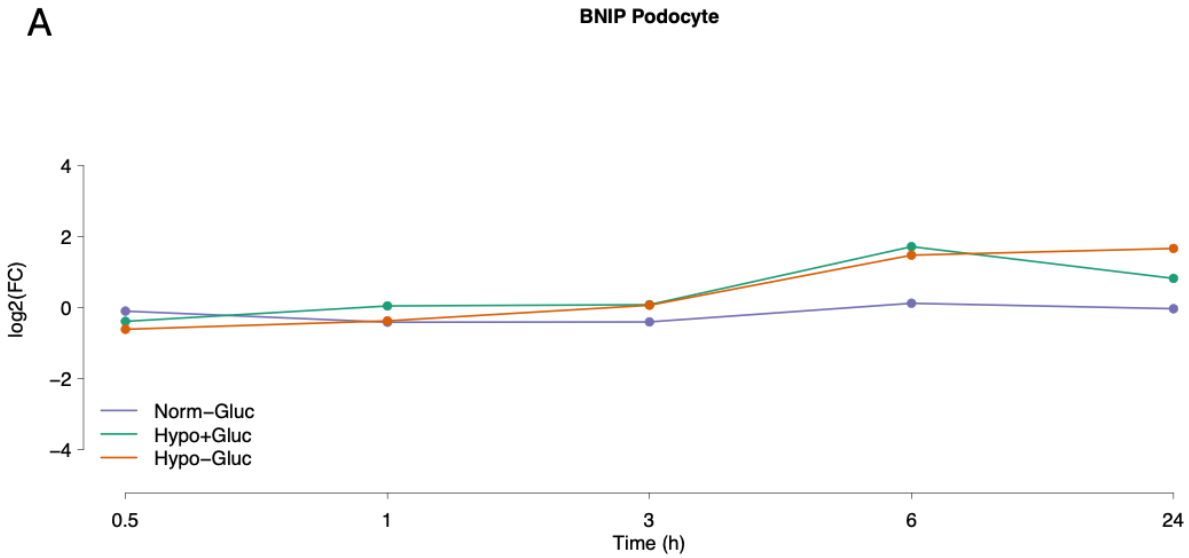
PTECs were cultured under normoxic and hypoxic conditions for 30m, 1h, 3h, 6h and 24h in media +/- glucose. Cell mRNA was measured for PHD3 expression. (A) depicts expression of PHD3 in PTECs across the time course, highlighting changes in expression at each time point based on treatment. (B) maps change in PHD3 expression with cell treatments across the different time points. (C) shows t-test p.values comparing each condition to Norm+Gluc, then between experimental conditions. PHD3 expression increased in Hypo+Gluc cells from 30m until 24h. PHD2 increased in Hypo-Gluc cells from 3h until 24h. Expression of PHD3 reduced in Norm-Gluc cells at 24h.

#### 5.4.4.3 BNIP3 expression increased with hypoxia over time in both podocytes and PTECs

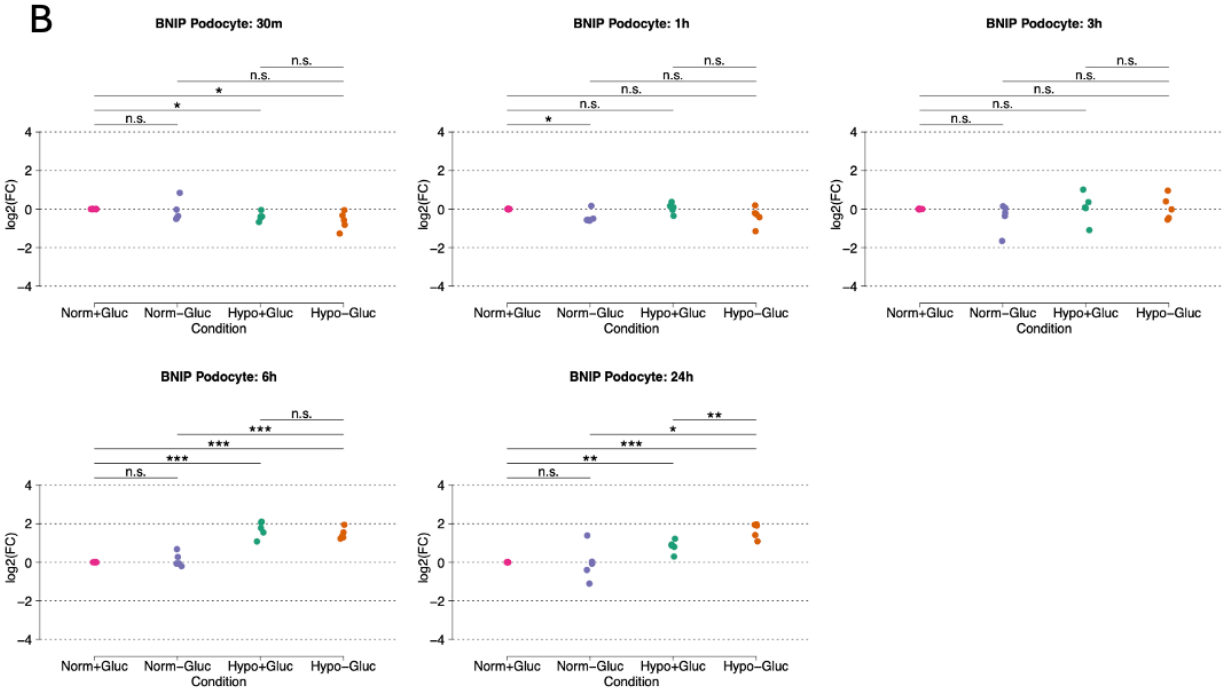
Bcl-2/adenovirus E1B 19-kDa interacting protein (BNIP3) is a pro-apoptotic protein belonging to the Bcl-2 family. BNIP3 regulates apoptosis and autophagy and is upregulated under hypoxic conditions by HIF1α binding to the HRE on the gene. BNIP3 expression was measured in the cells in this study, as an indicator of the downstream effects of hypoxia.

BNIP3 expression in hypoxic podocytes was decreased at 30m then started trending upwards. At 6h expression of BNIP was increased in the hypoxic cells. BNIP3 expression did not change in Norm-Gluc cells.

A




B




C

**T-test p.values**

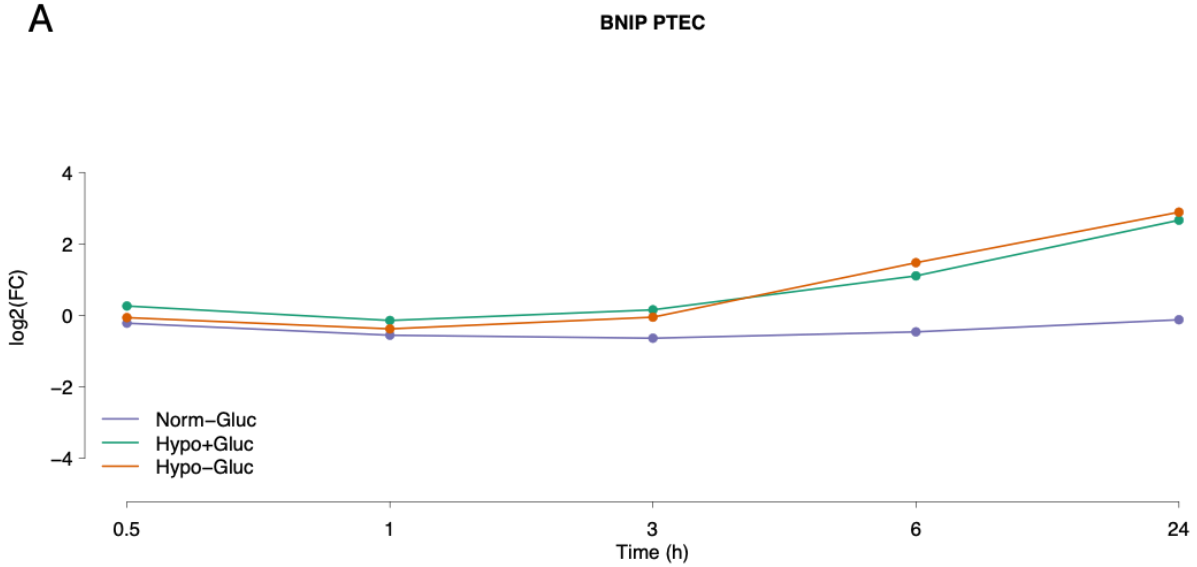
| Time Point | Norm-Gluc | Hypox+Gluc | Hypox-Gluc | Norm-Gluc Vs Hypo-Gluc | Hypo+Gluc Vs Hypo-Gluc |
|---|---|---|---|---|---|
| 30m | 0.7082 | 0.0182 | 0.0424 | 0.1564 | 0.3747 |
| 1h | 0.0467 | 0.7236 | 0.1627 | 0.8902 | 0.1422 |
| 3h | 0.2817 | 0.8240 | 0.8257 | 0.3060 | 0.9736 |
| 6h | 0.4916 | 0.0008 | 0.0003 | 0.0002 | 0.3264 |
| 24h | 0.9390 | 0.0054 | 0.0007 | 0.0105 | 0.0069 |

**Figure 5-Q: BNIP3 mRNA expression in podocytes cultured under normoxic and hypoxic conditions**

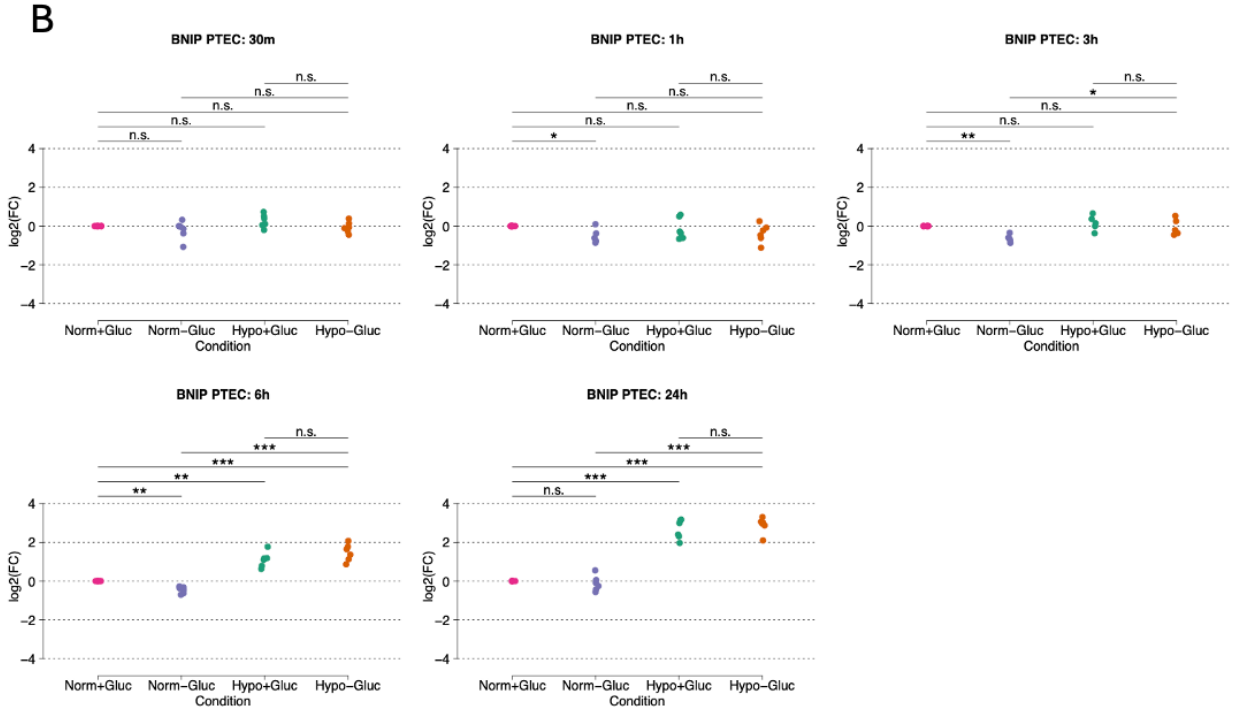
Podocytes were cultured under normoxic and hypoxic conditions for 30m, 1h, 3h, 6h and 24h in media +/- glucose. Cell mRNA was measured for BNIP3 expression. (A) depicts expression of BNIP3 in podocytes across the time course, highlighting changes in expression at each time point based on treatment. (B) maps change in BNIP3 expression with cell treatments across the different time points. (C) shows t-test p.values comparing each condition to Norm+Gluc, then between experimental conditions. BNIP3 expression was initially decreased in hypoxic cells at 30m but increased at 6h until 24h.

BNIP3 expression in PTECs, like podocytes, was initially reduced in treated cells. Expression of BNIP3 increased at 6h and 24h in the hypoxic PTECs. BNIP3 expression decreased in Norm-Gluc cells from 1h up to 6h.

A




B




C

**T-test p.values**

| Time Point | Norm-Gluc | Hypox+Gluc | Hypox-Gluc | Norm-Gluc Vs Hypo-Gluc | Hypo+Gluc Vs Hypo-Gluc |
|---|---|---|---|---|---|
| 30m | 0.31642 | 0.11686 | 0.63458 | 0.51412 | 0.10895 |
| 1h | 0.01317 | 0.55567 | 0.10922 | 0.48436 | 0.44455 |
| 3h | 0.00178 | 0.41407 | 0.80673 | 0.03205 | 0.44302 |
| 6h | 0.00123 | 0.00101 | 0.00045 | 0.00004 | 0.15910 |
| 24h | 0.49134 | 0.00005 | 0.00001 | 0.00000 | 0.41745 |

**Figure 5-R: BNIP3 mRNA expression in PTECs cultured under normoxic and hypoxic conditions**

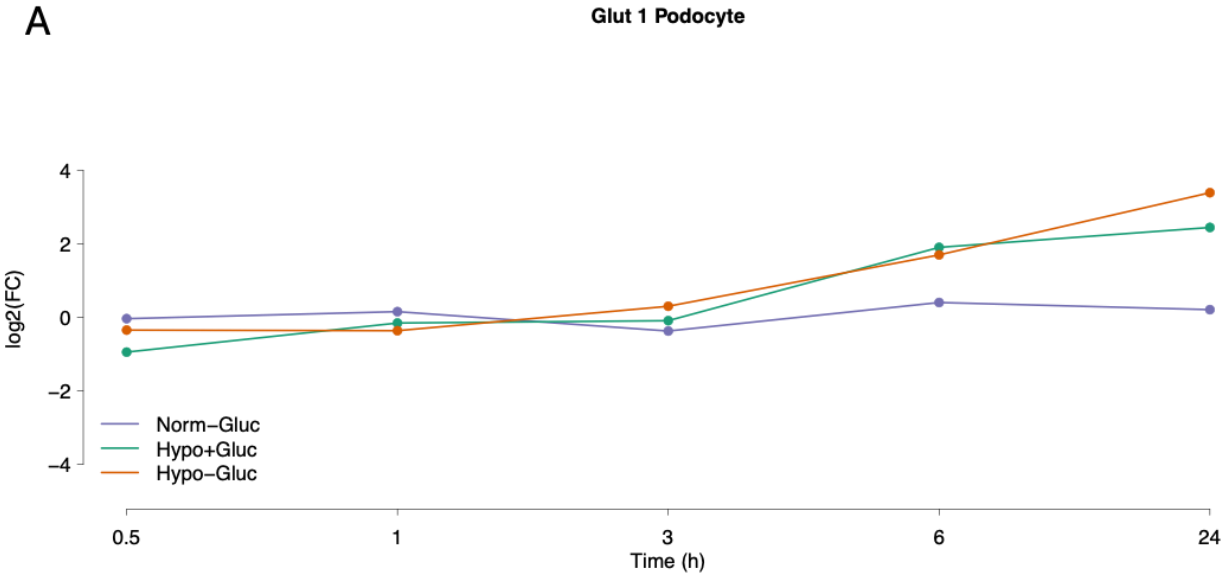
PTECs were cultured under normoxic and hypoxic conditions for 30m, 1h, 3h, 6h and 24h in media +/- glucose. Cell mRNA was measured for BNIP3 expression. (A) depicts expression of BNIP3 in PTECs across the time course, highlighting changes in expression at each time point based on treatment. (B) maps change in BNIP expression with cell treatments across the different time points. (C) shows t-test p.values comparing each condition to Norm+Gluc, then between experimental conditions. BNIP3 expression decreased in Norm-Gluc cells from 1h up to 6h. BNIP3 expression increased in hypoxic cells from 6h up to 24h.

#### 5.4.4.4 Glut1 increased gradually with hypoxia in podocytes and PTECs

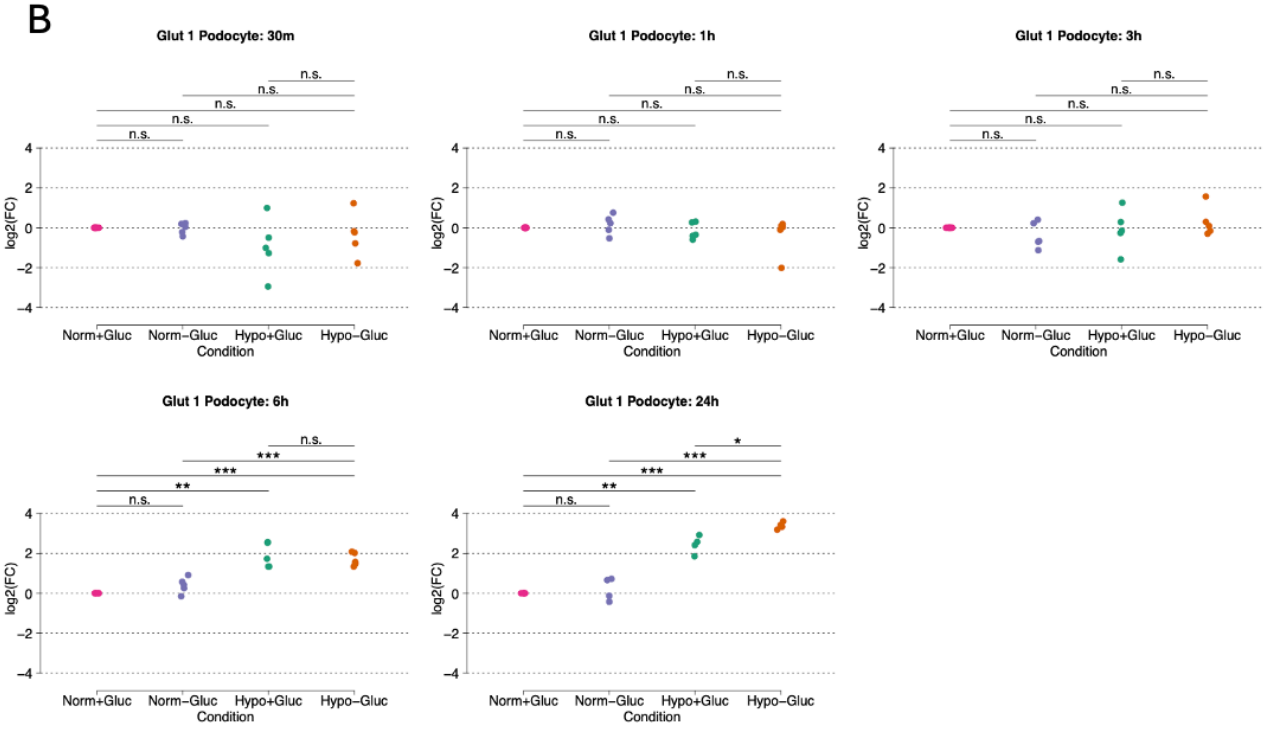
Glucose transporter 1 (Glut1) is a membrane protein, expressed mostly in plasma membranes, that transports glucose, galactose, mannose, glucosamine, and ascorbic acid. Glut1 expression is typically regulated by blood glucose concentrations, cell signalling and hormones; specifically, expression is upregulated under hypoglycaemic conditions. Expression and function of Glut1 increases under hypoxic conditions and is involved in glucose uptake. Glut1 expression has recently been shown to be upregulated by HIF1α binding to its HRE[193]. Glut1 expression was measured in podocytes and PTECs as a downstream marker of hypoxia.

Glut1 expression was increased in podocytes exposed to hypoxia from 6h up to 24h. Glut1 was increased in Hypo-Gluc cells compared to Hypo+Gluc. The expression of Glut1 did not change in Norm-Gluc cells.

A




B




C

**T-test p.values**

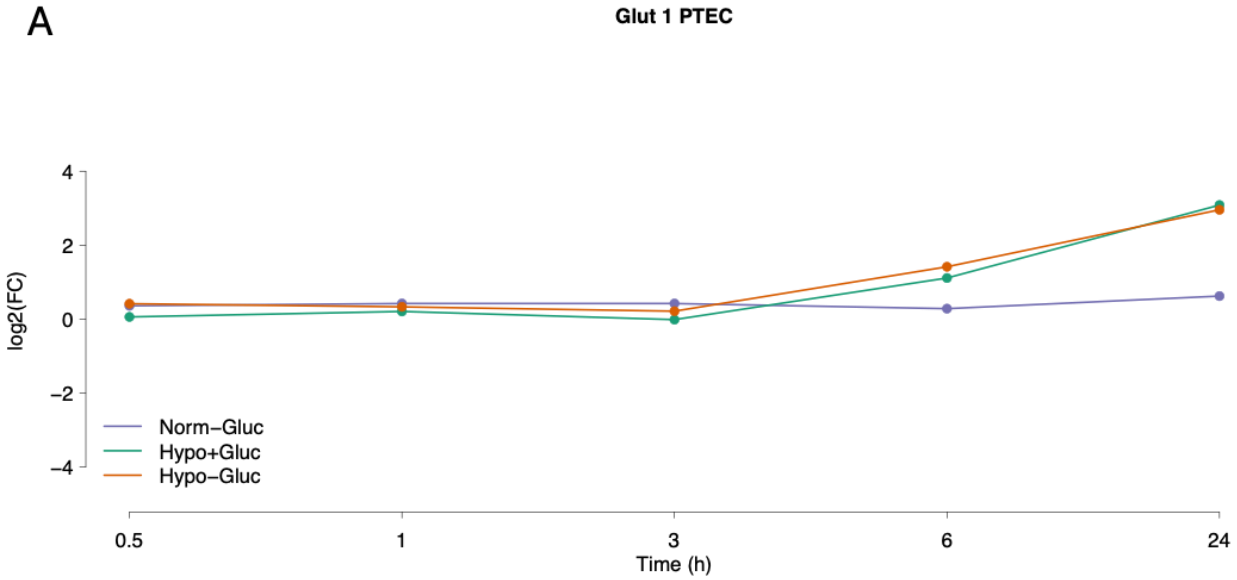
| Time Point | Norm-Gluc | Hypox+Gluc | Hypox-Gluc | Norm-Gluc Vs Hypo-Gluc | Hypo+Gluc Vs Hypo-Gluc |
|---|---|---|---|---|---|
| 30m | 0.78499 | 0.21079 | 0.51617 | 0.56782 | 0.47700 |
| 1h | 0.52461 | 0.45106 | 0.42956 | 0.31188 | 0.66300 |
| 3h | 0.27305 | 0.85247 | 0.41667 | 0.16783 | 0.51116 |
| 6h | 0.08446 | 0.00227 | 0.00034 | 0.00056 | 0.53610 |
| 24h | 0.51923 | 0.00161 | 0.00004 | 0.00080 | 0.01743 |

**Figure 5-S: Glut1 mRNA expression in podocytes cultured under normoxic and hypoxic conditions**

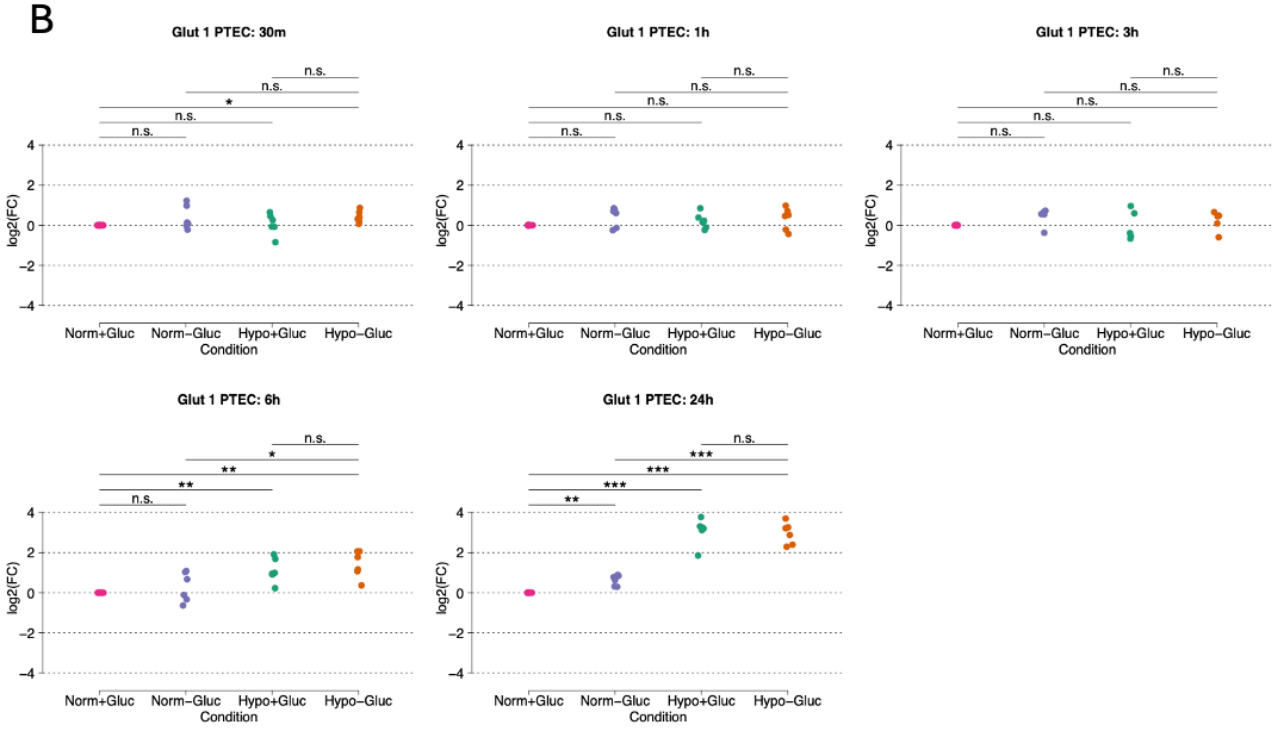
Podocytes were cultured under normoxic and hypoxic conditions for 30m, 1h, 3h, 6h and 24h in media +/- glucose. Cell mRNA was measured for Glut1 expression. (A) depicts expression of Glut1 in podocytes across the time course, highlighting changes in expression at each time point based on treatment. (B) maps changes in Glut1 expression with cell treatments across the different time points. (C) shows t-test p.values comparing each condition to Norm+Gluc, then between experimental conditions. Glut1 expression was increased in hypoxic cells from 6h until 24h.

Glut1 expression increased in Hypo-Gluc PTECs at 30m, and then in both hypoxic conditions at 6h and 24h. At 24h the expression of Glut1 also increased in the Norm-Gluc PTECs, yet expression of Glut1 in hypoxic PTECs was significantly higher.

A




B




C

**T-test p.values**

| Time Point | Norm-Gluc | Hypox+Gluc | Hypox-Gluc | Norm-Gluc Vs Hypo-Gluc | Hypo+Gluc Vs Hypo-Gluc |
|---|---|---|---|---|---|
| 30m | 0.19197 | 0.78883 | 0.01704 | 0.83958 | 0.18664 |
| 1h | 0.08506 | 0.24239 | 0.19544 | 0.76694 | 0.65986 |
| 3h | 0.10497 | 0.97165 | 0.38768 | 0.50966 | 0.58479 |
| 6h | 0.38911 | 0.00647 | 0.00353 | 0.01962 | 0.43007 |
| 24h | 0.00207 | 0.00008 | 0.00004 | 0.00002 | 0.71678 |

**Figure 5-T: Glut1 mRNA expression in PTECs cultured under normoxic and hypoxic conditions**

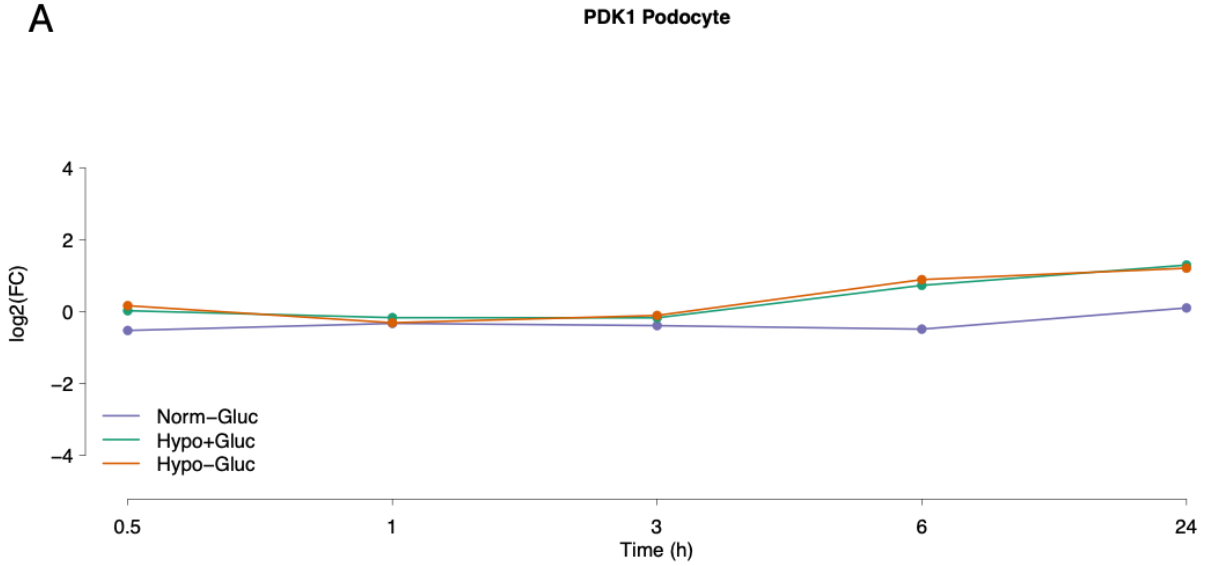
PTECs were cultured under normoxic and hypoxic conditions for 30m, 1h, 3h, 6h and 24h in media +/- glucose. Cell mRNA was measured for Glut1 expression. (A) depicts expression of Glut1 in PTECs across the time course, highlighting changes in expression at each time point based on treatment. (B) maps change in Glut1 expression with cell treatments across the different time points. (C) shows t-test p.values comparing each condition to Norm+Gluc, then between experimental conditions. Glut1 expression increased in Hypo-Gluc cells from 30m, and in both hypoxic cell groups from 6h. At 24h all experimental cell cohorts had increased expression of Glut1, yet Glut1 expression was significantly higher in the hypoxic PTECs.

#### 5.4.4.5 PDK1 expression changed over the time course in podocytes and PTECs

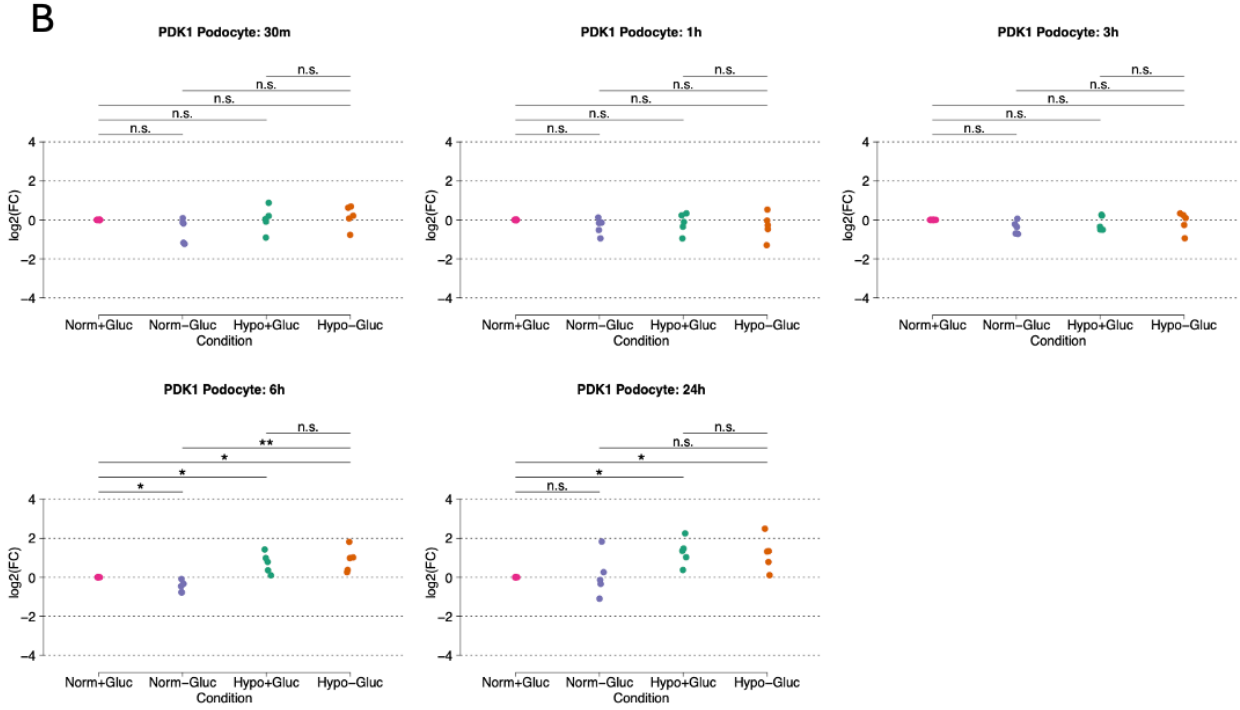
Pyruvate dehydrogenase kinase 1 (PDK1) is a mitochondrial enzyme that regulates glycolysis and oxidative phosphorylation. PDK1 is induced by HIF1α promoting glycolysis[273], and inhibits pyruvate dehydrogenase, reducing the conversion of pyruvate to acetyl-CoA in the CAC[274]. Here PDK1 expression should increase with hypoxia.

PDK1 expression increased in hypoxic podocytes at 6h and 24h and was observed to decreased in Norm-Gluc cells at 6h.

A




B




C

**T-test p.values**

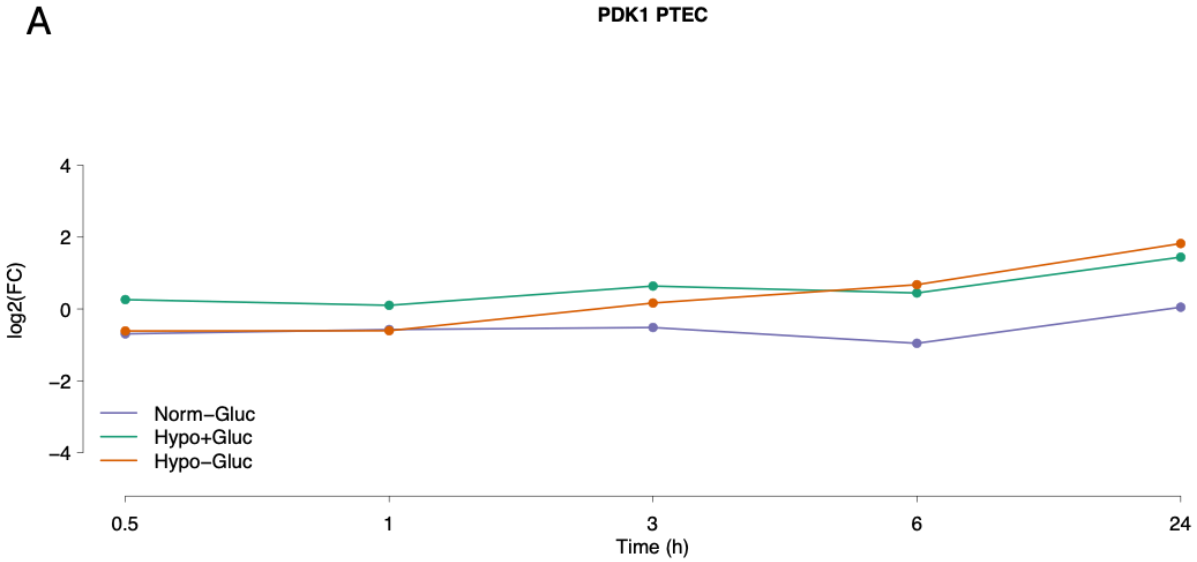
| Time Point | Norm-Gluc | Hypox+Gluc | Hypox-Gluc | Norm-Gluc Vs Hypo-Gluc | Hypo+Gluc Vs Hypo-Gluc |
|---|---|---|---|---|---|
| 30m | 0.13472 | 0.93346 | 0.55866 | 0.10920 | 0.72525 |
| 1h | 0.15271 | 0.50730 | 0.35795 | 0.96201 | 0.71636 |
| 3h | 0.05820 | 0.37074 | 0.67133 | 0.34006 | 0.82464 |
| 6h | 0.02073 | 0.03487 | 0.03272 | 0.00473 | 0.67120 |
| 24h | 0.84318 | 0.01331 | 0.03661 | 0.11589 | 0.86557 |

**Figure 5-U: PDK1 mRNA expression in podocytes cultured under normoxic and hypoxic conditions**

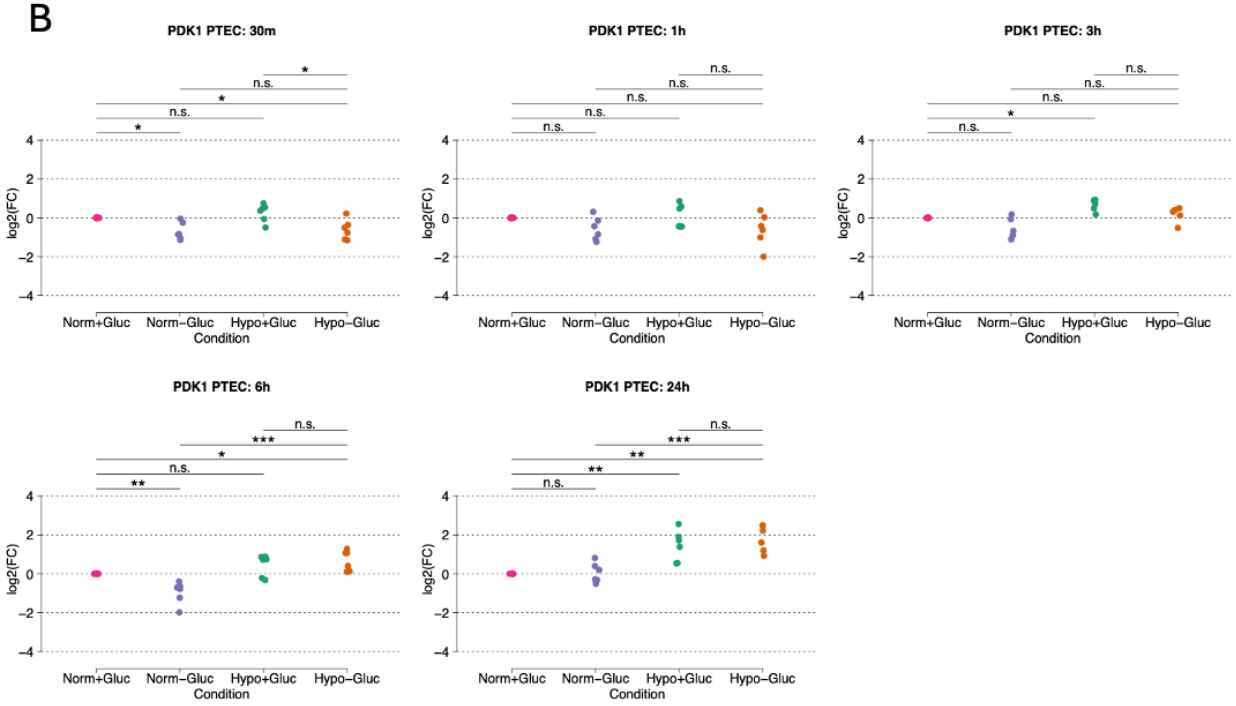
Podocytes were cultured under normoxic and hypoxic conditions for 30m, 1h, 3h, 6h and 24h in media +/- glucose. Cell mRNA was measured for PDK1 expression. (A) depicts expression of PDK1 in podocytes across the time course, highlighting changes in expression at each time point based on treatment. (B) maps change in PDK1 expression with cell treatments across the different time points. (C) shows t-test p.values comparing each condition to Norm+Gluc, then between experimental conditions. PDK1 expression decreased in Norm-Gluc cells from 6h and increased in hypoxic cells between 6h and 24h.

PDK1 expression decreased in Norm-Gluc PTECs and increased in Hypo-Gluc PTECs from 30m. Expression did not differ at 1h and 3h. At 6h and 24h PDK1 expression in hypoxic PTECs increased. PDK1 expression decreased at 6h in Norm-Gluc PTECs.

A




B




C

**T-test p.values**

| Time Point | Norm-Gluc | Hypox+Gluc | Hypox-Gluc | Norm-Gluc Vs Hypo-Gluc | Hypo+Gluc Vs Hypo-Gluc |
|---|---|---|---|---|---|
| 30m | 0.01217 | 0.22200 | 0.03334 | 0.77877 | 0.01138 |
| 1h | 0.06441 | 0.69828 | 0.13800 | 0.94038 | 0.12847 |
| 3h | 0.10288 | 0.01064 | 0.41171 | 0.05837 | 0.07584 |
| 6h | 0.00957 | 0.10797 | 0.02515 | 0.00045 | 0.47707 |
| 24h | 0.82229 | 0.00673 | 0.00118 | 0.00055 | 0.39371 |

**Figure 5-V: PDK1 mRNA expression in PTECs cultured under normoxic and hypoxic conditions**

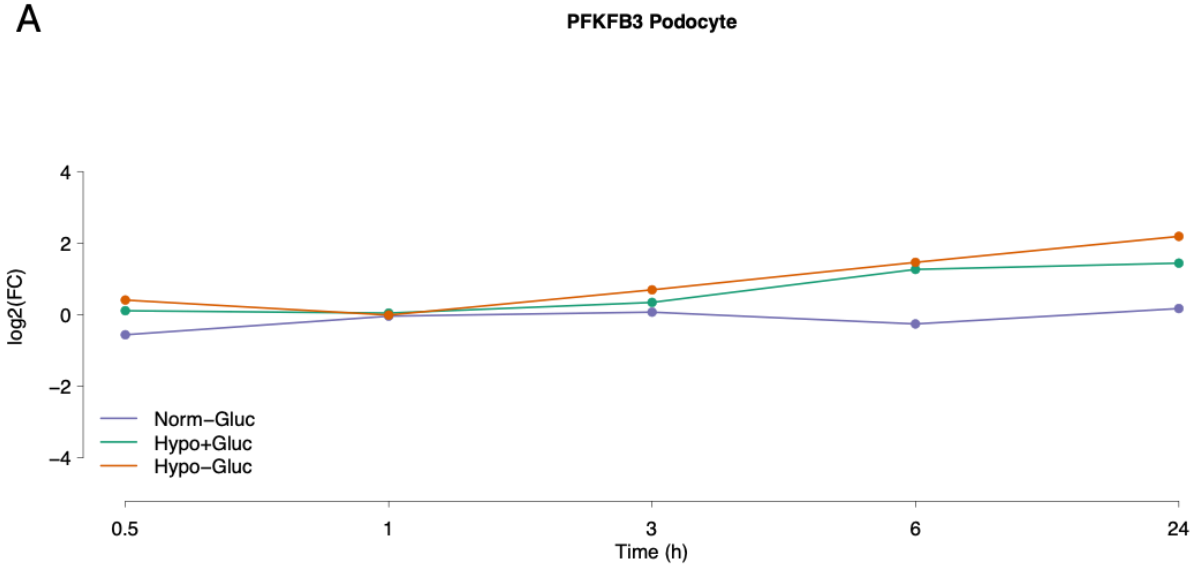
PTECs were cultured under normoxic and hypoxic conditions for 30m, 1h, 3h, 6h and 24h in media +/- glucose. Cell mRNA was measured for PDK1 expression. (A) depicts expression of PDK1 in PTECs across the time course, highlighting changes in expression at each time point based on treatment. (B) maps change in PDK1 expression with cell treatments across the different time points. (C) shows t-test p.values comparing each condition to Norm+Gluc, then between experimental conditions. PDK1 expression decreased in Norm-Gluc cells from 30m and at 6h and 24h. In Hypo-Gluc cells PDK1 expression increased at 6h up to 24h and increased in Hypo+Gluc cells from 24h

#### 5.4.4.6 PFKFB3 expression increased with hypoxia in both podocyte and PTECs

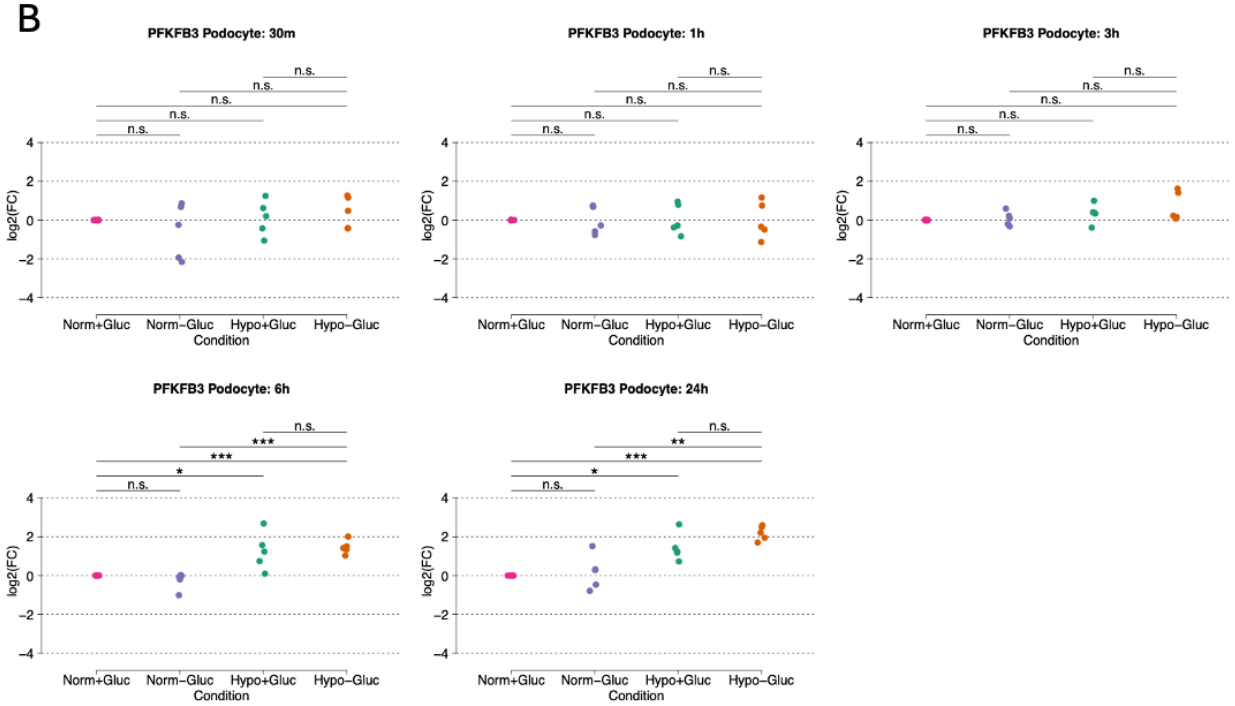
6-phosphofructo-2-kinase/fructose-2,6-biphosphatase 3 (PFKFB3) enzyme controls glycolytic flux by regulating intracellular concentrations of fructose 2,6-biphosphate, activating 6-phosphofructo-1-kinase *via* the glycolysis pathway (Figure 4-S). When PFKFB3 expression is low, glycolysis is downregulated. Hypoxia increases PFKFB3 expression and stimulates glycolytic pathways.

PFKFB3 expression increased in hypoxic podocytes at 6h and 24h of culture. Podocytes cultured under normoxic conditions did not have increased PFKFB3 expression.

A




B




C

**T-test p.values**

| Time Point | Norm-Gluc | Hypox+Gluc | Hypox-Gluc | Norm-Gluc Vs Hypo-Gluc | Hypo+Gluc Vs Hypo-Gluc |
|---|---|---|---|---|---|
| 30m | 0.42813 | 0.79245 | 0.32564 | 0.23152 | 0.59828 |
| 1h | 0.90704 | 0.90168 | 0.98261 | 0.95642 | 0.92155 |
| 3h | 0.67727 | 0.19223 | 0.10802 | 0.14867 | 0.41215 |
| 6h | 0.25244 | 0.04311 | 0.00076 | 0.00015 | 0.68601 |
| 24h | 0.68673 | 0.01082 | 0.00019 | 0.00461 | 0.08323 |

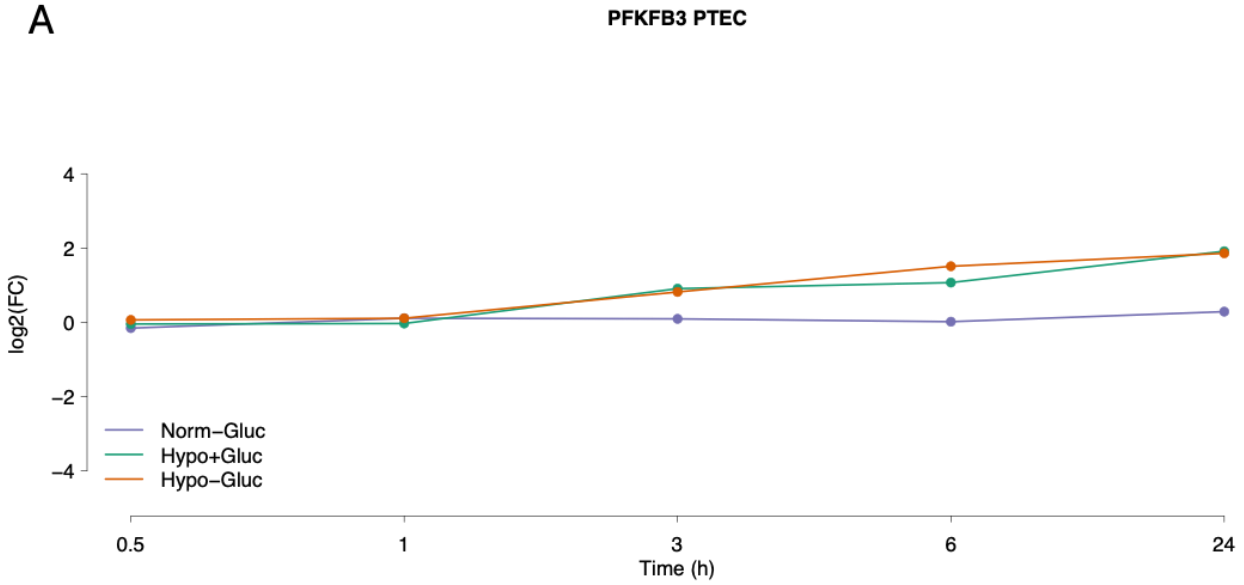
**Figure 5-W: PFKFB3 mRNA expression in podocytes cultured under normoxic and hypoxic conditions**

Podocytes were cultured under normoxic and hypoxic conditions for 30m, 1h, 3h, 6h and 24h in media +/- glucose. Cell mRNA was measured for PFKFB3 expression. (A) depicts expression of PFKFB3 in podocytes across the time course, highlighting changes in expression at each time point based on treatment. (B) maps change in PFKFB3 expression with cell treatments across the different time points. (C) shows t-test p.values comparing each condition to Norm+Gluc, then between experimental conditions. PFKFB3 expression increased in hypoxic cells from 6h up to 24h.

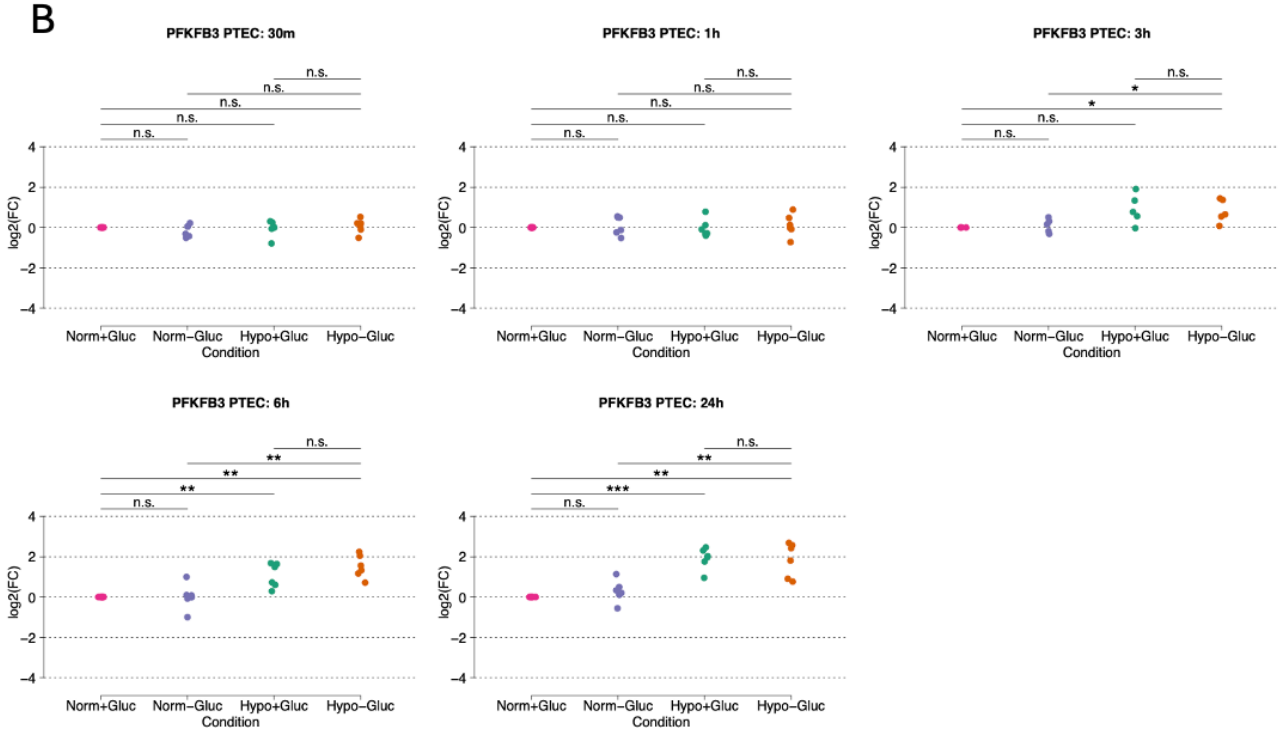
PFKFB3 expression in PTECs increased in hypoxic treated cells between 3h and 24h.

Expression of PFKFB3 did not change in Norm-Gluc treated PTECs.

A




B




C

**T-test p.values**

| Time Point | Norm-Gluc | Hypox+Gluc | Hypox-Gluc | Norm-Gluc Vs Hypo-Gluc | Hypo+Gluc Vs Hypo-Gluc |
|---|---|---|---|---|---|
| 30m | 0.26887 | 0.79293 | 0.66128 | 0.27121 | 0.61711 |
| 1h | 0.58170 | 0.87430 | 0.63930 | 0.99968 | 0.63324 |
| 3h | 0.56820 | 0.05210 | 0.03392 | 0.04936 | 0.83672 |
| 6h | 0.94561 | 0.00732 | 0.00126 | 0.00161 | 0.22282 |
| 24h | 0.25481 | 0.00031 | 0.00306 | 0.00466 | 0.89483 |

**Figure 5-X: PFKFB3 mRNA expression in PTECs cultured under normoxic and hypoxic conditions**

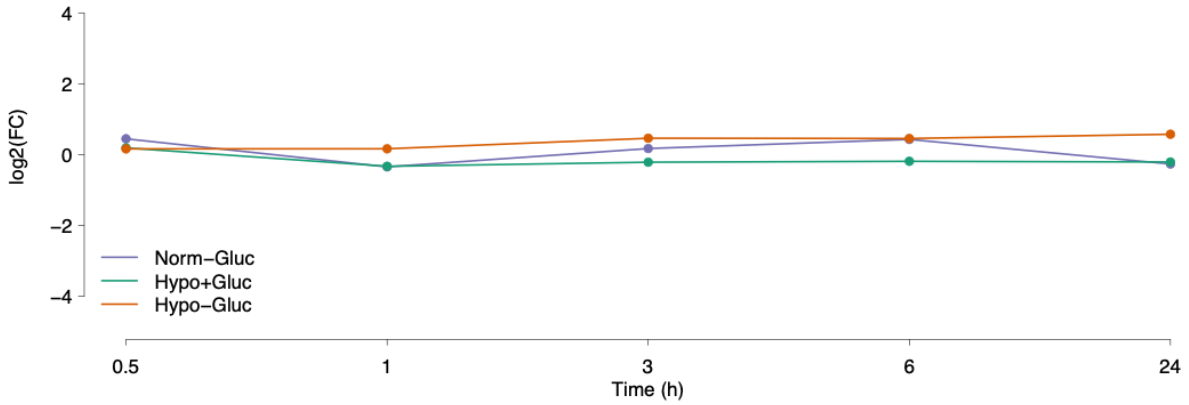
PTECs were cultured under normoxic and hypoxic conditions for 30m, 1h, 3h, 6h and 24h in media +/- glucose. Cell mRNA was measured for PDK1 expression. (A) depicts expression of PFKFB3 in PTECs across the time course, highlighting changes in expression at each time point based on treatment. (B) maps change in PFKFB3 expression with cell treatments across the different time points. (C) shows t-test p.values comparing each condition to Norm+Gluc, then between experimental conditions. PFKFB3 expression increased in Hypo-Gluc cells from 3h and in Hypo+Gluc cells from 6h. Expression was increased in hypoxic PTECs at 24h. There was no change in PFKFB3 expression in Norm-Gluc PTECs

#### 5.4.4.7 PGC1α expression did not change in podocytes despite treatment and was variably expressed in PTECs

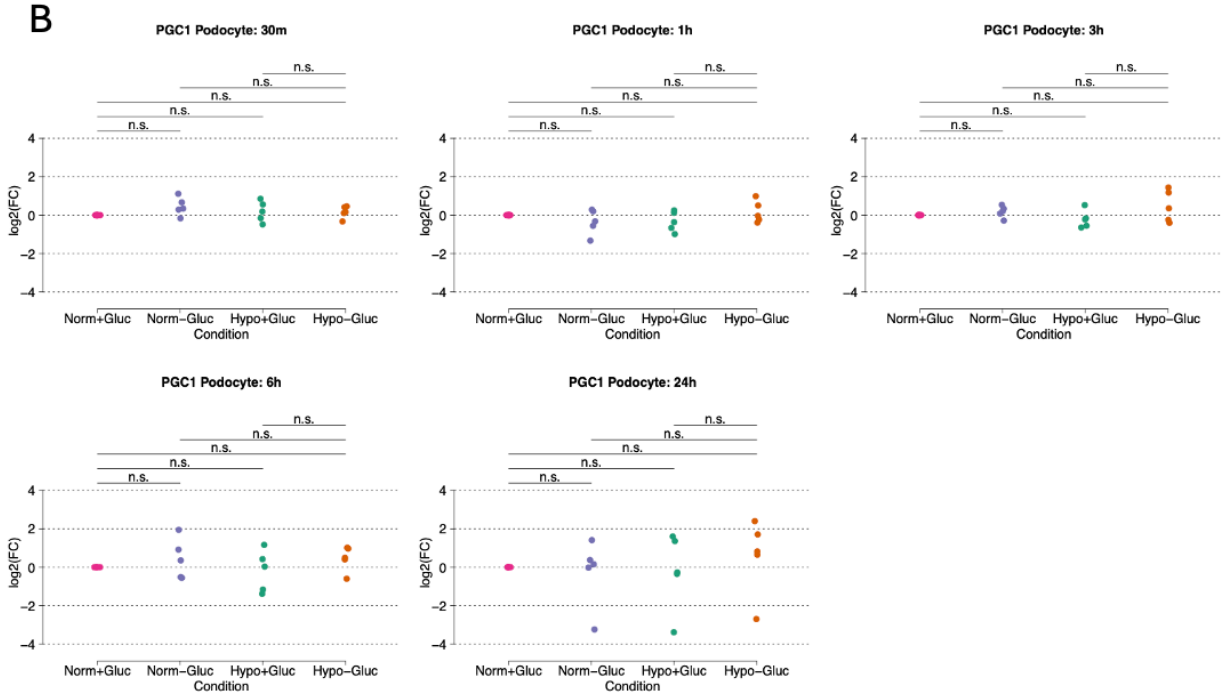
Peroxisome proliferator-activated receptor gamma coactivator 1-alpha (PGC1α) is a key regulator of genes associated with energy metabolism induced by various physiological conditions that demand increased mitochondrial energy production[275,276]. PGC1α expression is upregulated during hypoxia[276].

In podocytes, PGC1α expression did not change between 30m and 24h under normoxic or hypoxic conditions.

A




B




C

**T-test p.values**

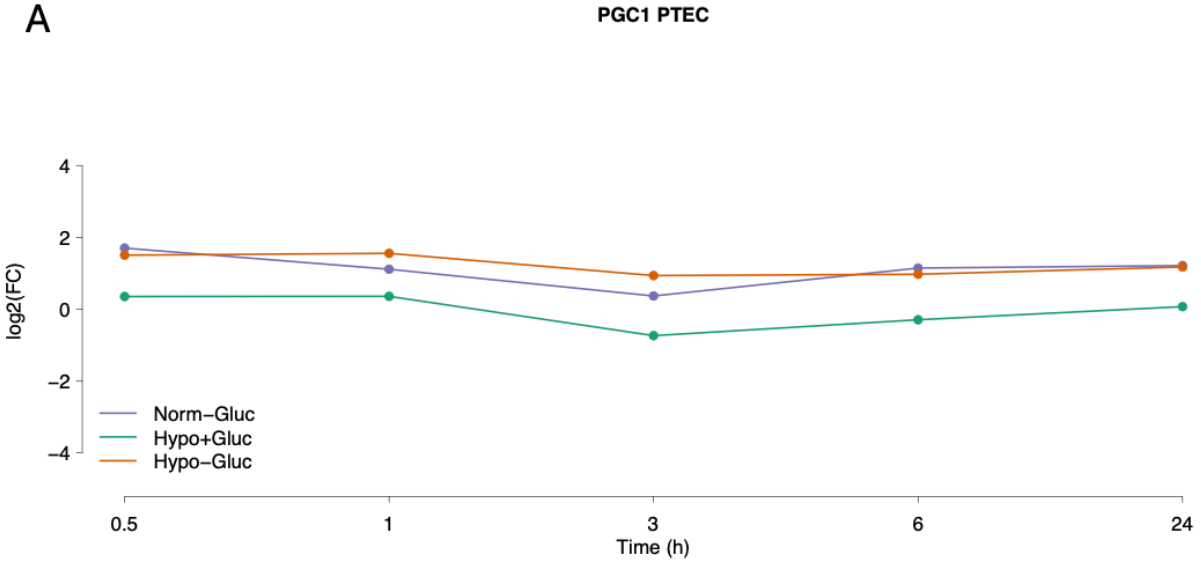
| Time Point | Norm-Gluc | Hypox+Gluc | Hypox-Gluc | Norm-Gluc Vs Hypo-Gluc | Hypo+Gluc Vs Hypo-Gluc |
|---|---|---|---|---|---|
| 30m | 0.10267 | 0.46869 | 0.30803 | 0.30074 | 0.92266 |
| 1h | 0.30316 | 0.23216 | 0.55112 | 0.22492 | 0.19063 |
| 3h | 0.27715 | 0.35670 | 0.27762 | 0.49377 | 0.15804 |
| 6h | 0.41098 | 0.71791 | 0.19270 | 0.96379 | 0.29292 |
| 24h | 0.75328 | 0.82683 | 0.54760 | 0.49603 | 0.54815 |

**Figure 5-Y: PGC1α mRNA expression in podocytes cultured under normoxic and hypoxic conditions**

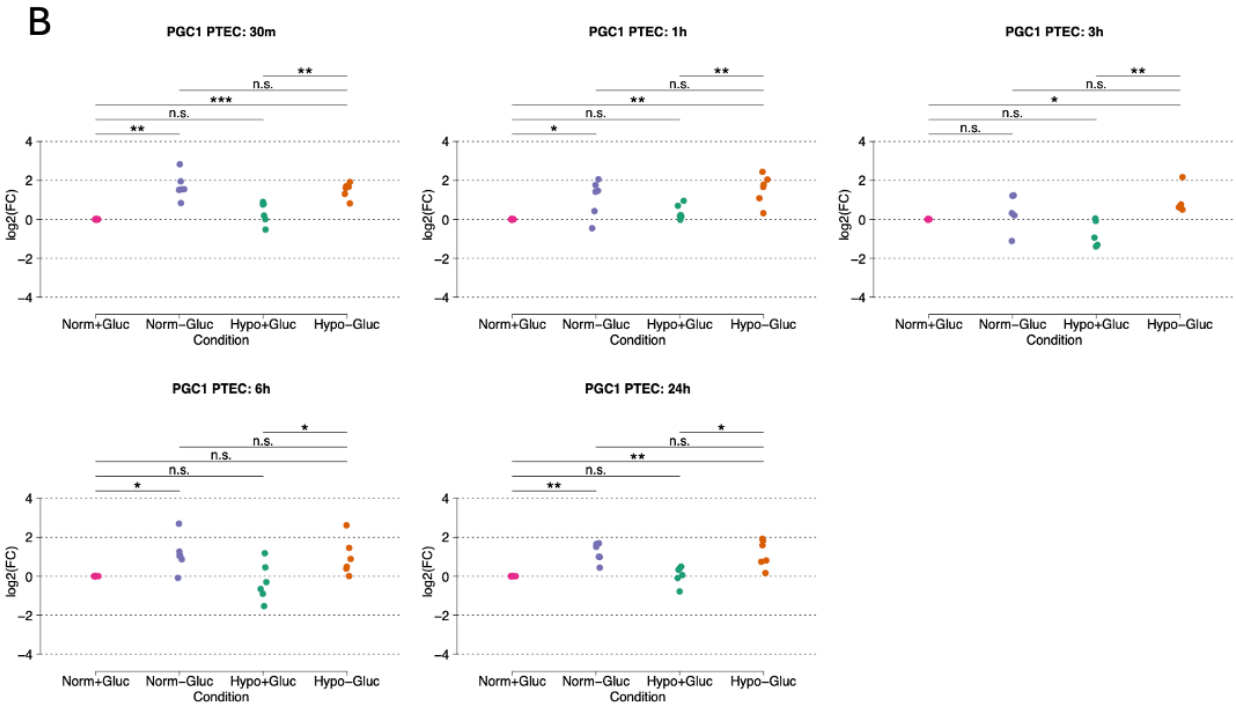
Podocytes were cultured under normoxic and hypoxic conditions for 30m, 1h, 3h, 6h and 24h in media +/- glucose. Cell mRNA was measured for PGC1α expression. (A) depicts expression of PGC1α in podocytes across the time course, highlighting changes in expression at each time point based on treatment. (B) maps change in PGC1α expression with cell treatments across the different time points. (C) shows t-test p.values comparing each condition to Norm+Gluc, then between experimental conditions. There was no difference in expression of PGC1α in podocytes cultured until normoxic or hypoxic conditions +/- glucose.

PGC1α expression in PTEC cells varied, dependent on culture conditions. At 30m up to 24h, PGC1α expression increased in the cells cultured without glucose. PGC1α expression in the Hypo+Gluc PTECs trended down compared with the Norm+Gluc cells, although this did not reach significance.

A




B




C

**T-test p.values**

| Time Point | Norm-Gluc | Hypox+Gluc | Hypox-Gluc | Norm-Gluc Vs Hypo-Gluc | Hypo+Gluc Vs Hypo-Gluc |
|---|---|---|---|---|---|
| 30m | 0.00145 | 0.18435 | 0.00022 | 0.54476 | 0.00264 |
| 1h | 0.03463 | 0.06738 | 0.00396 | 0.39301 | 0.00965 |
| 3h | 0.43844 | 0.07194 | 0.03949 | 0.31739 | 0.00486 |
| 6h | 0.02630 | 0.49321 | 0.05264 | 0.75315 | 0.04526 |
| 24h | 0.00182 | 0.72628 | 0.00953 | 0.91211 | 0.01161 |

**Figure 5-Z: PGC1α mRNA expression in PTECs cultured under normoxic and hypoxic conditions**

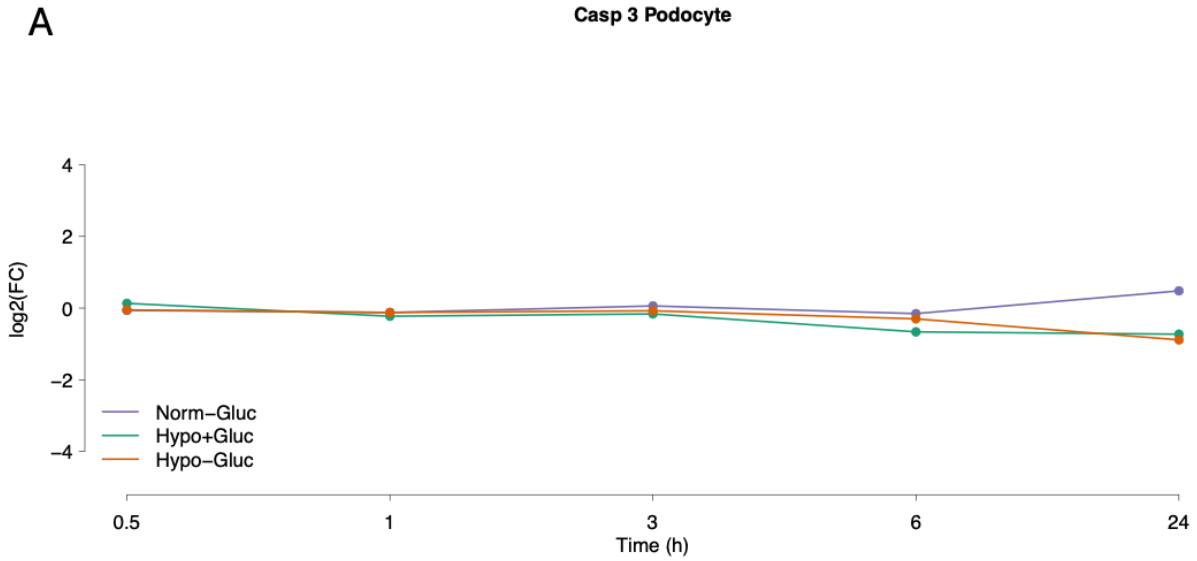
PTECs were cultured under normoxic and hypoxic conditions for 30m, 1h, 3h, 6h and 24h in media +/- glucose. Cell mRNA was measured for PGC1α expression. (A) depicts expression of PGC1α in PTECs across the time course, highlighting changes in expression at each time point based on treatment. (B) maps change in PGC1α expression with cell treatments across the different time points. (C) shows t-test p.values comparing each condition to Norm+Gluc, then between experimental conditions. PGC1α expression increased in Norm-Gluc cells from 30m up to 24h. Expression also increased in Hypo-Gluc cells from 30m up to 24h. PGC1α expression did not increase in Hypo+Gluc cells at any time point.

#### 5.4.4.8 Caspase-3 expression was variable in podocytes and PTECs cultured under normoxic and hypoxic conditions

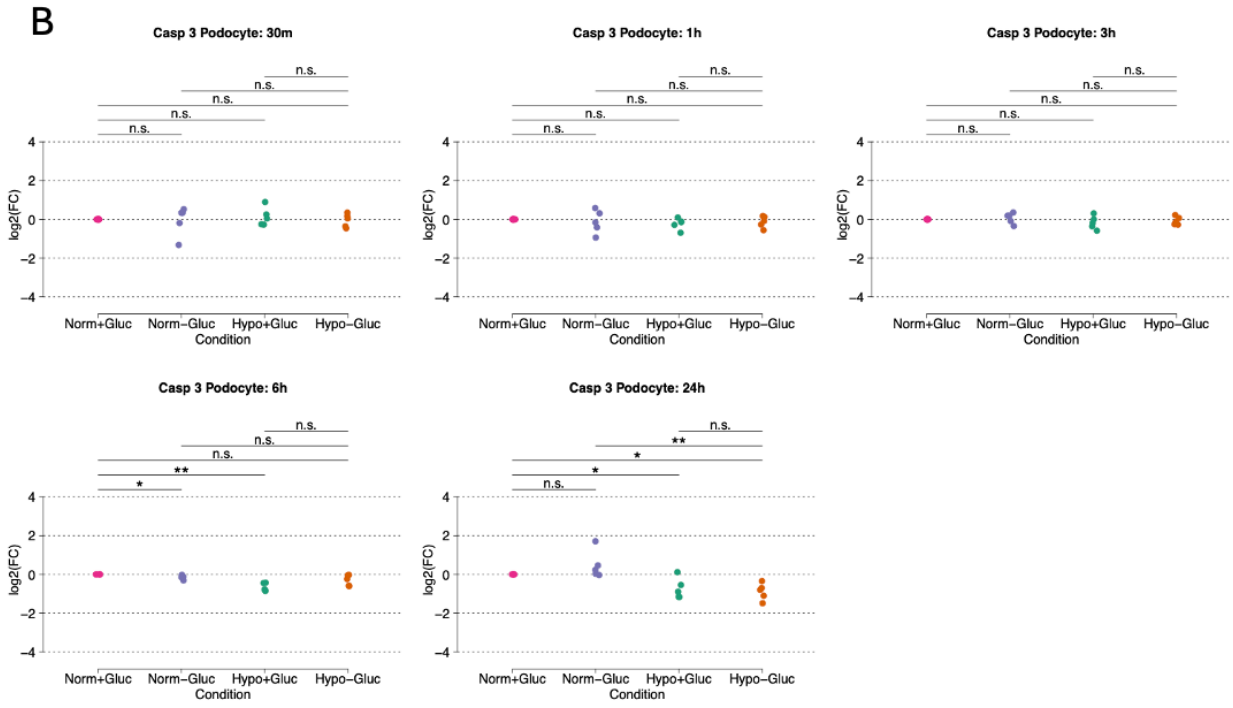
Caspase-3 (CASP3) is a cysteine protease commonly associated with the apoptotic pathway. Under hypoxic conditions, stimulation of the intrinsic or mitochondrial pathway leads to apoptosis. During apoptosis, CASP3 cleaves downstream substrates in the pathways causing morphological changes in apoptotic cells[277]. CASP3 is also associated with inflammation and fibrosis in the kidney and has previously been associated with renal scarring and kidney disease[278]. CASP3 expression increases with hypoxia.

Caspase-3 expression decreased in hypoxic cells at 6h and 24h. Expression of CASP3 trended upwards in Norm-Gluc cells at 24h yet did not reach significance.

A




B




C

**T-test p.values**

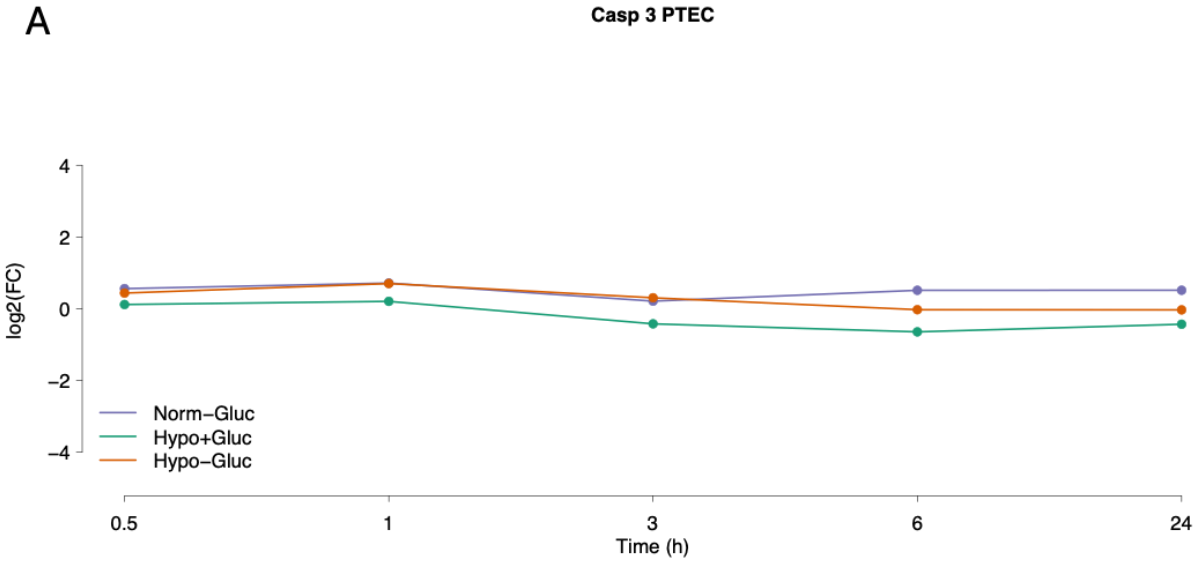
| Time Point | Norm-Gluc | Hypox+Gluc | Hypox-Gluc | Norm-Gluc Vs Hypo-Gluc | Hypo+Gluc Vs Hypo-Gluc |
|---|---|---|---|---|---|
| 30m | 0.86098 | 0.56861 | 0.75777 | 0.97602 | 0.50791 |
| 1h | 0.67000 | 0.15719 | 0.41089 | 0.99938 | 0.59282 |
| 3h | 0.64941 | 0.34494 | 0.48163 | 0.41499 | 0.63717 |
| 6h | 0.02789 | 0.00205 | 0.07488 | 0.32399 | 0.05110 |
| 24h | 0.20587 | 0.03843 | 0.01005 | 0.00886 | 0.62148 |

**Figure 5-AA: Caspase-3 mRNA expression in podocytes cultured under normoxic and hypoxic conditions**

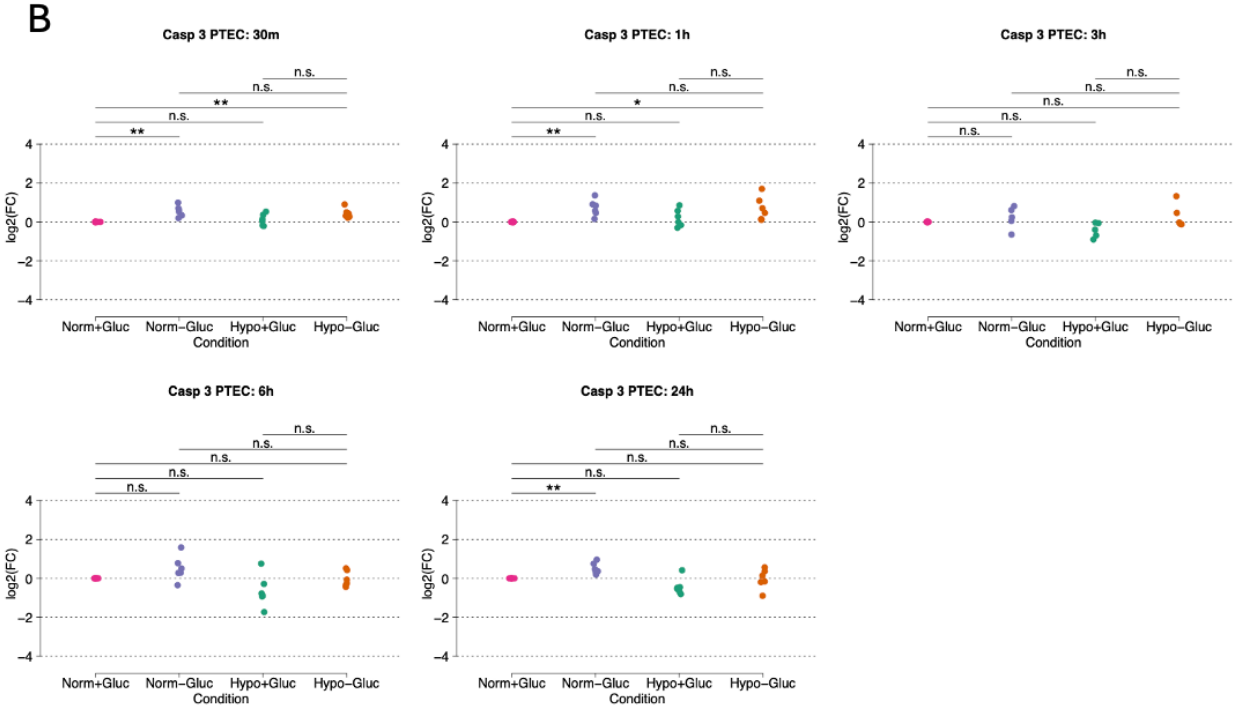
Podocytes were cultured under normoxic and hypoxic conditions for 30m, 1h, 3h, 6h and 24h in media +/- glucose. Cell mRNA was measured for Caspase-3 expression. (A) depicts expression of Caspase-3 in podocytes across the time course, highlighting changes in expression at each time point based on treatment. (B) maps change in Caspase-3 expression with cell treatments across the different time points. (C) shows t-test p.values comparing each condition to Norm+Gluc, then between experimental conditions. Caspase-3 expression increased in Norm-Gluc cells from 6h up to 24h but decreased in hypoxic cells at 6h and 24h.

Caspase-3 expression increased in Norm-Gluc PTECs at 30m, 1h and 24h. At 6h, expression of CASP3 started trending down in hypoxic treated PTECs. Increased expression in cells cultured without glucose indicates a potential hypoglycaemic stress response.

A




B




C

**T-test p.values**

| Time Point | Norm-Gluc | Hypox+Gluc | Hypox-Gluc | Norm-Gluc Vs Hypo-Gluc | Hypo+Gluc Vs Hypo-Gluc |
|---|---|---|---|---|---|
| 30m | 0.00456 | 0.36933 | 0.00764 | 0.43756 | 0.07005 |
| 1h | 0.00843 | 0.30897 | 0.03702 | 0.96627 | 0.14169 |
| 3h | 0.44923 | 0.06958 | 0.32933 | 0.80822 | 0.06194 |
| 6h | 0.10794 | 0.11515 | 0.87972 | 0.11794 | 0.14296 |
| 24h | 0.00696 | 0.05981 | 0.88771 | 0.05364 | 0.17820 |

**Figure 5-BB: Caspase-3 mRNA expression in PTECs cultured under normoxic and hypoxic conditions**

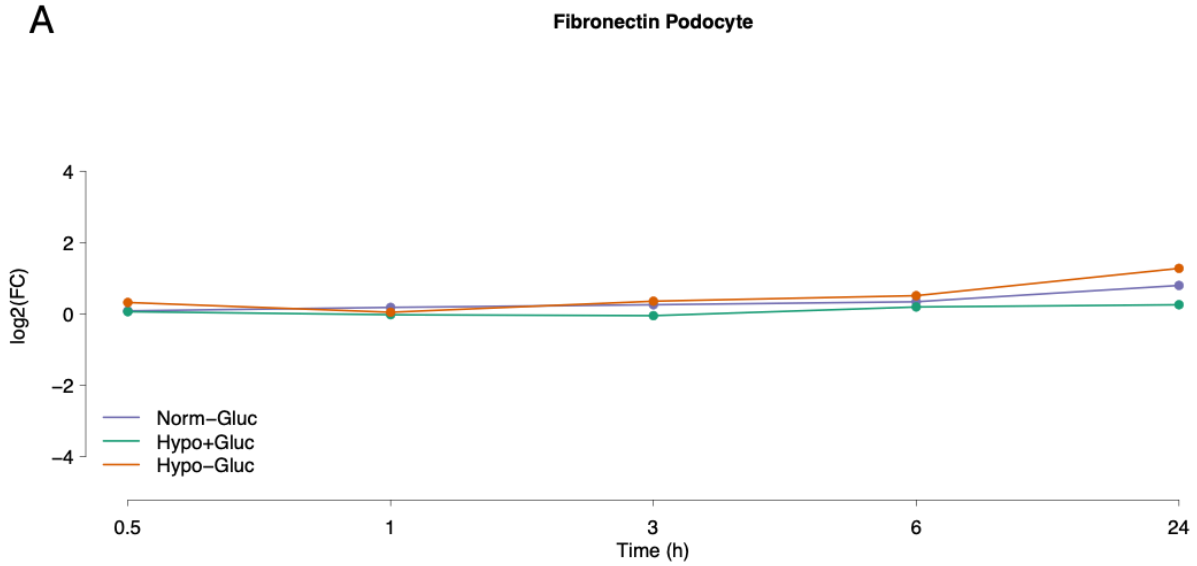
PTECs were cultured under normoxic and hypoxic conditions for 30m, 1h, 3h, 6h and 24h in media +/- glucose. Cell mRNA was measured for Caspase-3 expression. (A) depicts expression of Caspase-3 in PTECs across the time course, highlighting changes in expression at each time point based on treatment. (B) maps change in Caspase-3 expression with cell treatments across the different time points. (C) t-test p.values comparing each condition to Norm+Gluc, then between experimental conditions. Caspase-3 expression increased at 30m, 1h and 24h in Norm-Gluc PTECs. At 6h expression of Caspase-3 trended down in hypoxic cells however this did not reach significance.

#### 5.4.4.9 Fibronectin expression did not change in podocytes and PTECs under hypoxic conditions

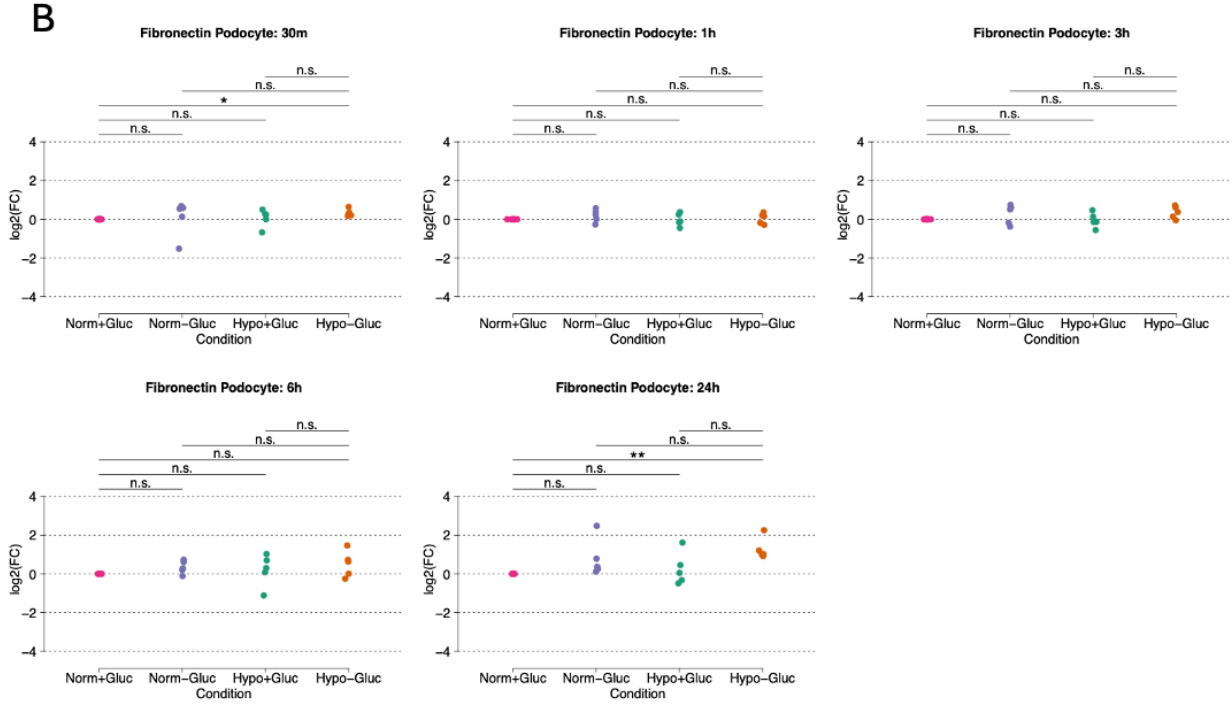
Fibronectin is a glycoprotein that interacts with other ECM proteins as well as other growth factors, small molecules, glycosaminoglycans, and cell surface receptors[279]. Through these connections, fibronectin provides essential structural and chemical signalling to regulate cellular behaviour[279]. Dysregulation in fibronectin expression is commonly associated with fibrosis in the kidney.

Fibronectin expression in Hypo-Gluc podocytes increased at 30m and 24h but did not change in podocytes cultured under other conditions.

A




B




C

**T-test p.values**

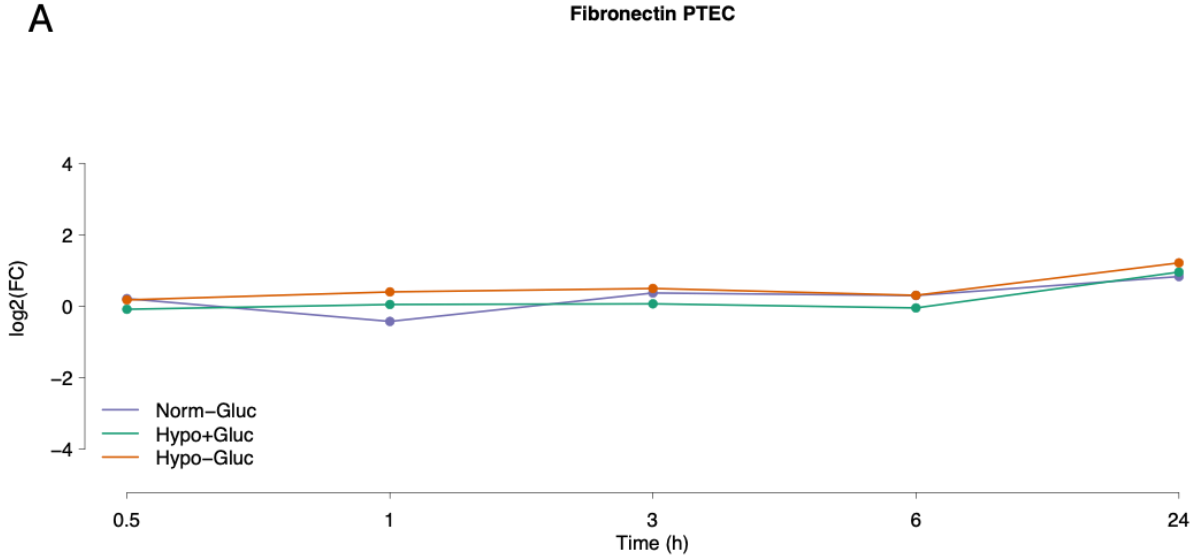
| Time Point | Norm-Gluc | Hypox+Gluc | Hypox-Gluc | Norm-Gluc Vs Hypo-Gluc | Hypo+Gluc Vs Hypo-Gluc |
|---|---|---|---|---|---|
| 30m | 0.84209 | 0.76282 | 0.01767 | 0.60243 | 0.28589 |
| 1h | 0.27390 | 0.89827 | 0.70906 | 0.49384 | 0.72840 |
| 3h | 0.31212 | 0.79463 | 0.06594 | 0.72142 | 0.10534 |
| 6h | 0.08462 | 0.61820 | 0.16241 | 0.63049 | 0.52300 |
| 24h | 0.13968 | 0.52734 | 0.00676 | 0.37360 | 0.05865 |

**Figure 5-CC: Fibronectin mRNA expression in podocytes cultured under normoxic and hypoxic conditions**

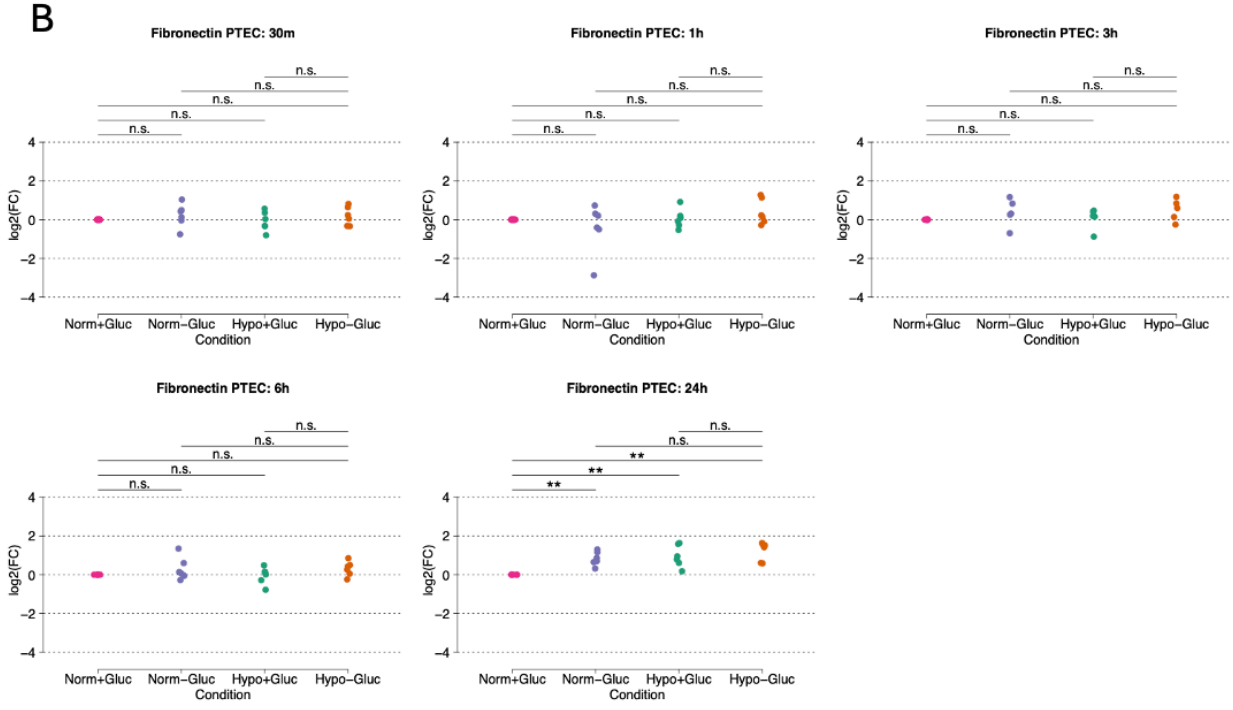
Podocytes were cultured under normoxic and hypoxic conditions for 30m, 1h, 3h, 6h and 24h in media +/- glucose. Cell mRNA was measured for Fibronectin expression. (A) depicts expression of fibronectin in podocytes across the time course, highlighting changes in expression at each time point based on treatment. (B) maps change in fibronectin expression with cell treatments across the different time points. (C) shows t-test p.values comparing each condition to Norm+Gluc, then between experimental conditions. Fibronectin was only increased in Hypo-Gluc podocytes at 30m and 24h.

Fibronectin expression increased in PTECs cultured for 24h, under both normoxic and hypoxic conditions.

A




B




C

**T-test p.values**

| Time Point | Norm-Gluc | Hypox+Gluc | Hypox-Gluc | Norm-Gluc Vs Hypo-Gluc | Hypo+Gluc Vs Hypo-Gluc |
|---|---|---|---|---|---|
| 30m | 0.42234 | 0.70067 | 0.40300 | 0.91131 | 0.37712 |
| 1h | 0.45587 | 0.81501 | 0.19061 | 0.20071 | 0.31827 |
| 3h | 0.30511 | 0.79060 | 0.12000 | 0.76306 | 0.25677 |
| 6h | 0.26545 | 0.80462 | 0.10294 | 0.98556 | 0.16478 |
| 24h | 0.00232 | 0.00896 | 0.00167 | 0.15354 | 0.41894 |

**Figure 5-DD: Fibronectin mRNA expression in PTECs cultured under normoxic and hypoxic conditions**

PTECs were cultured under normoxic and hypoxic conditions for 30m, 1h, 3h, 6h and 24h in media +/- glucose. Cell mRNA was measured for Fibronectin expression. (A) depicts expression of Fibronectin in PTECs across the time course, highlighting changes in expression at each time point based on treatment. (B) maps change in Fibronectin expression with cell treatments across the different time points. (C) shows t-test p.values comparing each condition to Norm+Gluc, then between experimental conditions. Fibronectin expression increased in all experimental groups at 24h.

### 5.4.5 Comparison of changes in gene expression in podocytes and PTECs cultured under normoxic and hypoxic conditions +/- glucose over culture time

To evaluate change in gene expression in podocytes and PTECs across the culture time course (24h), a one-way analysis of variance test (ANOVA) was used, comparing within the experimental groups. Two heatmaps, Figure 5-EE for podocytes and Figure 5-FF for PTECs are presented below and use a colour scale to highlight changes in mRNA expression over time. Significant p.values are highlighted in blue. In podocytes and PTECs cultured under hypoxic conditions, HIF1$\alpha$ and HIF2$\alpha$ expression is increased at 30minutes and decreases gradually over the culture time course. Expression of PHD2, PHD3, BNIP3, Glut1, PDK1, PFKFB3 and fibronectin in cells cultured under hypoxic conditions increased over the culture time course. Expression of these markers in Norm-Gluc cells was variable over the time course.

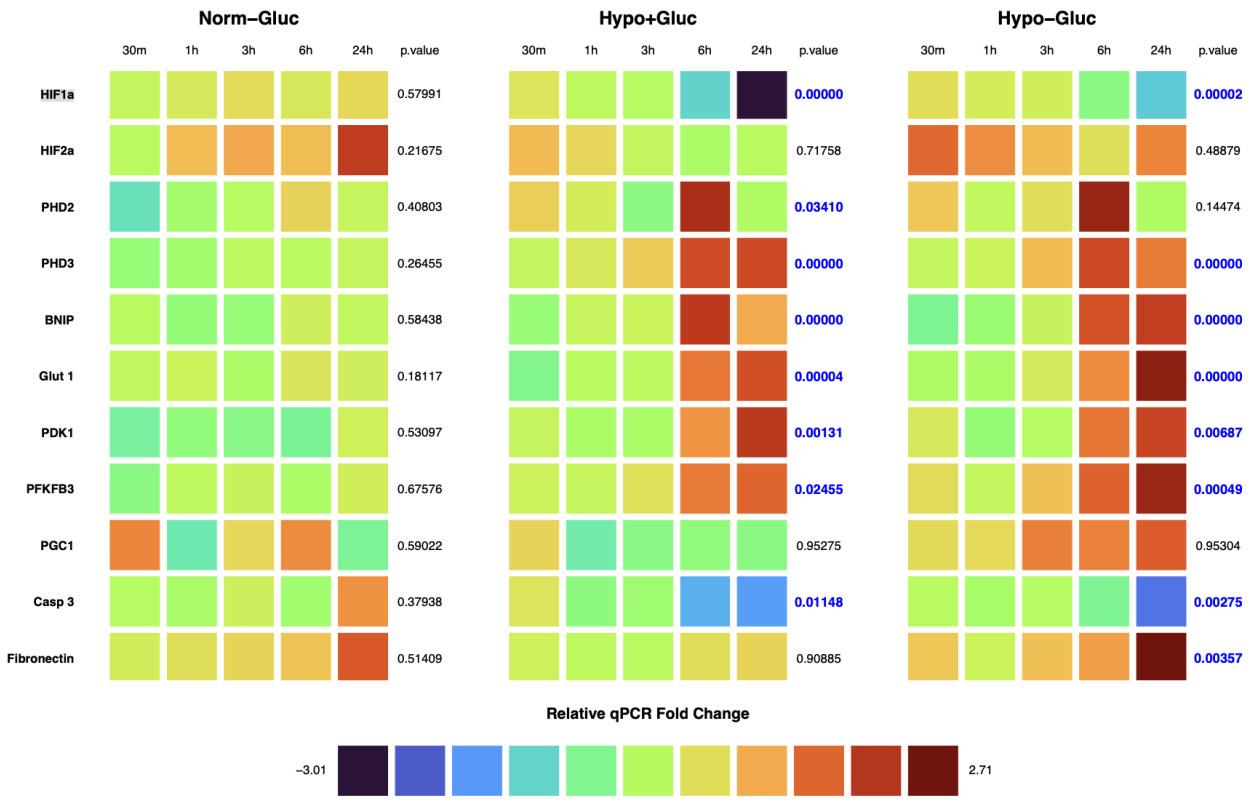



**Figure 5-EE: Summary of mRNA expression for all analytes in cultured podocytes**

Heatmap highlighting changes in mRNA expression for each analyte over the 24h culture. Colour change from blue to red indicate changes in mRNA expression. The p.values were derived from a one-way ANOVA comparing analyte expression within each condition over time – significant p.values are highlighted in blue.

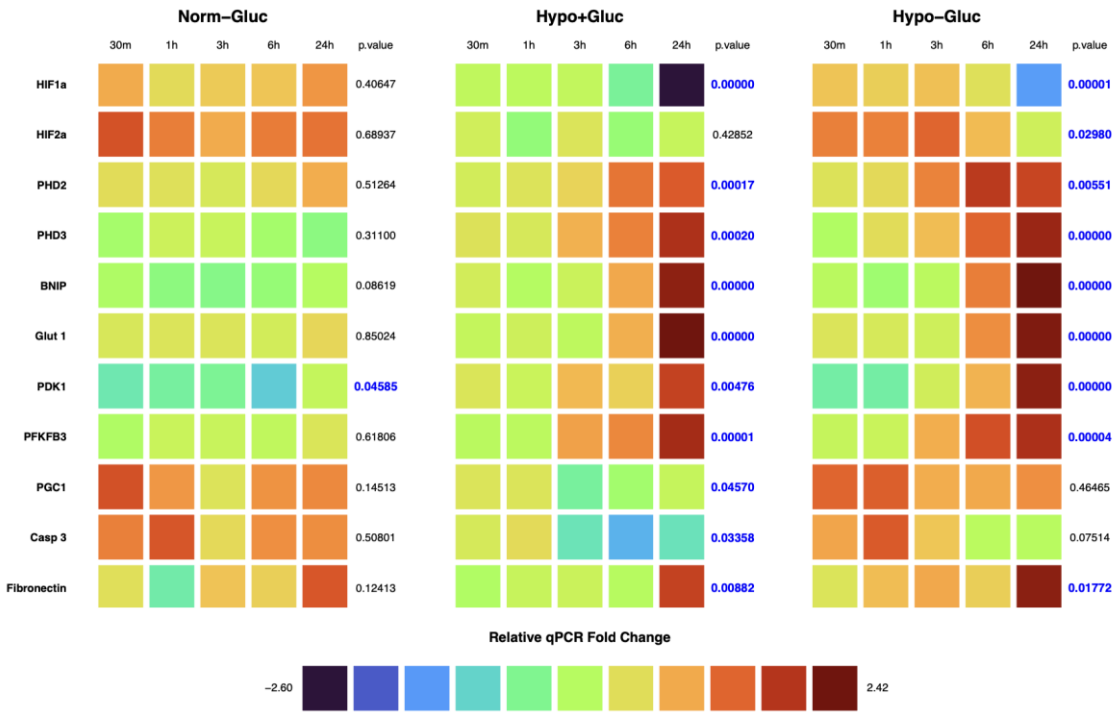



**Figure 5-FF: Summary of mRNA expression for all analytes in cultured PTECs**

Heatmap highlighting changes in mRNA expression for each analyte over the 24h culture. Colour change from blue to red indicate changes in mRNA expression over time. The p.values were derived from a one-way ANOVA comparing analyte expression within each condition over time – significant p.values are highlighted in blue.

## 5.5 Discussion

This chapter describes the optimisation of a hypoxic human immortalised podocyte and PTEC cell model. Three methods to induce hypoxia were tested, with GasPak-pouches selected as the best and most robust method to naturally induce hypoxia in the cells. Confirmation of a 'hypoxic cell response' was measured using qPCR (Figure 5-F).

### 5.5.1 Glucose concentration during cell culturing may influence metabolic processes in podocytes and PTECs

In Chapter 4, metabolic processes in DCD kidneys were shown to be significantly modified as fWIT was prolonged, specifically indicating changes in glucose utilisation in the kidney. Variance in glucose utilisation and metabolism has also been described in cultured cells. The Crabtree effect first described in cancer cells refers to the phenomena that cells cultured in glucose rich media will shift from aerobic respiration to glycolysis to generate ATP[268,280,281]. The mechanism driving this shift is poorly understood and does not occur in all cell types[268]. Previously, PTECs cultured in low glucose concentrations were shown to exhibit the Crabtree effect, however the reason for this is unclear[268].

In this study, to avoid drawing conclusions about hypoxic changes and later metabolic changes in podocytes and PTECs that are glucose driven, podocytes and PTECs were cultured under 'normal' glucose concentrations and without glucose. Further work is required in this area to understand difference in podocyte and PTEC response to hypoxic conditions associated with glucose, but this was beyond the scope of this thesis.

### 5.5.2 GasPak-pouches are a reliable method of inducing cell hypoxia

A tri-gas incubator connected to a nitrogen supply and $CoCl_2$ were the two alternative methods compared to induce hypoxia. The nitrogen-fed incubator was quickly ruled out

as a reliable way to induce hypoxia, as the incubator's internal environment could not maintain the hypoxic conditions when the incubator was accessed. Nitrogen incubators have previously been described in the literature, with nitrogen suppressing the oxygen concentration within the incubator, inducing hypoxia. Each time the incubator door was opened, the oxygen concentration increased and was not immediately reduced. This meant that hypoxia could not be reliably monitored over a definitive time course and therefore this method was quickly eliminated. An alternative incubator design or a hypoxic chamber may have been better suited to this experiment.

Cobalt chloride chemically mimics hypoxia by stabilising HIFs under normoxic conditions, *via* PHD inhibition, yet the mechanisms of this remain elusive[257]. In this study, several concentrations of $CoCl_2$ were tested to monitor the effect of the compound on the cells and to determine cellular toxicity. Concentrations <250µM were not toxic to the podocytes or PTECs. Use of $CoCl_2$ to induce hypoxia benefits from being affordable and not requiring additional large equipment[269]. However, the mechanism and reliability of $CoCl_2$ to mimic hypoxia remains underexplored especially in kidney cells. Previous studies comparing chemical to physical induced hypoxia have shown varying cellular, metabolic and physical responses to the 'hypoxic' insult. Muñoz-Sánchez and Chánez-Cárdenas[257] summarised various hypoxic cell model studies in 2019, showing variances in metabolic, transcriptional and signalling pathways in $CoCl_2$ compared to oxygen deprivation models[257]. More recently, Muniz *et al* has shown variance in moderate and severe hypoxia by comparing between chemical and physical hypoxia. In stem cells hypoxia-induced metabolic responses are different in moderate and severe hypoxia[269]. These studies have demonstrated that significant optimisation would be required to

proceed with a $CoCl_2$ model of hypoxia, which was also beyond the scope of this thesis. Following determination of the 'optimal' $CoCl_2$ concentration to induce hypoxia, any proceeding biological changes associated with hypoxia would need to be validated in a physical hypoxic culture system such as use of a hypoxic chamber, for the same cells. Therefore, this model was not used for this study.

Given the significant limitations of utilising a tri-gas incubator and $CoCl_2$ to induce hypoxia, the GasPak-pouch method was preferable. The GasPak-pouch has an incorporated monitoring system and naturally induces hypoxia by scavenging oxygen from the pouch's internal environment. As this method had not previously been used in cells before, confirmation of cell hypoxia was required. Analysis of gene expression in podocytes and PTECs cultured within the GasPak-pouches over the 24h culture period demonstrated that gene upregulation in response to hypoxia occurred as expected, providing additional confidence, that the GasPak-pouch model induces cell hypoxia.

### 5.5.3 HIF expression changed over time in Podocytes and PTECs

HIF1α and HIF2α are proteins commonly considered to be the master regulators of the cell's hypoxic response[161]. HIFs are differentially distributed in cells and when activated regulate hundreds of genes affecting cell metabolism, the cell cycle and inflammation[161]. Both HIFs regulate 'common' genes and specific targets, for example, HIF1α regulates glycolysis associated genes and HIF2α regulate TGFα genes[282]. HIF is a heterodimeric complex regulated by the oxygen regulated α-subunits (α1-3). During hypoxia the HIFα-subunits accumulate and enter the nucleus where they bind to the β subunit to form the HIF-dimer[113,283]. HIF activity is regulated by PHD enzymes that hydroxylate prolyl

residues. Under normoxic conditions, PHDs initiate HIF degradation *via* the von Hippel-Lindau proteasome pathway[282,284,285]. The HIF pathway is also regulated by factor inhibiting HIF (FIH), a hydroxylase that regulates HIFs transcriptional activity by inhibiting its interaction with P300/CRP[283] and is also implicated in other cellular processes including glucose metabolism, inflammation and CKD[286]. Under hypoxic conditions PHD and FIH activity is supressed. The α subunit subsequently accumulates and binds to the β subunit and recruits co-activators to HREs (Figure 5-GG)[282,285]. HIF signalling and PHD regulation respond promptly to changes in oxygenation[113]. HIF activation has been previously demonstrated in donor biopsies and associates with proximal tubule injury and survival[113,287].

In this study, HIF1α and HIF2α gene expression was measured using qPCR as an indicator of hypoxia in podocytes and PTECs cultured using GasPak-pouches. In podocytes and PTECs, HIF1α expression was increased in cells cultured without glucose and those under hypoxic conditions at 1h. HIF1α expression then decreased in the hypoxia treated cells at 6h. HIF2α expression increased in podocytes after 1h hypoxia but did not increase at later time points. In PTECs, HIF2α expression increased in cells without glucose as early as 30m, continuing up to 6h. These results are in line with those previous reported by Uchida *et al*[288] and Cavadas *et al*[289]. In both studies, in different cell types HIF1α mRNA expression increased initially with hypoxia exposure but decreased below baseline after 6h. Uchida *et al* also reported that HIF2α expression, although initially increased, did not decrease below baseline during prolonged hypoxia[288]. These results show the variability in HIFs response to reduced oxygenation and cellular stress. HIF1α and HIF2α expression increased in Norm-Gluc cells. HIF1α expression has previously been shown to increase

under hypoglycaemic culture conditions, promoting vascular endothelial growth factor expression and dysregulating metabolic processes including glycolysis[290]. HIF activation under normoxic conditions was associated with metabolic regulation[291,292], switching metabolic processes from oxidative phosphorylation to glycolysis[19], modulating intracellular glucose utilisation[292].

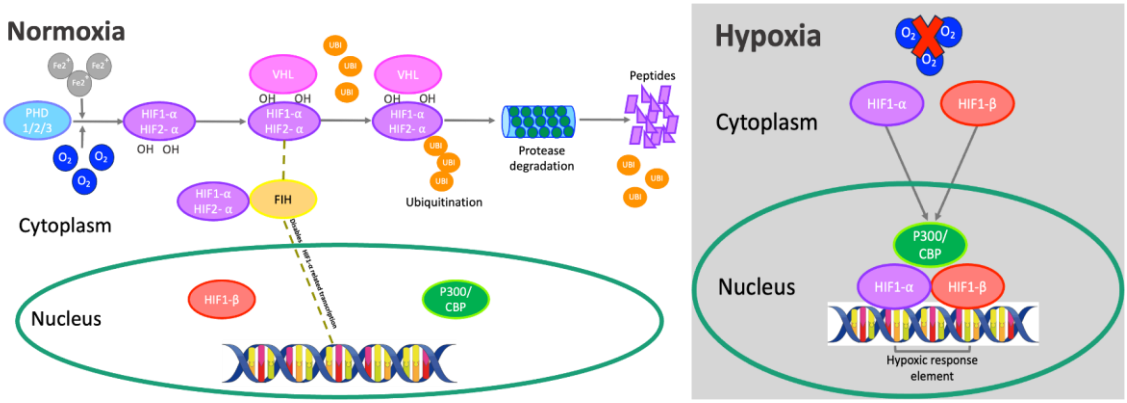



**Figure 5-GG – HIF under normoxic and hypoxic conditions**

Schematic diagram showing the tagging and subsequent degradation of HIFs during normoxia compared to its stabilisation under hypoxic conditions.

### 5.5.4 PHDs are key oxygen sensors and regulate HIF stability

Prolyl 4-hydroxylase domains (PHD) are the main oxygen sensors in cells[293]. PHDs hydroxylate HIFs under normoxic conditions at two proline residues, promoting their degradation *via* the von Hippel Lindau proteasome[294]. PHD expression varies among cells and tissues, whilst their activity varies between isoforms. PHD2 senses normoxia and mild hypoxia[293], and targets HIF1α specifically. PHD3 acts on both HIF1α and HIF2α, and has been found to be activated in higher concentrations under hypoxic condtions[272].

Both PHD2 and PHD3 mRNA expression increases with hypoxia, indicative of the ability of PHDs' to adjust to oxygen availability[295].

In this study, PHD2 and PHD3 mRNA expression was measured using qPCR to monitor the cells' response to the hypoxic conditions. In both podocytes and PTECs both PHD2 and PHD3 concentration increased with time in cells cultured under hypoxic conditions. In PTECs PHD2 and PHD3 expression increased from 30m in hypoxic cells. In podocytes, PHD2 expression increased from 6h, and PHD3 increased from 3h. Increased expression of PHD2 and PHD3 in cells cultured under hypoxic conditions confirmed that hypoxia was induced in the cells using the GasPak-pouch system, confirming it a viable model to induce hypoxia.

### 5.5.5 HIFs upregulate genes *via* the hypoxic response element (HRE)

When stabilised by hypoxia, HIF initiates a programme of gene expression aimed to overcome oxygen deprivation in the cell. The HIF dimer binds to HREs on target genes promoting transcription. There are hundreds of identified and described gene targets for HIFs, many of which regulate metabolic processes. Previously described gene targets of HIFs were measured here to demonstrate the downstream implications of HIF-activation in podocytes and PTECs cultured using GasPak-pouches.

HIF activation is associated with significant metabolic changes, especially the upregulation of glycolysis and downregulation of oxidative phosphorylation. Here genes associated with metabolic pathways were analysed, including BNIP3, Glut1, PDK1,

PFKFB3 and PGC1α. Caspase 3 and Fibronectin mRNA expression were also measured as indicators of apoptosis and fibrosis, respectively.

BNIP3 was upregulated in hypoxic podocytes and PTECs after 6h culture in the GasPak-pouch. In both podocytes and PTECs, BNIP3 expression was decreased below control levels, in cells cultured under Norm-Gluc and hypoxic conditions, at 30m, gradually increasing in hypoxic cells from 1h. Under normoxic conditions, BNIP3 transcription is silenced by NFKB *via* gene promotor binding. During hypoxia, BNIP3 transcription and translation is increased[296], the activity of NFKB is also upregulated during hypoxia. Binding of NFKB to the BNIP3 promoter region may potentially explain the reduction in BNIP3 mRNA expression at 30minutes and in Norm-Gluc PTECs. As BNIP3 mRNA levels typically parallel with BNIP3 protein expression[297], measuring BNIP3 protein expression in cultured cells could confirm whether BNIP3 transcription is reduced during early hypoxia. Additionally, measuring changes in NFKB expression in hypoxic cells could provide additional insight into the BNIP and NFKB relationship. BNIP3 regulates mitochondrial function and moderates mitophagy, the elimination of damaged mitochondria[298]. BNIP3 is also protective in the proximal tubule during IRI, mediating mitophagy[299], cell death and protecting against renal fibrosis[300]. Interestingly, mitophagy is increased in AKI but decreased in CKD[301]. The change in BNIP3 described in AKI and CKD should be explored as a potential marker of a good- and suboptimal-function in DD kidneys, especially in DCD kidneys where mitochondrial function is likely to be reduced with prolonged fWIT.

Glycolysis is upregulated during hypoxia, with HIF1$\alpha$ mediating increased glucose uptake by increasing the expression of glucose trasporters[19], including GLUT1. GLUT1 is one of two ways that glucose can be transported across cell membranes in the kidneys, and is expressed in both the glomerulus and tubular regions[302]. The efficient transport of glucose *via* GLUT1 is essential to the glycolytic flux described in hypoxia[283] and was evidenced in the hypoxic podocytes and PTECs. GLUT1 mRNA expression increased after 6h in both podocytes and PTECs, likely increasing their capacity to uptake glucose[303] and fuel glycolytic processes.

PDK1 transcription is also upregulated by HIF. PDK1 phosphorylates the pyruvate dehydrogenase complex supressing the conversion of pyruvate to acetyl-CoA inhibiting the CAC cycle (Figure 4-T)[304]. In podocytes and PTECs cultured in GasPak-pouches, PDK1 expression was increased after 6h and was downregulated in Norm-Gluc cells compared to Norm+Gluc. This indicates a suppression in pyruvate conversion to acetyl-CoA and a metabolic shift in both cell types, most probably to anaerobic processes.

PFKFB3 regulates glucose uptake and the glycolytic flux during hypoxia, and has also been associated with angiogenesis[283]. PFKFB3 knockout inhibits glycolysis, as PFKFB3 is involved in the generation of fructose 2,6-bisphosphate, an enzyme that regulates glycolytic activity[283]. In GasPak-pouch incubated podocytes and PTECs, PFKFB3 expression was increased at 6h, highlighting a HIF-driven switch to glycolytic metabolism in these cells. The upregulation of PFKFB3 may associate with kidney fibrosis as reported in mice by Wang *et al*[305]. Further assessment of the hypoxic podocytes and PTECS would be required to confirm this.

PGC1α is upregulated by HIF, boosting mitochondrial biogenesis[276]. It also has a critical role in regulating mitochondrial proteins[276] and in several metabolic pathways[306]. PGC1α prevents fibrosis and expression is reduced in AKI[306]. In this study the expression of PGC1α in hypoxic podocytes and PTECs were variable. There was no change in expression in podocytes, whilst regulation in PTECs was inconsistent across treatment and time. There was a trend observed where PGC1α increased in PTECs cultured without glucose, which was significant at 30m, 1h and 24h. Increased PGC1α expression in PTECs is not surprising, as PTECs are rich in mitochondria and have a high metabolic rate. Increased PGC1α expression may associate with its role in maintaining GLUT4 expression, another glucose transporter[307].

Caspase-3 is a well-known downstream mediator of apoptosis. In this study CASP3 was measured to monitor cell death in hypoxic cells. In podocytes CASP3 expression was decreased in hypoxia treated cells at 6h and 24h but increased in PTECS cultured without glucose at 30m and 1h and trended towards increased until 24h. This result suggests that glucose deprivation may invoke cell death in the proximal tubules, likely due to metabolic deprivation brought on by low glucose availability. PTECs have a high metabolic demand that cannot be sustained under anaerobic conditions. In this study, there was not visual evidence of significant cell death during the 24h culture period, however the observed trend towards increased CASP3 expression in PTECs cultured without glucose may indicate that prolonged glucose deprivation could lead to cell death. Further studies should monitor cell viability during the culture course and could examine earlier markers of cell death such as cytochrome C, Caspase-8 or Caspase-9.

Additionally, if the culture period is extended beyond 24h, monitoring CASP3 expression may be valuable to track the progression of cell death in these cells.

Fibronectin is an ECM protein that is upregulated in fibrosis and is a well-described substrate of LGMN. In this study, fibronectin expression was measured to monitor changes with hypoxia so that it could be associated with any measured changes in LGMN. Fibronectin increased in Hypo-Gluc podocytes at 30m and 24h. Fibronectin expression was increased compared to Norm+Gluc but did not reach significance at other time points. In PTECs fibronectin expression increased in all experimental groups at 24h. At 3h and 6h expression trended upwards in PTECs without glucose. These changes may associate with varying LGMN activity and warrants further investigation. In this study, fibronectin was not a reliable marker of induced hypoxia.

### 5.5.6 Conclusions, limitations and future work

The literature is rich with studies utilising hypoxic cells, many of which use hypoxic chambers. As this equipment was not available for this study and would require a large financial outlay, available nitrogen fed incubators were compared with $CoCl_2$ and GasPak-pouch methods to induce hypoxia.

As previously described in the literature, the 'Crabtree effect' can cause some cells to switch from normal metabolic processes to anaerobic glycolysis, utilising glucose available in the culture media. Unfortunately, it was not possible to test this in the podocytes and PTECs under normoxic or hypoxic conditions, due to several limitations associated with equipment and ability to maintain hypoxia during 'test' conditions. To

progress this work, methods to measure glucose consumption in podocytes and PTECs should be explored. Techniques including Seahorse analysis or secondary ion mass spectrometry could be used in future studies to monitor metabolic processes in cells during culture. For this study, use of a Seahorse analyser to measure glucose metabolism was considered however this would have required access specialised equipment to maintain the hypoxic conditions whilst the assay was being performed.

Due to the variability described in podocytes and PTECs cultured +/- glucose, follow up studies using this model should include a glucose titration experiment, monitoring how gene expression changes with glucose concentration over time. Future studies should also monitor the pH of the culture media over the time course and measure changes in metabolic markers including the accumulation of metabolic products as an indicator of changes in cell osmolarity. Changes in cell viability should be monitored as standard in all future studies using this cell model and can easily be done using trypan blue staining.

In this study, there was evidence of morphological changes in podocytes and PTECs associated with the length of hypoxia. Investigating the cause of these physiological changes was beyond the scope of this chapter but is something that should be investigated further. Morphological changes in the podocytes may associate with fibrotic pathways or changes in matrix proteins. This would be an interesting area for future investigation. Analysis of morphological changes could be performed using histological staining methods such as haematoxylin and eosin staining or by more in-depth analysis such as transcriptomics or proteomics.

Finally, in this chapter the impact of hypoxia on podocytes and PTECs has been monitored using previously described markers of hypoxia – these markers are not kidney or cell type specific. Future work using this model could look to evaluate changes in molecular markers and metabolic pathways that associated with prolonged periods of hypoxia as described in the degradomic data presented in Chapter 4. In this chapter there is preliminary evidence of a switch to glycolysis in both podocytes and PTECs, with hypoxia, yet this should be evaluated in more detail in both cell types, and related to other metabolic changes, including gluconeogenesis and mitochondrial capacity.

# Chapter 6 Validation of key HUNTER degradomic findings

## 6.1 Introduction

Chapter 4 describes the degradomic profiling of DCD kidneys with prolonged fWIT using the previously described HUNTER peptidomic technique. In this study, 42 DCD kidney biopsies were analysed using MS and bioinformatics. Increased abundance of seven endogenous peptides correlated to prolonged fWIT and subsequent ischaemia. Fifty-five biological pathways were significantly dysregulated with increasing fWIT. This analysis was the first to delve into molecular changes associated with increasing fWIT and demonstrated changes associated with cytoskeletal and matrix composition and metabolic regulation. Specifically, the analysis of the peptidomic data showed increased degradation of proteins integral to maintaining the cytoskeleton of glomerular and tubular cells and dysregulation of glucose metabolism in the kidney, which may limit cellular function, metabolic regulation and induce cell death. Pathway dysregulation indicated matrix and membrane disruption and dysregulation of metabolic pathways. Evaluation of protease activity revealed that increased LGMN activity correlated with longer fWIT. Activity of GRAM also increased with fWIT, whilst MMP3, CATB and TPP1 activity decreased as fWIT increased.

Proteostasis is the term used to refer to protein homeostasis – specifically, the regulated turnover and generation of proteins to maintain cellular function. Proteostasis regulates the cleavage of functional peptides that contribute to cellular functions including cell growth, stress response and immune signalling – the biological function of the generated peptides is often different to that of the derivative protein[308].

In humans, 600 different proteases have been identified[127] that have a critical role in most biological processes, including cell proliferation, migration, cell survival and protein turnover[309]. Proteases are expressed in their in-active zymogen form and are activated through autocatalytic activity or by another protease, protein or specific cofactors[128]. Regulation of the transcription and expression of proteases is poorly understood, but is likely controlled by hormones, growth factors, or immune driven mechanisms[128]. Protease dysregulation is associated with injury and disease states, including cancer, neurological disorders[309] and kidney disease[141]. Previously, dysregulation of calpain activity has been implicated in DBD kidneys causing cytoskeletal protein degradation, contributing to suboptimal kidney function posttransplant[16]. Proteases are promising therapeutic targets, yet our understanding of the impact of proteases activity in kidney injury is limited.

## 6.2 Hypothesis and aims

The degradomic analysis of DCD kidneys quantified changes of endogenous peptides with increasing fWIT and relevant protease activity associated with generation of the measured peptides. In this chapter, the degradation profiles of three proteins described in Chapter 4 as being degraded with increasing fWIT will be quantified in DCD kidney tissue. Western blotting will be used to visualise and quantify changes in protein and peptide abundance, as fWIT increases. The abundance of zymogen and active LGMN and CATB in kidney tissue and podocytes and PTECs cultured under normoxic and hypoxic conditions +/- glucose will also be quantified using Western blotting.

## 6.3 Materials and methods

### 6.3.1 Mapping endogenous peptides to each derivative protein

To validate changes in protein degradation in DCD kidneys, the measured peptides for three proteins – FBP1, NHERF1 and BHMT – were profiled. Using R Studio, the endogenous peptides associated with each protein to be validated were mapped using volcano plots. The sequence and length of each peptide was also retrieved from the raw data and listed for comparison. The molecular weight of each peptide was used to compare to degradation products quantified using Western blotting

### 6.3.2 Validation of peptidome changes using Western blotting

Western blotting was used to validate some of the key findings from the HUNTER study using kidney biopsies remaining from the HUNTER study and podocyte and PTEC homogenates. Antibodies were optimised to ensure that the antibody target epitopes would capture the degradation products identified in the HUNTER analysis. Methods for Western blotting can be found in Chapter 3 (3.7); kidney and cell homogenates were prepared into Laemmli buffer at a 1µg/µL (based on initial BCA), with 10-15µg of total protein loaded to each gel. Transferred membranes were probed with commercially available primary and secondary antibodies. Table 3-B lists the antibodies and dilutions used.

### 6.3.3 Analysis of Western blots

Quantification of Western blotting was performed using EMPIRIA studio (Li-cor, version 3.0.0.173), and analysed using R Studio. The expression of the full-length protein was compared to the endogenous peptide profiles. Protease zymogen and active form were

compared to determine the signal ratio in relation to fWIT. All quantified bands were normalised to β-actin. A linear model was used to analyse differences in protein and protease expression in kidney tissue, whilst a paired t-test compared expression in podocyte and PTECs. Tables with the p.values can be found in Chapter 8 (8.4).

### 6.3.4 Evaluation of protease targets

Protease activity for each endogenous protease is reported in relation to the peptides they are associated with. The online resource STRING was used to map the protein targets of each protease, providing additional insight into mechanisms of injury associated with fWIT.

## 6.4 Results

### 6.4.1 Validation of peptide and protease changes in DCD kidneys

Three proteins – FBP1, NHERF1 and BHMT – had increased endogenous peptide abundance in DCD kidneys with prolonged fWIT and were selected to be validated using Western blotting. LGMN and CATB peptidomic activity was quantified in DCD kidney tissue and *in vitro* normoxic/hypoxic podocyte and PTECs models also using Western blotting.

### 6.4.2 FBP1 endogenous peptides validated using Western blotting

Seven endogenous peptides were identified as being derived from the degradation of FBP1 and are listed in Figure 6A (A). These FBP1 peptides are also mapped on the volcano plot in Figure 6-A (B), in relation to all other measured endogenous peptides.

Two FBP1 peptides had increased abundances as fWIT increased, as indicated by the pink circles in the table (Figure 6-A (A)).

A

| Peptide number on plot | P1 Peptide | Peptide sequence | MW before peptide | MW of peptide and preceeding sequence |
|---|---|---|---|---|
| 1 | Q | APFDTDVNTLTR | 0.46350594 | 36.39698084 |
| 2 | T | AVKAISSAVR | 4.43099014 | 32.42949664 |
| 3 | S | EEDKHAIIVEPEKR | 10.30689104 | 26.55359574 |
| 4 | D | QAPFDTDVNTLTR | 0.33537524 | 36.52511154 |
| 5 | K | STDEPSEKDALQPGR | 15.45881894 | 21.40166784 |
| 6 | D | TDVNTLTR | 0.89396664 | 35.96652014 |
| 7 | C | VLVSEEDKHAIIVEPEKR | 9.90838824 | 26.95209854 |

B

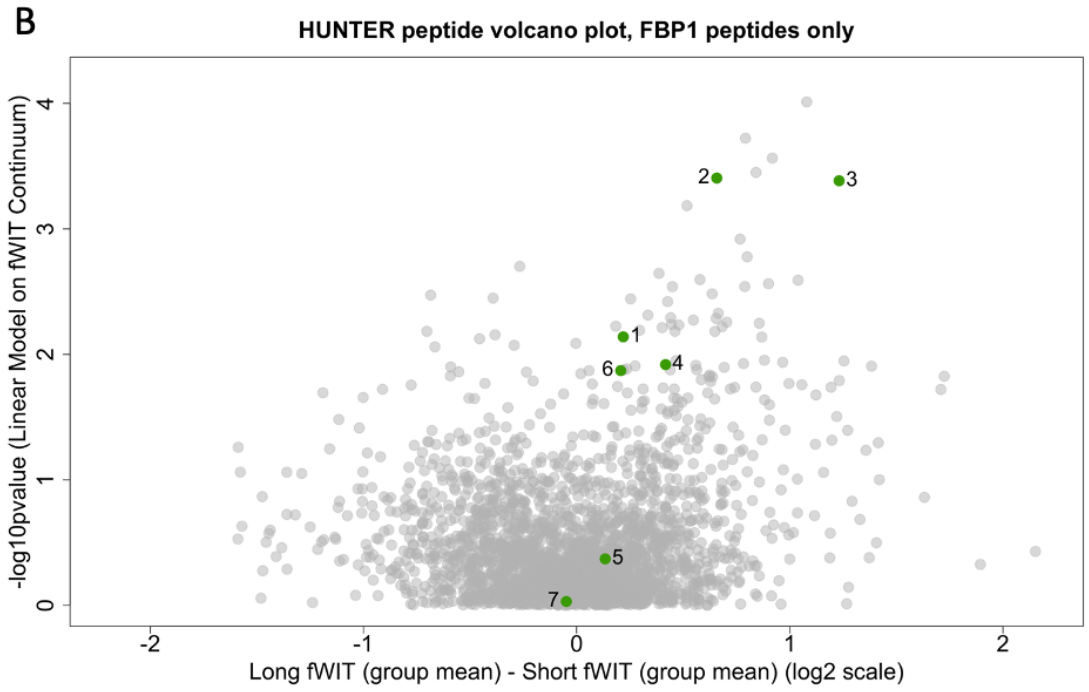



**Figure 6-A: Endogenous FBP1 peptides intensity increases with prolonged fWIT**

Endogenous peptides cleaved from the FBP1 protein are presented here. (A) provides a list of the seven peptides linked to FBP1. The two peptides indicated with pink circles increased in abundance with increasing fWIT. (B) shows a volcano plot of all identified endogenous peptides in the study. FBP1 peptides are numbered on the volcano plot (B) to match those in the table (A).

Western blotting was used to validate and quantify the expression of endogenous peptides in homogenised kidney biopsies. The full length FBP1 protein measured around 37kDa in size and can be visualised on the Western blot in Figure 6-B. The bands below 37kDa were degradation products cleaved from FBP1. The abundance of FBP1 increased with fWIT (left to right) which can be clearly seen on the Western blot in Figure 6-B (B). Increased FBP1 abundance was confirmed using densitometry. FBP1 degradation products were observed as increasing with fWIT; this was confirmed using densitometry (Figure 6-B (C)). There were four peptide bands (degradation products) visible on the Western blot, two of which had the same molecular weight as the two peptides measured by MS as increasing in abundance with fWIT. These peptides measured at 32 and 26kDa and are indicated with arrows on Figure 6-B (A). The abundance of endogenous peptides relative to full length FBP1 increased as fWIT was prolonged (Figure 6-B (D&E)).

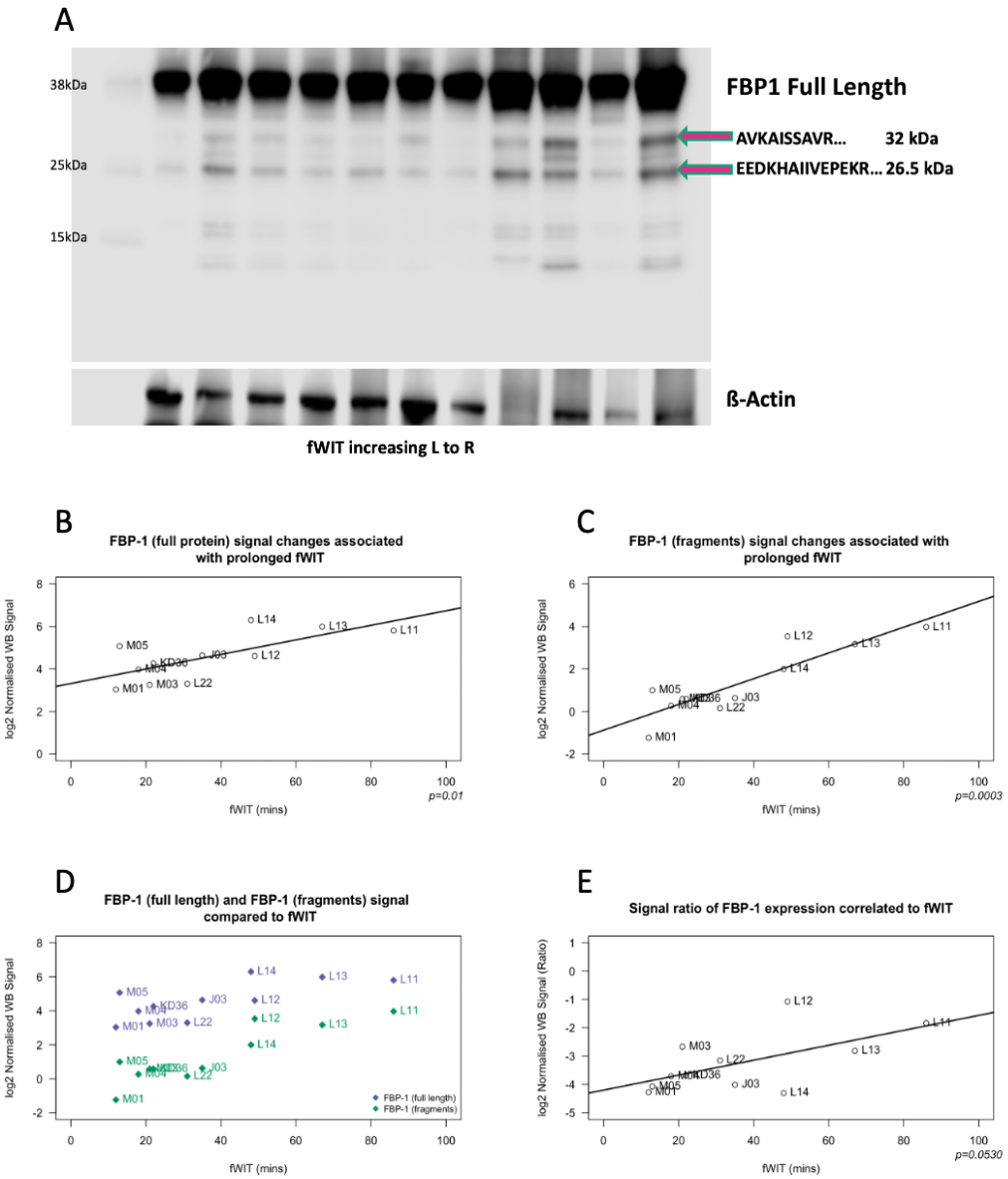



**Figure 6-B: Western blotting shows increased degradation of FBP1 with increasing fWIT**

Increased fWIT in DCD kidneys associates with increased expression of FBP1 endogenous peptides. (A) shows Western blot analysis of n=11 kidney biopsies with increasing fWIT (left-to-right). The two peptides that changed significantly with prolonged fWIT are indicated on the blot with arrows. (B) maps the quantitation of full length FBP1 showing increased FBP1 expression associated with increased fWIT (p=0.01). (C) maps the quantitation of degradation products showing that increased protein fragments associated with increased fWIT (p=0.0003). (D) shows the ratio of expression of full length FBP1 (purple) compared to expression of endogenous peptides (green), where increased abundance of FBP1 peptides with fWIT is apparent. (E) shows the signal ratio of peptide to full length FBP1 that increases with fWIT (p=0.053).

### 6.4.3 Western blotting to measure NHERF1

Several antibodies specific to NHERF1 were worked-up in attempts to validate the expression of NHERF1 derived endogenous peptides in kidney biopsy homogenates. Twelve endogenous peptides were mapped to NHERF1 and are listed in Figure 6-C (A). Each NHERF1 peptide is also mapped on the endogenous peptide volcano plot in part (B) of the figure. One NHERF1 endogenous peptide's abundance significantly increased with fWIT and is labelled as peptide 1. This peptide has a molecular weight of 38.5kDa, which is only 0.4kDa less than the full-length protein. Western blot analysis of NHERF1 was not possible due to poor specificity of the trialled antibodies, and because the significant peptide's molecular weight was too close to that of the full length NHERF1 protein.

A

| Peptide number on plot | P1 Peptide | Peptide sequence | MW before peptide | MW of peptide and preceeding sequence |
|---|---|---|---|---|
| 1 | D | AAAGAPLPR | 0.42245344 | 38.46399424 |
| 2 | Q | AEPPAAAEVQGAGNENEPR | 12.81558724 | 26.07086044 |
| 3 | Q | EAPGQAEPPAAAEVQGAGNENEPR | 12.33309364 | 26.55335404 |
| 4 | A | EPPAAAEVQGAGNENEPR | 12.88666604 | 25.99978164 |
| 5 | N | GENVEKETHQQVVSR | 6.54452924 | 32.34191844 |
| 6 | N | GVCMEGKQHGDVVSAIR | 21.92159564 | 16.96485204 |
| 7 | N | LHSDKSKPGQFIR | 18.01929994 | 20.86714774 |
| 8 | C | MEGKQHGDVVSAIR | 22.18091894 | 16.70552874 |
| 9 | V | NGENVEKETHQQVVSR | 6.43042544 | 32.45602224 |
| 10 | A | QEAPGQAEPPAAAEVQGAGNENEPR | 12.20496294 | 26.68148474 |
| 11 | R | SVDPDSPAEASGLR | 19.51401644 | 19.37243124 |
| 12 | V | VDPETDEQLQKLGVQVR | 9.55699464 | 29.32945304 |

B

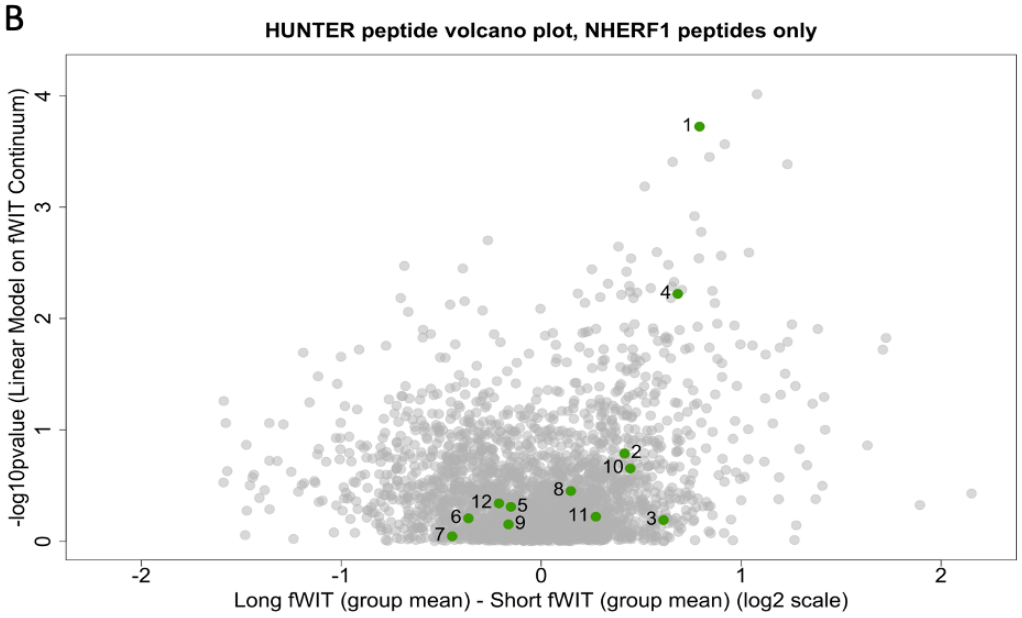



**Figure 6-C: Endogenous NHERF1 peptides intensity increases with prolonged fWIT**

Twelve endogenous peptides identified in the HUNTER study were mapped to the NHERF1 protein. (A) provides a list of the 12 endogenous NHERF1 peptides, including the peptide sequence. The significantly increased peptide is circled in pink. (B) shows a volcano plot of all endogenous peptides with the NHERF1 peptides highlighted in green and numbered in line with table (A).

### 6.4.4 BHMT endogenous peptides validated using Western blotting

The HUNTER analysis identified 19 endogenous peptides derived from BHMT that are listed in Figure 6-D (A). The endogenous peptides are numbered to correspond with the points on the endogenous peptide volcano plot in part (B) of the figure. One BHMT peptide – labelled as peptide 4 – was significantly increased (10% FDR) with fWIT in the HUNTER analysis. Several BHMT peptides were shown to have been cleaved by LGMN.

A

| Peptide number on plot | P1 Peptide | Peptide sequence | MW before peptide | MW of peptide and preceeding sequence |
|---|---|---|---|---|
| 1 | V | AATMCIGPEGDLHGVPPGECAVR | 19.90567514 | 25.11082754 |
| 2 | K | AGPWTPEAAVEHPEAVR | 4.24406734 | 40.77243534 |
| 3 | N | EAACDIAR | 11.04559564 | 33.97090704 |
| 4 | L | EKISGQEVNEAACDIAR | 10.06053394 | 34.95596874 |
| 5 | T | FYASEDKLENR | 8.16045624 | 36.85604644 |
| 6 | G | GCCGFEPYHIR | 32.58041914 | 12.43608354 |
| 7 | C | GFEPYHIR | 32.84374864 | 12.17275404 |
| 8 | S | GQEVNEAACDIAR | 10.51806114 | 34.49844154 |
| 9 | V | IGDGGFVFALEKR | 2.40592794 | 42.61057474 |
| 10 | C | IGPEGDLHGVPPGECAVR | 20.38326924 | 24.63323344 |
| 11 | K | ISGQEVNEAACDIAR | 10.31782354 | 34.69867914 |
| 12 | E | KISGQEVNEAACDIAR | 10.18964944 | 34.82685324 |
| 13 | V | LEKISGQEVNEAACDIAR | 9.94737454 | 35.06912814 |
| 14 | M | PPVGGKKAK | 0.14920784 | 44.86729484 |
| 15 | I | SGQEVNEAACDIAR | 10.43098294 | 34.58551974 |
| 16 | F | TFYASEDKLENR | 8.05935114 | 36.95715154 |
| 17 | A | TMCIGPEGDLHGVPPGECAVR | 20.04783274 | 24.96866994 |
| 18 | F | YASEDKLENR | 8.30763284 | 36.70886984 |
| 19 | N | YVLEKISGQEVNEAACDIAR | 9.68506594 | 35.33143674 |

B

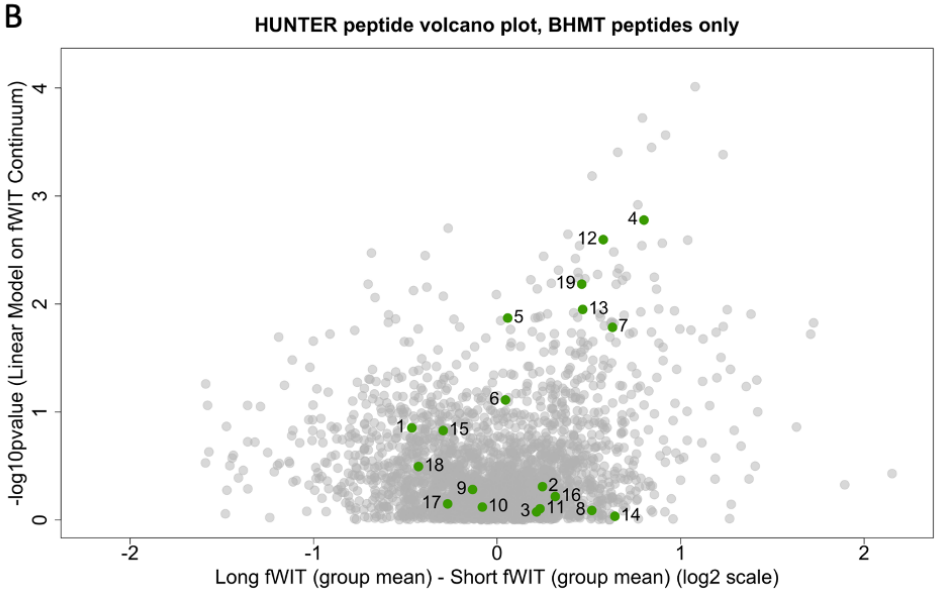



**Figure 6-D: Endogenous BHMT peptides intensity increases with prolonged fWIT**

Nineteen endogenous peptides derived from the BHMT protein were identified in homogenised kidney tissue. (A) provides a list of the measured BHMT endogenous peptides, including the peptide sequence, precursor amino acid and the molecular weight of the peptide and subsequent sequence. The peptide shown to increase (10% FDR) with prolonged fWIT is indicated by the pink circle. (B) shows a volcano plot of all endogenous peptides with BHMT peptides highlighted in green. The endogenous peptide measured to increase with prolonged fWIT is labelled number 4.

Western blotting was used to validate changes in endogenous peptide abundance for BHMT, a 45kDa protein, which can be viewed on the Western blot in Figure 6-E (A). A ~35kDa endogenous peptide was also visible on the Western blot, however it is difficult to conclude which peptide this is likely to be based on the listed peptides, as there are several endogenous peptides of similar molecular weights. This degradation product could represent the peptide measured as increasing with fWIT, but sequencing would be required to confirm. The abundance of the full length BHMT protein (Figure 6-E (B)) and peptide intensity (Figure 6 E (C)) trended downwards but did not significantly associate with prolonged fWIT. There was no difference in the signal ratio when the full length BHMT abundance was compared to the abundance of BHMT degradation products, as fWIT increased ($p=0.43$) (Figure 6 E (D & E)).

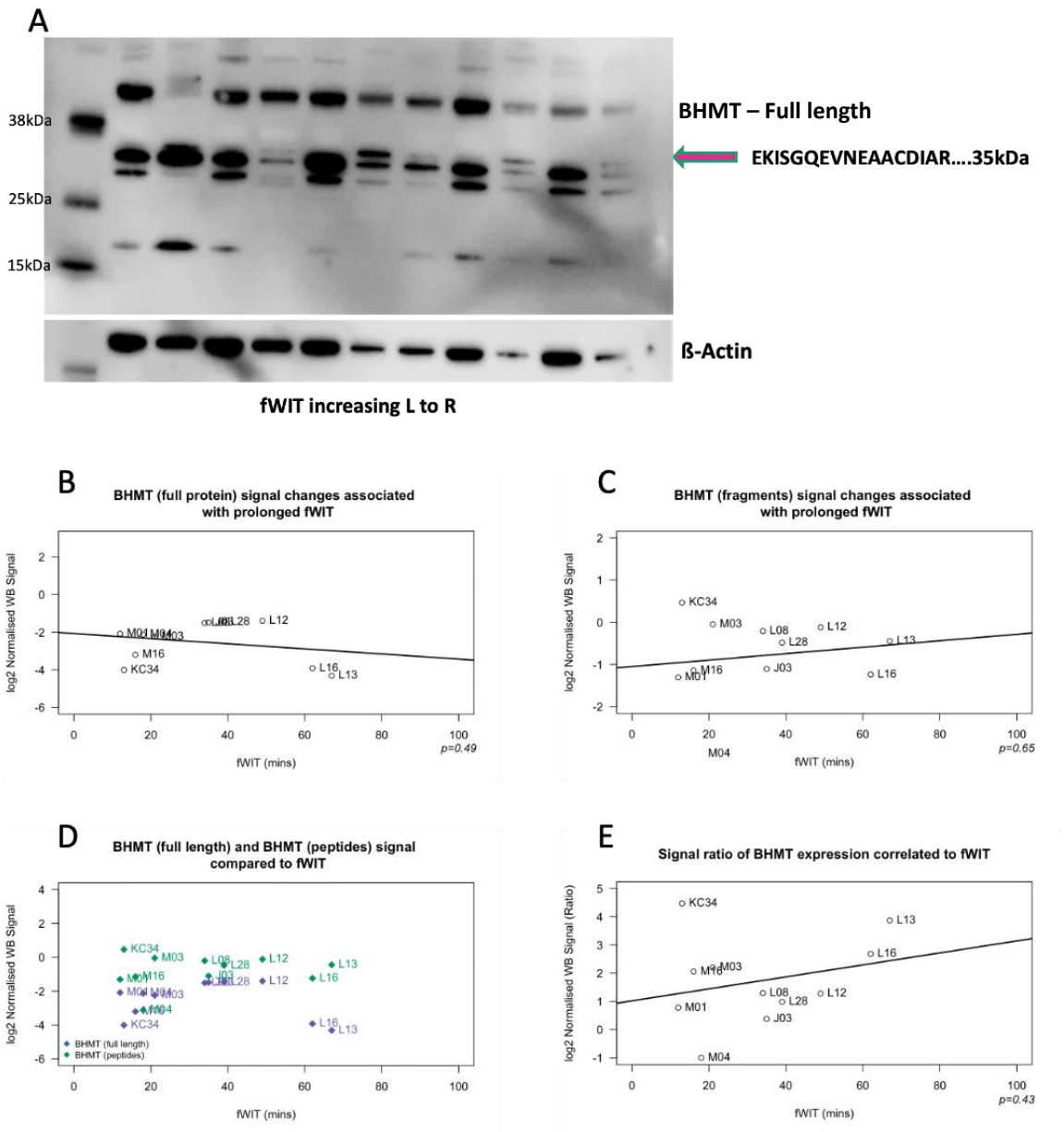



**Figure 6-E: Western blotting shows increased degradation of BHMT with increasing fWIT**

Western blotting was used to validate changes in BHMT endogenous peptides observed in the HUNTER peptidome study. (A) maps BHMT full length and endogenous peptide abundance using Western blotting. Full length BHMT protein is 45kDa. Densitometry analysis highlighted a trend in reduced expression of full length BHMT (B), and an increase in peptide expression (C). The endogenous peptides indicated as significantly increasing with fWIT in the HUNTER analysis is marked with a pink arrow on the Western blot. The signal ratio of full-length protein compared to fragment intensity is presented in parts D & E – there was no difference in signal ratio.

### 6.4.5 Abundance of active LGMN is greater than the zymogen form as fWIT increases in DCD kidneys

Legumain activity increased in DCD kidneys with fWIT (Figure 4-N). To determine whether LGMN activity correlated with its abundance, LGMN was measured in DCD kidneys using Western blotting (Figure 6-F (A)). Inactive zymogen LGMN has a molecular weight of 56kDa, compared to active LGMN which measures at 37kDa. The abundance of both zymogen and active LGMN trended downward as fWIT increased, and this result was confirmed using densitometry (Figure 6-F B & C). Comparison of zymogen and active LGMN abundance indicated a trend towards increased active LGMN abundance however this did not reach significance ($p=0.15$) (Figure 6-F (D)). These results suggest that protease activity is not dependent on protease abundance and is likely regulated by other factors such as cell pH, substrate availability, and inhibitor binding. Thus, protease activity in kidney tissue and the *in* vitro models should be measured separately. Changes in protease mRNA may indicate if glucose deprivation or hypoxia regulates gene transcription for the different proteases, which may have downstream implications on protease abundance and activity.

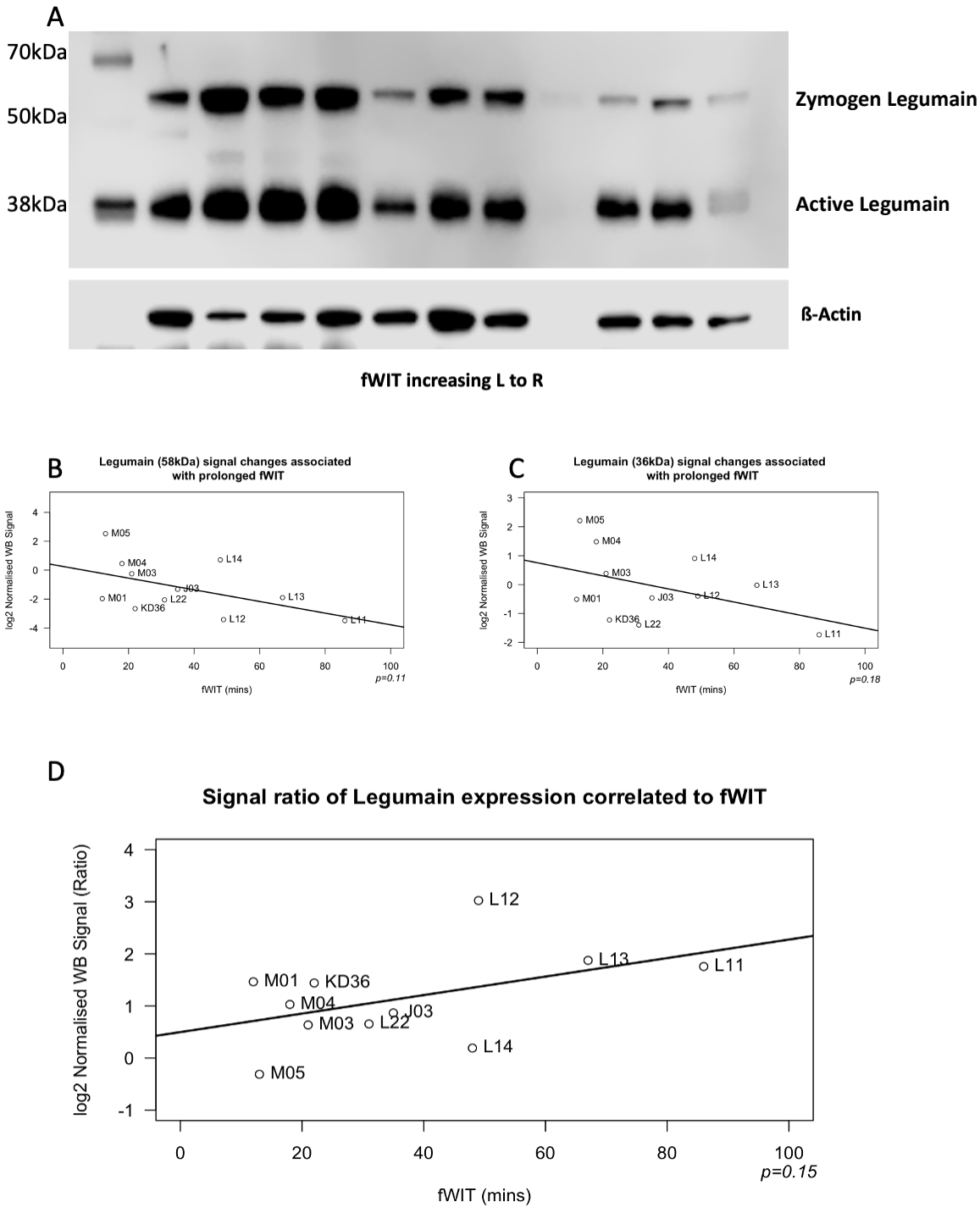



**Figure 6-F: Legumain expression in DCD kidneys with prolonged fWIT**

Legumain expression was measured using Western blotting (A). (B) maps the abundance of zymogen LGMN and (C) the abundance of active LGMN, both quantified using densitometry. (D) shows a comparison of signal expression as fWIT increases and there is a trend towards increased abundance of active LGMN compared to zymogen LGMN (p=0.15).

The endogenous peptides identified as being cleaved by LGMN in the degradomic study are listed in Figure 6-G (A). These peptides are derived from two parent proteins, BHMT (n=3 peptides) and HBA1 (n=3 peptides). A string analysis of these proteins showed that there is no pathway connection between BHMT and HBA1 (B).

A

| Protease | Preceding 10 residues | Peptide | Peptide Parent Proteins | Protein name | Peptide Parent Proteins |
|---|---|---|---|---|---|
| Legumain | LSPADKTNVK | AAWGKVGAHAGEYGAEALER | HBA1 | Hemoglobin subunit alpha | P69905 |
| Legumain | GKKVADALTN | AVAHVDDMPNALSALSDLHAHKLR | HBA1 | Hemoglobin subunit alpha | P69905 |
| Legumain | KLENRGNYVL | EKISGQEVNEAACDIAR | BHMT | Betaine-homocysteine S-methyltransferase 1 | Q93088 |
| Legumain | DKLENRGNYV | LEKISGQEVNEAACDIAR | BHMT | Betaine-homocysteine S-methyltransferase 1 | Q93088 |
| Legumain | MVLSPADKTN | VKAAWGKVGAHAGEYGAEALER | HBA1 | Hemoglobin subunit alpha | P69905 |
| Legumain | SEDKLENRGN | YVLEKISGQEVNEAACDIAR | BHMT | Betaine-homocysteine S-methyltransferase 1 | Q93088 |

B

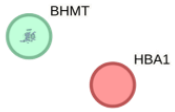



**Figure 6-G: Legumain cleaved two proteins in DCD kidneys**

The TopFIND online database was used to determine the protease that most likely cleaved each endogenous peptide. (A) lists endogenous peptides most likely cleaved by LGMN. The pink box highlights peptide significantly changed with fWIT (10% FDR). (B) shows a STRING analysis of proteins BHMT and HBA2, cleaved by LGMN, showing there is no biological pathway relationship between these proteins.

### 6.4.6 Legumain expression was variable in podocytes and PTEC cells, with active LGMN abundance reduced in PTECs cultured without glucose

Both zymogen and active LGMN levels were measured in podocytes and PTECs cultured under normoxic and hypoxic culture conditions in media +/- glucose, for up to 24h. β-actin was used to normalise LGMN abundance.

The abundance of LGMN was quantified in these cells by measuring and comparing the expression of zymogen and active LGMN. The abundance of zymogen LGMN decreased in podocytes cultured for 6h (Hypo+Gluc p=0.017, Hypo-Gluc p=0.004) and for 24h (Hypo-Gluc p=0.047) under hypoxic conditions. There was also less zymogen LGMN in the Hypo-Gluc cells compared to the Norm-Gluc cells at 6h (p=0.007) and 24h (p=0.049). No changes were observed in active LGMN levels in any culture conditions. Lack of glucose in culture media did not influence the abundance of zymogen or active LGMN. When comparing the signal ratio of zymogen and active LGMN, during earlier culture time points, there was a distinct difference in the abundance of active LGMN compared to the zymogen. However, as culture time increased, the abundance of active LGMN reduced in line with zymogen abundance, which may signal a loss of active LGMN or an increase in zymogen LGMN.

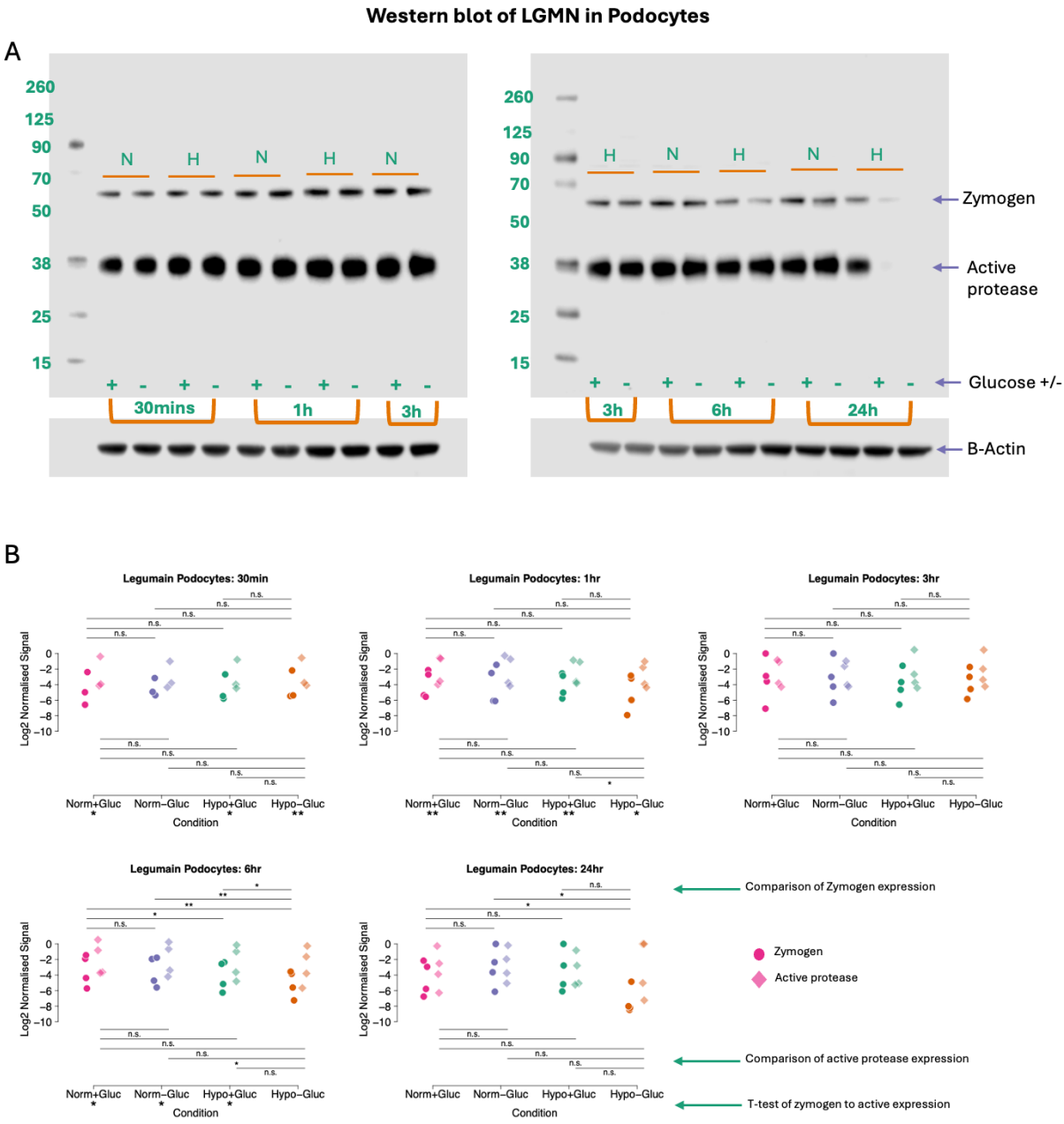
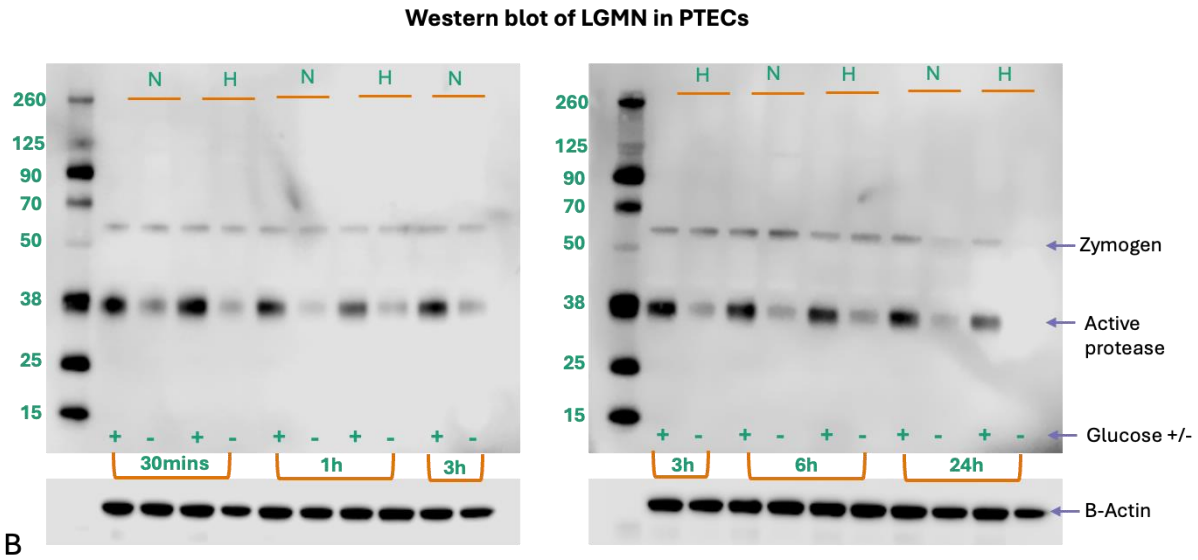



**Figure 6-H: Legumain abundance in podocyte cells exposed to normoxic and hypoxic conditions in media +/- glucose**

Zymogen LGMN abundance reduced in podocytes cultured under hypoxic conditions at 6h and 24h. (A) shows a Western blot probed for LGMN in podocyte homogenates collected post-culture over 24h. The culture time and conditions are indicated next to each well. Protein abundance is normalised to ß-actin. (B) shows the abundance of zymogen and active LGMN quantified using densitometry. Abundance of zymogen and active LGMN are compared according to culture time and condition. The signal ratio of zymogen compared to active LGMN is indicated below the individual plots as indicated by the arrow.

Analysis of LGMN expression in cultured PTECS is presented in Figure 6-I. The Western blot clearly shows a reduction in active LGMN abundance in PTECs cultured without glucose (A). PTECs cultured for 24h under Hypo-Gluc conditions, had no LGMN bands, showing a significant reduction in abundance. Densitometry analysis (B) confirmed that abundance of active LGMN reduced in PTECs cultured without glucose. Active LGMN expression decreased at 30m (Norm-Gluc p=0.002, Hypo-Gluc p=0.01), 1h (Norm-Gluc p=0.042, Hypo-Gluc p=0.07), 3h (Norm-Gluc p=0.06, Hypo-Gluc p=0.01) and 24h (Norm-Gluc p=0.02, Hypo-Gluc p=0.76). The expression of active LGMN differed in the hypoxic cultured cells (Hypo+Gluc vs Hypo-Gluc) at 30m (p=0.014), 1h (p=0.02), and 3h (p=0.03). Expression of zymogen LGMN did not differ between the experimental groups, however increased in Hypo-Gluc PTECs compared to Hypo+Gluc cells at 30min (p=0.01), 1h (p=0.02), and 3h (p=0.009). The signal ratio between zymogen and active LGMN was also calculated, at each time point and within treatment. Cells cultured under Norm-Gluc conditions up to 3h had a difference in zymogen and active abundance. Hypo+Gluc cells at 30m, 1h and 24h also had a difference in abundance. Abundance of zymogen and active LGMN did not differ in cells cultured without glucose.

A




B

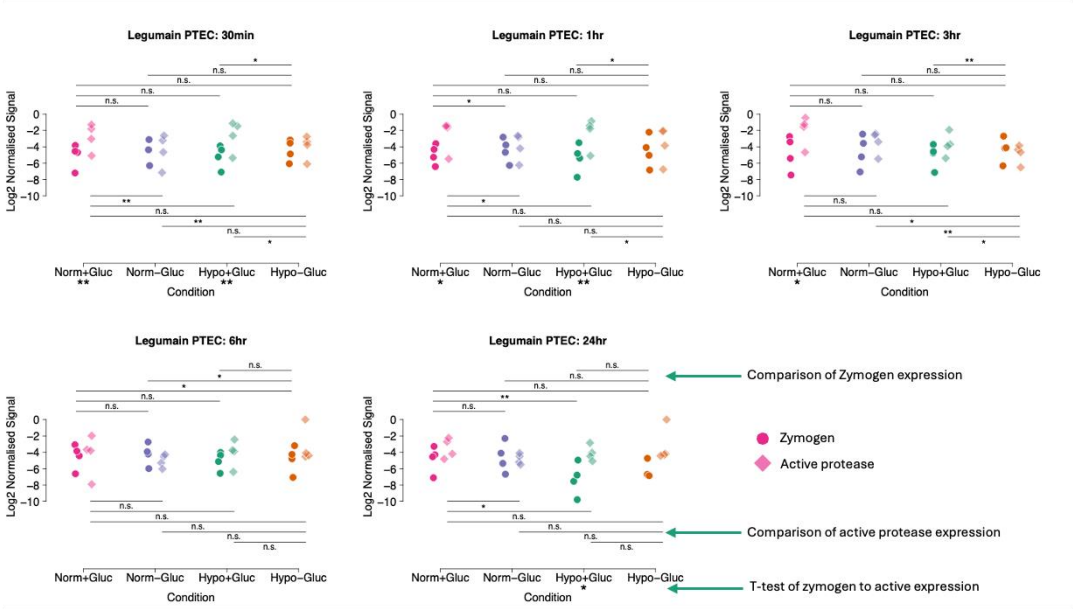



**Figure 6-I: Legumain abundance in PTEC cells cultured under normoxic and hypoxic conditions in media +/- glucose**

Active LGMN abundance was reduced in cells cultured without glucose under both normoxic and hypoxic conditions. Zymogen LGMN abundance reduced in hypoxic cells over time. (A) shows a Western blot used to measure LGMN abundance in PTECs cultured over 24h. The culture time and condition are indicated next to each well. Protein abundance was normalised to ß-actin. (B) shows zymogen and active LGMN abundance measured using densitometry. The abundance of zymogen and active LGMN were compared according to culture time and condition. The signal ratio of zymogen compared to active LGMN is indicated below the individual plots as indicated by the arrow.

### 6.4.7 Fibronectin expression did not change in podocytes or PTECs cultured under hypoxic conditions

Fibronectin is a substrate of LGMN and is well defined in the literature for its association with fibrosis in the kidney. Fibronectin was not a measured target of LGMN in the HUNTER study but was measured here to describe changes associated with hypoxia and as a marker of possible morphological changes in the cells that may be indicative of injury.

Comparison of the expression of fibronectin in the Western blot presented in Figure 6-J (A), indicate no change in fibronectin abundance in cells cultured for 24h. In the cells cultured under Hypo-Gluc conditions, there is a fainter band at 24h yet this was not significant following densitometry analysis of the blots (B). The expression of fibronectin was reduced in Norm-Gluc ($p=0.02$) and Hypo+Gluc ($p=0.02$) cells at 6h compared to Norm+Gluc. This change was not evident at other time points and can likely be explained by variability in the cell replicates analysed.

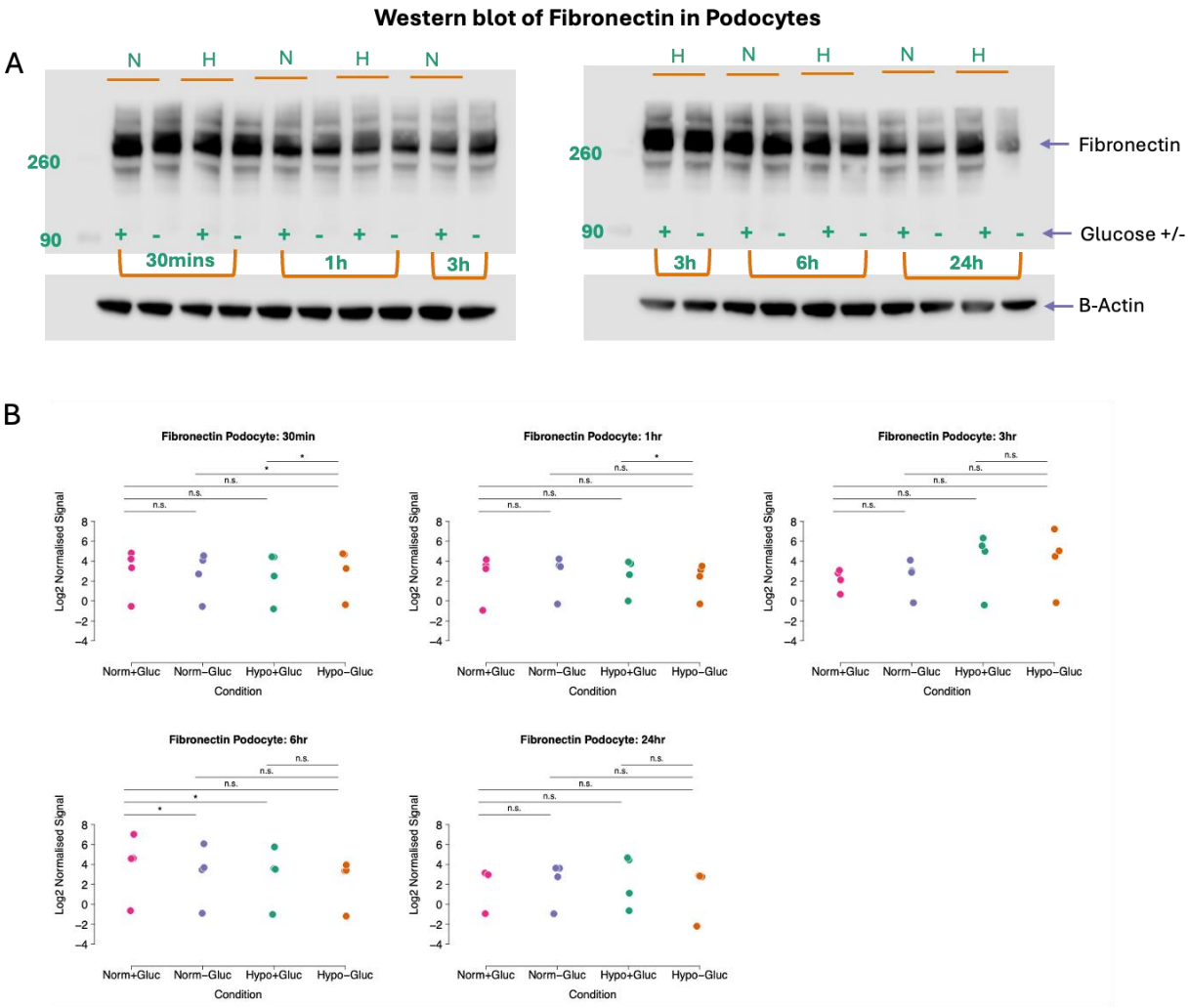



**Figure 6-J: Fibronectin measured in podocytes cultured under normoxic and hypoxic conditions in media +/- glucose**

Fibronectin was measured as a well-documented substrate of LGMN. In podocytes cultured under normoxic and hypoxic conditions, fibronectin was reduced in cells exposed to hypoxic conditions at 30m and 6h, but not at other time points. Changes in fibronectin are inconsistent, and therefore reliably conclusions cannot be drawn.

In Figure 6-K, the expression of fibronectin in cultured PTECs is presented. There is no evidence of changes in fibronectin expression under normoxic or hypoxic conditions over 24h in culture.

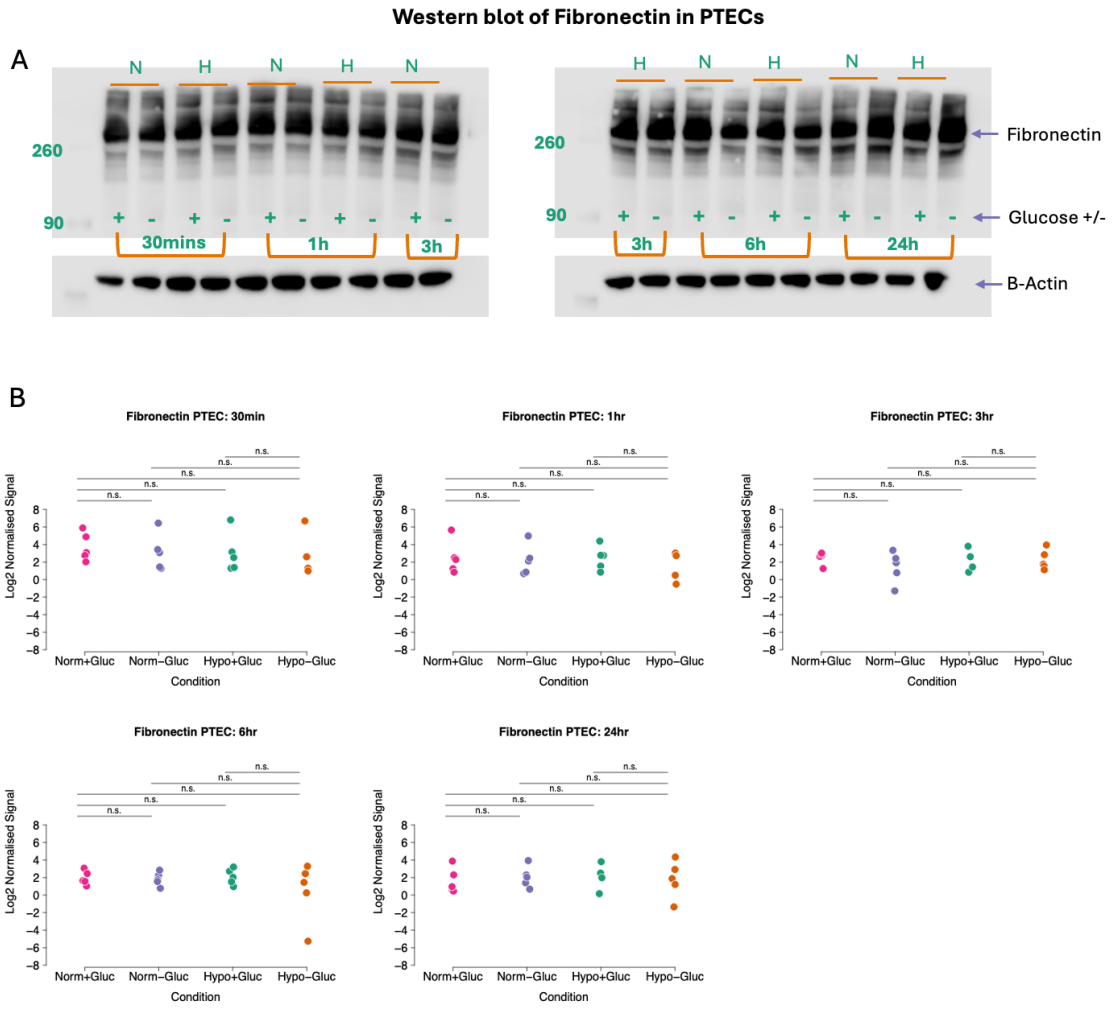



**Figure 6-K: Fibronectin measured in PTECs cultured under normoxic and hypoxic conditions in media +/- glucose**

Fibronectin was measured as a well-documented substrate of LGMN. In PTECs cultured under normoxic and hypoxic conditions, fibronectin did not change.

### 6.4.8 Active Cathepsin B abundance decreases as fWIT extends

Cathepsin B (CATB) is a cysteine protease that in its active form has a molecular weight of 25-32kDa and appears as two distinct bands on an immunoblot. Pro-CATB has a molecular weight of 38kDa. In Figure 4-N, CATB activity was seen to decrease as fWIT increased. This change was quantified using Western blotting and showed a decrease in

active CATB abundance as fWIT increased from left to right (Figure 6-L). Densitometry confirmed that active CATB abundance decreased with an increasing fWIT. The abundance of active CATB decreased with increasing fWIT, as shown in Figure 6-L (B). The abundance of active CATB trended down with an increasing fWIT (Figure 6-L (C)). The signal ratio of active CATB compared to pro-CATB reduced with increasing fWIT ($p=0.03$) (Figure 6-L (D)).

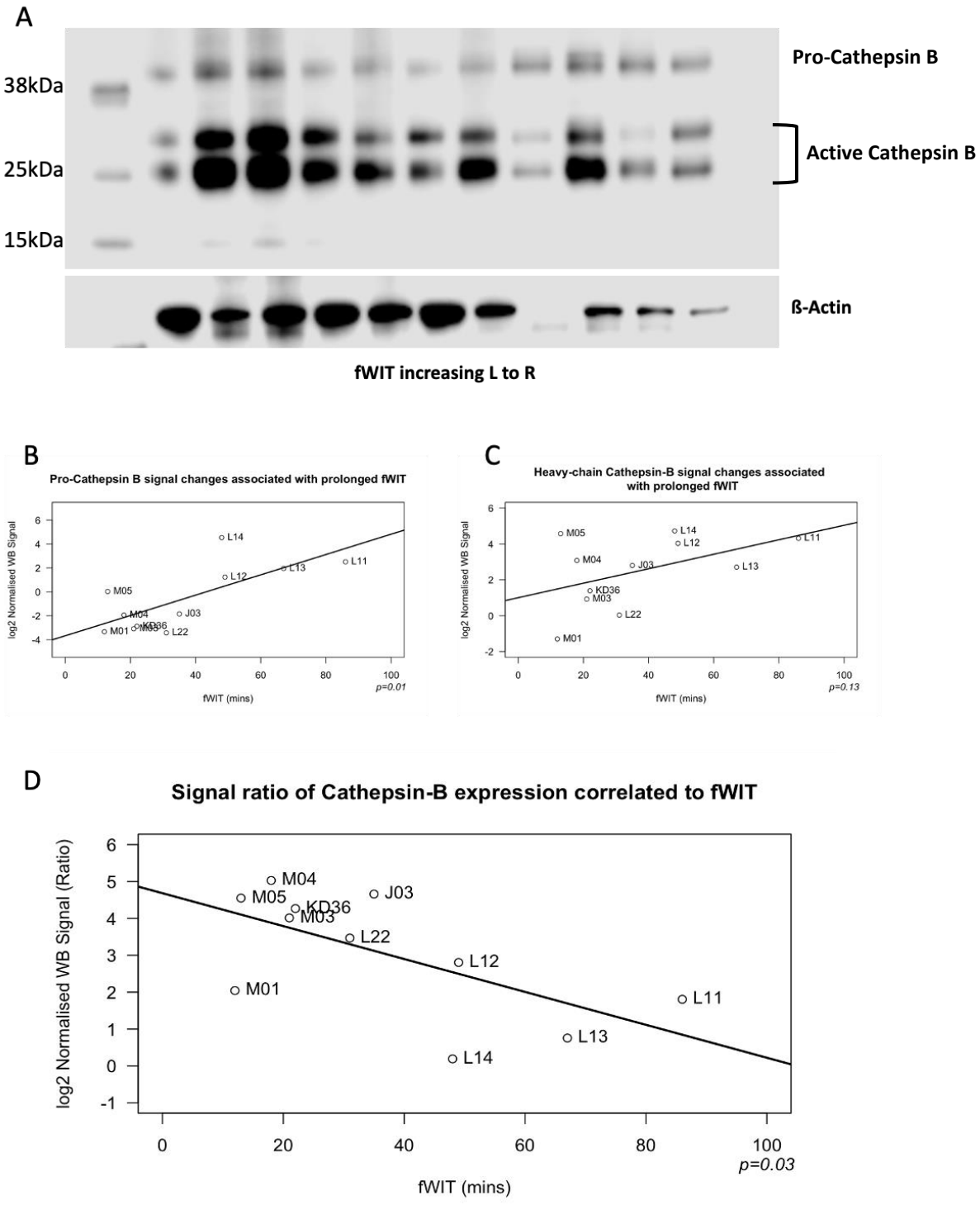



**Figure 6-L: Cathepsin B abundance in DCD kidneys with prolonged fWIT**

Cathepsin B abundance was quantified using Western blotting as shown in (A). The abundance of pro-CATB increased with fWIT (B), as did the abundance active CATB (C). (D) depicts the comparison between pro-CATB and active CATB abundance, showing that as fWIT increased the abundance of active CATB decreased in relation to pro-CATB abundance (p=0.03).

The endogenous peptides predicted to have been cleaved by CATB are listed in Table 6-A and were derived from 14 proteins: H1-6, ACTA1, ACTA2, PFN1, GADPH, GPI, ALDOA, ENO1, PRDX6, SOD1, PEBP1, PARK7, MAP4, SAA1. A STRING analysis indicated several pathway connections between the proteins targeted for cleavage by CATB, as seen in Figure 6-M. STRING indicated that the proteins targeted by CATB are associated with gluconeogenesis, glycolysis, cytoskeletal organisation, the regulation of macromolecules, metabolic process, and positive regulation of gene expression.

| Protease | Preceding 10 residues | Peptide | Peptide Parent Proteins | Protein name | Peptide Parent Proteins |
|---|---|---|---|---|---|
| Cathepsin B | MSLVALKKAL | AAAGYDVEKNNSR | H1-6 | Histone H1t | P22492 |
| Cathepsin B | SLVALKKALA | AAGYDVEKNNSR | H1-6 | Histone H1t | P22492 |
| Cathepsin B | VCDNGSGLCK | AGFAGDDAPR | ACTA2 | Actin, aortic smooth muscle | P62736 |
| Cathepsin B | MRRAGIKVTV | AGLAGKDPVQCSR | PARK7 | Parkinson disease protein 7 | Q99497 |
| Cathepsin B | IKVDKGVVPL | AGTNGETTTQGLDGLSER | ALDOA | Fructose-bisphosphate aldolase A | P04075 |
| Cathepsin B | IHQGTKMIPC | DFLIPVQTQHPIR | GPI | Glucose-6-phosphate isomerase | P06744 |
| Cathepsin B | MPGGLLLG | DVAPNFEANTTVGR | PRDX6 | Peroxiredoxin-6 | P30041 |
| Cathepsin B | DNGSGLCKAG | FAGDDAPR | ACTA2 | Actin, aortic smooth muscle | P62736 |
| Cathepsin B | SLVLGVSSRS | FFSFLGEAFDGAR | SAA1 | Serum amyloid A-1 protein | P0DJI8 |
| Cathepsin B | LGVSSRSFFS | FLGEAFDGAR | SAA1 | Serum amyloid A-1 protein | P0DJI8 |
| Cathepsin B | LVLGVSSRSF | FSFLGEAFDGAR | SAA1 | Serum amyloid A-1 protein | P0DJI8 |
| Cathepsin B | FTASAGIQVV | GDDLTVTNPKR | ENO1 | Alpha-enolase | P06733 |
| Cathepsin B | VSSRSFFSFL | GEAFDGAR | SAA1 | Serum amyloid A-1 protein | P0DJI8 |
| Cathepsin B | KGVVPLAGTN | GETTTQGLDGLSER | ALDOA | Fructose-bisphosphate aldolase A | P04075 |
| Cathepsin B | CDNGSGLCKA | GFAGDDAPR | ACTA2 | Actin, aortic smooth muscle | P62736 |
| Cathepsin B | SSMKKTTTLS | GTAPAAGVVPSR | MAP4 | Microtubule-associated protein 4 | P27816 |
| Cathepsin B | GIVEGLMTTV | HAITATQKTVDGPSGKLWR | GAPDH | Glyceraldehyde-3-phosphate dehydrogenase | P04406 |
| Cathepsin B | AYSDMREANY | IGSDKYFHAR | SAA1 | Serum amyloid A-1 protein | P0DJI8 |
| Cathepsin B | LVCDNGSGLC | KAGFAGDDAPR | ACTA2 | Actin, aortic smooth muscle | P62736 |
| Cathepsin B | GMSLVALKKA | LAAAGYDVEKNNSR | H1-6 | Histone H1t | P22492 |
| Cathepsin B | GVSSRSFFSF | LGEAFDGAR | SAA1 | Serum amyloid A-1 protein | P0DJI8 |
| Cathepsin B | LDSGKLYTLV | LTDPDAPSR | PEBP1 | Phosphatidylethanolamine-binding protein 1 | P30086 |
| Cathepsin B | DGLDSGKLYT | LVLTDPDAPSR | PEBP1 | Phosphatidylethanolamine-binding protein 1 | P30086 |
| Cathepsin B | WAAVPGKTFV | NITPAEVGVLVGKDR | PFN1 | Profilin-1 | P07737 |
| Cathepsin B | EFGDNTAGCT | SAGPHFNPLSR | SOD1 | Superoxide dismutase [Cu-Zn] | P00441 |
| Cathepsin B | CSLVLGVSSR | SFFSFLGEAFDGAR | SAA1 | Serum amyloid A-1 protein | P0DJI8 |
| Cathepsin B | VLGVSSRSFF | SFLGEAFDGAR | SAA1 | Serum amyloid A-1 protein | P0DJI8 |
| Cathepsin B | RKDLYANNVM | SGGTTMYPGIADR | ACTA1 | Actin, alpha skeletal muscle | P68133 |
| Cathepsin B | ADQAANEWGR | SGKDPNHFR | SAA1 | Serum amyloid A-1 protein | P0DJI8 |
| Cathepsin B | ADQAANEWGR | SGKDPNHFRPAGLPEKY | SAA1 | Serum amyloid A-1 protein | P0DJI8 |
| Cathepsin B | ADVSIEDSVI | SLSGDHCIIGR | SOD1 | Superoxide dismutase [Cu-Zn] | P00441 |
| Cathepsin B | GFHVHEFGDN | TAGCTSAGPHFNPLSR | SOD1 | Superoxide dismutase [Cu-Zn] | P00441 |
| Cathepsin B | WDGLDSGKLY | TLVLTDPDAPSR | PEBP1 | Phosphatidylethanolamine-binding protein 1 | P30086 |
| Cathepsin B | HEFGDNTAGC | TSAGPHFNPLSR | SOD1 | Superoxide dismutase [Cu-Zn] | P00441 |
| Cathepsin B | NFGIVEGLMT | TVHAITATQKTVDGPSGKLWR | GAPDH | Glyceraldehyde-3-phosphate dehydrogenase | P04406 |
| Cathepsin B | KFTASAGIQV | VGDDLTVTNPKR | ENO1 | Alpha-enolase | P06733 |
| Cathepsin B | FGIVEGLMTT | VHAITATQKTVDGPSGKLWR | GAPDH | Glyceraldehyde-3-phosphate dehydrogenase | P04406 |
| Cathepsin B | GLDSGKLYTL | VLTDPDAPSR | PEBP1 | Phosphatidylethanolamine-binding protein 1 | P30086 |
| Cathepsin B | RAYSDMREAN | YIGSDKYFHAR | SAA1 | Serum amyloid A-1 protein | P0DJI8 |

**Table 6-A: Endogenous peptides cleaved by Cathepsin B**

Fourteen proteins were predicted to have been cleaved by CATB, resulting in endogenous peptides measured in the HUNTER study. The endogenous peptides are listed above, along with the peptide sequence and preceding 10 amino acid residues. The parent proteins name, gene name and UniProt reference is also listed.

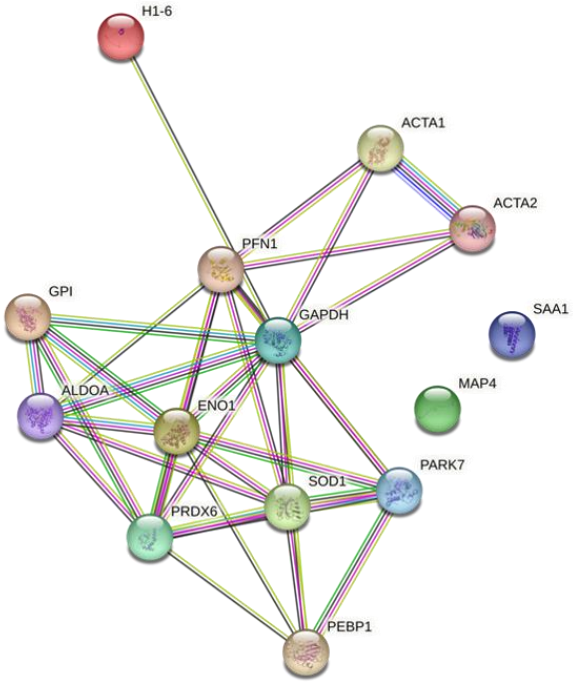



**Figure 6-M: STRING analysis of proteins cleaved by Cathepsin B**

Proteins perceived to have been cleaved by CATB generating the endogenous peptides identified in the HUNTER study were mapped using STRING to evaluate protein-protein interactions between the proteins targeted for degradation by CATB. These proteins are associated with gluconeogenesis, glycolysis and cytoskeletal organisation.

### 6.4.9 Cathepsin B abundance is not affected by hypoxia or glucose concentration in podocytes or PTECs

The abundance of pro-CATB and active-CATB was quantified in podocytes and PTECs cultured under normoxic and hypoxic conditions +/- glucose for up to 24h. In podocytes, pro-CATB and active CATB abundance did not change with culture conditions or time, as shown in Figure 6-N. The signal ratio of pro-CATB and active CATB was different at all time points and for each condition, with there being more active CATB than pro-CATB.

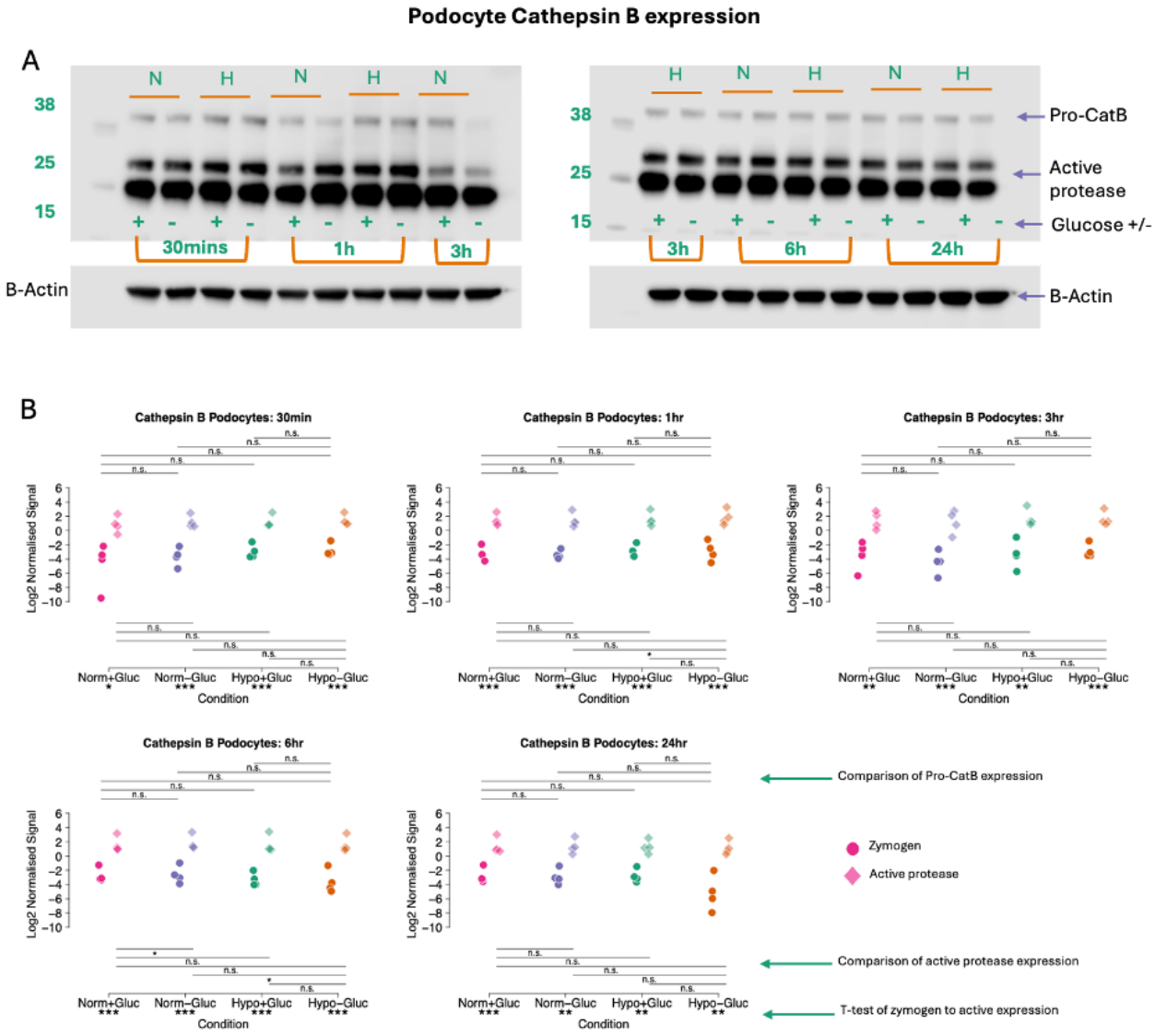



**Figure 6-N: Cathepsin B measured in podocytes cultured under normoxic and hypoxic conditions in media +/- glucose**

The abundance of pro-CATB and active-CATB did not change under hypoxic or glucose-starved conditions. (A) shows a Western blot measuring CATB abundance in podocytes cultured over 24h. The culture time and condition are indicated next to each well. Protein abundance is normalised to ß-actin. (B) shows plots of zymogen and active CATB abundance measured using densitometry. Abundance of zymogen and active CATB were compared according to culture time and condition. The signal ratio of zymogen to active CATB is indicated below the individual plots.

Figure 6-O shows Western blot quantification of pro- and active-CATB in PTECs. CATB abundance did not change with culture conditions or time (Figure 6-O (B & C)). The signal ratio of pro-CATB and active-CATB was different for each condition during the first 6h of culture. However, at 24h the abundance of pro- and active-CATB were similar in Hypo+Gluc PTECs.

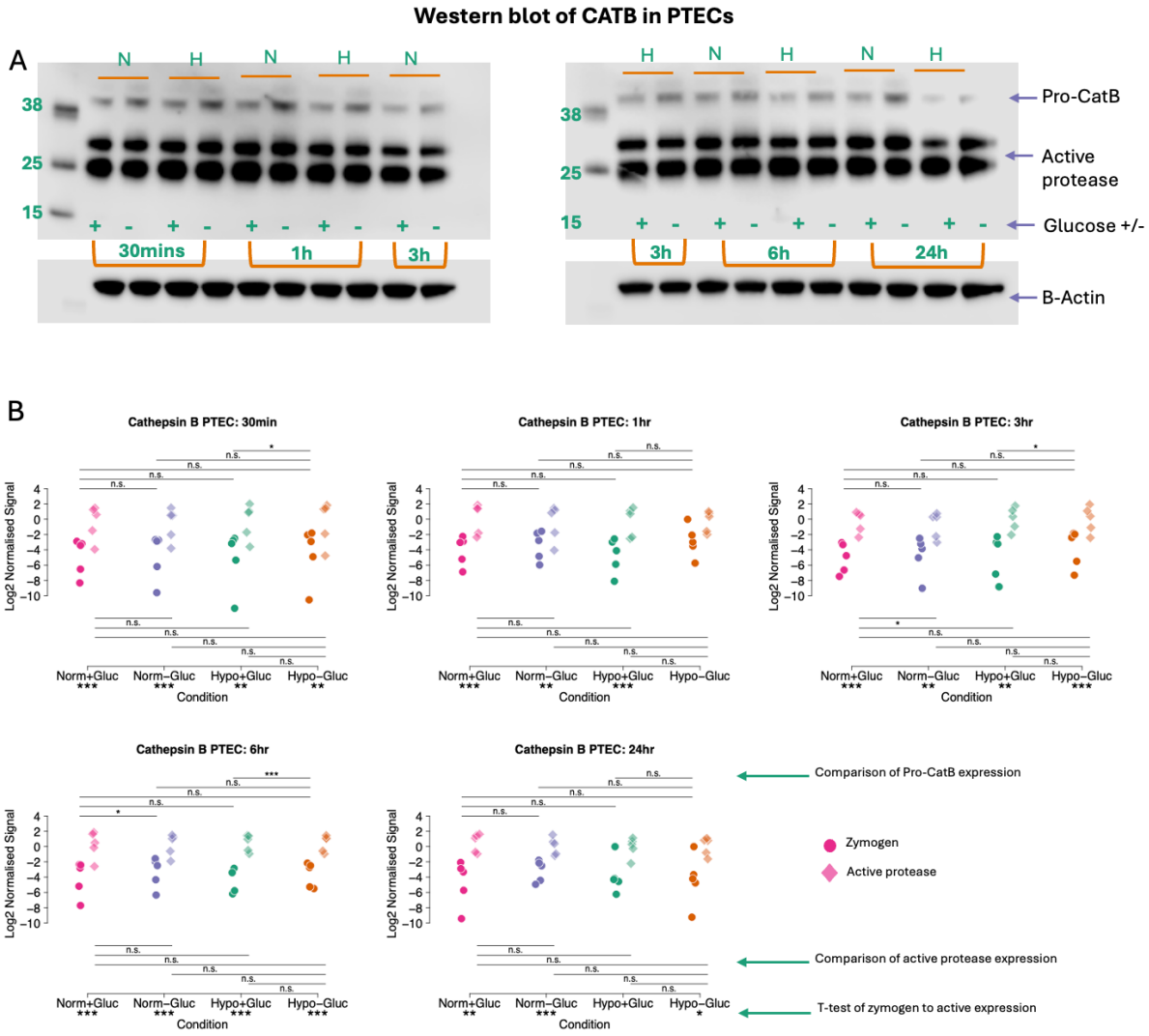



**Figure 6-O: Cathepsin B measured in PTECs cultured under normoxic and hypoxic conditions in media +/- glucose**

The abundance of active-CATB was significantly increased compared to pro-CATB. Hypoxia and glucose did not impact the CATB abundance. (A) shows a Western blot measuring CATB abundance in PTECs cultured over 24h. The culture time and condition are indicated next to each well. Protein abundance was normalised to ß-actin. (B) depicts pro- and active-CATB abundance measured using densitometry. The abundance of pro- and active-CATB are compared according to culture time and condition. The signal ratio of zymogen compared to active CATB is indicated at the bottom of each plot.

### 6.4.10 Granzyme M activity increased in DCD kidneys with prolonged fWIT

Granzyme M (GRAM) activity increased in DCD kidneys with prolonged fWIT as shown in Figure 4-N. The endogenous peptides predicted to have been cleaved by GRAM are listed in Table 6-B.

The endogenous peptides cleaved by GRAM were derived from 22 proteins: SERBP1, BCLAF1, EIF-1, SERPINA3, HNRNPU, HNRPC, HNRNPK, UBA1, MAP4, SLC93A3R1, PKM, ACTB, H1-10, ACTG1, CTTN, H2AC13, H1-4, TPI1, TUBA1A, NACA, TMBIM1 and NAP1L4. A STRING analysis indicated several protein-to-protein interactions between the parent proteins, including protein binding, nucleic acid binding, RNA binding, and structural molecule activity (Figure 6-P).

| Protease | Preceding 10 residues | Peptide | Peptide Parent Protein Gene name | Protein name | Peptide Parent Protein UniProt Id |
|---|---|---|---|---|---|
| Granzyme M | QATTQQAQLA | AAAEIDEEPVSKAKQSR | NACA | Nascent polypeptide-associated complex subunit alpha | Q13765 |
| Granzyme M | VSLAALKKAL | AAAGYDVEKNNSR | H1-4 | Histone H1.4 | P10412 |
| Granzyme M | SLAALKKALA | AAGYDVEKNNSR | H1-4 | Histone H1.4 | P10412 |
| Granzyme M | SLGELIGTLN | AAKVPADTEVVCAPPTAYIDFAR | TPI1 | Triosephosphate isomerase | P60174 |
| Granzyme M | DYRQFRKSVL | ADQGKSFATASHR | BCLAF1 | Bcl-2-associated transcription factor 1 | Q9NYF8 |
| Granzyme M | YLAAVLEYLT | AEILELAGNAAR | H2AC11 | Histone H2A type 1 | P0C0S8 |
| Granzyme M | LLRAQEAPGQ | AEPPAAAEVQGAGNENEPR | NHERF1 | Na(+)/H(+) exchange regulatory cofactor NHE-RF1 | O14745 |
| Granzyme M | AEGMAKKVTK | AGGSAALSPSKKR | H1-10 | Histone H1.10 | Q92522 |
| Granzyme M | MEEEIA | ALVIDNGSGMCKAGFAGDDAPR | ACTG1 | Actin, cytoplasmic 2 | P63261 |
| Granzyme M | RKSAGAAKRK | ASGPPVSELITKAVAASKER | H1-4 | Histone H1.4 | P10412 |
| Granzyme M | PSDSVEAAKN | ASNTEKLTDQVMQNPR | NAP1L4 | Nucleosome assembly protein 1-like 4 | Q99733 |
| Granzyme M | GPPVSELITK | AVAASKER | H1-4 | Histone H1.4 | P10412 |
| Granzyme M | GKSSGPTSLF | AVTVAPPGAR | HNRNPU | Heterogeneous nuclear ribonucleoprotein U | Q00839 |
| Granzyme M | SPSPLLSSSF | DLDYDFQR | HNRNPC | Heterogeneous nuclear ribonucleoproteins C1/C2 | P07910 |
| Granzyme M | MDDDIAALVV | DNGSGMCKAGFAGDDAPR | ACTB | Actin, cytoplasmic 1 | P60709 |
| Granzyme M | LRAQEAPGQA | EPPAAAEVQGAGNENEPR | NHERF1 | Na(+)/H(+) exchange regulatory cofactor NHE-RF1 | O14745 |
| Granzyme M | DMVPGKPMCV | ESFSDYPPLGR | EEF1A1P5 | Putative elongation factor 1-alpha-like 3 | Q5VTE0 |
| Granzyme M | MSAIQNLHS | FDPFADASKGDDLLPAGTEDYIHIR | EIF1 | Eukaryotic translation initiation factor 1 | P41567 |
| Granzyme M | SAGAAKRKAS | GPPVSELITKAVAASKER | H1-4 | Histone H1.4 | P10412 |
| Granzyme M | PRHQGVMVGM | GQKDSYVGDEAQSKR | ACTB | Actin, cytoplasmic 1 | P60709 |
| Granzyme M | SVPTNGMAKN | GSEADIDEGLYSR | UBA1 | Ubiquitin-like modifier-activating enzyme 1 | P22314 |
| Granzyme M | MEEEIAALV | IDNGSGMCKAGFAGDDAPR | ACTG1 | Actin, cytoplasmic 2 | P63261 |
| Granzyme M | KASGPPVSEL | ITKAVAASKER | H1-4 | Histone H1.4 | P10412 |
| Granzyme M | RSGVSLAALK | KALAAAGYDVEKNNSR | H1-4 | Histone H1.4 | P10412 |
| Granzyme M | GVSLAALKKA | LAAAGYDVEKNNSR | H1-4 | Histone H1.4 | P10412 |
| Granzyme M | SAATAVKITL | LSALVETR | SERPINA3 | Alpha-1-antichymotrypsin | P01011 |
| Granzyme M | RPRHQGVMVG | MGQKDSYVGDEAQSKR | ACTB | Actin, cytoplasmic 1 | P60709 |
| Granzyme M | NAVLDGADCI | MLSGETAKGDYPLEAVR | PKM | Pyruvate kinase PKM | P14618 |
| Granzyme M | TTLEHSDCAF | MVDNEAIYDICR | TUBA1A | Tubulin alpha-1A chain | Q71U36 |
| Granzyme M | GGGVGGPGAK | SAAQAAAQTNSNAAGKQLR | SERBP1 | SERPINE1 mRNA-binding protein 1 | Q8NC51 |
| Granzyme M | EHPSPSPLLS | SSFDLDYDFQR | HNRNPC | Heterogeneous nuclear ribonucleoproteins C1/C2 | P07910 |
| Granzyme M | VYLAAVLEYL | TAEILELAGNAAR | H2AC11 | Histone H2A type 1 | P0C0S8 |
| Granzyme M | SVEAAKNASN | TEKLTDQVMQNPR | NAP1L4 | Nucleosome assembly protein 1-like 4 | Q99733 |
| Granzyme M | GSKSTQTVAK | TTTAAAVASTGPSSR | MAP4 | Microtubule-associated protein 4 | P27816 |
| Granzyme M | VTQVSSAYQK | TVPVEAVTSKTSNIR | CTTN | Src substrate cortactin | Q14247 |
| Granzyme M | TLEHSDCAFM | VDNEAIYDICR | TUBA1A | Tubulin alpha-1A chain | Q71U36 |
| Granzyme M | VDMVPGKPMC | VESFSDYPPLGR | EEF1A1P5 | Putative elongation factor 1-alpha-like 3 | Q5VTE0 |
| Granzyme M | VGRPRHQGVM | VGMGQKDSYVGDEAQSKR | ACTB | Actin, cytoplasmic 1 | P60709 |
| Granzyme M | KSSGPTSLFA | VTVAPPGAR | HNRNPU | Heterogeneous nuclear ribonucleoprotein U | Q00839 |
| Granzyme M | MDDDIAAL | VVDNGSGMCKAGFAGDDAPR | ACTB | Actin, cytoplasmic 1 | P60709 |
| Granzyme M | TWSPSEWQMA | YEPQGGSGYDYSYAGGR | HNRNPK | Heterogeneous nuclear ribonucleoprotein K | P61978 |
| Granzyme M | MPPTHPMPMN | YGPGHGYDGEER | TMBIM1 | Protein lifeguard 3 | Q969X1 |
| Granzyme M | CPTGFKVGIN | YQPPTVVPGGDLAKVQR | TUBA1A | Tubulin alpha-1A chain | Q71U36 |

**Table 6-B: Endogenous peptides cleaved by Granzyme M**

Granzyme M (GRAM) activity significantly increased as fWIT was prolonged. Twenty-two proteins were predicted to have been cleaved by GRAM, generating the endogenous peptides identified in the HUNTER study. The endogenous peptides are listed in the table, with the peptide sequence and preceding 10 amino acid residues. The parent protein name, gene name and UniProt reference is also listed.

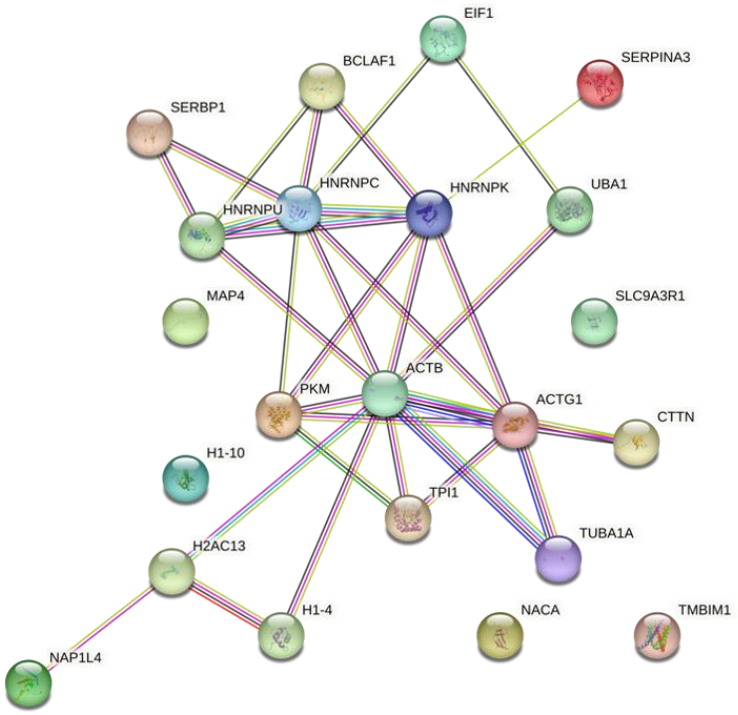



**Figure 6-P: STRING analysis of proteins cleaved by Granzyme M**

Proteins cleaved by GRAM identified in the HUNTER study were mapped using STRING to evaluate protein-protein interactions between the proteins targeted for degradation. The proteins degraded by GRAM are associated with protein binding, compound binding, nucleic acid binding and structural molecular activity.

### 6.4.11 Matrix metalloproteinase-3 activity decreased in DCD kidneys with prolonged fWIT

Matrix metalloproteinase-3 (MMP3) activity decreased as fWIT increased, as seen in Figure 4-N. The endogenous peptides cleaved by MMP3 are listed in Table 6-C, and were derived from four proteins: SAA1, FGA, SERPINA3 and SPP1. Protein-to-protein interaction of these proteins was analysed using STRING (Figure 6-Q) and were associated with amyloidosis, metabolism and the complement system.

| Protease | Preceding 10 residues | Peptide | Peptide Parent Proteins | Protein name | Peptide Parent Proteins |
|---|---|---|---|---|---|
| MMP3 | ESEELNGAYK | AIPVAQDLNAPSDWDSR | SPP1 | Osteopontin | P10451 |
| MMP3 | LGVSSRSFFS | FLGEAFDGAR | SAA1 | Serum amyloid A-1 protein | P0DJI8 |
| MMP3 | VSSRSFFSFL | GEAFDGAR | SAA1 | Serum amyloid A-1 protein | P0DJI8 |
| MMP3 | GVSSRSFFSF | LGEAFDGAR | SAA1 | Serum amyloid A-1 protein | P0DJI8 |
| MMP3 | SAATAVKITL | LSALVETR | SERPINA3 | Alpha-1-antichymotrypsin | P01011 |
| MMP3 | VLGVSSRSFF | SFLGEAFDGAR | SAA1 | Serum amyloid A-1 protein | P0DJI8 |
| MMP3 | VSPGTRREYH | TEKLVTSKGDKELR | FGA | Fibrinogen alpha chain | P02671 |

**Table 6-C: Endogenous peptides cleaved by matrix metalloproteinase-3**

Matrix metalloproteinase-3 (MMP3) activity significantly decreased as fWIT was prolonged. Four proteins were predicted to have been targeted for cleavage by MMP3 generating endogenous peptides identified in the HUNTER study. The endogenous peptides are listed in the table with the peptide sequence and preceding 10 amino acid residues. The parent protein name, gene name and UniProt reference is also listed.

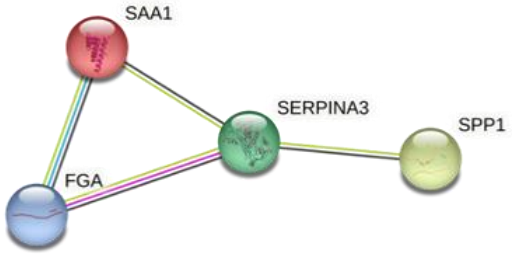



**Figure 6-Q: STRING analysis of proteins cleaved by Matrix metalloproteinase-3**

The proteins degraded by MMP3 are associated with metabolism and the complement system.

### 6.4.12 Tripeptidyl peptidase 1 cleaved itself, shows its autocatalytic activity

Tripeptidyl peptidase 1 (TPP1) activity decreased as fWIT was prolonged, as seen in

Figure 4-N. The activity of TPP1 was shown to be autocatalytic.

| Protease | Preceding 10 residues | Peptide | Peptide Parent Proteins | Protein name | Peptide Parent Proteins |
|---|---|---|---|---|---|
| Tripeptidyl peptidase 1 | RPEPQVTGTV | GLHLGVTPSVIR | TPP1 | Tripeptidyl-peptidase 1 | O14773 |
| Tripeptidyl peptidase 1 | QVTGTVGLHL | GVTPSVIR | TPP1 | Tripeptidyl-peptidase 1 | O14773 |
| Tripeptidyl peptidase 1 | EPQVTGTVGL | HLGVTPSVIR | TPP1 | Tripeptidyl-peptidase 1 | O14773 |
| Tripeptidyl peptidase 1 | PQVTGTVGLH | LGVTPSVIR | TPP1 | Tripeptidyl-peptidase 1 | O14773 |
| Tripeptidyl peptidase 1 | PEPQVTGTVG | LHLGVTPSVIR | TPP1 | Tripeptidyl-peptidase 1 | O14773 |

**Table 6-D: Endogenous peptides cleaved by Tripeptidyl peptidase 1**

Activity of TPP1 was reduced as fWIT was prolonged. Endogenous peptides cleaved by TPP1 were derived from TPP1. Five TPP1 peptides were measured in DCD kidneys with prolonged fWIT.

## 6.5 Discussion

In Chapter 4, the analysis of MS data from the HUNTER-prepared degradomic study was presented. Comparing the degradome of kidneys with a short and prolonged fWIT highlighted significant dysregulation of cytoskeletal and ECM-associated proteins and metabolic pathways in the DCD kidney associated with extended fWIT. Protease activity was also variably modified as fWIT was prolonged. To expand on the MS analysis of DCD kidneys in this chapter, three endogenous peptides shown to be differentially expressed in kidneys with an extended fWIT have been validated. Protease abundance of LGMN and CATB was measured and quantified using Western blotting in kidney tissue and cultured podocytes and PTECs. Protein targets for significant proteases were also explored in this chapter. A considered analysis of the literature has been undertaken to explain the function and potential implications of changes in protease activity in the kidney and to consider how this may affect kidney function.

Polyclonal antibodies were purchased commercially for the protein targets FBP1, NHERF1 and BHMT, and for the proteases LGMN and CATB. Additionally, antibodies targeting alternative proteins were also purchased, but are not included here as the antibody either did not reliably probe the expected protein/peptides or sample availability was limited. Polyclonal antibodies are produced with an affinity for the same antigen using different animals from the same species. This means that these antibodies can recognise multiple epitopes of the same antigen[310] and have increased sensitivity and specificity for the target, even when protein concentration is low[310,311]. Polyclonal antibodies are therefore more likely to bind to protein-specific peptides during immunoblotting. Each protein of interest was mapped to individual membranes, with

sample fWIT increasing from left to right. β-actin was measured on each membrane as a loading control.

### 6.5.1 Degradation of fructose-1,6-biphosphate increased with fWIT

Fructose-1,6-biphosphate (FBP1) is a rate-limiting enzyme involved in the gluconeogenesis pathway (Figure 4-S). The kidney contributes ~40% of systemic glucose *via* gluconeogenesis, predominantly from pyruvate entering the gluconeogenic pathway within the proximal tubules[185]. Glucose generated *via* gluconeogenesis is returned to the peritubular capillaries *via* GLUT transporters, where it is delivered to the distal tubule as an energy source for glycolysis, or back into the plasma[180] to regulate systemic glucose levels. The proximal tubules are the only segment in the kidneys to synthesise glucose *via* gluconeogenesis, with pathway-specific enzymes exclusively expressed in S1-S3 segments of the proximal tubules[187]. The role of FBP1 in disease is well established in the literature and has been described as a marker for numerous cancers and kidney diseases. However, little is understood about the role of gluconeogenesis and FBP1 dysregulation in AKI. Zhang *et al* recently reported that tissue level FBP1 is reduced in diabetic nephropathy associated kidney disease, yet FBP1 can reliably be measured in the urine of patients with diabetic nephropathy[181]. The authors also reported that urinary FBP1 correlated with tubular injury and loss in the kidney[181]. Loss of FBP1 in the liver promotes the expression of HMGB1, a DNA-binding non-histone nuclear binding protein implicated in fibrosis[312] and may activate senescence-driven tumorigenesis[313]. In IRI, anoxia induces a rapid switch to glycolysis increasing lactate release, which gluconeogenesis has a role in clearing. However when gluconeogenesis is performing inefficiently, increased lactate in the kidney induces hyperlactatemia and

hypoglycaemia[226]. After reperfusion, expression of gluconeogenesis enzymes are significantly reduced[226], perpetrating substantial metabolic dysregulation in IRI kidneys. Metabolic dysregulation is also reported in transplanted kidneys with DGF; 30 minutes after reperfusion, lactate levels are significantly increased indicating mitochondrial defects, confirmed by functional and morphological analysis of posttransplant biopsies[314]. Urinary excretion of FBP1 increases with CIT, correlating with poorer graft outcomes posttransplant[182].

In this study, seven FBP1 endogenous peptides were identified, two of which had an increased abundance with fWIT (Figure 6-A). The two significant peptides had a molecular weight of ~ 32 and 26kDa measured by MS. Using Western blotting these two peptides were visualised and shown to be more prominent in biopsies from kidneys with extended fWIT (Figure 6-B). Densitometry analysis showed an increase in FBP1 (full length) ($p=0.01$) and peptide expression ($p=0.0003$). The ratio of full length FBP1 to fragments was also calculated, indicating a trend of increased FBP1 degradation with increasing fWIT, however this did not reach significance ($p=0.0530$). The protease targeting FBP1 was not determined *via* a MEROPS search; under proteostasis, FBP1 is degraded via the proteasome[315]. Degradation of FBP1 with protracted fWIT is indicative of metabolic disruption in the kidney, specifically in the proximal tubule, where gluconeogenesis occurs. Increased degradation of FBP1 indicates an imbalance in glucose metabolism and possible lactate clearance that is likely to reduce the metabolic capabilities of the kidney and reduce ATP availability. Dysregulated FBP1 may associate with increased incidences of DGF in DCD kidneys, limiting long term outcomes. Understanding the impact of FBP1 dysregulation in the proximal tubules should be a

consideration for future work and could be addressed using the hypoxic PTEC model described in Chapter 5. Specifically, PTECs could be cultured under normoxic and hypoxic conditions with titered glucose, monitoring gene and protein changes associated with gluconeogenesis, glucose metabolism, senescence and cell survival.

### 6.5.2 Na/H exchange regulatory factor 1 degradation increased with fWIT, but could not be validated using Western blotting

Na/H exchange regulatory factor 1 (NHERF1) is a scaffolding protein with two tandem PDZ-binding domains, a carboxy terminal ezrin-binding domain and a cholesterol recognition amino acid domain, for which the function is relatively elusive[173]. Ezrin and other ERM proteins bind to the ezrin-binding domain on NHERF1, crosslinking membrane proteins with the actin cytoskeleton. NHERF1 also acts as an adaptor protein, anchoring ion channels and membrane receptors, and is thought to regulate cell polarity *via* cell junctions, microvillus formation, and the assembly of protein complexes[173]. NHERF1 expression correlates with inflammatory responses, interacting with several inflammatory proteins and pathways including IL-8 and NFκB [173]. It is also important in sodium absorption, chloride secretion in the brush border membrane[316] and in phosphate reabsorption in the proximal tubules[317]. NHERF1 binds to the main renal phosphate transporter NPT2a and to parathyroid hormone receptor *via* the PDZ-domains[318].

In proximal tubules, NHERF1 is highly expressed, specifically in the brush border membrane[319]. NHERF1 anchors parathyroid hormone receptor, adenylyl cyclase and NPT2a to the apical membrane *via* ezrin binding. Additionally NHERF1 maintains

phosphate and calcium homeostasis in the proximal tubules[319], and when interrupted causes phosphaturia, whereby phosphate is excreted in the urine due to impaired reabsorption from the glomerular filtrate and is associated with CKD[318]. NHERF1 also regulates protein transport, ion transport and hormone regulation in the proximal tubule cells.

NHERF1 dysregulation in the kidney associates with increased sensitivity to injury, as evidenced by a study by Gagnon *et al* (2022)[320]. In this study the authors induced kidney injury using four different injury models, including an IRI model. NHERF1 expression was increased at the brush border membrane of proximal tubules immediately post-injury, suggesting an injury response function. After 14 days, NHERF1 expression in the IRI model returned to baseline. NHERF1 knockout cells tend to grow slowly and are more likely to die in culture, however these cells do not have any obvious morphological differences compared to control cells. Proteomic studies comparing the brush border membrane from wild type and NHERF1 knockout mice show differential expression of proteins associated with cellular transport, signalling, trafficking and the cytoskeleton and cell junctions[316]. NHERF1 knockout human cells and mice show significant increase in malic enzyme and G6P-dehydrogenase, indicating increased PPP metabolism and decreased mitochondrial protein expression, but not a decrease in overall ATP content[174].

In the HUNTER analysis, 12 endogenous peptides were measured and mapped to NHERF1 (Figure 6-C). One NHERF1 peptide significantly increased with fWIT (Figure 4-N), and had a molecular weight of 38kDa – 0.4kDa less than the full length NHERF1 – making

it difficult to distinguish the peptide on a Western blot. Several of the other measured NHERF1 peptides were cleaved from a similar region and have not been described in the literature. Cleavage of the significant peptide was not mapped to a protease, however peptides numbered 2 and 4 in Figure 6-C were cleaved by GRAM. Several attempts were made to work up a NHERF1 antibody to quantify variance in NHERF1 peptide expression. Difficulties optimising antibodies to quantify the cleaved peptides may be due to the similar sizing of the endogenous peptide to the full-length protein, or due to epitope incompatibilities with the antibodies used.

NHERF1 is an integral scaffolding protein for PTECs, specifically modulating the structure of the actin cytoskeleton *via* the ERM axis and maintaining the brush border matrix. NHERF1 also regulates phosphate reabsorption in the proximal tubules and regulates metabolism including PPP and moderates inflammation. Therefore, NHERF1 is likely a valuable marker of proximal tubule injury and may serve as a marker of DCD kidney quality. The impact of NHERF1 degradation needs to be further investigated to establish its potential as an injury marker. As shown in this study, Western blotting is not a viable method to validate the degradation profile quantified in DCD kidneys, however, attempts to quantify NHERF1 degradation could be made using histological techniques or by assessing changes in NHERF1-associated proteins, such as actin or ERM proteins. Previously, studies have shown that ezrin expression is reduced in NHERF1 knockout mice[319], and is likely to also be dysregulated if NHERF1 is degraded. Metabolic changes associated with the PPP may also correlate with degraded NHERF1 in the DCD kidney.

### 6.5.3 Betaine-homocysteine S-methyltransferase degradation generated several previously described fragments and associates with increased Legumain activity and fWIT

Betaine-homocysteine S-methyltransferase (BHMT) is a cytosolic enzyme that catalyses the transfer of a methyl group from betaine to homocysteine to form dimethylglycine and methionine. BHMT is exclusively expressed in the liver and the kidneys, specifically in the proximal tubule of the cortex in the kidney. As discussed in Chapter 4, BHMT has a role in both methionine and, inadvertently, choline metabolism, but also acts as an osmolyte, providing protection against stress induced protein misfolding. Betaine is produced by the metabolism of choline, and dimethylglycine is further demethylated into the amino acid glycine, which can act as an amino acid or be degraded to pyruvate (Figure 4-W). Methionine is a dietary amino acid and the precursor for cellular methylation, succinyl-CoA, homocysteine, cysteine, creatine, and carnitine. Methionine also regulates metabolic processes, systemic immune responses and counteracts oxidative stress by catalysing the synthesis of glutathione, which is a cellular antioxidant reducing the formation of damaging free radicals[321]. Deficient methionine metabolism is a side effect of dysregulated BHMT and can cause hyperhomocysteinemia, a well described side effect of declining kidney function.

In Chapter 4, BHMT was shown to be degraded in kidneys with a prolonged fWIT. Twelve endogenous peptides were mapped to BHMT, many of which had similar molecular weights between 34 and 40kDa and were from overlapping regions (

Figure 6-D). Several measured BHMT peptides were predicted to have been cleaved by LGMN (Figure 6-G), which is minimally described in the literature. Western blot analysis showed the full length BHMT band at 45kDa and three fragments between 30-38kDa (Figure 6-E), one of which may represent the significant peptide estimated at 35kDa. However, as shown in Figure 6-D, there were two peptides with a molecular weight of 35kDa, and one with a molecular weight of 36kDa. Distinguishing which peptide is being amplified in the Western blot would require sequencing. Densitometry of the Western blot indicates trends in BHMT abundance changing with increased fWIT. Full-length BHMT abundance trended down as fWIT increased ($p=0.49$) whilst peptide abundance trended up with fWIT ($p=0.65$). The ratio of full length to fragment expression was not significantly different ($p=0.43$).

Legumain cleavage of BHMT, as illustrated in Figure 6-G, appears region-specific, cleaving peptides 4, 12 and 19 as ordered in Figure 6-D. The three LGMN cleaved peptides have overlapping sequence, slightly shifting the cleavage region. A literature search for the relationship between LGMN and BHMT indicated that the 35kDa fragments observed in this study have previously been described in both human and animal models. Specifically, this cleavage of BHMT is associated with autophagy, where cellular protein is degraded *via* the lysosomal system. The 35kDa BHMT peptide in this model was only described in the autolysosomal membrane and may serve as a marker for autophagy[322]. Specific to the findings reported here, further work is required to determine if BHMT degradation and change in LGMN activity have an impact on cell function, autophagy and choline metabolism. Furthermore, loss of BHMT may be

indicative of reduced osmoprotection against oxidative stress in the kidney concurrent with increased ischaemia.

### 6.5.4 Legumain activity was significantly increased in ischaemic kidneys, yet its expression was reduced as fWIT increased

Legumain (LGMN) activity was significantly increased in DCD kidneys with prolonged fWIT (Figure 4-N). However, the abundance of both zymogen and active LGMN was shown to be reduced as fWIT extended, whilst the ratio showed more active LGMN compared to zymogen (p=0.15). This discrepancy between LGMN activity and abundance is not surprising. LGMN activity was quantified from the peptide data in the peptidomic analysis by measuring the expression of endogenous peptides assumed to have been cleaved by LGMN, furthermore, protease activity is not dependent upon its abundance.

Protease activity is modulated by various influences, including environmental factors such as pH, substrate availability, protease inhibition and protease specificity. The observed trend of reduced LGMN abundance in DCD kidneys with fWIT may have a downstream posttransplant effect; reduced LGMN may reduce degradation of matrix proteins leaving the kidney susceptible to fibrosis.

Legumain is a lysosomal cysteine protease predominantly active under acidic conditions with a strong affinity for cleaving C-terminal side asparagine (ASN - N) or aspartic acid (ASP - D) (Figure 4-L). LGMN is less selective about the amino acids at P2, P3 and primed positions, and expressed predominantly in the kidney and testis, LGMN is found

ubiquitously in the body. It has been identified in the nucleus, extracellular space and cytosol, with its role and activity under a more basic pH being typically disease-related[237]. LGMN participates in several cellular pathways, including hydrolysing cathepsins, antigen processing, and protein degradation. In the kidney, LGMN is expressed in the endosomes and lysosomes of the proximal tubules where it processes cathepsins (B, H and L), cleaving them into their active two-chain forms[323], and controls ECM remodelling by degrading ECM proteins including fibronectin and collagens[237,324,325]. Other substrates of LGMN include cystatin C, tau, acetoacetyl-CoA synthase and p53[237]. LGMN has an immunity and immune response role by processing self and foreign proteins for presentation to the MHCII complex and for processing antigens in immune signalling, and in regulating the degradation of macromolecules in proximal tubule cells[236]. Deregulation of LGMN is associated with various pathological conditions; overexpression of LGMN correlates with poor cell survival, increased lactate dehydrogenase release[326] and is implicated in cancer growth and metastasis, Alzheimer's disease, and multiple sclerosis lesions[327,328]. LGMN deficiency associates with interstitial fibrosis, decreased eGFR, increased plasma creatinine, proteinuria in mice[237,323], and slower antigen processing[236]. LGMN knockout mice have impaired cathepsin cleavage, whilst proximal tubule lysosomes become enlarged as macromolecules accumulate[329]. In an IRI model, LGMN abundance reduced with hypoxia and immediately following reperfusion but returned to baseline levels within seven days[326]. In a LGMN knockout IRI model, LGMN deficiency attenuates tubular injury and inflammation, and suppresses ferroptosis[326], indicating that LGMN inhibition may protect the kidney from hypoxia related injury during transplantation. In this study, the authors found that LGMN degrades ferroptosis protective factors *via* autophagy, driving

pathogenesis and cell death in AKI[326]. Additionally cell survival and lactate dehydrogenase was affected by hypoxia in proximal tubule cells isolated from wild type mice, but not mimicked in proximal tubule cells isolated from LGMN knockout mice, indicating the role of LGMN in associated processes[326].

In the HUNTER analysis, LGMN cleaved two proteins: HBA1 and BHMT (Figure 6-G). A STRING analysis showed there was no relationship between these proteins. The HUNTER data did not show evidence of LGMN targeting its more well described substrates such as fibronectin, cystatin C or p53. BMHT has previously been described as a substrate of LGMN associated with lysosomal autophagy, with described fragments being of a similar molecular weight to those observed in the DCD kidneys. HBA1 degradation has not been described in the literature in relation to humans but has been described in blood-feeding ticks. Expression of LGMN was also shown to be variable in podocytes and PTECs when cultured under normoxic and hypoxic conditions +/- glucose. In podocytes LGMN abundance was stable during the first 6h of culture, but at 24h there was less zymogen LGMN and reduced LGMN in the Hypo-Gluc cells although this did not reach significance (this may be due to an outlier in the data) (Figure 6-H). Furthermore, the signal ratio comparing zymogen and active LGMN showed a realigning of expression levels at 24h, whilst at previous time points there was more active LGMN. Typically, LGMN expression is described in the proximal tubule region on the nephron. In PTECs, active LGMN was evidently affected by the availability of glucose during culture, as seen in the Western blot (Figure 6-I). Active LGMN band intensity was significantly reduced in PTEC culture under both normoxic and hypoxic conditions without glucose, indicating a relationship between LGMN and glucose that requires further investigation. It has previously been

reported that Simvastatin reduces glucose metabolism and LGMN activity in cultured cells, yet the relationship between glucose metabolism and LGMN has not been further explored[330].

The reduction of LGMN abundance in DCD kidneys is an interesting finding, considering the activity of LGMN was shown to increase with prolonged fWIT. This finding needs to be validated in a separate cohort of DCD kidneys with extending fWIT. Previously, reduced LGMN has been associated with ageing and the induction of premature senescence and fibrosis in the proximal tubules[324] and the enlargement of the lysosomes caused by macromolecule build up associated with reduced LGMN activity[323]. However, Chen *et al* reported that hypoxia-induced LGMN deficiency may prevent tubular injury, inflammation and cell death[326]. This variability regarding the implications of reduced LGMN in the kidney requires further study and is essential in a DD model.

In this study, LGMN activity was increased in DCD kidneys targeting HBA1 and BHMT, which are not typical targets of this protease. Understanding this change in LGMN target could provide insight into dysregulation in the kidney associated with fWIT and into novel substrates of LGMN. Furthermore, reduced zymogen and active LGMN in DCD kidneys may indicate changes in LGMN gene expression caused by biological ageing, hypoxic insult associated with the DCD pathway, or metabolic dysregulation. Following validation in a separate cohort of DCD kidneys with prolonged fWIT, reduced LGMN expression should be further studied in relation to metabolic changes, especially associated with glucose and choline, changes in fibrotic markers, senescence and early tubular injury. Further understanding of LGMN activity and abundance changes

associated with fWIT may provide insight into new markers of ischaemic injury and catalogue potential biological targets for intervention.

### 6.5.5 Cathepsin B expression decreased with fWIT

Cathepsin B (CATB) is another lysosomal cysteine protease that coordinates with other lysosomal proteins to maintain proteostasis. Active CATB is cleaved from the single-chain inactive form by LGMN[323]. Typically, CATB is active in the lysosomes under an acidic pH, however under pathophysiological conditions CATB can translocate from the lysosome into the cytosol, nucleus and extracellular space, and is active within a neutral pH[241]. Substrate specificity of CATB has been described as altering with pH. Substrate cleavage profiling reported by Yoon *et al* found that CATB prefers norleucine at P3, lysine and arginine in P2 regardless of pH, yet no definitive preference for an amino acid at the P1 position could be determined[241].

Cathepsins regulate ECM proteostasis, autophagy, apoptosis and inflammation. Specifically, CATB is involved in regulating glomerular permeability and endothelial function and, when dysregulated, associates with the onset and progression of kidney fibrosis and disease. The matrix proteins collagen, laminin, fibronectin, perlecan and aggrecan are the typical substrates of CATB, along with the antigens epithelial growth factor, glucagon and BCL2[240]. CATB acts as an endopeptidase cleaving within a protein or peptide but also as a carboxydipeptidase cleaving amino acid at the C-terminal end of a peptide[240].

Cathepsin B activity, like other proteases, is affected by various factors including environmental conditions. CATB can be inhibited by proteins and drug therapies including steroids[331]. Aberrant CATB activity has previously been associated with cytoskeletal dysregulation, fibrosis and cell death, however the role of CATB in kidney injury and disease is complex. CATB dysregulation causes inflammation in podocytes and endothelial cells and apoptosis and autophagy in proximal tubules[254]. Dysregulated CATB activity is well described in cancer biology and is indicated as a potential therapeutic target[332]. Under physiological conditions in the kidney, circulating CATB is continuously filtered into the glomeruli and then reabsorbed by the proximal tubule cells by megalin receptors, providing a fresh flux of enzymes to the proximal tubules, indicating that CATB levels in the proximal tubule can adapt as required[240]. Reduced CATB activity is associated with worsening renal function and AKI[254], and in IRI models induces inflammasome activation[333]. However, in a hypoxic rat model, CATB activity in proximal tubule cells does not change[334]. In diabetic nephropathy, CATB activity reportedly decreased in isolated rat glomeruli, whilst expression of fibronectin increased[243], demonstrating the delicate balance between CATB activity and matrix proteostasis. In nephrectomy samples from patients with chronic rejection, CATB activity was significantly increased[335,336], as was the expression of fibronectin and laminin in isolated glomeruli[337]; suggesting an ineffectiveness of CATB under stress conditions. Fibronectin and collagen urinary excretion, however, was increased post-reperfusion[338]. Interestingly, in a liver cell model CATB has been shown to have a HRE, making it a potential target gene for HIF regulation under hypoxic and stress conditions[339].

In Chapter 4 (Figure 4-N) CATB activity decreased with increasing fWIT. Here, Western blotting was used to measure CATB abundance in kidney biopsies and podocyte and PTECs cultured under normoxic and hypoxic conditions. In kidney tissue, pro-CATB abundance increased (p=0.01) with fWIT, whilst active-CATB (p=0.13) abundance did not change; there was less active-CATB compared to pro-CATB (p=0.03) (Figure 6-L). This finding indicates that CATB synthesis may increase with hypoxia, however, the cleavage of pro-CATB into its active form is decreased with prolonged fWIT. As previously reported in HEPG2 liver cells, CATB transcription in the kidney maybe upregulated by hypoxia through HIF stabilisation and HRE activity. However, this does not necessarily imply that pro-CATB will subsequently be cleaved into its active form. Therefore, future research should focus on determining whether hypoxia, upregulates CATB gene expression via its HRE, and what mechanism in the DCD kidney causes reduced CATB activity. The dysregulation of LGMN activity associated with prolonged fWIT may contribute to the reduced activation of CATB. This could be further explored by measuring LGMN activity and its cleavage of CATB using an *in vitro* hypoxic cell model, ensuring that factors that influence protease activity, such as pH, are continuously monitored.

In this study, initial measurements of CATB abundance did not change in podocytes or PTECs cultured under hypoxic conditions, despite increases in HIF and PHD expression. These findings contrast with the observations made in the kidney and suggest that hypoxia alone may not be the primary driver of reduced CATB activity or abundance. Rather, CATB abundance and activity are likely influenced by various factors that were not captured in the *in vitro* cell model. In the kidney, decreased CATB activity could be a

consequence of drug treatments during donor management prior to WLST (e.g steroids), reduced renal blood flow (limiting the delivery of circulating CATB to the kidney), or a loss of megalin activity in the PT. Quantifying CATB mRNA expression in these cells could help determine whether hypoxia regulates CATB expression under hypoxic conditions, *via* HRE activity as previously reported in HEPG2 liver cells[339]. Further studies using the podocyte and PTEC cell model could investigate the effects of additional factors, such as drug treatments, on CATB activity and abundance under both normoxic and hypoxic conditions potentially identifying the cause of the reduced CATB activity observed in DCD kidneys. Changes in CATB activity could be assessed using commercially available fluorometric assays or protease-specific activity probes.

Although reduced, CATB activity cleaved 14 endogenous peptides (Table 6-A), from ACTA1, PFN1, GAPDH, ALDOA, ENO1 and SOD1. In Figure 6-M a STRING analysis of the proteins cleaved by CATB is presented, showing distinct relationships between the proteins, several of which associate with the cytoskeleton, cleaving key proteins including actin. CATB also cleaved proteins involved in glucose metabolism. Reduced CATB activity may associate with cytoskeletal protein accumulation, potentially inducing fibrosis. Degradation of integral proteins involved in metabolism, such as SOD1 and ENO1 may regulate or limit the metabolic capabilities of the kidneys when fWIT is short. Decreased CATB activity with increased fWIT reduces the degradation of metabolic products which may exacerbate metabolic dysfunction and drive kidney injury. The accumulation of CATB substrates with decreased CATB activity requires confirmation. Most matrix proteins can be degraded by multiple proteases, therefore in the instance of DCD kidneys with prolonged fWIT, further work is required to quantify the effect of

reduced CATB activity, including whether it results in the accumulation of matrix proteins that could induce fibrosis.

### 6.5.6 Granzyme M activity increased with fWIT

Granzyme M (GRAM) activity was increased as fWIT was prolonged in DCD kidneys (Figure 4-N) and was associated with the degradation of 22 proteins (Table 6-B). A STRING analysis of the proteins cleaved by GRAM is indicative of degradation of proteins associated with core cellular function and interaction, including nucleic acid and protein binding, protein interaction and structural and molecular activity (Figure 6-P).

GRAM is a serine protease, commonly associated with inflammatory processes, and was originally thought to be innate to natural killer cells[239]. Increased GRAM activity in the kidney likely associates with increased inflammation in the DD kidney, yet this protease is poorly studied, especially in the context of transplantation[340]. GRAM is known to degrade cytoskeletal proteins including ezrin and α-tubulin, as found in this study, destabilising the microtubular network and cellular integrity[340]. Degradation of ezrin may associate with the degradation of NHERF1; further investigations are required to understand the impact of the ERM-axis in DCD kidneys. Most of the other identified substrates of GRAM identified in the degradome have not previously been associated with GRAM in the literature, making it difficult to draw conclusions about the increased activity of GRAM in the DCD kidney. The STRING analysis shows that the proteins cleaved by GRAM are associated with regulating cellular function and communication, and therefore increased GRAM may be indicative of base level kidney injury affecting cell-cell interactions and communications essential to the function of the nephron.

Evaluation of each GRAM substrate described here is required to quantify the implications of GRAM-driven degradation on outcomes.

### 6.5.7 Matrix metalloproteinase-3 activity reduces with increasing fWIT

Matrix metalloproteinase-3 (MMP3) belongs to the MMP family of enzymes that each have specific substrate preference for matrix proteins[246]. MMP3 is an endopeptidase that favours basement membrane proteins[341] including; collagens-II, -IV & -IX, a range of proteoglycans, elastin, fibronectin and laminin[246]. MMP3 also cleaves other MMPs[244], and pro-inflammatory proteins, including TNFα and osteopontin[247]. MMP expression in the kidney is variable, and often region-specific, MMP3 is expressed in all regions of the nephron including the glomerulus (mesangial and endothelial cells) and the tubules[247]. However, its activity is best characterised in the glomerulus. MMPs are inhibited by TIMPs (tissue inhibitors of metalloproteinases), with TIMP-1 being the primary inhibitor of MMP3[247,342]. Concise regulation of MMP activity and TIMP inhibition regulates matrix protein proteostasis especially during matrix remodelling[342], therefore when this equilibrium is disrupted, matrix proteins accumulate, inducing injury. Disruption of MMP3 activity likely impacts inflammatory processes and is associated with EMT *via* the degradation of E-cadherin in tubular cells[247].

MMP3 expression is reportedly increased in KTx recipients experiencing antibody mediated rejection, but not in recipients with T-cell mediated rejection[343]. Urine levels of MMP3 activity are decreased in diabetic patients with progressive diabetic kidney disease. In these incidences MMP3 activity in the urine decrease in line with kidney function and the accumulation of ECM proteins and kidney scarring[342]. In chronic

allograph nephropathy in rats, inhibition of MMPs (including MMP3) early after transplant improves graft outcomes, lowers proteinuria and macrophage infiltration and improves creatinine clearance[341]. It has been reported elsewhere that pro-MMP3 serum levels are increased in recipients with chronic allograph nephropathy and positively correlated with serum creatinine[344]. A measure of MMP3 activity in donor kidneys is lacking in the literature, as is the analysis of MMP3 activity in kidney disease.

In the HUNTER analysis, MMP3 activity was seen to decrease with elongated fWIT in (Figure 4-N). To quantify MMP3 expression in the kidney biopsies, two polyclonal antibodies were unsuccessfully tested; clear protein bands were not measurable. Quantifying zymogen and active MMP3 should be a continued focus of follow up work from this study. The MMP family is vast and well reported in the literature. Several MMPs, including MMP-2 and -9, are implicated in kidney disease. Therefore, further research into the role of MMP3 in kidney injury would be a valuable addition to the field. As discussed above, inhibition of MMPs (including MMP3) in rats, has been shown to improve graft viability, pointing to it being a potential target for intervention in humans. Reduced MMP3 activity in DCD grafts with increasing fWIT is most likely indicative of dysregulation and subsequent accumulation of matrix proteins, which may provoke injury, and analysis of MMP3 and TIMP-1 expression would support this claim.

In the degradomic study, four proteins – serum amyloid A1, osteopontin, fibrinogen alpha chain and alpha-1 antichymotrypsin-1 – were cleaved by MMP3 (Table 6-C). These proteins were mapped using STRING, highlighting changes in folate and vitamin B12 metabolic pathways and the complement system (Figure 6-Q). All four proteins are

implicated in AKI and CKD, and therefore reduced degradation of these proteins may indicate a switch in proteostasis and induced injury limiting graft recovery and posttransplant function.

### 6.5.8 Tripeptidyl peptidase 1 showed autocatalytic activity which was downregulated as fWIT increased

Tripeptidyl peptidase 1 (TPP1) is an aminopeptidase localised to the lysosomes, cleaving tripeptides *en bloc* from the N-termini of small unstructured polypeptides[345]. TPP1 is minimally expressed in glomerular cells but has increased expression in the tubules[249]. TPP1 has been observed to hydrolyse collagens and subunit C of mitochondrial ATP synthase, however other substrates are relatively under investigated, making it difficult to predict the role of TPP1 in the kidney.

In the HUNTER analysis, TPP1 activity was decreased with increasing fWIT (Figure 4-N), yet its activity was autocatalytic (Table 6-D). The peptide sequence of the five endogenous peptides measured were similar and ended in the same seven amino acids. It is unclear from this analysis if the observed cleavages of TPP1 are part of its autocatalytic activation or indicative of protein degradation.

### 6.5.9 Limitations and future work

In this chapter, Western blotting was used to visualise and validate endogenous peptide and protease changes associated with fWIT in DCD kidney homogenates and podocytes, and PTECs cultured under normoxic and hypoxic conditions. Several proteins and proteases were selected for validation, however not all yielded results. In some

instances, the antibodies selected did not probe the expected degradation products of the full-length protein, despite all primary antibodies being polyclonal antibodies. In addition, some commercial antibodies did not work as expected, as they did not reliably probe for the full-length protein, or as in the case of NHERF1, degradation products were not distinguishable from the full-length protein. Quantifying changes observed in the degradome is not straightforward for many reasons. Changes in protein abundance or protease activity can be caused by various biological functions, which requires specialist techniques to quantify. Furthermore, measuring differences in protein and peptide abundance with differences in protein isoforms and PTM are finite.

The study was also limited by sample availability to validate additional proteins and proteases. Some remaining kidney samples had diminished protein concentration for Western blot analysis, likely reflecting sample age, reduced tissue quality, and most probably a consequence of freeze/thaw cycles. The variability in sample protein concentration was evident in Figure 6-F and Figure 6-L. The inconsistency in ß-actin concentration between samples highlights the variability in protein levels between these samples and should be considered when interpreting the results. Whilst Western blot data were normalised to the housekeeping gene, such significant fluctuations in sample concentration could have impacted the findings. Therefore, further quantification of protein and protease abundance should be undertaken in an independent cohort. Continued validation of the degradome study is dependent upon the acquisition of additional DCD biopsies with prolonged fWIT; this is a challenge due to limited sample availability and data missingness, as previously described.

Alternatively, degradation products described in the DCD degradome study could be studied in urine samples from the same donors. Protocol optimisation to measure peptides in urine is required. Validating degradation of kidney proteins in the urine would be clinically beneficial, as urine is a non-invasive sample type that is available in large volume. Previously FBP1 and NHERF1 has been measured in urine samples from patients with kidney pathologies; FBP1 has been described as a novel biomarker for progression of diabetic nephropathy[181].

The validation of protease changes was also limited by the application of Western blotting, which allowed for protease abundance to be quantified in both the zymogen and active forms, but did not provide insight into the activity of the proteases. Overview of protease abundance may provide clues regarding the implication of protease activity posttransplant, however this would require recipient protocol biopsies to quantify. Protease activity probes are a viable way to measure protease activity in a biological sample but are currently better suited to cell lysates rather than organ homogenates. Future work could use the cell model described in Chapter 5 to measure changes in protease activity over time and culture condition. Based on the findings reported here, quantifying LGMN activity in PTECs cultured without glucose would provide additional insight into the relationship between LGMN and glucose. This is a key aim of research following on from this study.

Proteases are central to regulating kidney pathophysiology and are key modulators of glomerular function and inflammation and tubular injury in the proximal tubules. As such, proteases are potential therapeutic targets to treat and prevent disease or injury

associated with deceased donation. In transplantation, proteases may be targeted during donor management, during organ perfusion or immediately posttransplant in the recipient to minimise organ injury. However, this would require an in-depth understanding of protease activity and expression in the kidney as well as the implications of protease activity and inhibition in the short- and long-term. Innovative strategies are required to evaluate this and should be the focus of future work as a follow on from this study, to work towards improving transplant outcomes from DCDs.

### 6.5.10 Conclusions

Analysis of DCD kidney biopsies using a peptidomic protocol highlighted abundance changes in endogenous peptides and protease activity that was associated with prolonged fWIT. In this chapter, three proteins with increased degradation and two proteases with differing activity were validated using Western blotting. In kidney homogenates, protein and peptide expression could reliably be measured by Western blotting. However, analysis of protease expression did not necessarily match protease activity. LGMN activity was significantly increased with fWIT, yet the expression of active and zymogen LGMN was decreased as fWIT was prolonged. Expression of CATB was reduced, as was its activity with prolonged fWIT, which may associate with changes in LGMN activity and expression. Further validation of findings from the degradomic analysis is necessary and would benefit from assessing changes within biological pathways with which the endogenous peptides are associated. Further validation is required to attribute change in protease activity and abundance to posttransplant outcomes. Quantification of protein degradation products should be attempted in urine.

# Chapter 7 Summary and future work

## 7.1 Experimental findings

This study aimed to investigate mechanisms of organ injury in kidneys from DCDs, specifically related to the duration of fWIT. Between 2012 and 2022, 3,300 DCD kidney donors with a recorded fWIT were identified from the NHSBT transplant registry. The mean and median fWIT were 26.1 minutes and 18 minutes, respectively. These values were used to establish clinically relevant experimental groups for this study.

In Chapter 4, the peptidomic analysis of 42 DCD kidney biopsies collected at retrieval is described. Donors for this study were age, sex and cause of death matched and had either a short fWIT of <25minutes or a long fWIT of 30-120 minutes. Endogenous peptides were enriched according to the HUNTER protocol and analysed using mass spectrometry, resulting in the quantification of 2,565 endogenous peptides. Of these, seven peptides exhibited increased abundance in kidneys with increasing fWIT, indicating disruptions to the cytoskeleton and metabolic dysregulation. Further analysis of biological pathway regulation confirmed significant perturbations in metabolic processes, particularly glucose metabolism. Changes in matrix protein abundance and degradation and cell-to-cell communication were also evident in kidneys with increasing fWIT, highlighting the molecular consequences of prolonged fWIT in DCD kidneys.

Disturbances in glucose metabolism in the kidney is indicative of an energy crisis, resulting from reduced organ oxygenation following WLST and WI. In DCD kidneys, increased degradation of FBP1 is likely linked to dysregulated gluconeogenesis in the proximal tubules, which could lead to elevated lactate levels and impaired kidney function posttransplant. The kidneys play a critical role in glucose synthesis through

gluconeogenesis, which is tightly regulated by hormones such as insulin and the body's nutritional state. A reduction in gluconeogenesis can precipitate systemic metabolic dysfunction and is associated with both AKI and CKD. Thus, the failure to maintain proper glucose metabolic processes post-WLST likely exacerbates renal injury and hinders metabolic and functional recovery, limiting long-term transplant outcomes.

Protease activity in DCD kidneys was also observed as changing with prolonged fWIT and was determined using the cleavage motif of each endogenous peptide in relation to the canonical parent protein sequence. The activity of five proteases changed with increasing fWIT; LGMN and GRAM activity increased, whereas the activity of MMP3, CATB and TPP1 decreased. The abundance of LGMN and CATB were quantified in kidney tissue using Western blotting. The abundance of zymogen and active LGMN decreased as fWIT was prolonged, although this did not reach statistical significance.

To further investigate the impact of hypoxia on the kidney, immortalised human podocytes and PTECs were cultured under hypoxic conditions using a GasPak-pouch system. The optimisation of this model is detailed in Chapter 5. Gene expression associated with hypoxia was measured using qPCR to confirm the successful induction of hypoxia using this novel method. The expression levels of these genes varied depending on the culture condition and duration, confirming that the GasPak-pouch effectively induced hypoxia. Furthermore, cells cultured in the absence of glucose exhibited elevated expression of stress markers including HIFs, consistent with a cellular response to hypoxic stress. This finding underscores the critical role of glucose regulation in kidney cells, showing that glucose availability may influence cellular

responses to hypoxia and contribute to the adaptive mechanisms that mediate kidney cell function and survival under low-oxygen conditions.

To further understand the effect of hypoxia on LGMN and CATB, the abundance of both proteases was measured in normoxic and hypoxic podocytes and PTECs cultured +/- glucose (Chapter 6). Notably, the abundance of active LGMN reduced in cells cultured without glucose, under both normoxic and hypoxic conditions. This suggests a potential interaction between LGMN and glucose, a relationship which to date has not been well-characterised and warrants further exploration. The dysregulation of LGMN in response to glucose availability, particularly in the context of DCD kidneys, may present a promising therapeutic target for intervention, either in the donor or during organ recovery.

Legumain is a cysteine protease that plays a critical role in ECM remodelling by degrading ECM proteins such as fibronectin and collagens, as well as processing cathepsins. In the kidney[237], LGMN also degrades macromolecules involved in regulating kidney homeostasis[237]. Dysregulated LGMN activity has been associated with fibrosis, impaired kidney function and elevated plasma creatinine levels[237,323]. Moreover, ageing has been linked to a loss of LGMN activity, which has been shown to promote cellular senescence and fibrosis[324]. Given these associations, further investigation into the implications of altered LGMN abundance and activity, particularly in relation to hypoxia and glucose availability, is essential.

In DCD kidneys with prolonged fWIT, decreased CATB activity is likely linked to dysregulated LGMN activity, and may contribute to the development of fibrotic lesions in the donor kidney posttransplant. The association between reduced CATB activity and LGMN dysregulation requires further study. CATB, like LGMN, is a cysteine protease involved in cell death[346] and ECM remodelling[240], and has a crucial role in kidney function. Dysregulation of CATB has previously been associated with podocyte inflammation and apoptosis[254], both of which are implicated in kidney injury and the development of kidney diseases including AKI and CKD, underscoring its importance in cellular injury and kidney pathophysiology.

Hypoxia associated with prolonged fWIT, may induce transcription of CATB *via* stabilisation of HIF1α and its binding to the CATB promoter's HRE. Increased CATB levels posttransplant have been observed in chronic rejection[335,336], suggesting that monitoring CATB could be valuable for assessing kidney health pre- and posttransplant. Additionally, 14 proteins were identified as being cleaved by CATB, several of which are involved in glucose metabolism, further implicating dysregulation of glucose metabolism as a significant consequence of DCD donation and extended fWIT.

## 7.2 Study reflections

In Chapter 2, three objectives were outlined to investigate changes in the DCD kidney degradome associated with warm ischaemia. These objectives were as follows.

1. Investigate the effects of fWIT on the DCD kidney degradome, by profiling endogenous peptides, proteases and biological pathways.

2. Develop a hypoxic *in vitro* model of immortalised human podocyte and proximal tubule epithelial cells (PTEC) that allows a comparison of the effect of normoxic and hypoxic conditions over time.
3. Validate peptide profiles and proteases using complementary molecular techniques and *in vitro* models.

While successful in addressing its primary objectives, there are elements of this study which could be improved in future work. In each chapter, specific methodological limitations have been outlined (Chapter 4 (4.5.7), Chapter 5 (5.5.6), Chapter 6 (6.5.9)), yet there were broader limitations to the project in terms of sample availability and practicality of approaches.

A significant limitation was the availability and inconsistency in the size and protein concentration of kidney biopsies from the QUOD biobank. In 2018, QUOD revised its biopsy collection protocol to improve sample continuity and quality, as well as to increase sample volume. The benefits of this change were clearly demonstrated in this study. Had all the biopsies used in this study been collected under the revised protocol, the higher protein concentration of each sample would have facilitated the completion of proteomic profiling in conjunction with peptidomics, enabling a more in-depth analysis of protein changes associated with prolonged fWIT, and more measured peptidomic changes. Proteomics quantifies the entire set of proteins in a biological sample, offering insights into protein abundance, post-translational modifications and various protein isoforms. Combining proteomic and peptidomic analysis would have provided a more comprehensive profile of the biological implications and functional

dynamics of the DCD kidney following fWIT. An integrated analysis would have also afforded a deeper and more accurate understanding of changes in protein abundance and the associated biological pathways. Additionally, increased sample size would have facilitated additional validation of protein degradation profile. This work will be continued using a new cohort of biopsies.

Another limitation to this study was the reliance on outdated online resources for assessing protease activity, specifically, attempting to profile protease activity using both TopFIND (presented) and Proteasix. However, both tools are based on outdated versions of the UniProt and MEROPS databases, which resulted in matching only 14% of the identified endogenous peptides to cleaving proteases. This limitation could be addressed in future studies by developing an updated version of these tools, linked to the most recent version of the UniProt and MEROPS databases. Whilst this would have been of great benefit to this study – and future studies – it is a substantial undertaking that would require significant effort and specialised programming knowledge to establish. Alternatively, cleaving proteases can be assumed when cleavage preference of a protease is known. For example, peptides cleaved by LGMN can be presumed, as it is known that LGMN cleaves after either asparagine or aspartic acid. Identifying the cleaving proteases for each peptide identified in this study would be laborious, yet efforts could be made to identify other proteins cleaved by a protease of interest.

This study was also limited by challenges in validating the degradomic changes observed in the DCD kidneys. In Chapter 6, Western blotting was used to profile the degradation of three proteins, as quantified through MS. However, the effectiveness of Western

blotting was constrained by its limited sensitivity and the restricted availability of commercially accessible polyclonal antibodies. Polyclonal antibodies were specifically selected based on their epitope specificity, as they were expected to capture degradation of the target proteins. Despite this, the approach was not always successful, as illustrated by the difficulty in analysing NHERF1 degradation. Additionally, whilst useful for measuring protein concentration, Western blotting was not the most suitable technique for validating changes in protease activity. The abundance of active proteases does not correlate with enzymatic activity. Utilisation of protease activity assays would have been a more appropriate method to validate changes in protease activity.

## 7.3 Future work

This study has identified several distinct protein and pathway alterations associated with prolonged fWIT. However, the validation of these changes was constrained by limited sample availability. Future research should aim to establish a new cohort of DCD kidneys with varying fWIT lengths to further profile and validate the findings presented here. In addition, utilising a new set of donor kidneys will allow for a more detailed investigation of ischaemia-driven biological changes in a stepwise manner. For example, degradation of NHERF1, as quantified in the current cohort, likely associates with disruption to the actin cytoskeleton. In a new cohort, degradation of NHERF1 could be profiled and correlated to changes in actin and ezrin abundance or alterations in the morphology of the actin cytoskeleton in the kidney could be profiled, using histological techniques, providing a clearer picture of the cellular implications of ischaemia-driven injury in the kidney.

As outlined in section **7.2**, the changes in protease activity described in this study were not validated. Ongoing research stemming from this work is focused on assessing protease activity alterations in response to hypoxia using DCD kidney biopsies and kidney cells cultured under both normoxic and hypoxic conditions in media +/- glucose. Once the protocol for measuring protease activity is optimised, alternative proteases will be explored. By drawing on the literature and establishing collaborations with researchers proficient in quantifying protease activity, the use of different protease probes will be optimised to ensure specificity and reliability specific to the experimental conditions. In this study, protease abundance was found to be influenced by both hypoxia and glucose concentration. These findings suggest that protease modulation in response to hypoxia and glucose conditions may limit kidney function and KTx outcomes. Further validation of these changes is necessary, as targeting protease activity may offer new therapeutic strategies to enhance kidney preservation and improve transplant outcomes.

The Crabtree effect is a well-documented phenomena in which glucose in culture media inhibits normal metabolic processes, even under normoxic conditions. In this study, significant dysregulation of glucose metabolism was observed in kidneys with a prolonged fWIT. In Chapter 5, an *in vitro* hypoxic podocyte and PTEC model was optimised, with cells cultured +/- glucose. Cells cultured without glucose under both normoxic, and hypoxic conditions had increased expression of cell stress markers including HIFs. Ongoing work is necessary to determine how varying glucose concentrations influence podocyte and PTECs cultured under both normoxic and hypoxic conditions. Future studies should first establish whether podocytes and PTECs

under standard culture conditions are influenced by the Crabtree effect, as this could have important implications for the interpretation of changes in cellular metabolism described using this cell model.

Podocytes and PTECs cultured under hypoxic conditions +/- glucose exhibited time-dependent morphological changes. These alterations warrant further investigation as they may serve as potential indicators of hypoxia-induced pathophysiological changes. These changes could reflect cellular injury or impairment in cell function and a possible link in the pathogenesis of ischaemia-induced kidney dysfunction, as observed in DCD kidneys.

## 7.4 Study conclusions

The primary aim of this research was to investigate the impact of prolonged fWIT on the kidney peptidome, with a focus on identifying dysregulations in biological mechanisms and delineating key pathways that influence proteolytic activity in DCD kidneys. This study has characterised the alterations in DCD kidneys associated with prolonged fWIT, revealing significant changes in protease activity and the dysregulation of several critical biological pathways, including disruptions in metabolic processes and cytoskeletal integrity. These findings were validated using a range of laboratory techniques applied to kidney tissue samples and hypoxic immortalised kidney cells cultured +/- glucose. Notably, the research highlights a disruption in glucose metabolism in DCD kidneys as a direct consequence of prolonged fWIT, which may, in turn, impact protease activity. Targeting glucose metabolism represents a promising therapeutic strategy which could

be applied during donor management or organ reconditioning, to enhance the utilisation and posttransplant outcomes of DCD kidneys.

# Chapter 8 Appendix

## 8.1 Buffers

### 8.1.1 Laemmli buffer

10% (w/v) Sodium dodecyl sulphate (SDS) (75746, Sigma)

50% (v/v) Glycerol (G5516, Sigma)

300mM Tris-Cl pH 6.8 (648313, Sigma)

0.05% (w/v) Bromophenol Blue (B-5525, Sigma)

100mM DTT (D5545, Sigma)

### 8.1.2 MOPS buffer

Prepared as a 5x buffer, to be diluted to 1x for use

250mM MOPS (M1254, Sigma)

250mM Tris (T1378, Sigma)

5mM Na-EDTA tetrahydrate (E5391, Sigma)

0.5% SDS (10% SDS solution, 20-40000-10, Severn biotechnology)

Mix the MOPS and Tris into 500mL of milli-Q water, check pH and adjust to 7.7.

Add the Na-EDTA tetrahydrate and SDS and make the volume up to 1L.

Store at room temperature of 4˚C for up to a week.

To prepare 1x MOPS for electrophoresis dilute 200mL of the 5xMOPS buffer into 800mL of Milli-Q water.

### 8.1.3 Transfer buffer

25mM Tris (T1378, Sigma)

190mM Glycine (G7126, Sigma)

Mix the Tris and glycine into 500mL of Milli-Q water and mix until dissolved. Make the volume up to 800mL with Milli-Q water. Store at 4˚C.

When ready to use, add 200mL of methanol to the buffer, mix and prepare transfer sandwich.

### 8.1.4 Tris-buffered saline with tween (TBST)

20x TBS buffer (28358, Thermo Scientific)

1% Tween 20 (J20605-AP, Thermo Scientific)

Dilute TBS buffer in water, then add Tween 20.

### 8.1.5 Bovine serum albumin (BSA) blocking buffer

3% BSA (A3059, Sigma)

0.1% Gelatin (G9391, Sigma)

TBST

Mix gently.

### 8.1.6 BSA TBST antibody diluent

0.5% BSA (A3059, Sigma)

TBST

Mix until BSA is fully dispersed.

### 8.1.7 5% Milk blocking buffer/Antibody diluent

5% Skim milk powder (LP0033B, Oxoid)

TBST

Mix until milk is dissolved.

### 8.1.8 6M Guanidine hydrochloride (GuHCl)

6M Guanidine hydrochloride (GuHCl)

Nanopure Water

### 8.1.9 1M HEPES

1M HEPES

Nanopure water

pH adjusted to 7.2-8

### 8.1.10 1M Sodium hydroxide (NaOH)

1M Sodium hydroxide (NaOH)

Nanopure water

### 8.1.11 100mM Sodium hydroxide (NaOH)

100mM Sodium hydroxide (NaOH)

Nanopure water

### 8.1.12 5M Sodium hydroxide (NaOH)

5M Sodium hydroxide (NaOH)

Nanopure water

### 8.1.13 200mM tris-2-carboxyethyl phosphine (TCEP)

200mM TCEP (C4706, Sigma)

Nanopure water

### 8.1.14 100mM Iodoacetamide (IAA)

100mM Iodoacetamide (A39271, Thermo Scientific)

Nanopure water

### 8.1.15 1M Ethanolamine

1M Ethanolamine

Nanopure water

### 8.1.16 Buffer A

98% MilliQ water

2% $CH_3CN$

0.1% TFA

## 8.2 Kidney tissue homogenisation tests

### 8.2.1 Buffers compared.

Tissue protein lysis buffer (BSP006-20, NBS Biologicals) supplemented with provided protease inhibitors, dithiothreitol and phenylmethylsulphonyl fluoride (serine protease inhibitor) was compared to RIPA buffer (89901, Thermo Fisher) supplemented with protease inhibitor (P8340, Sigma), phosphatase inhibitors 2 (P5726, Sigma) and phosphates inhibitor 3 (P0044, Sigma) to lyse kidney tissue with a bead beater, sonic dismembrator (sonicator) and mortar/pestle tubes.

Kidney tissue samples were weighed (range 0.002-0.005g) and put into tubes with the assigned lysis buffer. Initial tests were performed with 50µL of RIPA buffer or 45µL of tissue lysis buffer; the volume was later increased to 100µL of each buffer for repeat tests. Both buffers and samples were kept cold using wet ice, where possible. The protein concentration of each sample was quantified using a BCA assay (3.6).

### 8.2.2 Homogenisation using a bead beater

Zirconia beads, 1.0mm (11079110zx, BioSpec Products), were added to four tubes, two with cold RIPA buffer and two with cold tissue lysis buffer. Kidney tissue was added to each tube and kept on wet ice. Samples were then placed onto the bead beater and spun for 30 seconds, then cooled on wet ice for four minutes, repeating the cycle a total of three times.

Tissue lysis in the low buffer volume was not successful using the bead beater. During spins, the buffer dried out deeming the tissue unusable. For the study design, it was important to not overly dilute the samples with buffer, thus this method was excluded.

### 8.2.3 Mortar and pestle homogenising

Specialised mortar and pestle tubes were purchased from VWR (431-0098). Kidney tissue was added to the provided tube with either tissue lysis buffer or RIPA buffer and pulverised with the pestle. Each buffer was tested in duplicate. Tissue was pulverised for between 60 and 90 seconds, stopping when all visible chunks of tissue were lysed.

### 8.2.4 Sonicator based tissue lysis

A sonic dismembrator ultrasonic processor (sonicator) (FN-705, Fisher Scientific) connected to a generator (Fisher Scientific) was used to homogenise the kidney tissue in tissue lysis buffer or RIPA buffer using a microtip connection. Again, each buffer was tested in duplicate, and the samples were kept on wet ice during homogenising, to minimise heat transference from the sonicator. The tissue was lysed using a microtip set to 50 amps, for 60 seconds.

### 8.2.5 Coomassie gel staining

Coomassie staining is a method for in-gel protein detection using Coomassie blue dye, that does not chemically modify proteins. Coomassie binds to the proteins in the gel to highlight the entire separated protein profile of a sample. After gel electrophoresis (3.7), gels were removed from their cassette and Coomassie blue dye stain (NB-45-0078-1L, Generon) applied. Gels were gently agitated on a gyro-rocker (Stuart) until the proteins

were stained blue, for a maximum of one hour. The dye was then decanted, and the gel washed in distilled water twice for three minutes and then for one hour at room temperature. Gels were imaged as required, using a Biorad Gel Doc EZ imager (Biorad) and Image Lab Software (V6.1).

### 8.2.6 Silver gel staining

Silver gel staining is an alternative protein stain that is more sensitive to low molecular weight proteins and fragments. Here, gels were stained using a ProteoSilver silver stain kit (1003331182, Sigma Aldrich), according to the manufacturers protocol. In brief, following electrophoresis, gels were placed in fixing solution on a rocker for 20 minutes, and then washed in 30% ethanol for 10 minutes followed by a wash in MilliQ water. The gels were then sensitised for 10 minutes, washed and equilibrated in the silver solution for an additional 10 minutes. The gels were then washed and developed in the provided developer solution. The staining reaction was stopped using the provided stop solution and incubated for five minutes. Gels were imaged using the Biorad Gel Doc EZ imager and Image Lab Software.

### 8.2.7 Comparison of homogenisation methods using protein staining

Following analysis using Coomassie (8.2.5) and silver staining (8.2.6) (Figure 8-A and Figure 8-B), there were no obvious differences in the protein profiles of kidney tissue homogenised in either buffer or by using the mortar and pestle versus sonicator. Additionally, there was no evidence of homogenisation-induced degradation to the proteins - confirmed by blotting and probing the samples with the housekeeping gene ß-actin (Figure 8-B). Comparison of protein concentration using BCA, found that samples

homogenised in RIPA buffer using the sonicator had a higher protein concentration compared to those homogenised using the mortar and pestle, and that these samples had a better reproducibility when the assay was repeated. Therefore, all kidney biopsies and cell samples were homogenised as described above in RIPA buffer supplemented with protease and phosphate inhibitors using the sonicator.

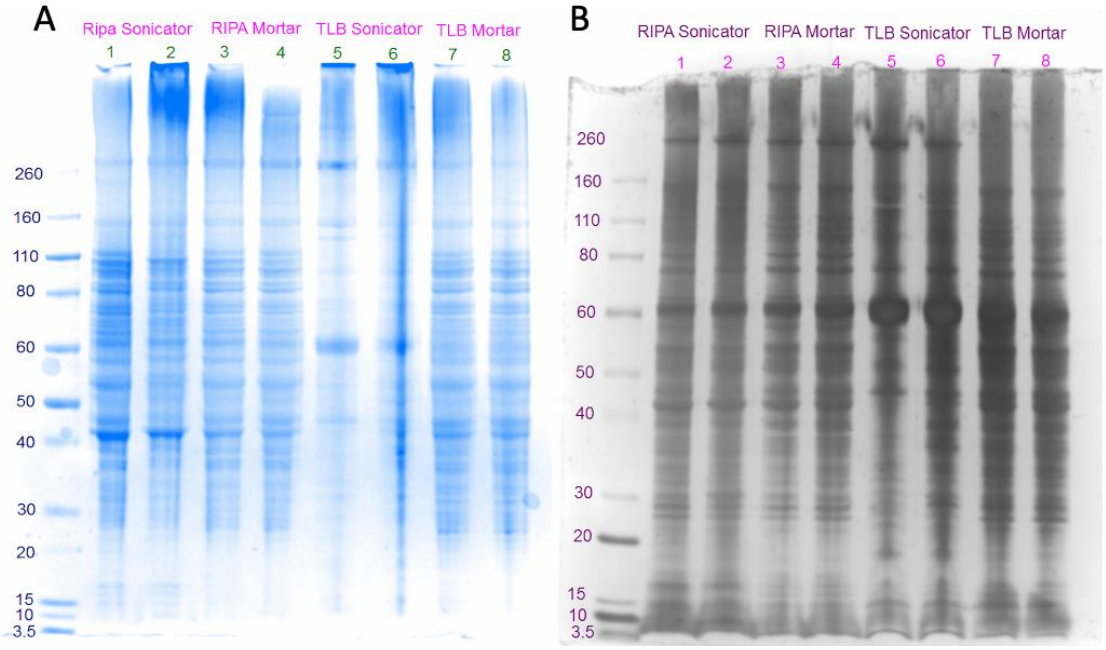



**Figure 8-A: Coomassie and silver staining of kidney tissue homogenised using tissue lysis buffer or RIPA buffer**

Coomassie and silver staining were used to compare the protein profiles of kidney biopsies homogenised in tissue lysis buffer or RIPA buffer using either sonication or mortar and pestle. Samples were run in 4-12% Bis Tris gels, loading between 10µg (Coomassie) or 15µg (silver staining) of total protein per well (quantified using BCA, samples were diluted in Laemmli buffer). Reproducibility was most consistent in tissue lysed in RIPA buffer.

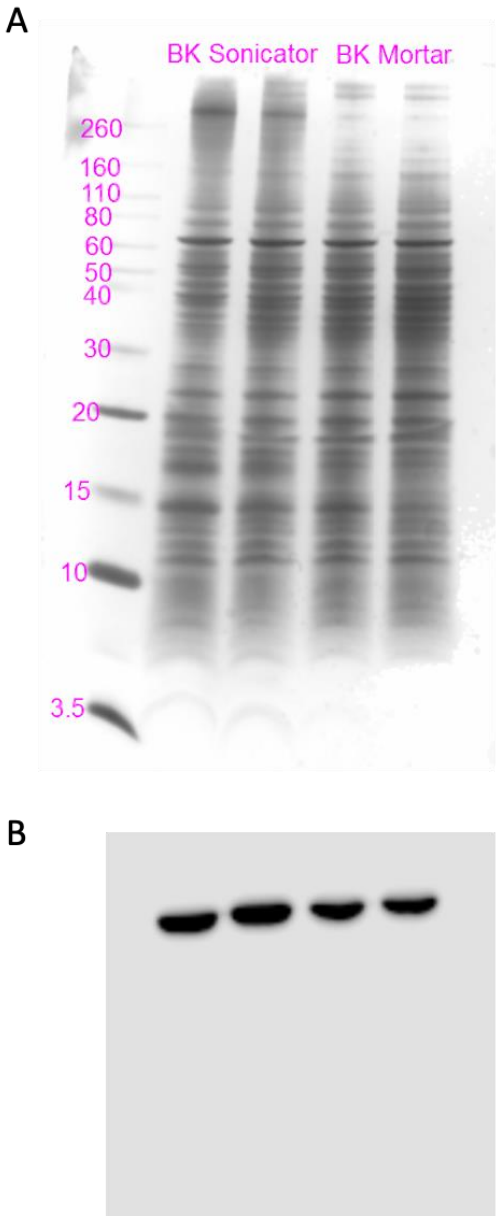



**Figure 8-B: Silver staining and β-actin probing of kidney tissue homogenised in RIPA buffer**

Kidney tissue from a deceased donor was homogenised in RIPA buffer and lysed using sonication or mortar and pestle. The samples were then diluted in Laemmli buffer and ran on a 16% Tricine gel. One gel was stained using silver staining whilst the other was transferred onto a PVDF membrane and probed with β-actin. There were minor differences in the protein profile of the technical replicates for each method, yet some differences in the size of proteins amplified with silver staining – RIPA buffer appears to better capture smaller proteins/peptides than the mortar and pestle method (A). For each homogenised sample there was no evidence of degradation of the key housekeeping protein β-actin (B).

## 8.3 HUNTER Study

### 8.3.1 Comparison between technical replicates across TMT batches

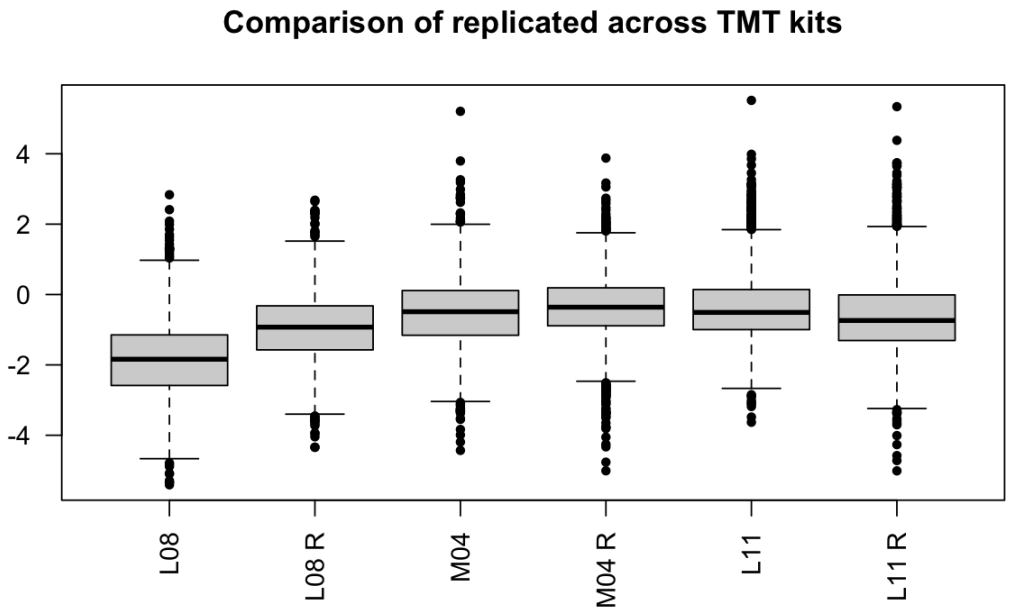



**Figure 8-C: Comparison in raw report ion values from technical replicates**

Three samples were analysed as technical replicates on two of the three TMT-kits (at random). A comparison between the raw report ion values can be seen in this box plot, which shows minimal difference in the raw ion values for each sample across the TMT-kits. The replicated sample has a 'R' after the sample id; these samples were not included in the analysis.

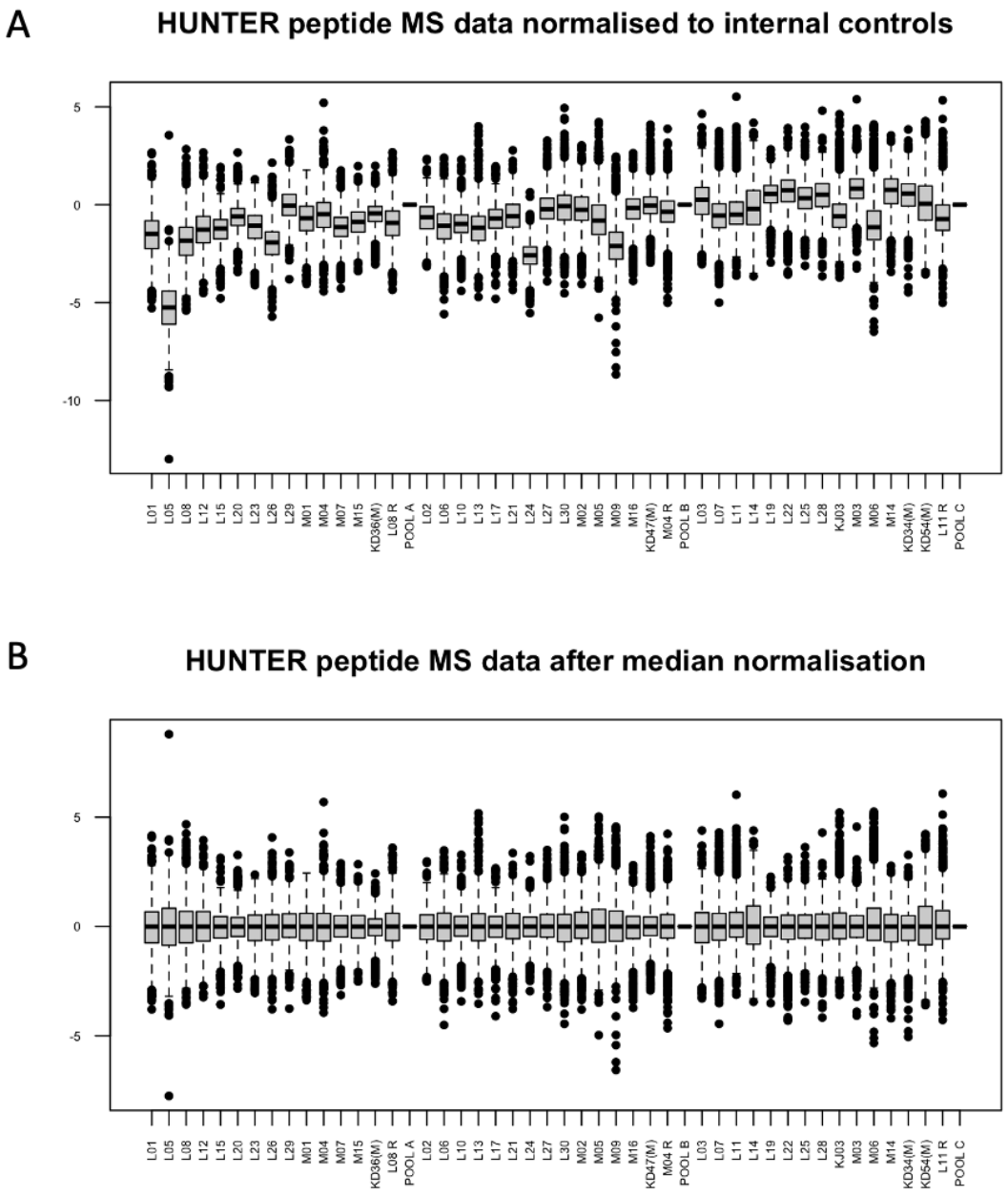



**Figure 8-D: Normalisation of peptide data from the HUNTER study**

Peptide raw intensity data was normalised against the control pooled sample analysed as part of each TMT-kit and then median normalised. (A) shows data normalised against the pooled samples. (B) shows data after median normalisation. For analysis, replicate samples were first removed.

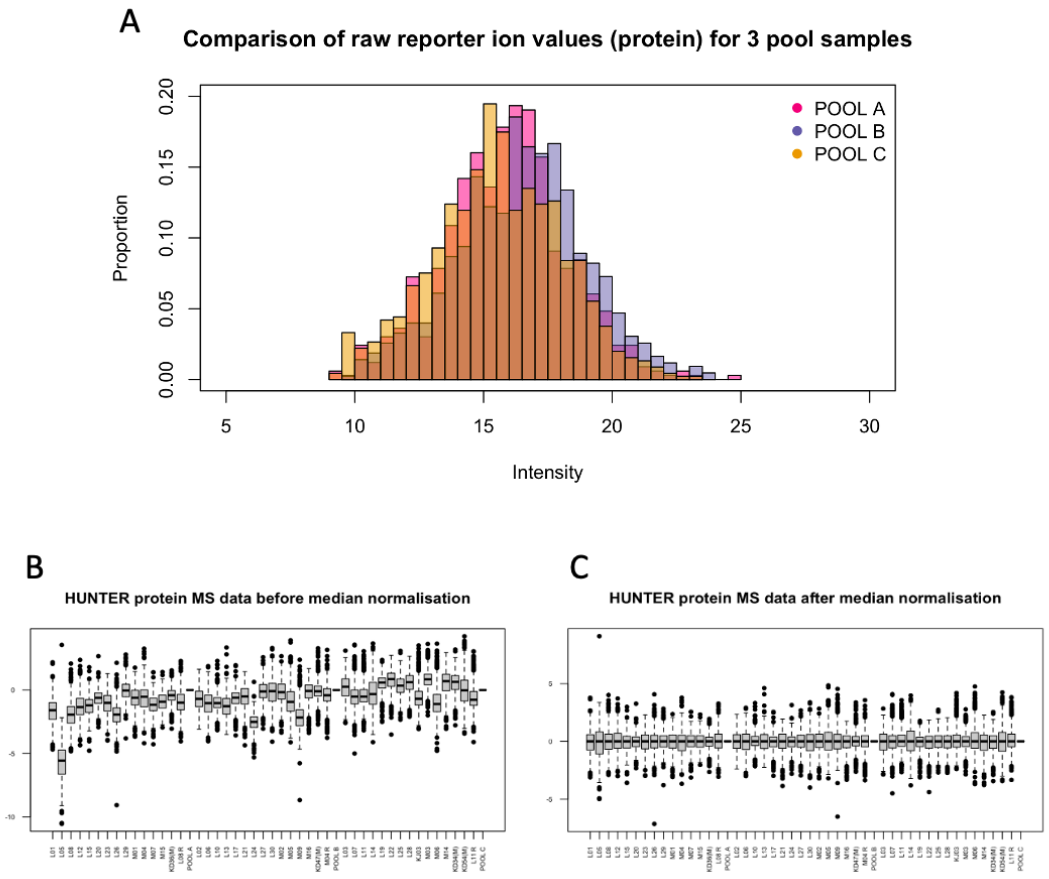



**Figure 8-E: Normalisation of the protein data from the HUNTER study**

Protein raw intensity data was normalised against the control pooled sample analysed as part of each TMT-kit and then median normalised (A). (B) shows data normalised against the pooled samples. (C) shows data after median normalisation. For analysis, replicate samples were first removed.

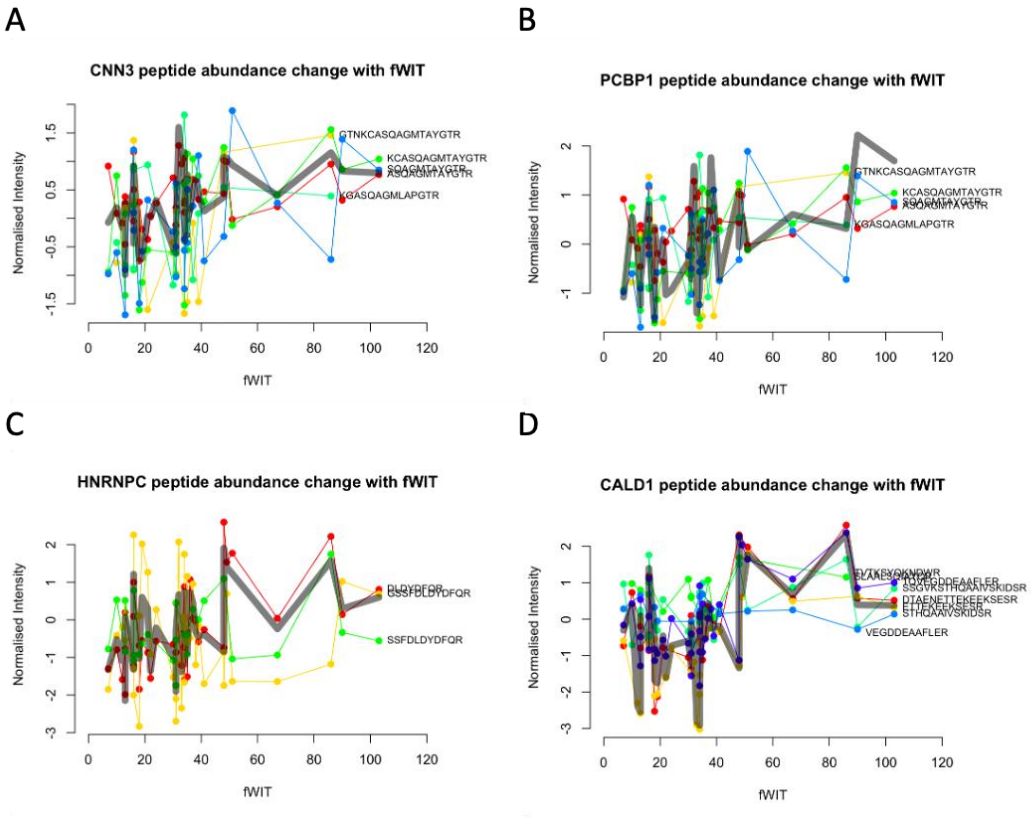



**Figure 8-F: Cumulative peptide abundance for proteins**

The cumulative peptide abundance for proteins is used by MaxQuant to determine protein abundance. These figures show individual peptide abundance derived from each protein, as well as the cumulative abundance of the peptides (grey line). CNN (A) and PCBP1 (B) abundance was increased in kidneys with a prolonged fWIT when analysed at the protein level but not at the peptide level. An endogenous peptide derived from HNRNPC (C) and CALD1 (D) was significantly increased in kidneys with a prolonged fWIT, and this effect was evident on the protein level.

## 8.4 Podocyte and PTEC Western blot analysis p.values

### Podocytes Western blot analysis p.values

A

| | | 30m | 1h | 3h | 6h | 24h |
|---|---|---|---|---|---|---|
| Zymogen LGMN | N+G vs N-G | 0.7995 | 0.7834 | 0.9954 | 0.2985 | 0.5007 |
| | N+G vs H+G | 0.9962 | 0.6485 | 0.6274 | 0.0169 | 0.6848 |
| | N+G vs H-G | 0.5578 | 0.1155 | 0.7953 | 0.0035 | 0.0466 |
| | N-G vs H-G | 0.7745 | 0.1485 | 0.7970 | 0.0067 | 0.0493 |
| | H+G vs H-G | 0.1236 | 0.2564 | 0.2260 | 0.0193 | 0.0703 |
| Active LGMN | N+G vs N-G | 0.5197 | 0.8551 | 0.1746 | 0.6357 | 0.1548 |
| | N+G vs H+G | 0.3490 | 0.4737 | 0.9056 | 0.1485 | 0.6424 |
| | N+G vs H-G | 0.9157 | 0.1286 | 0.6530 | 0.0876 | 0.9565 |
| | N-G vs H-G | 0.4800 | 0.1895 | 0.3499 | 0.0411 | 0.9118 |
| | H+G vs H-G | 0.3771 | 0.0365 | 0.1325 | 0.0925 | 0.8902 |
| Zymogen LGMN vs Active LGMN ratio | N+G | 0.0475 | 0.0018 | 0.6479 | 0.0247 | 0.0667 |
| | N-G | 0.0870 | 0.0049 | 0.7102 | 0.0298 | 0.8781 |
| | H+G | 0.0303 | 0.0046 | 0.0747 | 0.0480 | 0.9854 |
| | H-G | 0.0028 | 0.0176 | 0.0579 | 0.0718 | 0.1450 |

B

| | | 30m | 1h | 3h | 6h | 24h |
|---|---|---|---|---|---|---|
| Fibronectin | N+G vs N-G | 0.3756 | 0.2280 | 0.5830 | 0.0249 | 0.3596 |
| | N+G vs H+G | 0.2372 | 0.8642 | 0.1754 | 0.0175 | 0.7002 |
| | N+G vs H-G | 0.4803 | 0.3990 | 0.2021 | 0.0686 | 0.1456 |
| | N-G vs H-G | 0.0426 | 0.0844 | 0.1850 | 0.2386 | 0.0879 |
| | H+G vs H-G | 0.0293 | 0.0340 | 0.9266 | 0.2567 | 0.4013 |

C

| | | 30m | 1h | 3h | 6h | 24h |
|---|---|---|---|---|---|---|
| Pro CatB | N+G vs N-G | 0.3479 | 0.5023 | 0.1946 | 0.7910 | 0.4075 |
| | N+G vs H+G | 0.3326 | 0.1903 | 0.6705 | 0.0545 | 0.9526 |
| | N+G vs H-G | 0.2565 | 0.2648 | 0.5457 | 0.1098 | 0.0724 |
| | N-G vs H-G | 0.1413 | 0.3191 | 0.2100 | 0.0531 | 0.0967 |
| | H+G vs H-G | 0.3875 | 0.8844 | 0.5693 | 0.5491 | 0.0920 |
| Active CatB | N+G vs N-G | 0.2192 | 0.8199 | 0.5700 | 0.0221 | 0.8742 |
| | N+G vs H+G | 0.3159 | 0.2591 | 0.5328 | 0.9753 | 0.7637 |
| | N+G vs H-G | 0.1319 | 0.0594 | 0.6315 | 0.9403 | 0.2054 |
| | N-G vs H-G | 0.0606 | 0.0394 | 0.5869 | 0.0129 | 0.1021 |
| | H+G vs H-G | 0.1033 | 0.0539 | 0.4962 | 0.9986 | 0.2420 |
| Pro CatB vs Active CatB ratio | N+G | 0.0150 | 0.0001 | 0.0024 | 0.0000 | 0.0000 |
| | N-G | 0.0009 | 0.0002 | 0.0003 | 0.0003 | 0.0010 |
| | H+G | 0.0001 | 0.0001 | 0.0024 | 0.0004 | 0.0012 |
| | H-G | 0.0000 | 0.0002 | 0.0001 | 0.0004 | 0.0043 |

# PTEC Western blot analysis p.values

A

| | | 30m | 1h | 3h | 6h | 24h |
|---|---|---|---|---|---|---|
| Zymogen LGMN | N+G vs N-G | 0.0574 | 0.0309 | 0.2493 | 0.1610 | 0.6273 |
| | N+G vs H+G | 0.6421 | 0.2394 | 0.5680 | 0.2283 | 0.0050 |
| | N+G vs H-G | 0.1170 | 0.4106 | 0.4257 | 0.0200 | 0.1150 |
| | N-G vs H-G | 0.6759 | 0.5866 | 0.5531 | 0.0348 | 0.0699 |
| | H+G vs H-G | 0.0127 | 0.0244 | 0.0091 | 0.6507 | 0.2584 |
| Active LGMN | N+G vs N-G | 0.0022 | 0.0424 | 0.0607 | 0.5003 | 0.0194 |
| | N+G vs H+G | 0.3738 | 0.4279 | 0.0776 | 0.6461 | 0.2251 |
| | N+G vs H-G | 0.0096 | 0.0732 | 0.0102 | 0.6696 | 0.7572 |
| | N-G vs H-G | 0.2970 | 0.3817 | 0.0058 | 0.3042 | 0.1592 |
| | H+G vs H-G | 0.0144 | 0.0194 | 0.0305 | 0.6757 | 0.2762 |
| Zymogen LGMN vs Active LGMN ratio | N+G | 0.0074 | 0.0300 | 0.0405 | 0.8385 | 0.1818 |
| | N-G | 0.8348 | 0.5116 | 0.0655 | 0.1276 | 0.8400 |
| | H+G | 0.0040 | 0.0023 | 0.1048 | 0.2335 | 0.0314 |
| | H-G | 0.2902 | 0.3139 | 0.2957 | 0.4633 | 0.1084 |

B

| | | 30m | 1h | 3h | 6h | 24h |
|---|---|---|---|---|---|---|
| Fibronectin | N+G vs N-G | 0.2110 | 0.1431 | 0.2682 | 0.8019 | 0.2709 |
| | N+G vs H+G | 0.2925 | 0.9002 | 0.4127 | 0.6288 | 0.2691 |
| | N+G vs H-G | 0.1604 | 0.2528 | 0.6198 | 0.3942 | 0.8079 |
| | N-G vs H-G | 0.1940 | 0.3455 | 0.3306 | 0.3066 | 0.6264 |
| | H+G vs H-G | 0.1819 | 0.1389 | 0.1990 | 0.3159 | 0.6661 |

C

| | | 30m | 1h | 3h | 6h | 24h |
|---|---|---|---|---|---|---|
| Pro CatB | N+G vs N-G | 0.8652 | 0.0517 | 0.5831 | 0.0495 | 0.1573 |
| | N+G vs H+G | 0.7985 | 0.0924 | 0.8340 | 0.6826 | 0.7229 |
| | N+G vs H-G | 0.5668 | 0.3300 | 0.1092 | 0.3807 | 0.9015 |
| | N-G vs H-G | 0.4016 | 0.6492 | 0.3918 | 0.4246 | 0.4636 |
| | H+G vs H-G | 0.0172 | 0.1579 | 0.0109 | 0.0009 | 0.4575 |
| Active CatB | N+G vs N-G | 0.2208 | 0.1340 | 0.0348 | 0.9878 | 0.0733 |
| | N+G vs H+G | 0.4828 | 0.1089 | 0.1433 | 0.6079 | 0.1384 |
| | N+G vs H-G | 0.9971 | 0.3189 | 0.3153 | 0.7373 | 0.0612 |
| | N-G vs H-G | 0.5109 | 0.7829 | 0.0526 | 0.4712 | 0.9170 |
| | H+G vs H-G | 0.6581 | 0.9423 | 0.4727 | 0.5306 | 0.7829 |
| Pro CatB vs Active CatB ratio | N+G | 0.0000 | 0.0001 | 0.0006 | 0.0002 | 0.0038 |
| | N-G | 0.0008 | 0.0016 | 0.0076 | 0.0003 | 0.0005 |
| | H+G | 0.0042 | 0.0006 | 0.0019 | 0.0001 | 0.0666 |
| | H-G | 0.0013 | 0.0907 | 0.0007 | 0.0001 | 0.0345 |

# References


1. Cardinal, H. *et al.* Organ donor management and delayed graft function in kidney transplant recipients: A multicenter retrospective cohort study. *Am. J. Transplant* **19**, 277–284 (2019).
2. Schnitzler, M. A., Lentine, K. L. & Burroughs, T. E. The cost effectiveness of deceased organ donation. *Transplantation* vol. 80 1636–1637 (2005).
3. Gardiner, D., Charlesworth, M., Rubino, A. & Madden, S. The rise of organ donation after circulatory death: a narrative review. *Anaesthesia* **75**, 1215–1222 (2020).
4. Chakravorty, T. The Use of Deceased Donor Organs in Kidney Transplantation. *Journal of the Nuffield Department of Surgical Sciences* vol. 3 Preprint at https://doi.org/10.37707/jnds.v3i1.130 (2022).
5. Snoeijs, M. G. J. *et al.* Kidney transplantation from donors after cardiac death: a 25-year experience. *Transplantation* **90**, 1106–1112 (2010).
6. Vanholder, R. *et al.* Organ donation and transplantation: a multi-stakeholder call to action. *Nat. Rev. Nephrol.* **17**, 554–568 (2021).
7. Kidney disease: A UK public health emergency. (2023).
8. Leatherby, R. J., Theodorou, C. & Dhanda, R. Renal physiology: blood flow, glomerular filtration and plasma clearance. *Anaesthesia & Intensive Care Medicine* **22**, 439–442 (2021).
9. Theodorou, C., Leatherby, R. & Dhanda, R. Function of the nephron and the formation of urine. *Anaesthesia & Intensive Care Medicine* **22**, 434–438 (2021).
10. Park, J. C. & Hirschberg, R. Hormones and the kidney. in (Oxford University Press, 2011).

11. Scholz, H. *et al.* Kidney physiology and susceptibility to acute kidney injury: implications for renoprotection. *Nat. Rev. Nephrol.* **17**, 335–349 (2021).
12. Finch, N. C., Neal, C. R., Welsh, G. I., Foster, R. R. & Satchell, S. C. The unique structural and functional characteristics of glomerular endothelial cell fenestrations and their potential as a therapeutic target in kidney disease. *Am. J. Physiol. Renal Physiol.* **325**, F465–F478 (2023).
13. Miner, J. H. The glomerular basement membrane. *Exp. Cell Res.* **318**, 973–978 (2012).
14. Chew, C. & Lennon, R. Basement Membrane Defects in Genetic Kidney Diseases. *Front Pediatr* **6**, 11 (2018).
15. Rinschen, M. M. *et al.* N-Degradomic Analysis Reveals a Proteolytic Network Processing the Podocyte Cytoskeleton. *J. Am. Soc. Nephrol.* **28**, 2867–2878 (2017).
16. Vaughan, R. H. *et al.* Cytoskeletal protein degradation in brain death donor kidneys associates with adverse posttransplant outcomes. *Am. J. Transplant* **22**, 1073–1087 (2022).
17. Holcombe, J. & Weavers, H. Functional-metabolic coupling in distinct renal cell types coordinates organ-wide physiology and delays premature ageing. *Nat. Commun.* **14**, 1–18 (2023).
18. Mather, A. & Pollock, C. Glucose handling by the kidney. *Kidney Int. Suppl.* S1-6 (2011).
19. Zhu, Z. *et al.* Transition of acute kidney injury to chronic kidney disease: role of metabolic reprogramming. *Metabolism* **131**, 155194 (2022).
20. Kovesdy, C. P. Epidemiology of chronic kidney disease: an update 2022. *Kidney Int. Suppl.* **12**, 7–11 (2022).

21. Hirst, J. A. *et al.* Prevalence of chronic kidney disease in the community using data from OxRen: a UK population-based cohort study. *Br. J. Gen. Pract.* **70**, e285–e293 (2020).

22. Busink, E. *et al.* A systematic review of the cost-effectiveness of renal replacement therapies, and consequences for decision-making in the end-stage renal disease treatment pathway. *Eur. J. Health Econ.* **24**, 377–392 (2023).

23. Barlow, A. D. & Ghoneima, A. S. Kidney transplantation. *Surgery* (2023) doi:10.1016/j.mpsur.2023.06.005.

24. Mannon, R. B. Delayed Graft Function: The AKI of Kidney Transplantation. *Nephron* **140**, 94–98 (2018).

25. Gavriilidis, P. & Inston, N. G. Recipient and allograft survival following donation after circulatory death versus donation after brain death for renal transplantation: A systematic review and meta-analysis. *Transplant. Rev.* **34**, 100563 (2020).

26. Kaisar, M. *et al.* Subclinical changes in deceased donor kidney proteomes are associated with 12-month allograft function posttransplantation-A preliminary study. *Transplantation* **103**, 323–328 (2019).

27. UK Renal Registry (2024) UK Renal Registry 26th Annual Report – data to 31/12/2022, Bristol, UK. Preprint at Available from https://ukkidney.org/audit-research/annual-report.

28. Kostakis, I. D. *et al.* Hypoperfusion warm ischaemia time in renal transplants from donors after circulatory death. *Nephrol. Dial. Transplant* **35**, 1628–1634 (2020).

29. Port, F. K. *et al.* Donor characteristics associated with reduced graft survival: an approach to expanding the pool of kidney donors. *Transplantation* **74**, 1281–1286 (2002).

30. Rao, P. S. & Ojo, A. The alphabet soup of kidney transplantation: SCD, DCD, ECD--fundamentals for the practicing nephrologist. *Clin. J. Am. Soc. Nephrol.* **4**, 1827–1831 (2009).

31. Sharif, A. Deceased donor characteristics and kidney transplant outcomes. *Transpl. Int.* **35**, 10482 (2022).

32. Schold, J. D., Kaplan, B., Baliga, R. S. & Meier-Kriesche, H.-U. The broad spectrum of quality in deceased donor kidneys. *Am. J. Transplant* **5**, 757–765 (2005).

33. Summers, D. M. *et al.* Is the increase in DCD organ donors in the United Kingdom contributing to a decline in DBD donors? *Transplantation* **90**, 1506–1510 (2010).

34. Watson, C. J. E., Johnson, R. J. & Mumford, L. Overview of the Evolution of the UK Kidney Allocation Schemes. *Current Transplantation Reports* **7**, 140–144 (2020).

35. Ibrahim, M. *et al.* An international comparison of deceased donor kidney utilization: What can the United States and the United Kingdom learn from each other? *Am. J. Transplant* **20**, 1309–1322 (2020).

36. Callaghan, C. J. *et al.* The discard of deceased donor kidneys in the UK. *Clin. Transplant.* **28**, 345–353 (2014).

37. Ibrahim, M. *et al.* Outcomes of Declined Deceased Donor Kidney Offers That Are Subsequently Implanted: A UK Registry Study. *Transplantation* **107**, 1348–1358 (2023).

38. Carreras-Planella, L., Franquesa, M., Lauzurica, R. & Borràs, F. E. A brief history of kidney transplantation. *Hektoen International - A journal of medical humanities* https://hekint.org/2020/09/08/a-brief-look-to-the-history-of-the-kidney-and-kidney-transplantation/ (2020).

39. Shrestha, B., Haylor, J. & Raftery, A. Historical perspectives in kidney transplantation: an updated review. *Prog. Transplant.* **25**, 64–9, 76 (2015).

40. Ramirez, C. G. B. & McCauley, J. *Contemporary Kidney Transplantation*. (Springer International Publishing, 2018).

41. Hamilton, D. Kidney Transplantation: A History. in *Kidney Transplantation - Principles and Practice (Eighth Edition)* (eds. Knechtle, S. J., Marson, L. P. & Morris, P. J.) 1–8 (Elsevier, Philadelphia, 2019).

42. Tantisattamo, E., Maggiore, U. & Piccoli, G. B. History of kidney transplantation: a journey of progression and evolution for success. *J. Nephrol.* **35**, 1783–1786 (2022).

43. Langer, R. M. Donation after cardiac death - From then to now. *Transplant. Rep.* **8**, 100119 (2023).

44. Nordham, K. D. & Ninokawa, S. The history of organ transplantation. *Proc.* **35**, 124–128 (2022).

45. Hatzinger, M., Stastny, M., Grützmacher, P. & Sohn, M. The history of kidney transplantation. *Urologe A* **55**, 1353–1359 (2016).

46. Summers, D. M. *et al.* Analysis of factors that affect outcome after transplantation of kidneys donated after cardiac death in the UK: a cohort study. *Lancet* **376**, 1303–1311 (2010).

47. Organ and Tissue Donation and Transplantation Activity Report 2021/22. *NHS Blood and Transplant: Organ donation* https://www.organdonation.nhs.uk/ (2022).

48. Kootstra, G., Daemen, J. H. & Oomen, A. P. Categories of non-heart-beating donors. *Transplant. Proc.* **27**, 2893–2894 (1995).

49. Wu, D. A. *et al.* Barriers to living donor kidney transplantation in the United Kingdom: a national observational study. *Nephrol. Dial. Transplant* **32**, 890–900 (2017).

50. Thongprayoon, C. *et al.* Recent Advances and Clinical Outcomes of Kidney Transplantation. *J. Clin. Med. Res.* **9**, (2020).

51. Ribeiro, B. *et al.* Greater impact of living donation than HLA mismatching in short-term renal allograft survival. *Cureus* **15**, e34427 (2023).

52. Yoshikawa, M. H., Rabelo, N. N., Welling, L. C., Telles, J. P. M. & Figueiredo, E. G. Brain death and management of the potential donor. *Neurol. Sci.* **42**, 3541–3552 (2021).

53. Shemie, S. D. & Gardiner, D. Circulatory Arrest, Brain Arrest and Death Determination. *Front Cardiovasc Med* **5**, 15 (2018).

54. Kahan, B. D. DONATION AFTER CIRCULATORY DEATH: AN INTERNATIONAL VIEW. *Transplantation Reports* 100137 (2023).

55. Parrilla, G. A., Hunt, W. R. & Daneshmand, M. A. Lung transplantation following donation after circulatory death. *Transplant. Rep.* **7**, 100110 (2022).

56. Corbett, S., Trainor, D. & Gaffney, A. Perioperative management of the organ donor after diagnosis of death using neurological criteria. *BJA Educ* **21**, 194–200 (2021).

57. Taylor, M. E. *et al.* Mitochondrial responses to brain death in solid organ transplant. *Frontiers in Transplantation* **2**, (2023).

58. Kumar, L. Brain death and care of the organ donor. *J. Anaesthesiol. Clin. Pharmacol.* **32**, 146–152 (2016).

59. de Vries, D. K. *et al.* Donor brain death predisposes human kidney grafts to a proinflammatory reaction after transplantation. *Am. J. Transplant* **11**, 1064–1070 (2011).

60. Nijboer, W. N. *et al.* Effects of brain death on stress and inflammatory response in the human donor kidney. *Transplant. Proc.* **37**, 367–369 (2005).

61. Martin-Loeches, I. *et al.* Management of donation after brain death (DBD) in the ICU: the potential donor is identified, what's next? *Intensive Care Med.* **45**, 322–330 (2019).

62. Bezeljak, N. & Večerić-Haler, Ž. Pathophysiological changes and systemic inflammation in brain dead organ donors: effect on graft quality. in *Organ Donation and Transplantation.* 3–14 (IntechOpen, 2020).

63. Gordon, J. K. & McKinlay, J. Physiological changes after brain stem death and management of the heart-beating donor. *Contin. Educ. Anaesth. Crit. Care Pain* **12**, 225–229 (2012).

64. van Leeuwen, L. L. *et al.* Proteomic analysis of machine perfusion solution from brain dead donor kidneys reveals that elevated complement, cytoskeleton and lipid metabolism proteins are associated with 1-year outcome. *Transpl. Int.* **34**, 1618–1629 (2021).

65. Westendorp, W. H., Leuvenink, H. G. & Ploeg, R. J. Brain death induced renal injury. *Curr. Opin. Organ Transplant.* **16**, 151 (2011).

66. Bera, K. D., Shah, A., English, M. R., Harvey, D. & Ploeg, R. J. Optimisation of the organ donor and effects on transplanted organs: a narrative review on current practice and future directions. *Anaesthesia* **75**, 1191–1204 (2020).

67. Nunez, M. *et al.* Diabetes insipidus in deceased donors and outcomes in kidney transplant recipients. *Am. J. Kidney Dis.* **84**, 129–132 (2024).

68. Cugini, D. *et al.* Inhibition of the chemokine receptor CXCR2 prevents kidney graft function deterioration due to ischemia/reperfusion. *Kidney Int.* **67**, 1753–1761 (2005).

69. Manara, A. R., Thomas, I. & Harding, R. A case for stopping the early withdrawal of life sustaining therapies in patients with devastating brain injuries. *J. Intensive Care Soc.* **17**, 295–301 (2016).

70. Manara, A. R. & Thomas, I. Current status of organ donation after brain death in the UK. *Anaesthesia* **75**, 1205–1214 (2020).

71. Prescott, J., Gardiner, D., Hogg, L. & Harvey, D. How the mode of organ donation affects family behaviour at the time of organ donation. *J. Intensive Care Soc.* **20**, 204–207 (2019).

72. Cooper, M. *et al.* Understanding Delayed Graft Function to Improve Organ Utilization and Patient Outcomes: Report of a Scientific Workshop Sponsored by the National Kidney Foundation. *Am. J. Kidney Dis.* (2023) doi:10.1053/j.ajkd.2023.08.018.

73. Smith, S. F., Hosgood, S. A. & Nicholson, M. L. Ischemia-reperfusion injury in renal transplantation: 3 key signaling pathways in tubular epithelial cells. *Kidney Int.* **95**, 50–56 (2019).

74. Li, C. *et al.* The emerging role of regulated cell death in ischemia and reperfusion-induced acute kidney injury: current evidence and future perspectives. *Cell Death Discovery* **10**, 1–10 (2024).

75. Watts, R. P., Thom, O. & Fraser, J. F. Inflammatory signalling associated with brain dead organ donation: from brain injury to brain stem death and posttransplant ischaemia reperfusion injury. *J. Transplant.* **2013**, 521369 (2013).

76. Kalogeris, T., Baines, C. P., Krenz, M. & Korthuis, R. J. Cell biology of ischemia/reperfusion injury. *Int. Rev. Cell Mol. Biol.* **298**, 229–317 (2012).

77. Saat, T. C. *et al.* A comparison of inflammatory, cytoprotective and injury gene expression profiles in kidneys from brain death and cardiac death donors. *Transplantation* **98**, 15–21 (2014).

78. Barreda Monteoliva, P., Redondo-Pachón, D., Miñambres García, E. & Rodrigo Calabia, E. Kidney transplant outcome of expanded criteria donors after circulatory death. *Nefrologia* **42**, 135–144 (2022).

79. Lomero, M. *et al.* Donation after circulatory death today: an updated overview of the European landscape. *Transpl. Int.* **33**, 76–88 (2020).

80. Jericho, B. G. Organ Donation After Circulatory Death: Ethical Issues and International Practices. *Anesthesia & Analgesia* **128**, 280 (2019).

81. Wu, D. A. & Oniscu, G. C. Piloting Uncontrolled DCD Organ Donation in the UK; Overview, Lessons and Future Steps. *Current Transplantation Reports* **9**, 250–256 (2022).

82. Smith, M., Dominguez-Gil, B., Greer, D. M., Manara, A. R. & Souter, M. J. Organ donation after circulatory death: current status and future potential. *Intensive Care Med.* **45**, 310–321 (2019).

83. Phillips, B. L. *et al.* Effect of delayed graft function on longer-term outcomes after kidney transplantation from donation after circulatory death donors in the United Kingdom: A national cohort study. *Am. J. Transplant* **21**, 3346–3355 (2021).

84. Schröppel, B. & Legendre, C. Delayed kidney graft function: from mechanism to translation. *Kidney Int.* **86**, 251–258 (2014).

85. Ponticelli, C., Reggiani, F. & Moroni, G. Delayed Graft Function in Kidney Transplant: Risk Factors, Consequences and Prevention Strategies. *J Pers Med* **12**, (2022).

86. Dumbill, R. *et al.* Transplant and Recipient Factors in Prediction of Kidney Transplant Outcomes: A UK-Wide Paired Analysis. *J. Clin. Med. Res.* **11**, (2022).

87. Tennankore, K. K., Kim, S. J., Alwayn, I. P. J. & Kiberd, B. A. Prolonged warm ischemia time is associated with graft failure and mortality after kidney transplantation. *Kidney Int.* **89**, 648–658 (2016).

88. Butala, N. M., Reese, P. P., Doshi, M. D. & Parikh, C. R. Is delayed graft function causally associated with long-term outcomes after kidney transplantation? Instrumental variable analysis. *Transplantation* **95**, 1008–1014 (2013).

89. de Kok, M. J. C. *et al.* Improving outcomes for donation after circulatory death kidney transplantation: Science of the times. *PLoS One* **15**, e0236662 (2020).

90. Brennan, C. *et al.* Impact of warm ischemia time on outcomes for kidneys donated after cardiac death Post-KAS. *Clin. Transplant.* **34**, e14040 (2020).

91. Heylen, L. *et al.* The duration of asystolic ischemia determines the risk of graft failure after circulatory-dead donor kidney transplantation: A Eurotransplant cohort study. *Am. J. Transplant* **18**, 881–889 (2018).

92. Franzin, R. *et al.* Inflammaging and complement system: A link between acute kidney injury and chronic graft damage. *Front. Immunol.* **11**, 734 (2020).

93. de Kok, M. J. *et al.* The neglectable impact of delayed graft function on long-term graft survival in kidneys donated after circulatory death associates with superior organ resilience. *Ann. Surg.* **270**, 877–883 (2019).

94. Schaapherder, A. *et al.* Equivalent Long-term Transplantation Outcomes for Kidneys Donated After Brain Death and Cardiac Death: Conclusions From a Nationwide Evaluation. *eClinicalMedicine* **4**, 25–31 (2018).

95. Zhang, R. *et al.* Assessment of biological organ age using molecular pathology in pre-transplant kidney biopsies. *Kidney Int.* (2024) doi:10.1016/j.kint.2024.03.028.

96. Lo Faro, M. L. *et al.* Kidney Tissue Proteome Profiles in Short Versus Long Duration of Delayed Graft Function - A Pilot Study in Donation After Circulatory Death Donors. *Kidney International Reports* (2024) doi:10.1016/j.ekir.2024.02.012.

97. Zwaini, Z. *et al.* Comparative Analysis of Risk Factors in Declined Kidneys from Donation after Brain Death and Circulatory Death. *Medicina* **56**, (2020).

98. Eleftheriadis, T., Pissas, G., Antoniadi, G., Liakopoulos, V. & Stefanidis, I. Cell Death Patterns Due to Warm Ischemia or Reperfusion in Renal Tubular Epithelial Cells Originating from Human, Mouse, or the Native Hibernator Hamster. *Biology* **7**, (2018).

99. Akalay, S. & Hosgood, S. A. How to Best Protect Kidneys for Transplantation-Mechanistic Target. *J. Clin. Med. Res.* **12**, (2023).

100. Summers, D. M. *et al.* Kidney donation after circulatory death (DCD): state of the art. *Kidney Int.* **88**, 241–249 (2015).

101. Sánchez-Cámara, S. *et al.* Critical warm ischemia time point for cardiac donation after circulatory death. *Am. J. Transplant* **22**, 1321–1328 (2022).

102. Pol, R. A. & Moers, C. Minimizing warm ischemic injury in the recipient: don't rush the anastomosis, but keep the kidney cool. *Kidney Int.* **90**, 226–227 (2016).

103. Urbanellis, P. *et al.* Prolonged warm ischemia time leads to severe renal dysfunction of donation-after-cardiac death kidney grafts. *Sci. Rep.* **11**, 1–11 (2021).

104. Phillips, B. *et al.* British Transplantation Society guidelines on abdominal organ transplantation from deceased donors after circulatory death. *Transplant. Rev.* 100801 (2023).

105. Coffey, J. C. *et al.* The influence of functional warm ischemia time on DCD liver transplant recipients' outcomes. *Clin. Transplant.* **31**, (2017).

106. Bruinsma, B. G. *et al.* Warm ischemic injury is reflected in the release of injury markers during cold preservation of the human liver. *PLoS One* **10**, e0123421 (2015).

107. Waikar, S. S. & Bonventre, J. V. Creatinine kinetics and the definition of acute kidney injury. *J. Am. Soc. Nephrol.* **20**, 672–679 (2009).

108. Chen, Y.-L., Li, H.-K., Wang, L., Chen, J.-W. & Ma, X. No safe renal warm ischemia time-The molecular network characteristics and pathological features of mild to severe ischemia reperfusion kidney injury. *Front Mol Biosci* **9**, 1006917 (2022).

109. van Leeuwen, L. Molecular signatures underlying kidney transplantation: towards a tailored treatment. (2022) doi:10.33612/diss.248377050.

110. Tang, W. & Wei, Q. The metabolic pathway regulation in kidney injury and repair. *Front. Physiol.* **14**, (2024).

111. Szeto, H. H., Liu, S., Soong, Y. & Birk, A. V. Improving mitochondrial bioenergetics under ischemic conditions increases warm ischemia tolerance in the kidney. *Am. J. Physiol. Renal Physiol.* **308**, F11-21 (2015).

112. Santos Dias, F., Metelo Coimbra, C. & Roncon-Albuquerque, R., Jr. Renal Warm Ischemia in Organ Donors After Circulatory Death. *Exp. Clin. Transplant.* **19**, 179–189 (2021).

113. Akhtar, M. Z., Sutherland, A. I., Huang, H., Ploeg, R. J. & Pugh, C. W. The role of hypoxia-inducible factors in organ donation and transplantation: the current perspective and future opportunities. *Am. J. Transplant* **14**, 1481–1487 (2014).

114. Baan, C. *et al.* Living kidney donors and hypoxia-inducible factor-1alpha. *Transplantation* **75**, 570–571 (2003).

115. Sethi, K., Rao, K., Bolton, D., Patel, O. & Ischia, J. Targeting HIF-1*α* to Prevent Renal Ischemia-Reperfusion Injury: Does It Work? *Int. J. Cell Biol.* **2018**, (2018).

116. Maxwell, P. H., Pugh, C. W. & Ratcliffe, P. J. Inducible operation of the erythropoietin 3' enhancer in multiple cell lines: evidence for a widespread oxygen-sensing mechanism. *Proc. Natl. Acad. Sci. U. S. A.* **90**, 2423–2427 (1993).

117. Moroz, E. *et al.* Real-time imaging of HIF-1alpha stabilization and degradation. *PLoS One* **4**, e5077 (2009).

118. Jaakkola, P. *et al.* Targeting of HIF-alpha to the von Hippel-Lindau ubiquitylation complex by O2-regulated prolyl hydroxylation. *Science* **292**, 468–472 (2001).

119. Maxwell, P. H. *et al.* The tumour suppressor protein VHL targets hypoxia-inducible factors for oxygen-dependent proteolysis. *Nature* **399**, 271–275 (1999).

120. Yasuda, M., Hatanaka, T., Shirato, H. & Nishioka, T. Cell type-specific reciprocal regulation of HIF1A gene expression is dependent on 5'- and 3'-UTRs. *Biochem. Biophys. Res. Commun.* **447**, 638–643 (2014).

121. Martinez, C.-A., Bal, N., Cistulli, P. A. & Cook, K. M. Intermittent hypoxia enhances the expression of HIF1A by increasing the quantity and catalytic activity of KDM4A-C and demethylating H3K9me3 at the HIF1A locus. *bioRxiv* 2021.07.25.453726 (2021) doi:10.1101/2021.07.25.453726.

122. Jaśkiewicz, M. *et al.* The transition from HIF-1 to HIF-2 during prolonged hypoxia results from reactivation of PHDs and HIF1A mRNA instability. *Cell. Mol. Biol. Lett.* **27**, 109 (2022).

123. Wang, B. *et al.* Hypoxia and chronic kidney disease. *EBioMedicine* **77**, 103942 (2022).

124. Ajouaou, Y. *et al.* The oxygen sensor prolyl hydroxylase domain 2 regulates the in vivo suppressive capacity of regulatory T cells. *Elife* **11**, e70555 (2022).

125. Rinschen, M. M. & Saez-Rodriguez, J. The tissue proteome in the multi-omic landscape of kidney disease. *Nat. Rev. Nephrol.* **17**, 205–219 (2021).

126. Tojo, A. The role of the kidney in protein metabolism: the capacity of tubular lysosomal proteolysis in nephrotic syndrome. *Kidney Int.* **84**, 861–863 (2013).

127. Grozdanić, M., Vidmar, R., Vizovišek, M. & Fonović, M. Degradomics in Biomarker Discovery. *Proteomics Clin. Appl.* **13**, e1800138 (2019).

128. López-Otín, C. & Bond, J. S. Proteases: multifunctional enzymes in life and disease. *J. Biol. Chem.* **283**, 30433–30437 (2008).

129. Overall, C. M. A Better Understanding of Protease Degradomics. *Journal of Proteomics & Bioinformatics* (2023) doi:10.35248/0974-276X.23.16.640.

130. Hipp, M. S., Kasturi, P. & Hartl, F. U. The proteostasis network and its decline in ageing. *Nat. Rev. Mol. Cell Biol.* **20**, 421–435 (2019).

131. Li, J. *et al.* The plasma degradome reflects later development of NASH fibrosis after liver transplant. *Sci. Rep.* **13**, 1–15 (2023).

132. Dallas, D. C. *et al.* Current peptidomics: applications, purification, identification, quantification, and functional analysis. *Proteomics* **15**, 1026–1038 (2015).

133. Gao, Q.-F., Zhang, X.-H., Yuan, F.-L., Zhao, M.-D. & Li, X. Recombinant human endostatin inhibits TNF-alpha-induced receptor activator of NF-κB ligand expression in fibroblast-like synoviocytes in mice with adjuvant arthritis. *Cell Biol. Int.* **40**, 1340–1348 (2016).

134. Digtyar, A. V., Pozdnyakova, N. V., Feldman, N. B., Lutsenko, S. V. & Severin, S. E. Endostatin: current concepts about its biological role and mechanisms of action. *Biochemistry* **72**, 235–246 (2007).

135. Zhao, H. *et al.* Matrix metalloproteinases contribute to kidney fibrosis in chronic kidney diseases. *World J Nephrol* **2**, 84–89 (2013).

136. Shechter, P., Boner, G. & Rabkin, R. Tubular cell protein degradation in early diabetic renal hypertrophy. *J. Am. Soc. Nephrol.* **4**, 1582 (1994).

137. Cavallo-Medved, D., Moin, K. & Sloane, B. Cathepsin B: Basis Sequence: Mouse. *AFCS Nat Mol Pages* **2011**, (2011).

138. Otlewski, J., Jelen, F., Zakrzewska, M. & Oleksy, A. The many faces of protease-protein inhibitor interaction. *EMBO J.* **24**, 1303–1310 (2005).

139. Zhong, G., Chang, X., Xie, W. & Zhou, X. Targeted protein degradation: advances in drug discovery and clinical practice. *Signal Transduct. Target. Ther.* **9**, 308 (2024).

140. Craik, C. S., Page, M. J. & Madison, E. L. Proteases as therapeutics. *Biochem. J.* **435**, 1–16 (2011).

141. Demir, F. *et al.* Proteolysis and inflammation of the kidney glomerulus. *Cell Tissue Res.* **385**, 489–500 (2021).

142. Fakhouri, F., Schwotzer, N., Golshayan, D. & Frémeaux-Bacchi, V. The rational use of complement inhibitors in kidney diseases. *Kidney Int. Rep.* **7**, 1165–1178 (2022).

143. Al-Amrani, S., Al-Jabri, Z., Al-Zaabi, A., Alshekaili, J. & Al-Khabori, M. Proteomics: Concepts and applications in human medicine. *World J. Biol. Chem.* **12**, 57–69 (2021).

144. Cui, M., Cheng, C. & Zhang, L. High-throughput proteomics: a methodological mini-review. *Lab. Invest.* **102**, 1170–1181 (2022).

145. Hellinger, R. *et al.* Peptidomics. *Nat Rev Methods Primers* **3**, (2023).

146. Weng, S. S. H. *et al.* Sensitive Determination of Proteolytic Proteoforms in Limited Microscale Proteome Samples. *Mol. Cell. Proteomics* **18**, 2335–2347 (2019).

147. Di Meo, A., Pasic, M. D. & Yousef, G. M. Proteomics and peptidomics: moving toward precision medicine in urological malignancies. *Oncotarget* **7**, 52460–52474 (2016).

148. Rinschen, M. M., Huesgen, P. F. & Koch, R. E. The podocyte protease web: uncovering the gatekeepers of glomerular disease. *Am. J. Physiol. Renal Physiol.* **315**, F1812–F1816 (2018).

149. NHS Blood and Transplant Annual Report on Kidney Transplantation, report for 2023/2024. Preprint at https://www.odt.nhs.uk/statistics-and-reports/organ-specific-reports/ (2024).

150. Saleem, M. A. *et al.* A conditionally immortalized human podocyte cell line demonstrating nephrin and podocin expression. *J. Am. Soc. Nephrol.* **13**, 630–638 (2002).

151. Ni, L., Saleem, M. & Mathieson, P. W. Podocyte culture: tricks of the trade. *Nephrology* **17**, 525–531 (2012).

152. Wilmer, M. J. *et al.* Novel conditionally immortalized human proximal tubule cell line expressing functional influx and efflux transporters. *Cell Tissue Res.* **339**, 449–457 (2010).

153. Mirshekar-Syahkal, B. *et al.* Local Expansion of Donation After Circulatory Death Kidney Transplant Activity Improves Waitlisted Outcomes and Addresses Inequities of Access to Transplantation. *Am. J. Transplant* **17**, 390–400 (2017).

154. Rijkse, E. *et al.* Implementation of donation after circulatory death kidney transplantation can safely enlarge the donor pool: A systematic review and meta-analysis. *Int. J. Surg.* **92**, 106021 (2021).

155. McFarlane, L., Nelson, P., Dugbartey, G. J. & Sener, A. Pre-Treatment of Transplant Donors with Hydrogen Sulfide to Protect against Warm and Cold Ischemia-Reperfusion Injury in Kidney and Other Transplantable Solid Organs. *Int. J. Mol. Sci.* **24**, (2023).

156. Yin, M. *et al.* Different patterns of renal cell killing after warm and cold ischemia. *Ren. Fail.* **24**, 147–163 (2002).

157. van Smaalen, T. C. *et al.* Presence of Cytotoxic Extracellular Histones in Machine Perfusate of Donation After Circulatory Death Kidneys. *Transplantation* **101**, e93–e101 (2017).

158. van Smaalen, T. C. *et al.* Extracellular histone release by renal cells after warm and cold ischemic kidney injury: Studies in an ex-vivo porcine kidney perfusion model. *PLoS One* **18**, e0279944 (2023).

159. Malek, M. & Nematbakhsh, M. Renal ischemia/reperfusion injury; from pathophysiology to treatment. *J Renal Inj Prev* **4**, 20–27 (2015).

160. van Leeuwen, L., Venema, L. H., Heilig, R., Leuvenink, H. G. D. & Kessler, B. M. Doxycycline Alters the Porcine Renal Proteome and Degradome during Hypothermic Machine Perfusion. *Curr. Issues Mol. Biol.* **44**, 559–577 (2022).

161. Hong, S.-S., Lee, H. & Kim, K.-W. HIF-1alpha: a valid therapeutic target for tumor therapy. *Cancer Res. Treat.* **36**, 343–353 (2004).

162. Pang, L. *et al.* Hypoxia-driven protease legumain promotes immunosuppression in glioblastoma. *Cell Rep Med* 101238 (2023).

163. Bonanni, A. *et al.* Protein-energy wasting and mortality in chronic kidney disease. *Int. J. Environ. Res. Public Health* **8**, 1631–1654 (2011).

164. Haack, A. M., Overall, C. M. & Auf dem Keller, U. Degradomics technologies in matrisome exploration. *Matrix Biol.* **114**, 1–17 (2022).

165. Rawlings, N. D. *et al.* The MEROPS database of proteolytic enzymes, their substrates and inhibitors in 2017 and a comparison with peptidases in the PANTHER database. *Nucleic Acids Res.* **46**, D624–D632 (2018).

166. Bunkenborg, J., Espadas, G. & Molina, H. Cutting Edge Proteomics: Benchmarking of Six Commercial Trypsins. *J. Proteome Res.* **12**, 3631–3641 (2013).

167. Walmsley, S. J. *et al.* Comprehensive analysis of protein digestion using six trypsins reveals the origin of trypsin as a significant source of variability in proteomics. *J. Proteome Res.* **12**, 5666–5680 (2013).

168. Soh, W. T. *et al.* ExteNDing Proteome Coverage with Legumain as a Highly Specific Digestion Protease. *Anal. Chem.* **92**, 2961–2971 (2020).

169. Nankivell, B. J., Nankivell, L. F. J., Elder, G. J. & Gruenewald, S. M. How unmeasured muscle mass affects estimated GFR and diagnostic inaccuracy. *EClinicalMedicine* **29–30**, 100662 (2020).

170. Steichen, C., Hervé, C., Hauet, T. & Bourmeyster, N. Rho GTPases in kidney physiology and diseases. *Small GTPases* **13**, 141–161 (2022).

171. Cao, Y. *et al.* A systematic pan-cancer analysis of SPATS2L, a potential new immunological and prognostic biomarker. *Research Square* (2023) doi:10.21203/rs.3.rs-2494003/v1.

172. Li, F. *et al.* Spermatogenesis associated serine rich 2 like plays a prognostic factor and therapeutic target in acute myeloid leukemia by regulating the JAK2/STAT3/STAT5 axis. *J. Transl. Med.* **21**, 115 (2023).

173. Bushau-Sprinkle, A. M. & Lederer, E. D. New roles of the Na+/H+ exchange regulatory factor 1 scaffolding protein: a review. *Am. J. Physiol. Renal Physiol.* **318**, F804–F808 (2020).

174. Bushau-Sprinkle, A. *et al.* NHERF1 Loss Upregulates Enzymes of the Pentose Phosphate Pathway in Kidney Cortex. *Antioxidants (Basel)* **9**, (2020).

175. Weinman, E. J. *et al.* Longitudinal study of urinary excretion of phosphate, calcium, and uric acid in mutant NHERF-1 null mice. *Am. J. Physiol. Renal Physiol.* **290**, F838-43 (2006).

176. Kha, M. *et al.* Injured proximal tubular epithelial cells lose hepatocyte nuclear factor 4α expression crucial for brush border formation and transport. *Am. J. Pathol.* (2025) doi:10.1016/j.ajpath.2025.01.011.

177. Khundmiri, S. J. *et al.* Parathyroid hormone regulation of NA+,K+-ATPase requires the PDZ 1 domain of sodium hydrogen exchanger regulatory factor-1 in opossum kidney cells. *J. Am. Soc. Nephrol.* **16**, 2598–2607 (2005).

178. Martino, F. *et al.* The mechanical regulation of RNA binding protein hnRNPC in the failing heart. *Sci. Transl. Med.* **14**, eabo5715 (2022).

179. Wu, J. *et al.* Essential m6A Methylation Regulator HNRNPC Serves as a Targetable Biomarker for Papillary Renal Cell Carcinoma. *J. Oncol.* **2022**, 9411692 (2022).

180. Hotait, Z. S., Lo Cascio, J. N., Choos, E. N. D. & Shepard, B. D. The sugar daddy: the role of the renal proximal tubule in glucose homeostasis. *American Journal of Physiology-Cell Physiology* **323**, C791–C803 (2022).

181. Zhang, M. *et al.* Urinary FBP1 as a novel biomarker for the diagnosis and progression of diabetic nephropathy. *Research Square* (2023) doi:10.21203/rs.3.rs-2438025/v1.

182. Kotanko, P., Margreiter, R. & Pfaller, W. Graft ischemia correlates with urinary excretion of the proximal marker enzyme fructose-1,6-bisphosphatase in human kidney transplantation. *Nephron* **77**, 62–67 (1997).

183. Kepka, A. *et al.* Urinary fructose-1,6-bisphosphatase activity as a marker of the damage to the renal proximal tubules in children with idiopathic nephrotic syndrome. *Clin. Chem. Lab. Med.* **46**, 831–835 (2008).

184. Kepka, A., Szajda, S. D. & Zwierz, K. [Fructose-1,6-bisphosphatase--marker of damage to proximal renal tubules]. *Pol. Merkur. Lekarski* **24**, 125–130 (2008).

185. Legouis, D. *et al.* Altered proximal tubular cell glucose metabolism during acute kidney injury is associated with mortality. *Nat Metab* **2**, 732–743 (2020).

186. Li, B. *et al.* Fructose-1,6-bisphosphatase opposes renal carcinoma progression. *Nature* **513**, 251–255 (2014).

187. Verissimo, T. *et al.* Decreased Renal Gluconeogenesis Is a Hallmark of Chronic Kidney Disease. *J. Am. Soc. Nephrol.* **33**, 810–827 (2022).

188. Dalga, D., Verissimo, T. & de Seigneux, S. Gluconeogenesis in the kidney: in health and in chronic kidney disease. *Clin. Kidney J.* **16**, 1249–1257 (2023).

189. Ando, Y. *et al.* Enhanced interstitial expression of caldesmon in IgA nephropathy and its suppression by glucocorticoid-heparin therapy. *Nephrol. Dial. Transplant* **14**, 1408–1417 (1999).

190. Patel, S. J. *et al.* The iron chaperone and nucleic acid–binding activities of poly(rC)-binding protein 1 are separable and independently essential. *Proceedings of the National Academy of Sciences* **118**, e2104666118 (2021).

191. Nandal, A. *et al.* Activation of the HIF prolyl hydroxylase by the iron chaperones PCBP1 and PCBP2. *Cell Metab.* **14**, 647–657 (2011).

192. Wojtaszek, E., Glogowski, T. & Malyszko, J. Iron and chronic kidney disease: Still a challenge. *Front. Med. (Lausanne)* **7**, 565135 (2020).

193. Taylor, C. T. & Scholz, C. C. The effect of HIF on metabolism and immunity. *Nat. Rev. Nephrol.* **18**, 573–587 (2022).

194. Sunden, S. L., Renduchintala, M. S., Park, E. I., Miklasz, S. D. & Garrow, T. A. Betaine-homocysteine methyltransferase expression in porcine and human tissues and chromosomal localization of the human gene. *Arch. Biochem. Biophys.* **345**, 171–174 (1997).

195. Delgado-Reyes, C. V. & Garrow, T. A. High sodium chloride intake decreases betaine-homocysteine S-methyltransferase expression in guinea pig liver and kidney. *American Journal of Physiology-Regulatory, Integrative and Comparative Physiology* **288**, R182–R187 (2005).

196. Mcgregor, D. O. *et al.* Betaine supplementation decreases post-methionine hyperhomocysteinemia in chronic renal failure. *Kidney Int.* **61**, 1040–1046 (2002).

197. Shibukawa, Y. *et al.* Calponin 3 regulates actin cytoskeleton rearrangement in trophoblastic cell fusion. *Mol. Biol. Cell* **21**, 3973–3984 (2010).

198. Yuasa, T., Yano, R., Izawa, T., Kuwamura, M. & Yamate, J. Calponin expression in renal tubulointerstitial fibrosis induced in rats by Cisplatin. *J. Toxicol. Pathol.* **27**, 97–103 (2014).

199. Ahn, S.-Y., Kim, Y., Kim, S. T., Swat, W. & Miner, J. H. Scaffolding proteins DLG1 and CASK cooperate to maintain the nephron progenitor population during kidney development. *J. Am. Soc. Nephrol.* **24**, 1127–1138 (2013).

200. Jiang, Y. *et al.* LAD1 promotes malignant progression by diminishing ubiquitin-dependent degradation of vimentin in gastric cancer. *J. Transl. Med.* **21**, 632 (2023).

201. Gharib, S. A. *et al.* Transcriptional landscape of glomerular parietal epithelial cells. *PLoS One* **9**, e105289 (2014).

202. Edwards, J. C. What's a CLIC doing in the podocyte? *Kidney international* vol. 78 831–833 (2010).

203. Chou, S.-Y. *et al.* CLIC4 regulates apical exocytosis and renal tube luminogenesis through retromer- and actin-mediated endocytic trafficking. *Nat. Commun.* **7**, 10412 (2016).

204. Suh, K. S., Mutoh, M., Gerdes, M. & Yuspa, S. H. CLIC4, an Intracellular Chloride Channel Protein, Is a Novel Molecular Target for Cancer Therapy. *J. Investig. Dermatol. Symp. Proc.* **10**, 105–109 (2005).

205. Snider, N. T. Kidney keratins: cytoskeletal stress responders with biomarker potential. *Kidney Int.* **89**, 738–740 (2016).

206. Djudjaj, S. *et al.* Keratins are novel markers of renal epithelial cell injury. *Kidney Int.* **89**, 792–808 (2016).

207. Ronsin, C., Benard, L., Mourtada, A., Perrin, F. & Boukerroucha, Z. Acute tubulointerstitial nephritis revealing VEXAS syndrome. *Kidney Int.* **101**, 1295–1297 (2022).

208. Baumgartner, M. R. *et al.* The molecular basis of human 3-methylcrotonyl-CoA carboxylase deficiency. *J. Clin. Invest.* **107**, 495–504 (2001).

209. Lee, S.-K., Son, L. T., Choi, H.-J. & Ahnn, J. Dicarbonyl/l-xylulose reductase (DCXR): The multifunctional pentosuria enzyme. *Int. J. Biochem. Cell Biol.* **45**, 2563–2567 (2013).

210. Jin, Y. *et al.* DCXR promotes cell proliferation by promoting the activity of aerobic glycolysis in breast cancer. *Mol. Med. Rep.* **27**, 1–10 (2023).

211. Lu, H., Kapur, G., Mattoo, T. K. & Lyman, W. D. Hypoxia decreases podocyte expression of slit diaphragm proteins. *Int. J. Nephrol. Renovasc. Dis.* **5**, 101–107 (2012).

212. Hu, S. *et al.* Crosstalk among podocytes, glomerular endothelial cells and mesangial cells in diabetic kidney disease: an updated review. *Cell Commun. Signal.* **22**, 136 (2024).

213. Nezu, M., Suzuki, N. & Yamamoto, M. Targeting the KEAP1-NRF2 System to Prevent Kidney Disease Progression. *Am. J. Nephrol.* **45**, 473–483 (2017).

214. Dinkova-Kostova, A. T. & Copple, I. M. Advances and challenges in therapeutic targeting of NRF2. *Trends Pharmacol. Sci.* **44**, 137–149 (2023).

215. Nezu, M. & Suzuki, N. Roles of Nrf2 in Protecting the Kidney from Oxidative Damage. *Int. J. Mol. Sci.* **21**, (2020).

216. Rush, B. M. *et al.* Genetic or pharmacologic Nrf2 activation increases proteinuria in chronic kidney disease in mice. *Kidney Int.* **99**, 102–116 (2021).

217. Kanda, H. & Yamawaki, K. Bardoxolone methyl: drug development for diabetic kidney disease. *Clin. Exp. Nephrol.* **24**, 857–864 (2020).

218. Nezu, M. *et al.* Transcription factor Nrf2 hyperactivation in early-phase renal ischemia-reperfusion injury prevents tubular damage progression. *Kidney Int.* **91**, 387–401 (2017).

219. Ma, S., Qiu, Y. & Zhang, C. Cytoskeleton Rearrangement in Podocytopathies: An Update. *Int. J. Mol. Sci.* **25**, (2024).

220. Prakash, J. *et al.* Inhibition of renal rho kinase attenuates ischemia/reperfusion-induced injury. *J. Am. Soc. Nephrol.* **19**, 2086–2097 (2008).

221. Gopalakrishnan, S., Raman, N., Atkinson, S. J. & Marrs, J. A. Rho GTPase signaling regulates tight junction assembly and protects tight junctions during ATP depletion. *Am. J. Physiol.* **275**, C798-809 (1998).

222. Borza, C. M., Chen, X., Zent, R. & Pozzi, A. Cell Receptor-Basement Membrane Interactions in Health and Disease: A Kidney-Centric View. *Curr. Top. Membr.* **76**, 231–253 (2015).

223. Fernandez-de-Cossio-Diaz, J. & Vazquez, A. A physical model of cell metabolism. *Sci. Rep.* **8**, 1–13 (2018).

224. Deshpande, O. A. & Mohiuddin, S. S. *Biochemistry, Oxidative Phosphorylation*. (StatPearls Publishing, 2022).

225. Chaudhry, R. & Varacallo, M. *Biochemistry, Glycolysis*. (StatPearls Publishing, 2023).

226. Legouis, D., Faivre, A., Cippà, P. E. & de Seigneux, S. Renal gluconeogenesis: an underestimated role of the kidney in systemic glucose metabolism. *Nephrol. Dial. Transplant* **37**, 1417–1425 (2022).

227. Tian, Z. & Liang, M. Renal metabolism and hypertension. *Nat. Commun.* **12**, 1–12 (2021).

228. Brinkkoetter, P. T. *et al.* Anaerobic Glycolysis Maintains the Glomerular Filtration Barrier Independent of Mitochondrial Metabolism and Dynamics. *Cell Rep.* **27**, 1551-1566.e5 (2019).

229. Schaub, J. A., Venkatachalam, M. A. & Weinberg, J. M. Proximal Tubular Oxidative Metabolism in Acute Kidney Injury and the Transition to CKD. *Kidney360* **2**, 355 (2021).

230. Wang, G. *et al.* Analyzing cell-type-specific dynamics of metabolism in kidney repair. *Nat Metab* **4**, 1109–1118 (2022).

231. Huskisson, E., Maggini, S. & Ruf, M. The Role of Vitamins and Minerals in Energy Metabolism and Well-Being. *J. Int. Med. Res.* **35**, 277–289 (2007).

232. Zeisel, S. H., Klatt, K. C. & Caudill, M. A. Choline. *Adv. Nutr.* **9**, 58–60 (2018).

233. Long, Y. & Nie, J. Homocysteine in Renal Injury. *Kidney Dis (Basel)* **2**, 80–87 (2016).

234. Martínez, Y. *et al.* The role of methionine on metabolism, oxidative stress, and diseases. *Amino Acids* **49**, 2091–2098 (2017).

235. Poreba, M. Recent advances in the development of legumain-selective chemical probes and peptide prodrugs. *Biol. Chem.* **400**, 1529–1550 (2019).

236. Dall, E. & Brandstetter, H. Structure and function of legumain in health and disease. *Biochimie* **122**, 126–150 (2016).

237. Solberg, R. *et al.* The Mammalian Cysteine Protease Legumain in Health and Disease. *Int. J. Mol. Sci.* **23**, (2022).

238. Hay, Z. L. Z. & Slansky, J. E. Granzymes: The Molecular Executors of Immune-Mediated Cytotoxicity. *Int. J. Mol. Sci.* **23**, (2022).

239. Souza-Fonseca-Guimaraes, F. *et al.* Granzyme M has a critical role in providing innate immune protection in ulcerative colitis. *Cell Death Dis.* **7**, e2302 (2016).

240. Saudenova, M. *et al.* Behind every smile there's teeth: Cathepsin B's function in health and disease with a kidney view. *Biochimica et Biophysica Acta (BBA) - Molecular Cell Research* **1869**, 119190 (2022).

241. Yoon, M. C. *et al.* Distinct Cleavage Properties of Cathepsin B Compared to Cysteine Cathepsins Enable the Design and Validation of a Specific Substrate for Cathepsin B over a Broad pH Range. *Biochemistry* **62**, 2289–2300 (2023).

242. Makita, Y. Effect of high glucose on the expression of cathepsin B, L and cystatin β in cultured rat mesangial cells. *Juntendo Med. J.* **42**, 82–91 (1996).

243. Wyczalkowska-Tomasik, A., Bartlomiejczyk, I., Gornicka, B. & Paczek, L. Strong association between fibronectin accumulation and lowered cathepsin B activity in glomeruli of diabetic rats. *J. Physiol. Pharmacol.* **63**, 525–530 (2012).

244. Tan, R. J. & Liu, Y. Matrix metalloproteinases in kidney homeostasis and diseases. *Am. J. Physiol. Renal Physiol.* **302**, F1351-61 (2012).

245. Lim, A. I. *et al.* Distinct role of matrix metalloproteinase-3 in kidney injury molecule-1 shedding by kidney proximal tubular epithelial cells. *Int. J. Biochem. Cell Biol.* **44**, 1040–1050 (2012).

246. Fu, Y. *et al.* Clinical value of serum MMP-3 in chronic kidney disease. *Clin. Chim. Acta* **553**, 117725 (2024).

247. Zakiyanov, O., Kalousová, M., Zima, T. & Tesař, V. Matrix Metalloproteinases in Renal Diseases: A Critical Appraisal. *Kidney Blood Press. Res.* **44**, 298–330 (2019).

248. Solé-Domènech, S. *et al.* Lysosomal enzyme tripeptidyl peptidase 1 destabilizes fibrillar Aβ by multiple endoproteolytic cleavages within the β-sheet domain. *Proceedings of the National Academy of Sciences* **115**, 1493–1498 (2018).

249. Kida, E. *et al.* Distribution of Tripeptidyl Peptidase I in Human Tissues Under Normal and Pathological Conditions. *J. Neuropathol. Exp. Neurol.* **60**, 280–292 (2001).

250. Clotet-Freixas, S. *et al.* Proteomics Reveals Extracellular Matrix Injury in the Glomeruli and Tubulointerstitium of Kidney Allografts with Early Antibody-Mediated Rejection. *bioRxiv* 2020.03.03.975672 (2020) doi:10.1101/2020.03.03.975672.

251. Li, M. T. *et al.* Effects of Delayed Graft Function on Transplant Outcomes: A Meta-analysis. doi:10.1097/TXD.0000000000001433.

252. Kinney, C. J. & Bloch, R. J. μ-Crystallin: A thyroid hormone binding protein. *Endocr. Regul.* **55**, 89–102 (2021).

253. Al-Kafaji, G. & Malik, A. N. Hyperglycemia induces elevated expression of thyroid hormone binding protein in vivo in kidney and heart and in vitro in mesangial cells. *Biochem. Biophys. Res. Commun.* **391**, 1585–1591 (2010).

254. Cocchiaro, P. *et al.* The Multifaceted Role of the Lysosomal Protease Cathepsins in Kidney Disease. *Front Cell Dev Biol* **5**, 114 (2017).

255. Cocchiaro, P. *et al.* Lysosomal protease cathepsin D; a new driver of apoptosis during acute kidney injury. *Sci. Rep.* **6**, 27112 (2016).

256. Fox, C. *et al.* Inhibition of lysosomal protease cathepsin D reduces renal fibrosis in murine chronic kidney disease. *Sci. Rep.* **6**, 1–15 (2016).

257. Muñoz-Sánchez, J. & Chánez-Cárdenas, M. E. The use of cobalt chloride as a chemical hypoxia model. *J. Appl. Toxicol.* **39**, 556–570 (2019).

258. Fu, Q., Colgan, S. P. & Shelley, C. S. Hypoxia: The force that drives chronic kidney disease. *Clin. Med. Res.* **14**, 15–39 (2016).

259. Balzer, M. S., Rohacs, T. & Susztak, K. How Many Cell Types Are in the Kidney and What Do They Do? *Annu. Rev. Physiol.* **84**, 507–531 (2022).

260. Pavenstädt, H. Roles of the podocyte in glomerular function. *Am. J. Physiol. Renal Physiol.* **278**, F173-9 (2000).

261. Ozawa, S. *et al.* Glycolysis, but not Mitochondria, responsible for intracellular ATP distribution in cortical area of podocytes. *Sci. Rep.* **5**, 1–15 (2015).

262. Nakuluri, K. *et al.* Hypoxia induces ZEB2 in podocytes: Implications in the pathogenesis of proteinuria. *J. Cell. Physiol.* **234**, 6503–6518 (2019).

263. Nakuluri, K. *et al.* Cerebral ischemia induces TRPC6 via HIF1α/ZEB2 axis in the glomerular podocytes and contributes to proteinuria. *Sci. Rep.* **9**, 1–13 (2019).

264. Nakhoul, N. & Batuman, V. Role of proximal tubules in the pathogenesis of kidney disease. *Contrib. Nephrol.* **169**, 37–50 (2011).

265. Wang, D., Sant, S., Lawless, C. & Ferrell, N. A kidney proximal tubule model to evaluate effects of basement membrane stiffening on renal tubular epithelial cells. *Integr. Biol.* (2022) doi:10.1093/intbio/zyac016.

266. Shu, S. *et al.* Hypoxia and Hypoxia-Inducible Factors in Kidney Injury and Repair. *Cells* **8**, (2019).

267. Hall, A. M. & de Seigneux, S. Metabolic mechanisms of acute proximal tubular injury. *Pflugers Arch.* **474**, 813–827 (2022).

268. Darshi, M. *et al.* Crabtree effect in kidney proximal tubule cells via late-stage glycolytic intermediates. *iScience* **26**, 106462 (2023).

269. Moniz, I., Ramalho-Santos, J. & Branco, A. F. Differential Oxygen Exposure Modulates Mesenchymal Stem Cell Metabolism and Proliferation through mTOR Signaling. *Int. J. Mol. Sci.* **23**, (2022).

270. Rana, N. K., Singh, P. & Koch, B. CoCl2 simulated hypoxia induce cell proliferation and alter the expression pattern of hypoxia associated genes involved in angiogenesis and apoptosis. *Biol. Res.* **52**, 12 (2019).

271. Downes, N. L., Laham-Karam, N., Kaikkonen, M. U. & Ylä-Herttuala, S. Differential but Complementary HIF1α and HIF2α Transcriptional Regulation. *Mol. Ther.* **26**, 1735–1745 (2018).

272. Fujita, N. *et al.* Expression of prolyl hydroxylases (PHDs) is selectively controlled by HIF-1 and HIF-2 proteins in nucleus pulposus cells of the intervertebral disc: distinct roles of PHD2 and PHD3 proteins in controlling HIF-1α activity in hypoxia. *J. Biol. Chem.* **287**, 16975–16986 (2012).

273. Semba, H. *et al.* HIF-1α-PDK1 axis-induced active glycolysis plays an essential role in macrophage migratory capacity. *Nat. Commun.* **7**, 11635 (2016).

274. Lee, H.-C., Lin, S.-C., Wu, M.-H. & Tsai, S.-J. Induction of Pyruvate Dehydrogenase Kinase 1 by Hypoxia Alters Cellular Metabolism and Inhibits Apoptosis in Endometriotic Stromal Cells. *Reprod. Sci.* **26**, 734–744 (2019).

275. Finck, B. N. & Kelly, D. P. PGC-1 coactivators: inducible regulators of energy metabolism in health and disease. *J. Clin. Invest.* **116**, 615–622 (2006).

276. Zhu, L. *et al.* Hypoxia induces PGC-1α expression and mitochondrial biogenesis in the myocardium of TOF patients. *Cell Res.* **20**, 676–687 (2010).

277. Eskandari, E. & Eaves, C. J. Paradoxical roles of caspase-3 in regulating cell survival, proliferation, and tumorigenesis. *J. Cell Biol.* **221**, (2022).

278. Yang, B. *et al.* Caspase-3 and apoptosis in experimental chronic renal scarring. *Kidney Int.* **60**, 1765–1776 (2001).

279. Dalton, C. J. & Lemmon, C. A. Fibronectin: Molecular Structure, Fibrillar Structure and Mechanochemical Signaling. *Cells* **10**, (2021).

280. Crabtree, H. G. Observations on the carbohydrate metabolism of tumours. *Biochem. J.* **23**, 536–545 (1929).

281. de Kok, M. J. C. *et al.* Circumventing the Crabtree effect in cell culture: A systematic review. *Mitochondrion* **59**, 83–95 (2021).

282. Foresto-Neto, O., da Silva, A. R. P. A., Cipelli, M., Santana-Novelli, F. P. R. & Camara, N. O. S. The impact of hypoxia-inducible factors in the pathogenesis of kidney diseases: a link through cell metabolism. *Kidney Res Clin Pract* **42**, 561–578 (2023).

283. Wei, X., Hou, Y., Long, M., Jiang, L. & Du, Y. Molecular mechanisms underlying the role of hypoxia-inducible factor-1 α in metabolic reprogramming in renal fibrosis. *Front. Endocrinol.* **13**, (2022).

284. Haase, V. H. Hypoxia-inducible factors in the kidney. *Am. J. Physiol. Renal Physiol.* **291**, F271-81 (2006).

285. Kapitsinou, P. P. & Haase, V. H. Molecular mechanisms of ischemic preconditioning in the kidney. *Am. J. Physiol. Renal Physiol.* **309**, F821-34 (2015).

286. Faivre, A. *et al.* Evolution of hypoxia and hypoxia-inducible factor asparaginyl hydroxylase regulation in chronic kidney disease. *Nephrol. Dial. Transplant* **38**, 2276–2288 (2023).

287. Conde, E. *et al.* Hypoxia inducible factor 1-alpha (HIF-1 alpha) is induced during reperfusion after renal ischemia and is critical for proximal tubule cell survival. *PLoS One* **7**, e33258 (2012).

288. Uchida, T. *et al.* Prolonged Hypoxia Differentially Regulates Hypoxia-inducible Factor (HIF)-1α and HIF-2α Expression in Lung Epithelial Cells: IMPLICATION OF NATURAL ANTISENSE HIF-1α*. *J. Biol. Chem.* **279**, 14871–14878 (2004).

289. Cavadas, M. A. S. *et al.* REST mediates resolution of HIF-dependent gene expression in prolonged hypoxia. *Sci. Rep.* **5**, 1–12 (2015).

290. Guo, C. *et al.* HIF-1α accumulation in response to transient hypoglycemia may worsen diabetic eye disease. *Cell Rep.* **42**, 111976 (2023).

291. Cimmino, F. *et al.* HIF-1 transcription activity: HIF1A driven response in normoxia and in hypoxia. *BMC Med. Genet.* **20**, 37 (2019).

292. Lum, J. J. *et al.* The transcription factor HIF-1alpha plays a critical role in the growth factor-dependent regulation of both aerobic and anaerobic glycolysis. *Genes Dev.* **21**, 1037–1049 (2007).

293. Chan, Y. Y., Mbenza, N. M., Chan, M. C. & Leung, I. K. H. Assays to Study Hypoxia-Inducible Factor Prolyl Hydroxylase Domain 2 (PHD2), a Key Human Oxygen Sensing Protein. *Methods Mol. Biol.* **2648**, 187–206 (2023).

294. Ginouvès, A., Ilc, K., Macías, N., Pouysségur, J. & Berra, E. PHDs overactivation during chronic hypoxia "desensitizes" HIFα and protects cells from necrosis. *Proceedings of the National Academy of Sciences* **105**, 4745–4750 (2008).

295. Stiehl, D. P. *et al.* Increased Prolyl 4-Hydroxylase Domain Proteins Compensate for Decreased Oxygen Levels: EVIDENCE FOR AN AUTOREGULATORY OXYGEN-SENSING SYSTEM*. *J. Biol. Chem.* **281**, 23482–23491 (2006).

296. Shaw, J. *et al.* Antagonism of E2F-1 regulated Bnip3 transcription by NF-kappaB is essential for basal cell survival. *Proc. Natl. Acad. Sci. U. S. A.* **105**, 20734–20739 (2008).

297. Lee, H. & Paik, S.-G. Regulation of BNIP3 in normal and cancer cells. *Mol. Cells* **21**, 1–6 (2006).

298. Glick, D. *et al.* BNip3 regulates mitochondrial function and lipid metabolism in the liver. *Mol. Cell. Biol.* **32**, 2570–2584 (2012).

299. Fu, Z.-J. *et al.* HIF-1α-BNIP3-mediated mitophagy in tubular cells protects against renal ischemia/reperfusion injury. *Redox Biol.* **36**, 101671 (2020).

300. Li, J. *et al.* HIF1α-BNIP3-mediated mitophagy protects against renal fibrosis by decreasing ROS and inhibiting activation of the NLRP3 inflammasome. *Cell Death Dis.* **14**, 200 (2023).

301. Wang, Y., Song, D. & Tang, L. Mitophagy, Inflammasomes and Their Interaction in Kidney Diseases: A Comprehensive Review of Experimental Studies. *J. Inflamm. Res.* **16**, 1457–1469 (2023).

302. Mogyorósi, A. & Ziyadeh, F. N. GLUT1 and TGF-beta: the link between hyperglycaemia and diabetic nephropathy. *Nephrol. Dial. Transplant* **14**, 2827–2829 (1999).

303. Zhang, J. Z., Behrooz, A. & Ismail-Beigi, F. Regulation of glucose transport by hypoxia. *Am. J. Kidney Dis.* **34**, 189–202 (1999).

304. Kierans, S. J. & Taylor, C. T. Regulation of glycolysis by the hypoxia-inducible factor (HIF): implications for cellular physiology. *J. Physiol.* **599**, 23–37 (2021).

305. Wang, Y. *et al.* The glycolytic enzyme PFKFB3 drives kidney fibrosis through promoting histone lactylation-mediated NF-κB family activation. *Kidney Int.* **0**, (2024).

306. Lynch, M. R., Tran, M. T. & Parikh, S. M. PGC1α in the kidney. *Am. J. Physiol. Renal Physiol.* **314**, F1–F8 (2018).

307. Rowe, G. C. & Arany, Z. Genetic models of PGC-1 and glucose metabolism and homeostasis. *Rev. Endocr. Metab. Disord.* **15**, 21–29 (2014).

308. Lyapina, I., Ivanov, V. & Fesenko, I. Peptidome: Chaos or Inevitability. *Int. J. Mol. Sci.* **22**, (2021).

309. Poreba, M. Protease-activated prodrugs: strategies, challenges, and future directions. *FEBS J.* **287**, 1936–1969 (2020).

310. Lipman, N. S., Jackson, L. R., Trudel, L. J. & Weis-Garcia, F. Monoclonal versus polyclonal antibodies: distinguishing characteristics, applications, and information resources. *ILAR J.* **46**, 258–268 (2005).

311. Ascoli, C. A. & Aggeler, B. Overlooked benefits of using polyclonal antibodies. *Biotechniques* **65**, 127–136 (2018).

312. Delgado, M. E., Cárdenas, B. I., Farran, N. & Fernandez, M. Metabolic Reprogramming of Liver Fibrosis. *Cells* **10**, (2021).

313. Li, F. *et al.* FBP1 loss disrupts liver metabolism and promotes tumorigenesis through a hepatic stellate cell senescence secretome. *Nat. Cell Biol.* **22**, 728–739 (2020).

314. Wijermars, L. G. M. *et al.* Defective postreperfusion metabolic recovery directly associates with incident delayed graft function. *Kidney Int.* **90**, 181–191 (2016).

315. Ghanem, A., Kitanovic, A., Holzwarth, J. & Wölfl, S. Mutational analysis of fructose-1,6-bis-phosphatase FBP1 indicates partially independent functions in gluconeogenesis and sensitivity to genotoxic stress. *Microb. Cell* **4**, 52–63 (2017).

316. Donowitz, M. *et al.* Alterations in the proteome of the NHERF1 knockout mouse jejunal brush border membrane vesicles. *Physiol. Genomics* **42A**, 200–210 (2010).

317. Courbebaisse, M. *et al.* A new human NHERF1 mutation decreases renal phosphate transporter NPT2a expression by a PTH-independent mechanism. *PLoS One* **7**, e34764 (2012).

318. Friedman, P. A. & Mamonova, T. The molecular sociology of NHERF1 PDZ proteins controlling renal hormone-regulated phosphate transport. *Biosci. Rep.* **44**, (2024).

319. Hatano, R. *et al.* Ezrin, a membrane cytoskeletal cross-linker, is essential for the regulation of phosphate and calcium homeostasis. *Kidney Int.* **83**, 41–49 (2013).

320. Gagnon, K. B. *et al.* Kidney injury stimulates apical translocation of NHERF1. *FASEB J.* **36 Suppl 1**, (2022).

321. Catanesi, M. *et al.* L-methionine protects against oxidative stress and mitochondrial dysfunction in an in vitro model of Parkinson's disease. *Antioxidants (Basel)* **10**, 1467 (2021).

322. Øverbye, A., Sætre, F., Hagen, L. K., Johansen, H. T. & Seglen, P. O. Autophagic activity measured in whole rat hepatocytes as the accumulation of a novel BHMT fragment (p10), generated in amphisomes by the asparaginyl proteinase, legumain. *Autophagy* **7**, 1011–1027 (2011).

323. Shirahama-Noda, K. *et al.* Biosynthetic processing of cathepsins and lysosomal degradation are abolished in asparaginyl endopeptidase-deficient mice. *J. Biol. Chem.* **278**, 33194–33199 (2003).

324. Wang, D. *et al.* Loss of legumain induces premature senescence and mediates aging-related renal fibrosis. *Aging Cell* **21**, e13574 (2022).

325. Wang, D. *et al.* Legumain, an asparaginyl endopeptidase, mediates the effect of M2 macrophages on attenuating renal interstitial fibrosis in obstructive nephropathy. *Kidney Int.* **94**, 91–101 (2018).

326. Chen, C. *et al.* Legumain promotes tubular ferroptosis by facilitating chaperone-mediated autophagy of GPX4 in AKI. *Cell Death Dis.* **12**, 1–13 (2021).

327. Lunde, N. N., Bosnjak, T., Solberg, R. & Johansen, H. T. Mammalian legumain – A lysosomal cysteine protease with extracellular functions? *Biochimie* **166**, 77–83 (2019).

328. Schwarz, G. *et al.* Characterization of legumain. *Biol. Chem.* **383**, 1813–1816 (2002).

329. Chan, C.-B. *et al.* Mice lacking asparaginyl endopeptidase develop disorders resembling hemophagocytic syndrome. *Proc. Natl. Acad. Sci. U. S. A.* **106**, 468–473 (2009).

330. Smith, R. *et al.* Simvastatin inhibits glucose metabolism and legumain activity in human myotubes. *PLoS One* **9**, e85721 (2014).

331. Korytowska, N. *et al.* Activity of Cathepsin B in Serum of Patients after Kidney Transplantation Depends on Glucocorticosteroids Treatment. *Ann. Transplant.* **20**, 622–626 (2015).

332. Aggarwal, N. & Sloane, B. F. Cathepsin B: multiple roles in cancer. *Proteomics Clin. Appl.* **8**, 427–437 (2014).

333. Tang, T.-T. *et al.* Hydroxychloroquine attenuates renal ischemia/reperfusion injury by inhibiting cathepsin mediated NLRP3 inflammasome activation. *Cell Death Dis.* **9**, 351 (2018).

334. Edelstein, C. L. *et al.* The role of cysteine proteases in hypoxia-induced rat renal proximal tubular injury. *Proc. Natl. Acad. Sci. U. S. A.* **92**, 7662–7666 (1995).

335. Zegarska, J. *et al.* Extracellular matrix proteins, proteolytic enzymes, and TGF-beta1 in the renal arterial wall of chronically rejected renal allografts. *Transplant. Proc.* **35**, 2193–2195 (2003).

336. Paczek, L. *et al.* Human chronic kidney allograft rejection is accompanied by increased intraglomerular cathepsin B and L activity. *Transpl. Int.* **7 Suppl 1**, S311-3 (1994).

337. Paczek, L. *et al.* INCREASED CONTENT OF FIBRONECTIN AND LAMININ IN GLOMERULI ISOLATED FROM CHRONICALLY REJECTED HUMAN RENAL ALLOGRAFTS1. *Transplantation* **61**, 654 (1996).

338. Paczek, L. *et al.* Chronic kidney allograft rejection is accompanied by increased urinary excretion of fibronectin. *Transplant. Proc.* **32**, 1333–1334 (2000).

339. Xiaofei, C. *et al.* Identification of cathepsin B as a novel target of hypoxia-inducible factor-1-alpha in HepG2 cells. *Biochem. Biophys. Res. Commun.* **503**, 1057–1062 (2018).

340. de Poot, S. A. H. & Bovenschen, N. Granzyme M: behind enemy lines. *Cell Death Differ.* **21**, 359–368 (2014).

341. Lutz, J. *et al.* Inhibition of matrix metalloproteinases during chronic allograft nephropathy in rats. *Transplantation* **79**, 655–661 (2005).

342. Altemtam, N., Nahas, M. E. & Johnson, T. Urinary matrix metalloproteinase activity in diabetic kidney disease: a potential marker of disease progression. *Nephron Extra* **2**, 219–232 (2012).

343. Kollar, B. *et al.* MMP3 Is a Non-invasive Biomarker of Rejection in Skin-Bearing Vascularized Composite Allotransplantation: A Multicenter Validation Study. *Front. Immunol.* **10**, 2771 (2019).

344. Rodrigo, E. *et al.* Circulating levels of matrix metalloproteinases MMP-3 and MMP-2 in renal transplant recipients with chronic transplant nephropathy. *Nephrol. Dial. Transplant* **15**, 2041–2045 (2000).

345. Golabek, A. A., Dolzhanskaya, N., Walus, M., Wisniewski, K. E. & Kida, E. Prosegment of tripeptidyl peptidase I is a potent, slow-binding inhibitor of its cognate enzyme. *J. Biol. Chem.* **283**, 16497–16504 (2008).

346. Xie, Z. *et al.* Cathepsin B in programmed cell death machinery: mechanisms of execution and regulatory pathways. *Cell Death Dis.* **14**, 1–18 (2023).